Alma Mater Studiorum · Università di Bologna

Scuola di Scienze
Corso di Laurea Magistrale in Fisica

Role of the stratospheric dynamics in the Southern Hemisphere long-term climate change

Relatore:
Prof. Andrea Buzzi

Correlatore:
Dott.ssa Chiara Cagnazzo

Presentata da:
Gloria Rea

Sessione II
Anno Accademico 2012/2013

Sommario

Le variazioni a lungo termine nella regione polare dell'Emisfero Sud sono dovute all'aumento antropico dei gas ad effetto serra (GHG) e alla riduzione dell'ozono stratosferico, a causa delle emissioni di sostanze in grado di distruggerlo dal 1970 circa. Se l'aumento delle concentrazioni di GHG porta ad un riscaldamento della troposfera e ad un raffreddamento radiativo della stratosfera globale, la riduzione dell'ozono e la sua grande distruzione sull'Antartide portano ad un raffreddamento a lungo termine della stratosfera che si sovrappone al raffreddamento indotto dai GHG, che è però caratterizzato da una forte stagionalità. Studi precedenti hanno dimostrato che la riduzione dell'ozono nella tarda primavera australe è la principale forzante dei cambiamenti a lungo termine nell'Emisfero Sud dalla stratosfera fino alla superficie. Il raffreddamento stratosferico associato alla riduzione dell'ozono, dal momento che questo assorbe radiazione solare, porta infatti al rafforzamento dei venti occidentali nella stratosfera con una più tarda transizione a venti orientali (influenzando quindi la stagionalità della circolazione media zonale stratosferica), ad uno spostamento verso il polo e ad un'intensificazione della corrente a getto (jet) troposferica delle medie latitudini (attraverso una complessa catena di meccanismi ancora in studio), con l'espansione della cella di Hadley in troposfera e una proiezione di questi cambiamenti a lungo termine sulla polarità ad alto indice di un modo di variabilità climatica alla superficie, il *Southern Annular Mode* (SAM). Questo può spiegare perché i cambiamenti climatici sull'Antartide sono caratterizzati da un raffreddamento sul continente e un riscaldamento sulla penisola. Alla superficie, i venti occidentali alle medie latitudini guidano la *Corrente Circumpolare Antartica* influenzando la circolazione oceanica meridionale e probabilmente l'estensione del ghiaccio marino. Inoltre, come indicano recenti studi modellistici e osservativi, variazioni nel pattern del vento associate a variazioni dei venti occidentali superficiali possono indurre dei trend nella circolazione oceanica e quindi dei flussi di carbonio aria-mare sull'Oceano Meridionale, responsabile dell'accumulo di quantità importanti (circa il 40%) del biossido di carbonio oceanico globale. Se la catena di meccanismi che collega il raffreddamento stratosferico, associato alla riduzione dell'ozono, alle variazioni climatiche in superficie è ancora oggetto di studio, recentemente è stato proposto che una limitata rappresentazione dei processi stratosferici nei modelli

climatici per la simulazione del passato e la previsione dei cambiamenti climatici futuri, potrebbe portare ad una distorsione nella rappresentazione dei cambiamenti troposferici a lungo termine nelle simulazioni di quei modelli climatici. Fino a che punto è possibile che il ruolo della dinamica stratosferica possa essere richiamato per spiegare parte dei cambiamenti stimati nell'Emisfero Sud? E quali sono le possibili implicazioni per i flussi di carbonio dell'Emisfero Sud e per quelli globali?

In questa tesi viene condotta un'analisi multi-model mettendo insieme i dati di output derivati da diverse simulazioni di modelli climatici accoppiati oceano-atmosfera, che partecipano al progetto *Coupled Model Intercomparison Project-phase5* (CMIP5), con l'obiettivo di comprendere come le diverse rappresentazioni della dinamica stratosferica possano portare ad una differente rappresentazione dei cambiamenti climatici a lungo termine alla superficie. I risultati vengono poi confrontati con quelli ottenuti tramite le stesse analisi condotte però su un set di dati di reanalisi meteorologiche globali disponibili (ERA-40, *ECMWF 40 Year Re-analysis*).

Dopo aver descritto ed esaminato la fenomenologia specifica coinvolta, che collega variazioni nell'ozono stratosferico a variazioni nella dinamica del sistema accoppiato stratosfera-troposfera, viene mostrato come la rappresentazione e l'intensità del raffreddamento radiativo iniziale e di quello dinamico nella bassa stratosfera, nei modelli, siano i fattori chiave che controlla la successiva risposta troposferica, e come il raffreddamento stesso dipenda dalla rappresentazione della dinamica stratosferica. Nello specifico, per capire come modelli diversi rispondono alla forzante della deplezione di ozono nella stratosfera e nella troposfera, vengono analizzate le climatologie (medie a lungo termine su 20-40 anni) con i trend lineari dei campi di temperatura e di vento zonale medio. In particolare, concentro la mia attenzione sul campo di temperatura nella bassa stratosfera a latitudini comprese tra 60°S e 90°S e su quello del vento zonale medio tra 50°S e 70°S nella stagione tra Novembre e Marzo, per un sottoinsieme di modelli detti *High Top* (HT), caratterizzati da una buona rappresentazione della dinamica stratosferica, per un altro di modelli *Low Top* (LT), che ne hanno invece una limitata rappresentazione, e per le reanalisi di ERA-40. Questo viene eseguito per quantificare in che misura i diversi modelli sono in grado di rappresentare il raffreddamento della bassa stratosfera e le variazioni stratosferiche e troposferiche del vento zonale medio in risposta ad esso. Viene riscontrato che modelli HT tendono in media a

rappresentare un raffreddamento della bassa stratosfera più intenso rispetto ai modelli LT. Come suggerito dalla letteratura recente, attribuiamo la differenza dei modelli nella risposta alla stessa (o simile) forzante alla rappresentazione della stratosfera stessa: nei modelli LT manca in generale la risposta dinamica a lungo termine nella stratosfera, cioè il raffreddamento adiabatico associato ai cambiamenti nella circolazione di Brewer-Dobson che si sovrappone al raffreddamento radiativo dovuto alla riduzione dell'ozono. Il diverso raffreddamento stratosferico porta ad una risposta media del vento zonale più forte nei modelli HT, a seguito della relazione di vento termico, avviando quindi una catena di effetti che portano ad una risposta più forte nel jet troposferico in DJF (stagione data da dicembre, gennaio e febbraio). Nella sezione successiva si cerca di differenziare i modelli in base alla loro rappresentazione del raffreddamento radiativo e dinamico nella bassa stratosfera e alla risposta del jet troposferico. Si riscontra infatti che la trend del jet dalla tropopausa fino alla superficie è significativamente correlata linearmente al raffreddamento stesso della bassa stratosfera nei modelli, con le reanalisi che fittano molto bene questa relazione lineare. È interessante notare che i modelli HT sembrano avere un raffreddamento e una risposta del jet più forte ma mostrano uno spread maggiore, mentre i modelli LT tendono a riportare una risposta a lungo termine più piccola, ma più simile. Interpretiamo la differenza nello spread con il fatto che i modelli LT sono ancora privi di una componente (in questo caso una corretta rappresentazione della variabilità stratosferica), e quindi la loro risposta a lungo termine è meno variabile nei modelli. Sebbene le grandi differenze nei modelli utilizzati in questo lavoro potrebbero rendere difficile derivare un chiaro e coerente ruolo della dinamica stratosferica, la nostra analisi sottolinea che nella risposta a lungo termine ai cambiamenti antropici la rappresentazione della stratosfera può essere importante. Ciò può essere importante anche per produrre proiezioni future realistiche dei cambiamenti climatici sull'Antartide perché si prevede che in futuro l'ozono stratosferico sarà recuperato e le variazioni di GHG e ozono quindi non saranno più combinate nelle proiezioni sulla polarità della SAM. Pertanto, confermiamo l'importanza di includere una corretta rappresentazione della stratosfera, almeno con un certo grado di dettaglio, al fine di ottenere simulazioni climatiche a lungo termine e proiezioni nei pattern di circolazione dell'Emisfero Sud più affidabili. Si conferma inoltre che la rappresentazione e l'intensità del raffreddamento iniziale nella bassa stratosfera (a seconda della rappresentazione della stratosfera stessa nel modello) è l'ingrediente fondamentale.

Abstract

Past long-term changes in the polar Southern Hemisphere (SH) are characterized by an increase of greenhouse gases (GHGs) and a reduction of stratospheric ozone caused by anthropogenic emissions of ozone-depleting gases since about the 1970s. If the increase in GHGs has led to a warming of the troposphere and a radiative cooling of the global stratosphere, the ozone reduction and its strong depletion over Antarctica has led to a long-term cooling of the stratosphere that overimposes to the GHG cooling, however characterized by a strong seasonality. Previous studies have demonstrated that the late austral spring ozone depletion is the main forcing of SH long-term changes from the stratosphere down to the surface. Stratospheric cooling associated to ozone reduction, because ozone absorbs solar radiation, has led indeed to the strengthening of westerly winds into the stratosphere with a later transition to easterlies (therefore impacting the seasonality of the zonal mean circulation), a poleward displacement and a strengthening of the midlatitude tropospheric jet (via a not fully clarified mechanism) with an expansion of the Hadley cell in the troposphere and a projection of these long-term changes onto a high-index polarity of the *Southern Annular Mode* (SAM) at the surface. Here, the projection onto the SAM positive polarity can explain why climate change over Antarctica is characterized by a cooling over the continent and a warming over the peninsula, whereas mid-latitude westerlies drive the *Antarctic Circumpolar Current* influencing the ocean meridional overturning and likely sea ice extent. Moreover, as recent model and observational studies indicate, changes in wind patterns associated to changes of surface westerlies can cause trends in the oceanic circulation and therefore on the air-sea carbon fluxes over the Southern Ocean, responsible for the storage of substantial portions (up to about 40 %) of the global oceanic carbon dioxide.

If the chain of mechanisms linking stratospheric cooling associated to ozone depletion to long-term surface changes are still under investigation, recently, it has been proposed that a limited representation of stratospheric processes in climate models aiming to simulate past and predict future SH climate change could lead to a bias in the representation of tropospheric long-term changes in those climate model simulations. To which extent it is possible that a role of the dynamical stratosphere can be invoked in explaining part of the estimated changes in SH ? And which are the possible implications for the SH and global carbon fluxes?

Abstract

In this work a multi-model analysis has been conducted-by putting together output data derived from different coupled atmosphere-ocean climate model simulations participating to the *Coupled Model Intercomparison Project-phase 5* (CMIP5), with the aim of understanding how different representations of stratospheric dynamics in state-of-the-art models can lead to different representation of long-term surface climate changes. Results have been compared with the same analysis conducted on a set of available global meteorological reanalyses (ERA-40, *ECMWF 40 Year Re-analysis*).

After describing and reviewing the specific involved phenomenology that links stratospheric ozone changes to changes in the dynamics of the stratosphere-troposphere coupled system, we show how the representation and magnitude of the initial radiative and dynamical cooling in the lower stratosphere in models is the key factor controlling the subsequent tropospheric response, and how the cooling itself depends on the representation of the stratospheric dynamics.

Specifically, in order to understand how different models respond to ozone depletion forcing in the stratosphere and in the troposphere, climatologies (20-40 years long-term mean) and linear trends of the temperature and of the zonal mean zonal wind fields have been analyzed. In particular, I have focused my attention onto the lower stratosphere temperature field at latitudes between 60°S and 90°S and zonal mean zonal winds between 50°S and 70°S in the November to March season, for a subset of High Top (HT) models (i.e. models that have a good representation of the stratospheric dynamics) and Low Top (LT) models (models that have a limited representation of stratospheric dynamics) and for the ERA-40 reanalyses. This has been performed in order to quantify to which extent the different models are able to represent the lower stratospheric cooling and the stratospheric and tropospheric zonal mean zonal wind changes in response to it. We have found that HT models on average tend to represent a stronger lower stratospheric cooling with respect to LT models. As suggested in recent literature, we ascribe the different response in the models to the same (or similar) forcing to the representation of the stratosphere itself: LT models are in general missing the dynamical long-term response into the stratosphere, i.e. the adiabatic cooling associated to changes in the Brewer-Dobson circulation overimposing to the radiative cooling due to ozone reduction. The different stratospheric cooling leads to a stronger zonal mean zonal wind response in HT models, following the thermal

wind relationship, therefore initiating a chain of effects that lead to a stronger response in the DJF (December-January-February season) tropospheric jet.

In the following section we try to stratify the models in terms of their representation of lower stratospheric radiative and dynamical cooling and in terms of their tropospheric jet response. We found indeed that the jet trend from the tropopause down to the surface is significantly linearly correlated to the lower stratospheric cooling itself across the models, with reanalyses very well fitting this linear relationship. Interestingly, HT models appear to have a stronger cooling and stronger jet response but do show a larger spread, whereas LT models tend to report a smaller but more similar long-term response. We interpret the difference in the spread by the fact that LT models are again missing a component (in this case a correct representation of the stratospheric variability), and therefore their long-term response is less variable across the models. Although large differences in the models used in this work could render it not very easy to derive a clear and consistent role of the dynamical stratosphere, our analysis points out that in the long-term response to anthropogenic changes the representation of the stratosphere can be important. This can be important also for producing realistic climate change future projection over Antarctica because in the future, it is expected that stratospheric ozone will recover and in this case GHG and ozone changes will no longer combine to project onto the SAM high-index polarity. Therefore we confirm the importance of including a proper representation of the stratosphere, at least with a certain degree of detail, in order to obtain more reliable long-term climate simulations and projections in the SH circulation patterns. We also confirm that the representation and the magnitude of the initial cooling in the lower stratosphere (depending on the model representation of the stratosphere itself) is the essential ingredient.

Contents

Chapter 1

Introduction

1.1 General phenomenology and aim of the thesis

Climate in a narrow sense is usually defined as the "average weather," or more rigorously, as the statistical description in terms of the mean and variability of relevant quantities over a period ranging from months to thousands or millions of years. The classical period is 30 years, as defined by the World Meteorological Organization[1] (WMO). These quantities are most often surface variables such as temperature, precipitation, and wind. Climate in a wider sense is the state, including a statistical description, of the climate system[2].

This is how the Intergovernmental Panel on Climate Change[3] (IPCC) defines climate, implying that its study involves the whole climate system trough a balance of the total energy and its distribution in the different "reservoirs" that constitute this particular system. The climate system, in fact, is composed by a set of non

[1] The World Meteorological Organization (WMO) is a specialized agency of the United Nations, of which is the authoritative voice on the state and behaviour of the Earth's atmosphere, its interaction with the oceans, the climate it produces and the resulting distribution of water resources (http://www.wmo.int/pages/index_en.html).

[2] Appendix I-Glossary from the Intergovernmental Panel on Climate Change (IPCC).

[3] The IPCC is the leading international body for the assessment of climate change, established by the United Nations Environment Programme (UNEP) and the WMO in 1988 to provide the world with a clear scientific view on the current state of knowledge in climate change and its potential environmental and socio-economic impacts. See the website: http://www.ipcc.ch/

linearly mutually interacting subsystems: the atmosphere, the ocean, the cryosphere, the lithosphere (restricted to the surface soils, rocks, and sediments) and the biosphere (Peixoto and Oort, 1992). Factors that can shape climate, i.e. the so-called forcing mechanisms, include natural processes such as variations in solar radiation, variations in the Earth's orbit, continental drift and human induced changes in green-house gas[4] (GHG) and ozone-depleting gas concentrations. Besides, the initial forcing can be later either amplified or diminished by a variety of climate change feedbacks.

The response of the climate system might be fast, but the full response to forcing mechanisms might not be fully developed for centuries or even longer. For example, some parts of the climate system like the oceans and ice caps respond very slowly in reaction to changes in climate forcings.

Therefore, the variables which determine climate are numerous and the interactions within the climate system are complex, but there is a general agreement that the broad outlines are understood, at least insofar as the determinants of historical *climate change* are concerned (Ledley *et al.*, 1999).

The climate change term means the variation in global or regional climates over time, more precisely it reflects changes in the variability or average state of the atmosphere over time scales ranging from decades to millions of years. These changes can be caused by processes internal to the Earth, by external forces (e.g. variations in sunlight intensity) or, more recently, human activities (e.g. variations in GHG and ozone-depleting gas concentrations).

In recent usage, especially in the context of environmental policy, the above-mentioned term often refers only to changes in modern climate, including the rise in average surface temperature, the so-called *global warming*, and, in some cases, the term is also used with a presumption of human causation.

In the past, Earth has undergone periodic climate shifts, including four major ice ages, consisting of glacial periods where conditions are colder than normal, separated by interglacial periods. The accumulation of snow and ice during a glacial period increases the surface albedo[5], reflecting more of the Sun's energy into space and maintaining a lower atmospheric temperature. Increases in GHGs instead, such as by volcanic activity, can increase the global temperature and produce an

[4] GHGs changes are also due to natural causes.

[5] Albedo is the diffuse reflectivity or reflecting power of a surface. It is defined as the ratio of reflected radiation from the surface to incident radiation upon it.

interglacial age. Suggested causes of ice age periods include the positions of the continents, variations in the Earth's orbit, changes in the solar output, and volcanism (Wignall, 2001).

In the last 50 years some regions of the Earth have experienced large changes in terms of temperature, precipitation and circulation. For example climate change over Antarctic region is quite pronounced and results in a warming of several K over the Peninsula region during the past decades, and a cooling over the interior. The warming at low elevations on the Bellingshausen Sea is as large as any increase observed on Earth over the last 50 years.

The scientific interest of studying climate and the necessity of understanding how the Earth system responds to climate changes have led, during the last decades, to the development of appropriate numerical models, able to investigate the dynamics of the present climate and its changes in future scenarios of the Earth climate. These numerical models, called "Earth System Models", represent the fundamental physical processes as a set of discretised differential equations describing processes within and between the atmosphere, the ocean, the cryosphere, and the land and marine biosphere. These equations contain information about physical, chemical and biological mechanisms governing the rates of change of the elements of the global Earth system.

Among the different Earth system components that are represented in state-of-the-art climate and Earth System Models, the stratosphere is one of the newest ones included[6]. There is indeed a growing body of evidence that variability in the stratosphere has a significant impact on modes of variability of the tropospheric and surface climate (Baldwin and Dunkerton, 2001). In addition, the impact of climate change on the thermal and dynamical structure of the stratosphere is a topic of current research (Butchart and Scaife, 2001, Butchart et al., 2006) and its feedback on stratospheric composition and surface climate is largely unknown.

The discovering of two-way interactions between the stratosphere and the Earth system have induced the World Climate Research Programme's (WRCP) Stratospheric Processes and Their Role in Climate (SPARC) Dyn Var[7] activity to

[6] Here we refer at a full representation of the stratospheric dynamics, as detailed in Chapter 2.

[7] SPARC is a core project of the World Climate Research Program (WCRP) and Dyn Var is part of this project promoting the development and use of coupled atmosphere-ocean-sea ice general circulation models to study the influence of the stratospheric circulation on the global climate system, with a particular emphasis on the two-way dynamical coupling between the troposphere and the stratosphere.

study the effect of stratospheric dynamics and variability on climate by means of numerical climate models (Gerber et al., 2011). This assessment is made possible by new simulations performed with models that include a well resolved stratosphere[8], so that it becomes possible understand the important role of the stratosphere in the natural and forced variability of the Earth system and determine whether incorporating knowledge of the middle atmosphere may lead to improved seasonal forecasts and climate projections.

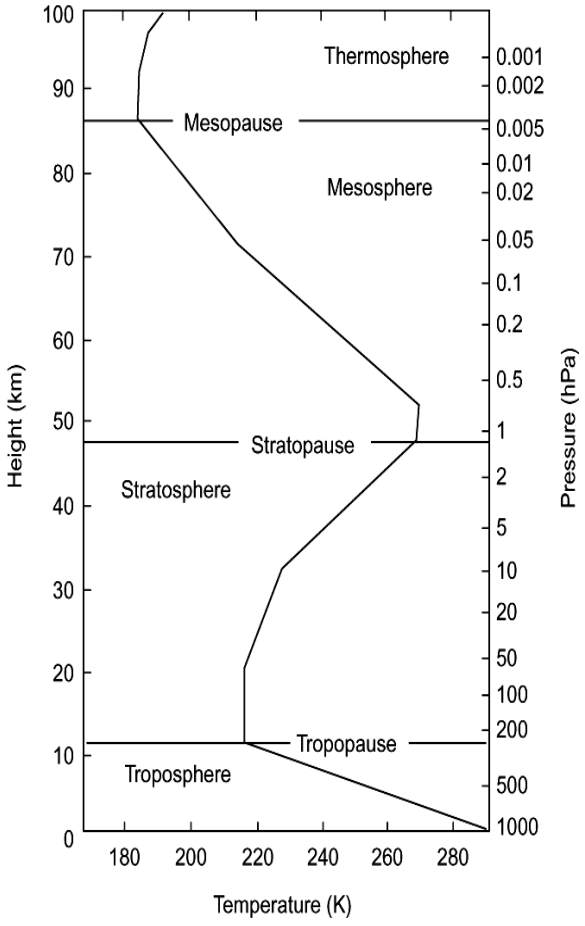

Figure 1.1: Midlatitude mean temperature profile. Based on the U.S. Standard Atmosphere (1976).

In this work of thesis it is possible to identify two main purposes. Firstly, one of these is managing to understand how stratospheric dynamics and ozone depletion

[8] A well-resolved stratosphere will be defined in Chapter 2.

can influence tropospheric jet, oceanic circulation, sea-ice trend and air-to-sea carbon fluxes in the Southern Hemisphere (SH). The second purpose is understanding how different representations of stratospheric dynamics in several climate models can produce different stratospheric temperature and wind changes.

I will make use of an extended dataset that includes climate simulations performed with state-of-the-art climate models including a different representation of the stratosphere. These simulations are performed within the CMIP5[9] (Coupled Model Intercomparison Project Phase 5) exercise and will be described in Section 2.2.

The focus of this work is to look at the ozone trend effect on the SH long term changes considering different representation of stratospheric dynamics[10]. Therefore, after basically introducing the mean state of the atmosphere, the stratospheric and tropospheric dynamics, I have dedicated Chapter 2 to describe CMIP5 Climate Models, with their general features, and to explain the differences between High Top (representing quite realistically the stratosphere and its processes) and Low Top Models (representing a stratosphere with a weak variability), concluding with a brief mention to observation techniques and reanalyses data.

In Chapter 3 the known mechanisms linking the ozone depletion to surface climate change are revised, based on published literature. This chapter also explains in detail the specific starting point of this study.

To understand how different models respond to ozone depletion forcing, in Chapter 4 zonal mean temperature and zonal wind climatologies and linear trends are analyzed. In particular, I have reserved my attention to 12 high top models and 8 low top models, quantifying long term changes in the stratosphere and in the troposphere down to the surface within the year.

In Chapter 5, I have constructed trend indices to investigate the correlation degree between jet magnitude (and jet shift) and cooling trend, for both High Top and Low Top Model data. These indices have been used to realize scatter plots that make possible to study the cooling-jet trends relationships and identify the possible role of the representation of the stratosphere. In Chapter 6, conclusions of this work

[9] The CMIP5 project is an extensive modeling effort, involving more than 20 climate modeling groups, that aims at evaluating the last generation of coupled models through the comparison of predefined experiments. Such experiments involves simulations of both the past and future climate, decadal predictions, etc. Further detail may be find in chapter 2.

[10] They also differ in the radiative schemes and chemical representation but considering a high margin of error we can neglect these differences with a good approximation.

are drawn.

1.2 The stratosphere and the ozone

The stratosphere is the lower layer of the middle atmosphere, located above the troposphere and below the mesosphere (Fig.1.1). Thus, this region extends from the tropopause at about 10-16 km altitude, according to the latitude[11], to the stratopause at about 50 km altitude.

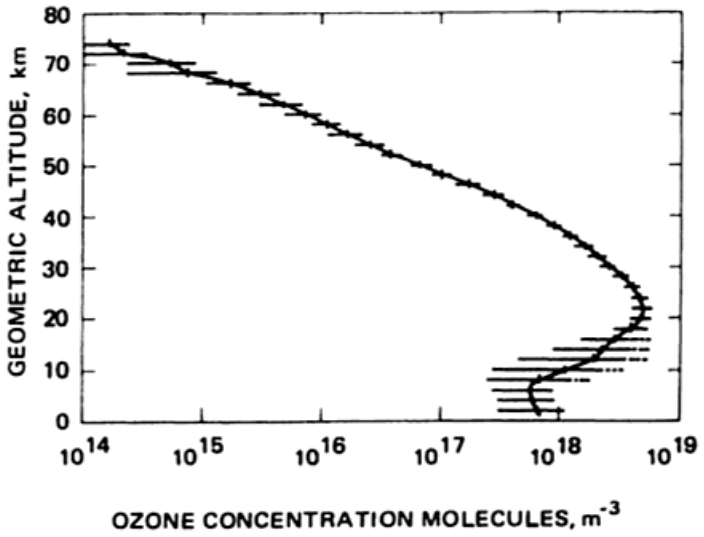

Figure 1.2: Midlatitude standard ozone concentration profile (molecules m^{-3}). Horizontal bars show the standard deviation about the mean for observed profiles. From the U.S. Standard Atmosphere (1976). Derived from Andrews *et al.* (1987).

Therefore, ozone, absorbing incoming solar radiation of wavelength less than 300 nm, provides the main heat source causing the observed-global mean vertical increase of temperature in the stratosphere. Ozone has a maximum molecular concentration of about $7x10^{12}$ molecules cm^{-3} at about 22 km altitude (Fig. 1.2), whereas the maximum mixing ratio occurs near 35 km altitude (Andrews *et al.*, 1987).

[11] At high latitudes the stratosphere is situated between about 8 km and 50 km altitude above the surface, while near the equator it may start at altitudes as high as 18 km.

The stratospheric ozone layer is really important because it protects life on Earth by absorbing UV radiation from the Sun (Jacob, 1999). On average 90% of atmospheric ozone is found in the lower stratosphere (Thompson *et al.*, 2011), where it is accumulated by Brewer-Dobson stratospheric circulation[12].

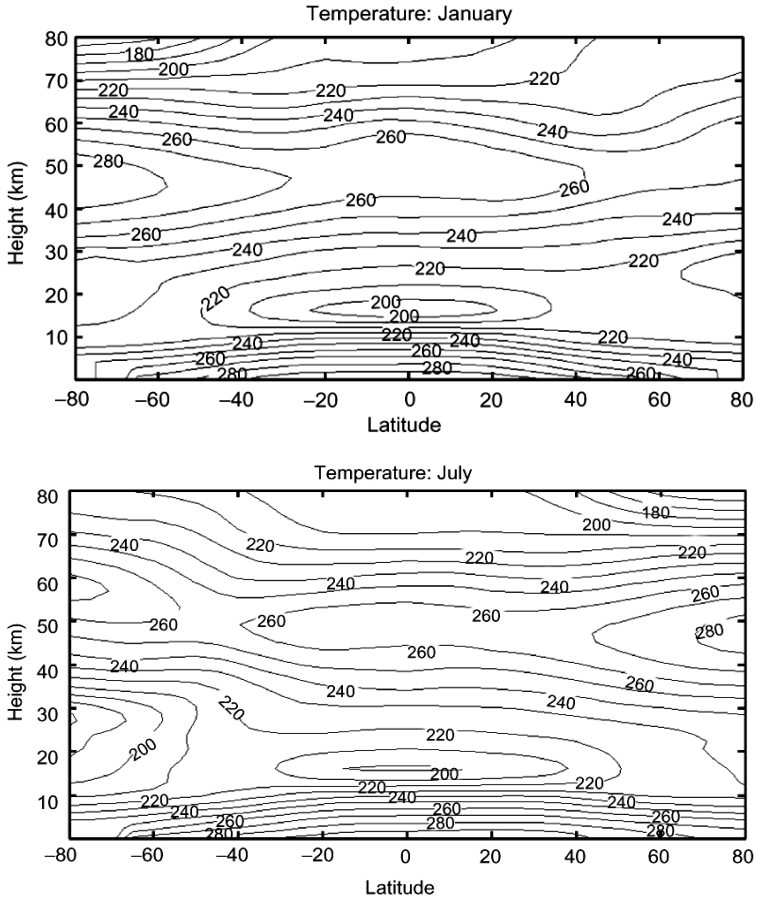

Figure 1.3: Observed monthly and zonally averaged temperature (K) for January and July. From Fleming *et al.* (1990).

As Figure 1.3 shows, in the lower stratospheres there is a temperature minimum at the equator due to a radiative cause (the ozone is taken away from lower latitudes by residual circulation, implying a lower ozone concentration in tropical belt) and a dynamical cause (rising motion of residual circulation implies an adiabatic cooling by expansion, as explained in the next sections). Instead, at the summer hemisphere

[12] The mechanism that explains how Brewer-Dobson circulation works is reported in Section 1.3.4.

pole and in winter hemisphere midlatitudes a maximum can be observed in the upper stratosphere. Furthermore, above 30 hPa the temperature decreases uniformly from summer pole to winter pole, in accord with radiative equilibrium conditions (Holton, 2004).

A theory for the origin of this ozone layer was proposed in 1930 by Sydney Chapman, who supposed that ozone originates from the photolysis of atmospheric oxygen molecule O_2. Since the bond energy of O_2 (498 kJ mol^{-1}) corresponds to the energy of a 240 nm UV photon, thus, only photons of a wavelength less than 240 nm are necessary to photolyze the O_2 molecule, and such high-energy photons are present in the solar spectrum at high altitude (Jacobs, 1999).

The Chapman reactions can be written as follows:

$$O_2 + h\nu \rightarrow 2O \tag{1.1a}$$

$$O + O_2 + M \rightarrow O_3 + M \tag{1.1b}$$

$$O_3 + h\nu \rightarrow O + O_2 \tag{1.1c}$$

$$O + O_3 \rightarrow 2O_2 \tag{1.1d}$$

where M is a *third body*[13], and the quantity $h\nu$ represents a photon of solar ultraviolet radiation (where ν is the frequency). In the stratosphere, (1.1b) and (1.1c) are fast reactions, while (1.1a) and (1.1d) are slow (Jacobs, 1999). The first two equations govern the production of ozone with a net result:

$$3O_2 \rightarrow 2O_3$$

The reaction (1.1c) instead doesn't actually destroy ozone, because the atomic oxygen just formed immediately reacts with O_2 to form ozone again, by reaction (1.1b). In the original scheme the fourth reaction (1.1d) is the only one that serves to destroy ozone, but this is much too slow to provide the rate of ozone destruction required to establish the observed stratospheric ozone profile. Therefore, most ozone production occurs in the tropical stratosphere where very energetic solar radiation is

[13] A third body is any inert molecule that can remove the excess energy from the reaction product and eventually dissipate it as heat.

able to break apart oxygen molecules (O_2) into oxygen atoms (O). However, the spatial distribution of ozone reports a minimum at equatorial regions.

In the stratosphere important sinks of ozone are represented by a set of catalytic cycles and heterogeneous reactions that involve free radicals of the nitrogen, chlorine, bromine and hydrogen families. Those reactions are particularly important over the polar regions.

Over Antarctica heterogeneous chemistry is fundamental to understand the ozone loss because these processes convert reservoir species such as HCl (hydrochloric acid) and $ClONO_2$ (chlorine nitrate) into active chlorine species such as ClO that can destroy it. Heterogeneous processes are different from homogeneous processes, that involve chemical reactions in the gas phase only, whereas the first type processes occur on the solid surfaces of particles.

Conditions necessary for ozone loss is the existence of Polar Stratospheric Clouds (PSCs), that are fundamental to let heterogeneous reactions act over Antarctic region. Because midlatitude air contains high concentrations of NO and NO2, it is necessary also that the polar vortex is isolated to prevent these reactive nitrogen compounds from reacting with the ClO, hence interrupting the ClO-ClO and ClO-BrO catalytic loss processes, other important ozone sinks. A third necessary condition is that there must be a small amount of sunlight to drive the catalytic loss process by splitting the Cl_2 (molecular chlorine) into highly reactive free chlorine. Another condition is that there be sufficient chlorine, otherwise ozone loss is too small.

The main chemical and physical processes that occur for ozone loss are:

- HCl and $ClONO_2$ react on PSCs to form Cl_2;
- The Cl_2 is degassed while HNO_3 remains on the surfaces of the PSCs.
- Sunlight returns in spring and the Cl_2 is immediately photolyzed into free chlorine, Cl.
- The free Cl then destroys ozone primarily via the ClO-ClO and ClO-BrO reactions.

An additional condition is imposed by the consideration that PSCs existence is due to very cold temperature over the polar regions, and this condition is encountered in the winter stratosphere over Antarctica. The temperatures there are so cold because of the feedbacks between radiation and dynamics.

As it was said above, ozone absorbs incoming solar radiation, so it defines the

thermal profile and therefore also the dynamical pattern of the stratosphere. A strong jet stream appears in the lower to middle stratosphere at the edge of the polar night region because it is here that solar radiation disappears, allowing temperatures inside the stratospheric polar night to fall to extremely low values. The different distribution of diabatic heating indeed, caused by the latitudinal distribution of ozone, implies a meridional temperature gradient that, from thermal wind considerations (see Appendix A), implies the existence of strong westerly jet stream called the *polar night jet* (Andrews et al., 1987). Hence, winds in the stratosphere are strongest at the edge of the stratospheric jet, where the temperature gradients are strongest. The region of extremely cold temperatures inside the polar night is known as the polar vortex.

In the SH the polar vortex is very strong and lasts more than in the NH. It is in this very cold and stable region that PSCs are able to form easily[14] and act as sinks for ozone-depleting-substances that are the main responsible of rapid ozone loss by chemical reactions, leading to the Antarctic ozone hole. In fact, the heterogeneous reactions of chlorine compounds on the surfaces of PSCs cause Antarctic ozone loss:

$$ClNO_3 + HCl \xrightarrow{PSC} Cl_2 + HNO_3 \quad (1.2a)$$

$$Cl_2 + h\nu \longrightarrow 2Cl \quad (1.2b)$$

Nitric acid (HNO_3), produced by heterogeneous reaction, is retained on the PSC cloud particle surfaces, through a process known as denoxification (as opposed to dentrification which carries reactive nitrogen out of the stratosphere). Without reactive nitrogen compounds to act as a brake on reactive chlorine compounds, the chlorine compounds are free to destroy ozone (the second reaction shows how chlorine molecule is transformed into its active form with solar radiation incoming in spring). In fact, HNO_3 must be photolyzed by sunlight to form reactive nitrogen compounds, and there is no sunlight during the wintertime polar night:

$$HNO_3 + h\nu \rightarrow NO_2 + OH \quad (1.3a)$$

$$ClO + NO_2 + M \rightarrow ClNO_3 + M \quad (1.3b)$$

[14] These clouds only form when temperatures in the stratosphere get extremely cold, below -78 °C.

The removal of ClOx by nitric acid is found to be inefficient also in spring because of exceedingly low HNO3 concentrations in the polar vortex. In fact, over the course of the winter, HNO_3-containing PSC particles are removed by sedimentation.

However, once the chlorine is freed by the heterogeneous reactions (1.3), seen before, the weak levels of sunlight initiate and maintain the catalytic ozone loss photochemistry. The chlorine compounds are principally of manmade origin: the chlorofluorocarbons (CFCs),were the safe, inert compounds developed in the late 1920s for refrigeration and aerosol propellants. CFCs gained enormous usage worldwide since their creation. Measurement of extremely high levels of chlorine monoxide over Antarctica has provided clear evidence that the CFCs were the culprit behind these ozone losses (Cordero *et al.*, 2012). These compounds initially exist as inactive, so-called reservoir species, so, this type of substances, to initiate the chemical reaction, first they have to be converted into other forms that can directly attack ozone molecules and part of this conversion process is catalyzed by the surfaces of tiny crystals and droplets in PSCs.

1.3 Atmospheric mean state

In this section we will briefly introduce to the main elements of the atmospheric circulation that are analyzed in the course of this work.

1.3.1 The zonal mean circulation

If the Earth had perfect zonally symmetric boundary conditions, because of the rotational symmetric of the system, it would necessarily feature a zonally symmetric climate. Therefore, the zonal asymmetries in the Earth boundary conditions are necessarily the reason of the zonal asymmetries in the observed time mean state, which are generally called *stationary* or *eddies waves*. The zonal mean circulation is instead depending on the net meridional transport of heat and momentum by the whole set of atmospheric motions, which results as instabilities forced by the vertical and meridional distribution in the incoming solar radiation.

So it is possible to distinguish between the zonal mean (i.e. the average around latitude circles) and its departure, the above-mentioned eddies waves, that are wave-

like oscillations of the midlatitude circulation at planetary scale, often associated to Rossby waves (see Section 1.3.3). Moreover to describe the general circulation, the transient eddies are deviations from the mean and they are represented by synoptic scale phenomena like cyclones, with time scales of few days.

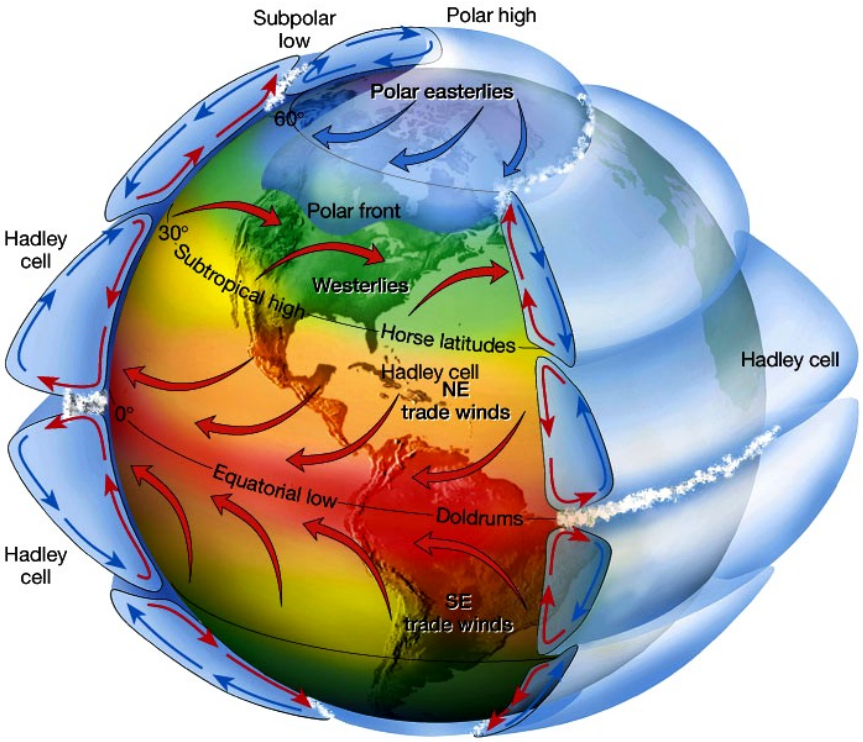

Figure 1.4: A schematic overview of the general circulation of the atmosphere. From Lutgens and Tarbuck (2001).

The zonal mean tropospheric circulation is associated to a meridional circulation, that features three overturning cells, respectively called, moving from the equator to the pole, the Hadley, the Ferrel and the Polar cell. The Hadley cell is associated to convection of rising warm air close to the equator, poleward flowing in the upper troposphere and sinking in the subtropics, where an adiabatic warming leads to the formation of the subtropical high pressure system (Held and Hou, 1980). This is wrong for the two extratropical meridional cells, which are instead consequence of the meridional heat and momentum transport by extratropical eddies (Peixoto and Oort, 1992). The general circulation of the atmosphere (shown in Fig. 1.4) is forced by the thermal difference between the equator and the poles

and by the angular momentum conservation.

The zonal wind field is characterized by tropical surface easterlies, known as *trade winds*, opposed to extratropical westerlies, that are organized in vertically coherent structures featuring maximum winds in the upper troposphere. These strong extratropical westerly winds in the upper troposphere are called *jet streams* (see Section 1.3.6) and are located at the latitude band of highest average meridional temperature gradient. Around the pole, instead, weak surface easterlies emerge.

Due to the drag exerted by the Earth surface on the air motions in the lowest atmospheric layers, tropical easterlies and extratropical westerlies represent respectively a source and a sink of atmospheric angular momentum. Considering long time averages, in fact, the total angular momentum in every latitude bands has to remain constant, hence atmospheric motions have to compensate the surface sources and sinks by meridionally redistributing momentum from the tropics to the extratropics. While the redistributing of momentum in the tropics is mainly accomplished by the Hadley cell circulation, extratropical waves provide essential transport in the extratropics (Peixoto and Oort, 1992).

In the stratosphere, the main features of the zonal mean flow are an easterly jet in the summer hemisphere and a westerly jet in the winter hemisphere, with a maxima in speed occurring near 60 km altitude (Holton, 2004). This is mainly due to the contribution of a differential heat distribution in latitude, as mentioned in previous section. In fact, a circulation develops in the meridional plane to dynamically balance the differential radiative heating, and this is often called *diabatic circulation*. In reality, this circulation is primarily driven by eddy forcing, not by radiative heating directly. At the solstices the diabatic circulation consists of rising motion near the summer pole, a meridional drift into the winter hemisphere, and sinking motion close to the winter pole. The responsible of the meridional drift is the Coriolis torque that tends to generate mean zonal westerlies in the winter hemisphere and easterlies in the summer hemisphere (Fig. 1.5) which are in approximate geostrophic balance with the meridional pressure gradient. At the equinoxes, the differential radiative drive is associated with rising in the equatorial region and a poleward meridional drift in both the hemispheres, so that the Coriolis torque generates weak mean zonal westerlies in both hemispheres (Andrews *et al.*, 1987).

The cross section of Figure 1.5 should not be regarded as definitive climatology because, in reality, there are substantial differences between the Northern and SH

solstice circulations and a remarkable interannual variability in the middle atmosphere (especially in the winter hemisphere).

However, the study of the atmospheric mean state can't be really separated from the study of its variability, as the non-uniform landmass distribution of the Earth creates several land-sea contrasts, that significantly alters the zonal perspective.

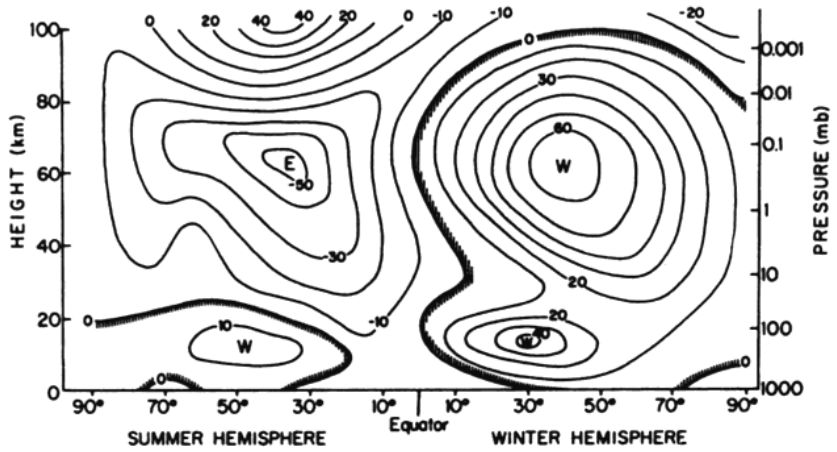

Figure 1.5: Schematic latitude-height section of zonal mean zonal wind (m s^{-1}) for solstice conditions; W and E indicate centers of westerlies and easterlies respectively. Courtesy of R. J. Rees.

For such reasons, it is necessary to describe more in detail the eddy flux effect on the zonal mean flow (Section 1.3.2), the jet streams (Section 1.3.6) and introduce the concept of the planetary waves (Section 1.3.3) and Hadley cell (Section 1.3.7). For this particular case it is important to focus also on the stratosphere dynamics reporting detailed explanations of the residual stratospheric circulation of Brewer-Dobson (Section 1.3.4) and the stratospheric polar vortex (Section 1.3.5).

1.3.2 Eddies and the stratospheric mean state

In the absence of eddy motions, the middle atmosphere should be close to radiative equilibrium at all latitudes with a zonal mean temperature distribution (Fig. 1.6) which is determined, except for a small lag due to thermal inertia, by an annually varying radiative equilibrium following the annual cycle in solar heating

(Holton, 2004). In this hypothetic case, the circulation would consist only of a zonal mean zonal flow (seen in the previous section) in thermal wind balance with the meridional temperature gradient, without any meridional and vertical circulation and without any stratosphere-troposphere interaction.

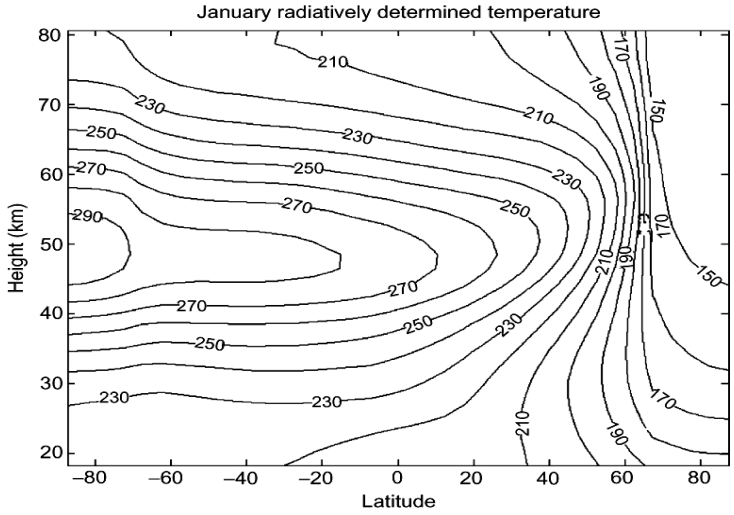

Figure 1.6: Radiatively determined temperature distribution (K) for Northern winter solstice from a radiative model that is time marched through an annual cycle. Realistic tropospheric temperatures and cloudiness are used to determine the upward radiative flux at the tropopause. From Shine (1987).

By observing Figure 1.6 and comparing it with the temperature profile for the same month of the Figure 1.2, we can note that the temperature difference between the two poles is much smaller than in the hypothetic radiatively determined state, although the quite uniform temperature increasing from winter pole to summer pole in a region that extends from 30 to 60 km altitude is qualitative consistent with the merely radiative distribution (Holton, 2004). The departure from this purely radiative state must be maintained by eddy transports.

Hence, rather than causing the mean circulation, the radiative heating and cooling patterns observed in the middle atmosphere are a result of the eddies driving the flow away from a radiative balance state. In this way, the eddies disturbances drive meridional and vertical circulations that give an important contribution in the heat redistribution, allowing substantial local departures from radiative equilibrium, especially in the winter stratosphere.

To understand how eddies can lead to departures of the zonal mean temperature distribution in the middle atmosphere from its radiatively determined state, it is useful to use the Transformed Eulerian Mean[15] (TEM) system of equations to consider an idealized model of extratropical forcing (Holton, 2004).

Considering the TEM equations, for quasi-geostrophic motions on the β-plane, we can see how the eddy fluxes can influence the zonal mean flow:

$$\frac{\partial \bar{u}}{\partial t} - f_0 \bar{v}^* - \bar{X} = -\frac{1}{\rho_0} \boldsymbol{\nabla} \cdot \mathbf{F} \tag{1.4a}$$

$$\frac{\partial \theta}{\partial t} + \bar{w}^* \frac{\partial \theta_0}{\partial z} - \bar{Q} = 0 \tag{1.4b}$$

$$\frac{\partial \bar{v}^*}{\partial y} + \frac{1}{\rho_0} \frac{\partial (\rho_0 \bar{w}^*)}{\partial z} = 0 \tag{1.4c}$$

$$f_0 \frac{\partial \bar{u}}{\partial z} + \frac{Re^{-kz/H}}{H} \frac{\partial \bar{\theta}}{\partial y} = 0 \tag{1.4d}$$

where $(\bar{v}^*, \bar{w}^*)$ are respectively the meridional and the vertical component of the residual stratospheric eddy-driven circulation, whereas the vector $\mathbf{F} \equiv (0, -\rho_0 \overline{v'u'}, \rho_0 \overline{v'\theta'}/\theta_{0z})$, represents the *Eliassen-Palm flux* (EP flux), in the transformed mean zonal momentum equation (1.4a). In this way, the eddy momentum flux $\overline{v'u'}$ and eddy heat flux $\overline{v'\theta'}$ act in combination, through the divergence of the EP flux **F** (see Appendix A), transporting momentum and heat along a meridional plane. Instead $\bar{Q}$ is the diabatic heating term, due to radiation contribution in terms of heating.

In reality, the interaction between eddy disturbances and mean flow is a two-way process, because the mean-flow configuration can strongly modify the propagation of the disturbances, while the disturbances themselves can bring about significant mean-flow changes, through rectified nonlinear effects (Andrews *et al.*, 1987). It's clear that eddies are important aspects of the circulation because they can affect the zonally averaged flow by producing fluxes and flux convergences.

It's also possible to distinguish between *stationary* eddies, which are anchored to features (such as mountain ranges) on the Earth's surface and so appear in time averaged (e.g. monthly mean) maps, and *transient* eddies that move and so are

[15] To know how TEM equations have been obtained see Appendix A.

hidden in time averages (Randall, 2013).

The stationary wave field, i.e. the time mean zonally asymmetric part of the circulation, is a key dynamical quantity that contributes significantly to the flux of wave activity (EP flux) from the troposphere to the stratosphere and to the driving of the Brewer-Dobson circulation. The stationary wave field can be used to characterize the vertical and meridional structure of zonal asymmetries, the shape and position of the polar vortex, and long-term trends in the zonally asymmetric flow. The climatological stationary wave field, i.e. the zonally asymmetric part of the climatological mean circulation, is observed to have a well-defined maximum in latitude at each altitude in the extra-tropical troposphere and stratosphere. The structure of the polar vortex is reflected in the stratospheric stationary wave field when decomposed into its dominant wave-1 component, which describes the location of the centre of the vortex relative to the pole, and its weaker wave-2 component, which describes the orientation and distortion of the vortex.

There is also significant small-scale, high-frequency motion in the stratosphere and mesosphere, driven by the dominant eddies. Much of this is associated with inertio-gravity waves, which are forced in the troposphere by flow over topography, convection, shear instability, and sometimes by spontaneous emission from the large-scale flow. These inertio-gravity waves propagate up into the stratosphere and mesosphere where they break and dissipate.

1.3.3 The planetary waves

Land-sea contrasts, orography and seasonality lead to considerable zonal asymmetries that support a characteristic wave-like pattern, especially in the Northern Hemisphere (NH) where there is the greater presence of lands and orographic surveys.

The *Rossby waves* or *planetary waves* are the most important wave type for large-scale meteorological processes (Holton, 2004) and were first identified in the Earth's atmosphere in 1939 by Carl-Gustaf Arvid Rossby who went on to explain their motion.

The planetary waves in the Earth's atmosphere are easy to observe as large-scale modulation of the jet stream (with very long wavelengths, upward of 10000 kilometers).

A single free propagating Rossby wave may be forced by tropical convection or by other sources of vorticity, even though the classical stationary wave pattern is caused by the orographic barriers and land-sea contrasts. They can be considered the main component of the Ferrel cell, being excited by longitudinally dependent diabatic heating patterns or by flow over topography, transporting momentum and heat from the equator up to the poles.

However, the physical origin of Rossby waves is connected to the conservation of the potential vorticity.

In fact, if a westerly flow has a curved path northward, initially it has a positive relative vorticity. Moving in this direction, in fact, the planetary vorticity increases, thus reducing the relative vorticity. When the relative vorticity reaches a negative value, instead, the flow curves southward. In this movement there is a similar mechanism, because of which the relative vorticity returns to increase and the flow turns back northward.

Hence, the planetary waves emerge due to shear in rotating fluids, because of the variation of the Coriolis parameter with latitude, the so-called *β-effect*, in an inviscid[16] barotropic[17] fluid of constant depth (where the divergence of the horizontal velocity must vanish).

Rossby waves are linear, dispersive (i.e. their frequency is not a linear function of the wavenumber) and they can be identified in that its phase velocity always has a westward component. However, the wave's group velocity (associated with the energy flux) can be in any direction. In general, shorter waves have an eastward group velocity and long waves a westward group velocity (Holton, 2004), thus, in the case of the planetary waves, that are large-scale waves, an easterly flow is observed.

Deep convection and heat transfer to the troposphere is enhanced over anomalously warm sea surface temperatures in the tropics, such as during El Niño events. This tropical forcing generates atmospheric Rossby waves that propagates poleward and eastward and are subsequently refracted back from the pole to the tropics. In this way they are responsible for the momentum convergence and for the eddy-driven acceleration of the jet streams (Vallis, 2006).

[16] In presence of a inviscid fluid, viscosity has a null value.

[17] The terms "barotropic" and "baroclinic" Rossby waves are used to distinguish their vertical structure. Barotropic Rossby waves do not vary in the vertical, and have the fastest propagation speeds. The baroclinic wave modes are slower, with speeds of only a few centimeters per second or less.

Conversely, when their amplitude become too large, they can break just like a surface sea wave, in a phenomena called Rossby Wave Breaking (RWB; McIntyre and Palmer, 1983). The RWB is defined as a rapid (few days) and irreversible mixing of materials contours of some meteorological field (e.g. potential vorticity). These events are typical occurring on the poleward and equatorward flanks of the jet streams (Strong and Magnusdottir, 2008). Therefore, since these deviations become very pronounced, these waves detach the masses of cold, or warm, air that become cyclones and anticyclones and are responsible for day-to-day weather patterns at midlatitudes. Rossby waves may be partly responsible for the fact that eastern continental edges, such as the Northeast United States and Eastern Canada, are colder than Europe at the same latitudes (Kaspi and Schneider, 2011).

Poleward propagating Rossby waves explain many of the observed statistical teleconnections between low latitude and high latitude climate (Hoskins and Karoly, 1981). Poleward propagating Rossby waves are an important and unambiguous part of the variability in the NH, as expressed in the Pacific North America pattern. Similar mechanisms apply in the SH and partly explain the strong variability in the Amundsen Sea region of Antarctica (Lachlan-Cope and Connolley, 2006).

However, the planetary-scale Rossby waves are an important part of the dynamics of the stratosphere. They, after being excited in the troposphere, by flow over topography, by latent heat release, or through the nonlinear evolution of tropospheric eddies (Scinocca & Haynes 1998), then propagate up from the troposphere into the stratosphere and mesosphere. Given that the dominant forcing of stratospheric Rossby waves is geographically stationary, this provides a basic explanation of why the winter stratosphere (with eastward flow around the pole) is much more disturbed than the summer stratosphere (with westward flow around the pole) and why the disturbances in the winter stratosphere tend to have much larger scales than is typical of the troposphere below.

Most planetary waves in the stratosphere, in fact, appear to propagate upward from forcing regions in the troposphere, and a useful way to model their middle atmosphere behaviour is to consider quasi-geostrophic disturbances forced by fluctuations in the height of some isobaric surface below. Thus, for analyzing extratropical planetary wave motions in the middle atmosphere, it is useful use β-plane, rather than spherical, geometry and work with quasi-geostrophic theory (see Appendix A). Furthermore, it is necessary to assume that the motion consists of a

small-amplitude disturbance superposed on a constant zonal mean flow, so that the eddy waves allow to drive the quasi-stationary waves vertically propagating. The potential vorticity also will have a fluctuating component that will satisfy the vorticity linearized equation, which will have solutions in the form of harmonic waves with zonal and meridional wave numbers k and l, zonal phase speed c_x and vertical wave number defined by:

$$m^2 \equiv \frac{N^2}{f_0^2}\left[\frac{\beta}{(\bar{u}-c_x)} - (k^2 + l^2)\right] - \frac{1}{4H^2} \tag{1.5}$$

where f_0 is a constant midlatitude reference value of the Coriolis parameter, β the Coriolis parameter derivative $\beta = 2\Omega a^{-1}\cos\phi$, with a^{-1} Earth radius and ϕ the latitudinal coordinate. The term N is the log-pressure buoyancy frequency corresponding to the reference temperature profile and representing the most convenient measure of atmospheric stability[18] (Andrews *et al.*, 1987). Besides, $\bar{u}$ is the zonal mean zonal wind, before mentioned in the previous sections, and H represents the vertical scale-length. The sign of m is very important because the buoyancy conditions allow the vertical propagation only if $m^2 > 0$. In this way, it is possible obtain a condition for vertically propagating modes and to more simplify we can consider the stationary waves case with $c_x = 0$. Hence, this condition is given by mean zonal flow that satisfies the following relation:

$$0 < \bar{u} < \beta\left[(k^2 + l^2) + \frac{f_0^2}{4N^2H^2}\right]^{-1} \equiv U_c \tag{1.6}$$

where U_c is the *Rossby critical velocity*. Thus, vertical propagation of stationary waves can occur only in presence of westerly winds weaker than a critical value that depends strongly on the wavelength of the waves. In the summer hemisphere the stratospheric mean zonal winds are easterlies so that stationary planetary waves are trapped vertically. In reality, the mean zonal wind is not constant, but depends on latitude and height. However, (1.6) seems to be a rather good qualitative guide for estimating vertical propagation of planetary waves (Holton, 2004).

[18] If $N^2 > 0$ the atmosphere is statically stable. In the stratosphere $N^2 \approx 5 \times 10^{-4} s^{-2}$.

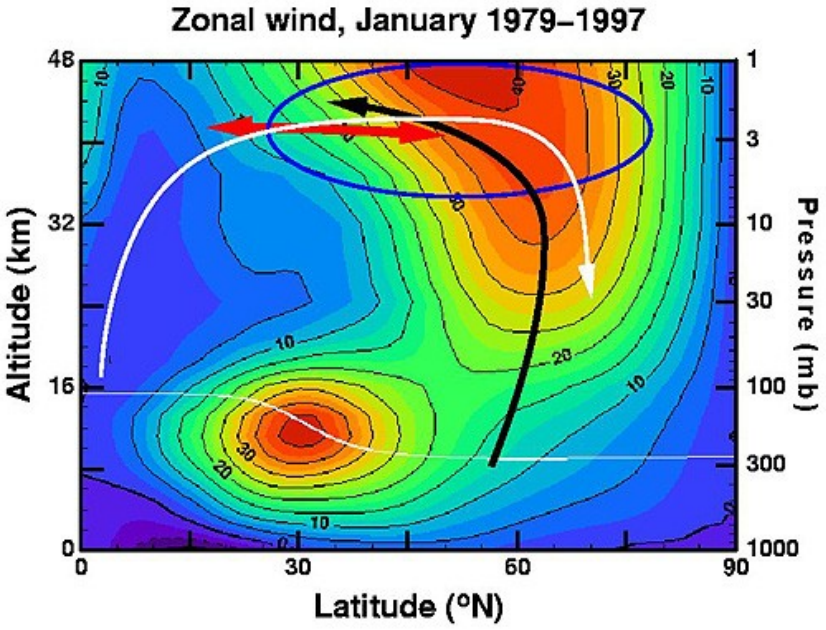

Figure 1.7: January zonal wind (1979-1997 average) for the NH showing vertical propagation of planetary waves into the stratosphere. From Cordero *et al.* (2012).

In Figure 1.7, the propagation of a planetary wave for the NH is schematically illustrated by the thick black arrow. The wave develops in the troposphere, propagates vertically into the stratosphere, through the tropopause shown by the thin white line under 16 km altitude, along the axis of the jet core, eventually bending towards the tropics.

The wave decelerates the polar night jet (in the region encircled by the blue line) by depositing easterly momentum into the fast moving westerly jet. As it will be explained in Section 1.3.6, the Brewer-Dobson circulation (shown as the white arrow) is induced by this wave deceleration and the accompanying stratospheric sudden warming (Cordero *et al.*, 2012).

Anyhow, we'll see more in detail how the planetary waves influence zonal mean flow in Section 1.4.

1.3.4 The Brewer-Dobson circulation

As it was previously observed in Section (1.33) about the planetary waves, the upward propagation of these Rossby waves is allowed only in presence of a mean

zonal wind that is westerly and less than a critical value. Hence, in the extratropical stratosphere it is possible to expect a strong annual cycle, with strong departure from radiative equilibrium, in winter and small in summer. Since the eddy forcing maintains the observed temperature above its radiative equilibrium in the extratropical stratosphere, there will be a radiative cooling and a downward residual vertical motion. By mass continuity, it is necessary that the residual vertical motion be upward in the tropics, implying that the temperature must be below radiative equilibrium in that region. Therefore, it is the dynamical driving by extratropical eddies that is responsible for the upward residual motion and net radiative heating in the tropical stratosphere, not a local forcing.

This residual circulation, being generated by planetary waves, is known as *Brewer-Dobson circulation*, from the names of the scientists that had proposed this model of atmospheric circulation, Alan Brewer in 1949 and Gordon Dobson in 1956. This model is very important because it explains why tropical air is lower in ozone than polar air, even though the photochemical source region of ozone is in the tropics. In fact, most ozone production occurs in the tropical stratosphere because here the Sun, positioned high overhead during the day all year long, is most intense and, thus, there is enough of the necessary sufficiently energetic UV light to split apart molecular oxygen, and form ozone. The problem is that most of the ozone is found outside of its natural tropical stratospheric source region. This higher latitude ozone results from the slow atmospheric circulation that moves ozone from the tropics where it is produced into the middle and polar latitudes.

The Brewer-Dobson circulation transfers mass and trace chemicals upward across the tropopause in the tropics and downward in the extratropics, and is closed in the lower stratosphere by a poleward meridional drift balanced by EP flux convergence (Holton, 2004). It's necessary to point out that descending motions in both the stratospheric middle and polar latitudes have important differences. The midlatitude descending air is transported back into the troposphere, while the polar latitude descending air is transported into the polar lower stratosphere, where it accumulates (Fig. 1.8).

The air that is slowly lifted out of the tropical troposphere into the stratosphere is very dry, with low ozone, and high CFC (chlorofluorocarbon[19]) levels. This tropical lifting circulation out of the lower stratosphere is quite slow, on the order of

[19] CFC is an organic compound that contains only carbon, chlorine, and fluorine, that contributes to ozone depletion.

20-30 meters per day. Most of the air rising into the stratosphere at the tropopause never makes it into the upper stratosphere. Between 16 and 32 km, in fact, the air density decreases by about 90%. This means that of the mass coming into the stratosphere at 16 km, approximately 90% of that mass will move towards the middle latitudes rather than be carried up to 32 km.

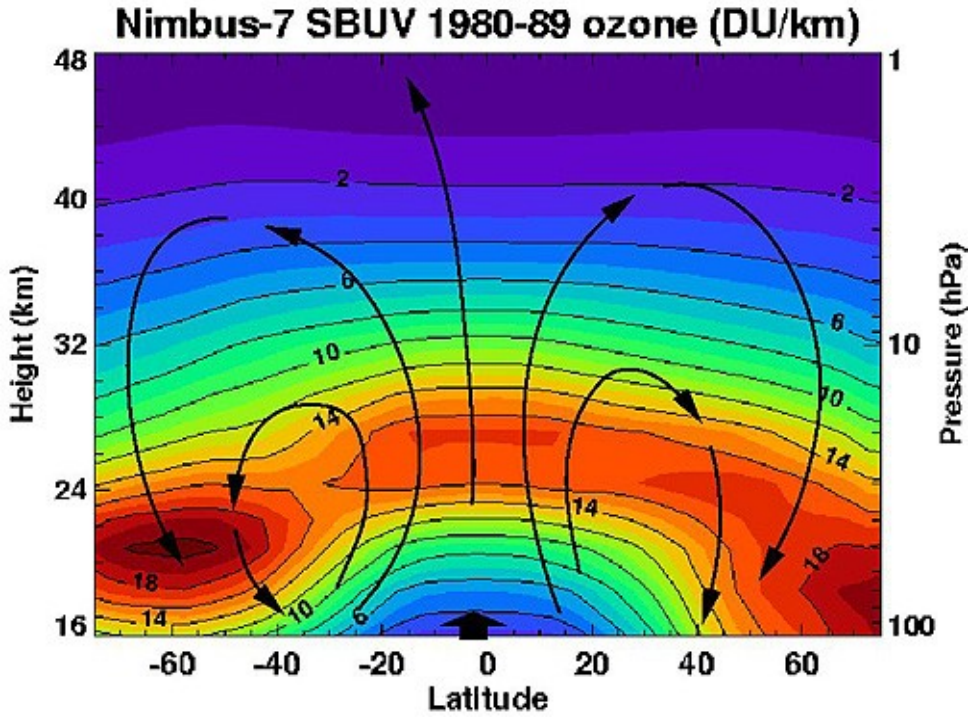

Figure 1.8: Schematic diagram of Brewer-Dobson circulation (depicted by the black arrows) with zonally circulation in the middle atmosphere superimposed on top of an annual average ozone density (in Dobson Units per kilometer). The ozone data is based on 1980-1989 Nimbus-7 SBUV data. (From Cordero *et al.*, 2012)

Even though ozone production is small and slow in the lower tropical stratosphere, the slow lifting circulation allows enough time for ozone to build-up.

Figure 1.8 shows that ozone density maximum extends up to 27 km, defining the ozone layer. Furthermore, another reason that ozone amounts increase in the lower stratosphere in the extratropical latitudes is that the lifetime of an ozone molecule gets longer here. To understand the reason of this it is necessary to consider that ozone is produced by molecular oxygen photolysis, and it is destroyed in catalytic reactions, generally utilizing free O atoms. Because most of the UV

necessary to produce O atoms is absorbed at higher altitudes, there are very few of them in the lower stratosphere and, thus, the lifetime of ozone is very long, so that it is not easily destroyed in the lower stratosphere.

Another important result of this mass circulation is that most CFCs are carried from the troposphere into the stratosphere in the tropics, and are then recycled back into the troposphere in the middle-to-high latitudes. Since the intense UV in the upper stratosphere breaks down molecules, and since very few CFCs makes it to the upper stratosphere, the lifetime of CFCs are quite long. It is estimated that the time scale needed to reduce CFC-12 by 63% is approximately 120 years (Cordero *et al.*, 2012). This lifetime results from the very slow circulation and the decrease of density, which both significantly impact the rate at which CFCs reach the upper stratosphere and are broken down by UV light.

1.3.5 The stratospheric polar vortex

The mean atmospheric circulation of the mid-high latitudes in both hemispheres is dominated by a westerly circumpolar vortex that extends from the surface to the stratosphere. This vortex is strongest during midwinter in the stratosphere, when polar temperatures are coldest, and is weakest during the summer months, when the circulation at levels above 30 hPa reverses sign and becomes weak easterly. Thus, as the thermal wind equation (1.7; see also Appendix A) shows, a jet stream, similar to the upper tropospheric jet streams, develops along the zone of sharp temperature contrasts during the 6-month long wintertime polar night, so this jet stream is commonly referred to as the *polar night jet*.

$$f_0 \frac{\partial \bar{u}}{\partial z} + RH^{-1} \frac{\partial \bar{T}}{\partial y} = 0 \qquad (1.7)$$

Since coldest temperatures are found over Antarctica during winter (on average 183K or -90°C at 50 hPa in early August), the Antarctic polar vortex is stronger than the Arctic one.

The vortex described by this jet stream exhibits considerable variability on month-to-month and year-to-year time scales.

At higher altitudes, the southern polar vortex starts to develop in the March-April period and is fully developed by May, corresponding to the beginning of a

complete darkness period in the SH. However, the polar night jet reaches its maximum wind speed in the August-September period and this results to be centered at 60°S. At lower altitudes, instead, the vortex develops more slowly, reaching its full development around the June-July period (early midwinter).

The polar night jet is highly important because it acts as a barrier to transport between the polar region and the midlatitudes. In fact, it effectively blocks any mixing between air inside and outside the vortex during the winter. Therefore, ozone-rich air in the midlatitudes cannot be transported into the polar region, allowing the ozone loss processed to proceed unimpeded with no replenishment by intrusion of ozone-rich air from midlatitudes. Furthermore, the very cold temperatures, that derive also from the polar vortex isolation, allow the PSCs formation providing the necessary solid surfaces for the heterogeneous chemical reactions that catalytically destroy ozone (Cordero *et al.*, 2012), as said in Section 1.1.

Radiative cooling during the polar night leads to a powerful westerly jet in the stratosphere. This polar vortex however, can be significantly displaced from the pole, strongly deformed in shape, or even split into two by bursts of planetary wave activity from the troposphere in just a matter of days (Matsuno, 1971), if the wave forcing is strong enough. In fact, when a standing planetary wave reaches the stratosphere, it deposits its easterly momentum, decelerating the polar night jet (*wave breaking*). Hence, the stratospheric jet slows and can even be displaced, involving also the polar vortex region displacement.

Associated with the weakening of the stratospheric westerly winds is a dramatic warming of the polar stratosphere, locally up to 80 K, as warmer middle latitude and even tropical air intrudes into the geographic polar region, so that these event is known as Stratospheric Sudden Warming (SSW; Scherhag, 1952; Labitzke, 1972).

SSW has been observed only once in the SH, in September 2002, where planetary wave forcing is weaker because of the relative lack of topography and greater proportion of ocean versus land. As a consequence, wintertime radiative cooling in the polar stratosphere quickly begins to manage to reach thermodynamic balance.

However, the mechanisms which act in the stratosphere-troposphere coupling will be described in Selection 1.4.

1.3.6 The jet streams

The horizontal temperature gradient, deriving from a different heat meridional distribution, contributes to formation of a theoretic wind, called *thermal wind* (see Appendix A). This substantially is the vertical shear of geostrophic wind, caused by the presence of that horizontal temperature gradient just mentioned[20]. Because thermal wind causes an increase in wind velocity with height, the westerly pattern increases in intensity up until the tropopause, creating a strong wind current known as the *jet stream*.

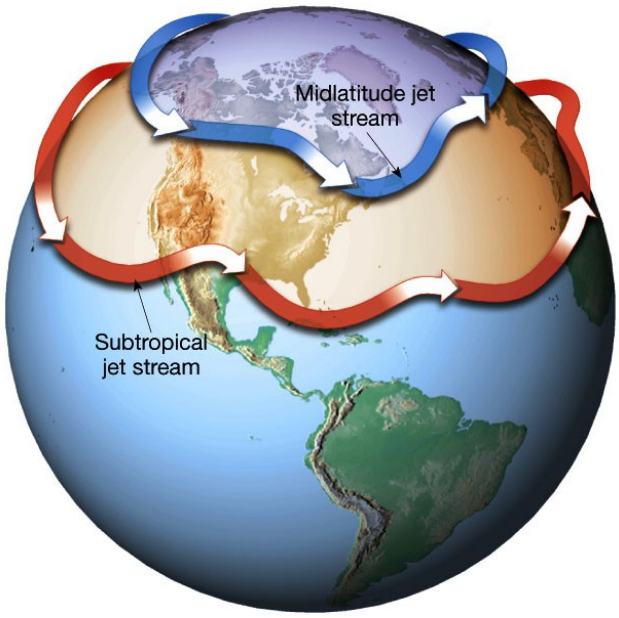

Figure 1.9: Location in map view of the jet streams. From Lutgens and Tarbuck, (2001).

Really, it is possible to classify the jet streams into two categories: the *midlatitude eddy-driven jet* and the *subtropical thermally-driven jet stream* (Fig. 1.9).

Subtropical jet streams are found close to the descending branch of the Hadley cell, so that also the angular momentum conservation in this cell provides an explanation of their increasing strength with altitude, as well as thermal wind

[20] For further information about thermal and geostrophic wind see Appendix A.

considerations. Thus, subtropical jets are typical of a *baroclinic* atmosphere[21].

The Hadley cell determines a flux of westerly momentum from the equator up to the subtropics, that contributes to the jet intensification near the descending region of the Hadley cell (Schneider, 2006).

On the other hand, eddy-driven jets, defined also as *sub-polar jets*, are connected with frontogenesis (baroclinic eddies) which occurs in the midlatitudes. The subtropical jets, instead, are more intense in the low-middle troposphere, being substantially *barotropic*[22], and are often associated to the *storm tracks*[23]. Therefore, the reasons of the formation of such jets have to be researched in land-sea contrasts and in momentum convergence by eddies.

The eddy-driven jet develops in regions of strong temperature gradient, allowing the formation of baroclinic transient eddies, that, as they propagate both equatorward and poleward, grow involving the westward meridional convergence of momentum. This leads to the acceleration of the westerly mean flow and to the jet formation (Hoskins *et al.*, 1983).

Due to the setup of the continents in the NH, largest temperature contrasts are observed on the east coast of North America and Eurasia. Continental landmasses are characterized by strong surface drag, especially over orographic reliefs and that leads to the weakening of the winds over the western side of the landmasses and favors the formation of baroclinic zones over the eastern side (Brayshaw *et al.*, 2009). A less friction is encountered when the stronger winds move over the ocean, where the baroclinicity is powered.

A similar argument can be applied to the SH, where the lack of continents lead to a more constant jet with longitude (i.e. a more zonally symmetric jet).

In Figure 1.10, it is possible to identify two jets in the NH, the first one around 40°N over the Western Atlantic, the second from Eurasia up to the Central Pacific a few degrees southward respect the first.

While the Atlantic jet is substantially an eddy-driven jet, its Pacific counterpart is a mixture of the thermally-driven component and the eddy-driven component over the Western Pacific (Li and Wettstein, 2012).

Furthermore the winter jet streams are stronger because of the increased

[21] Baroclinic atmosphere is an atmosphere where the density of the air column depends on both temperature and pressure. See also Appendix A.

[22] Barotropic atmosphere is an atmosphere where the density of the air column depends only on pressure. See also Appendix A.

[23] Storm tracks are the area where the most of the extratropical cyclones travel.

meridional thermal gradient and increased land-sea contrasts (Peixoto and Oort, 1992).

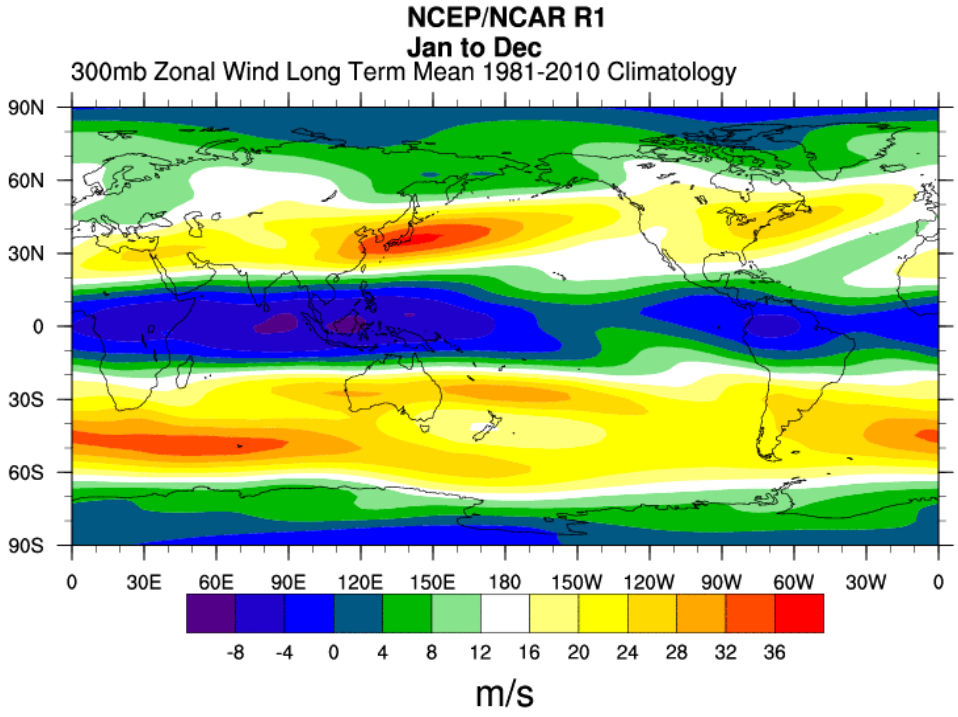

Figure 1.10: Long term mean (climatology) taken from NCEP/NCAR Reanalyses time series between 1981 and 2010 of 300-hPa zonal winds. Derived from the website http://www.esrl.noaa.gov/

As regards the SH, the topography uniformity implies an absence of drag that lets the jet blow more fast, and it is possible to see, again in Figure 1.10, the summer jet tending to split into two different jet streams, that instead conversely in the austral winter (Held, 2000).

In the stratosphere, instead, there is another kind of jet stream, the so-called polar night jet (mentioned also previously), which surrounds the circumpolar region representing the meridional boundary of the stratospheric polar vortex. This jet is a strong westerly wind blowing in the wintertime stratosphere around 60 degrees in latitude and we'll see it more in detail after a brief introduction of the planetary waves that is necessary to really understand the processes of interaction between the

midlatitude tropospheric jet and stratospheric mean flow through the eddies disturbances.

1.3.7 Hadley cell

In the mean the net solar energy absorbed by the atmosphere and the Earth must equal the infrared energy radiated back to space by the planet. The annually averaged solar heating is strongly dependent on latitude, with a maximum at the equator and minima at the poles. The outgoing infrared radiation, instead, is only weakly dependent on latitude, therefore there is a net radiative surplus in the tropical region and a deficit in the polar regions. This heating difference creates a pole-to-equator temperature meridional gradient.

Since a growing store of zonal mean available potential energy is produced, the westerly thermal wind becomes baroclinically unstable, generating baroclinic waves to transport heat poleward, reducing the resulting temperature meridional gradient. These waves will intensify until their heat transport is sufficient to balance the radiation deficit in the polar regions. At the same time these perturbations convert potential energy into kinetic energy, maintaining the circulation against frictional dissipation (Holton, 2004).

Between 30°N and 30°S latitude, this energy transport is accomplished by a relatively simple meridional overturning circulation, with rising tropospheric motion near the equator, poleward motion near the tropopause, sinking motion in the subtropics, and an equatorward return flow near the surface. The tropical overturning cell is called the *Hadley cell*. This cell carries heat and moisture from the tropics to the northern and southern midlatitudes, being trapped into tropical latitudes. Furthermore, this circulation is affected by the Coriolis force that deflects the poleward moving air at the upper levels to the east, creating the subtropical jet streams, and the equatorward moving air near the surface to the west (trade winds).

1.4 Stratosphere-troposphere interaction

In the past, firstly, interactions between the stratosphere and troposphere were believed primarily one way, so that the stratosphere passively responding to forcing from the more massive troposphere below. After the 1980s, with advances in

observational analysis and modeling capability, it became possible establish two-way interactions between the stratosphere and world below, setting the stage for recent studies on the role of the stratosphere in the Earth system (Gerber *et al.*, 2012).

Nowadays it is widely accepted that the troposphere has a strong dynamical effect on the stratosphere, primarily through the upward propagation of waves, both low-frequency large-scale Rossby waves (planetary waves, seen also previously in Section 1.3.3) and high-frequency inertia-gravity waves. Understanding of this effect is based on simple theories of wave propagation (including the Charney-Drazin[24] criterion for vertical Rossby wave propagation), experiments in many different types of numerical models, plus observational indicators such as differences in stratospheric circulation between summer and winter, and between the hemispheres.

An important aspect of this effect is that in the stratosphere there is a wave mean-flow interaction, i.e. a two-way process in which the mean-flow can strongly modify the propagation of the eddies, while the disturbances can bring about significant mean-flow changes through nonlinear effects (Andrews *et al.*, 1987).

Breaking or dissipating waves exert a systematic mean force that changes the mean flow. The mean flow, on the other hand, affects the propagation, breaking and dissipation of waves.

The stronger polar vortex changes the background conditions for planetary wave propagation: the amplitude and location of planetary wave breaking change in stratosphere. This variation drives changes in atmospheric vertical motion that extend to the surface of the Earth (via the downward control mechanism that will be explained below) and adjust the horizontal gradients in temperature through adiabatic expansion and compression.

As numerical experiments suggest, changes in the lower stratospheric flow influence the fluxes of momentum by synoptic waves in the upper troposphere. The phase speed and direction of propagation determine where the waves will break and decelerate tropospheric westerly flow. If the jet changes its position, the poleward displacement may preferentially occur when the climatological jet is located in the lower latitudes. In fact, it was observed that models with an equatorward bias in the climatology of the SH jet stream appear more sensitive to stratospheric

[24] Charney and Drazin in 1961 showed that in the absence of friction and heating, small amplitude (linear), stationary Rossby waves in a vertical shear flow is not able to alter the mean flow. This is called Charney-Drazin's non-acceleration theory or non-interaction theory.

perturbations and the climatological jet tends to move much more poleward than a high-latitude jet (Son *et al.*, 2010).

The dynamical effect of the stratosphere on the troposphere is now a major research activity (Gillett *et al.,* 2003; Hartmann 2004). Whereas for some time there has been significant evidence from numerical model studies (e.g. Boville, 1984; Kodera *et al.,* 1990), that imposed perturbations to the stratosphere lead to changes in the tropospheric circulation and that the mechanism for communication of these changes is dynamical, much of the recent interest in this topic has come from studies of the NH and SH Annular Modes (See Section 1.5). Methods such as EOF (Empirical Orthogonal Function) analysis have identified these as dominant signals in variability in both troposphere (e.g. Thompson and Wallace 2000) and stratosphere (e.g. Baldwin and Dunkerton 1999), where the annular modes are associated with variation in the strength and position of the jet (the midlatitude jet in the troposphere, the polar night jet in the stratosphere). However, in the troposphere the annular mode variability is believed to derive from two-way interaction between baroclinic eddies and the tropospheric midlatitude jet (e.g. Robinson, 1991; Feldstein and Lee, 1998; Hartmann and Lo, 1998), whereas in the stratosphere this variability is a manifestation of the variation in the strength of the polar-night jet, driven by the wave force, but what is more interesting is that there seem to be strong correlations between the annular mode variability in the troposphere and that in the stratosphere. In fact, in SH winter there is significant correlation between the annular mode index defined on the basis of the surface pressure field and the stratospheric circulation, so that when there is a strong pole-to-equator pressure gradient at the surface, indicating strong westerly surface flow, there are also strong westerly winds throughout the midlatitude troposphere and in the mid-to-high latitude stratosphere (Thompson and Wallace, 2000). Although these correlations strongly suggest dynamical connections between troposphere and stratosphere, it is not easy to establish from the correlations alone whether the stratosphere affects the troposphere, or vice versa.

There are several possible dynamical mechanisms by which the stratosphere might affect the troposphere, summarized schematically in the diagram in Figure 1.11. The issues discussed in this scheme can be organized in the following points:

1) *Planetary wave propagation*: a first distinct mechanism for communication in the vertical is via Rossby wave propagation. Using a linear model, the vertical propagation of planetary waves from the troposphere to the stratosphere results

to be sensitive to the vertical wind shear across the extratropical tropopause (Chen and Robinson, 1992). This shear is found to vary with the annular modes (Limpasuvan and Hartmann 1999). The propagation of Rossby waves out of the troposphere might be sensitive to by variation in the 'refractive' properties of the lower stratospheric flow (Hartmann *et al.*, 2000, see also Limpasuvan and Hartman 2000), or indeed there might be downward reflection of Rossby waves from higher in the stratosphere (e.g. Perlwitz and Harnik 2003, 2004).

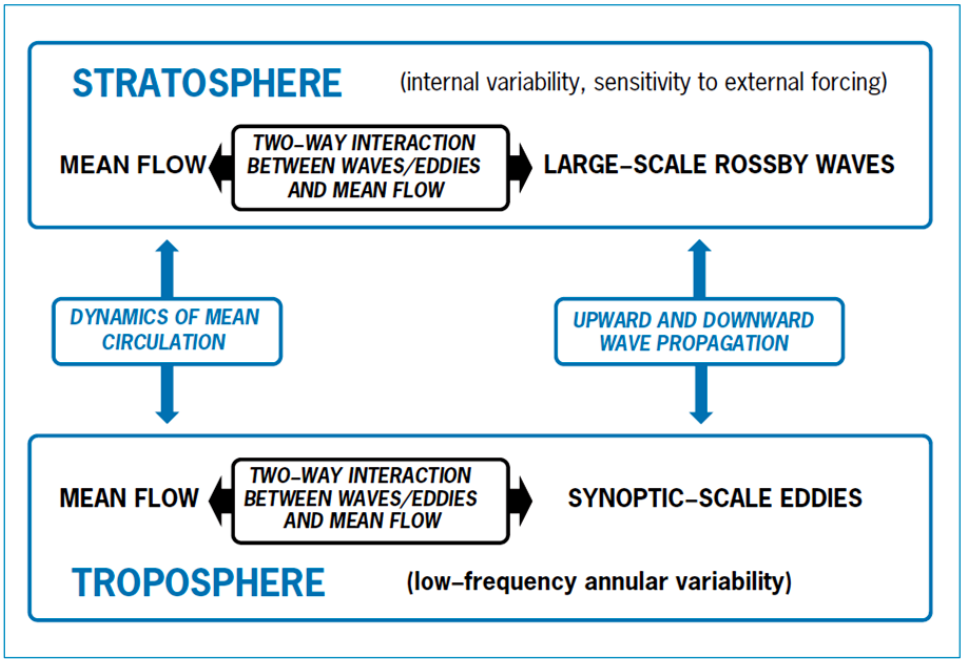

Figure 1.11: Schematic diagram indicating the role of different aspects of the dynamics in the dynamical mechanisms discussed in the text. Note that 'dynamics of mean circulation' includes non-local PV inversion (or equivalently the short-time effect of the meridional circulation) and the effect of the meridional circulation on longer time scales, including the 'downward control' limit. From SPARC newsletter n°25.

2) *Wave–zonal flow interaction*: A second mechanism for downward propagation of wind anomalies in the stratosphere might be through a two-way interaction between planetary waves and zonal mean flow (Holton and Mass 1976; Christiansen 1999), which could continue into the troposphere and reach the surface. Recent investigation (Steven Hardiman, personal communication) has

shown no evidence of any distinct downward propagation of the effect of imposed upper level stratospheric perturbations through a such a mechanism when stratospheric Rossby wave amplitudes are weak. When stratospheric wave amplitudes are large, however, the dynamics of waves and mean flow is highly nonlinear and imposed upper level perturbations can have significant effects at lower levels. Furthermore, the two-way interaction between baroclinic waves and mean flow in the troposphere, that gives rise to annular mode variability, may also serve as an amplifier for external forcing (including dynamical forcing from the stratosphere) (e.g. Hartmann *et al.* 2000). This may allow the tropospheric response to be significantly larger than might be expected from zonal mean dynamics, for example.

3) Remote responses to the rearrangement of *stratospheric potential vorticity*: a third mechanism arises from the rapid propagation of inertio-gravity waves, required to maintain a state of geostrophic and hydrostatic balance (see Appendix A), that through an inversion operator allows to determine quantities such as velocity or temperature from the potential vorticity (PV) distribution. Baldwin and Dunkerton (1999) suggested that the redistribution of mass in the stratosphere, in response to changes in wave driving, may be sufficient to influence the surface pressure significantly, consistent with the theoretical results of Haynes and Shepherd (1989). From calculated changes in the tropospheric flow induced by stratospheric redistributions of potential vorticity, changes in the zonal flow in the lower stratosphere, through the instantaneous induced meridional circulation, can give rise to an acceleration in the troposphere below with significant changes in the tropopause height and tropospheric winds. (Hartley *et al.*, 1998; Black; 2002).

4) *Downward control*: on sufficiently long timescales, the wave transport of potential vorticity equilibrates with its creation and destruction by radiative damping (Song and Robinson, 2004). In this equilibrium, the influence of altered stratospheric wave driving is transmitted to the surface through secondary circulations that extend downward from the region of anomalous wave driving, and close in the planetary boundary layer, allowing use of the term "downward control" (Song and Robinson, 2004). An important refinement is that in this conditions, the meridional circulation tends to be narrower and deeper in the troposphere below (Haynes *et al.* 1991, Holton *et*

al. 1995) potentially allowing an enhanced tropospheric response to a stratospheric wave force.

The conclusion is therefore that the Rossby waves play a significant role in downward communication of information. Other strong evidence that the stratosphere plays an active, rather than a passive, role in tropospheric variations associated with the annular modes comes from observed and modeled changes on the timescale of the annular mode variations. This timescale results to be significantly longer at times of the year (NH winter, SH spring) when there is strong Rossby wave propagation into the stratosphere (Baldwin *et al.*, 2003). Correspondingly, artificial suppression of stratospheric variability in model simulations reduces the time scale of the tropospheric annular mode (Norton, 2003).

The dynamical mechanism here is likely to be that, when there is significant flux of Rossby waves into the stratosphere, the flow in the stratosphere acts as an integrator, and hence low-pass-filter, of the variability in this flux, since stratospheric damping times are relatively long. Any stratospheric effect on the troposphere will therefore tend to increase the time scales of the variability. When there is little flux of Rossby waves into the stratosphere (in NH summer, or in SH midwinter) the effect is absent.

Therefore, the possibility of significant stratospheric effects on the troposphere has implications or many aspects of month-to-month and year-to-year variability and systematic change in the tropospheric circulation, suggesting possible mechanisms for explaining apparent signals in the tropospheric circulation of the solar cycle or inputs of volcanic aerosol to the stratosphere. It also strengthens the link between possible climate change in the troposphere and changes in the stratosphere, due to ozone depletion or increasing greenhouse gases. The dynamical mechanisms required to explain these effects are still being investigated.

1.5 The Southern Annular Mode

The SH high-latitude climate variability is dominated by the Southern Annular Mode (SAM), also known as the Antarctic Oscillation (AO), a large-scale pattern of variability characterized by north-south fluctuations of the westerly wind belt that circles Antarctica. It is essentially a zonally symmetric structure, but with a zonal

wave three pattern superimposed. It is associated with synchronous pressure or height anomalies of opposite sign in mid- and high-latitudes, and therefore reflects changes in the main belt of subpolar westerly winds. It can also be considered as the normalized difference in the zonal mean sea-level pressure between 40°S and 64°S.

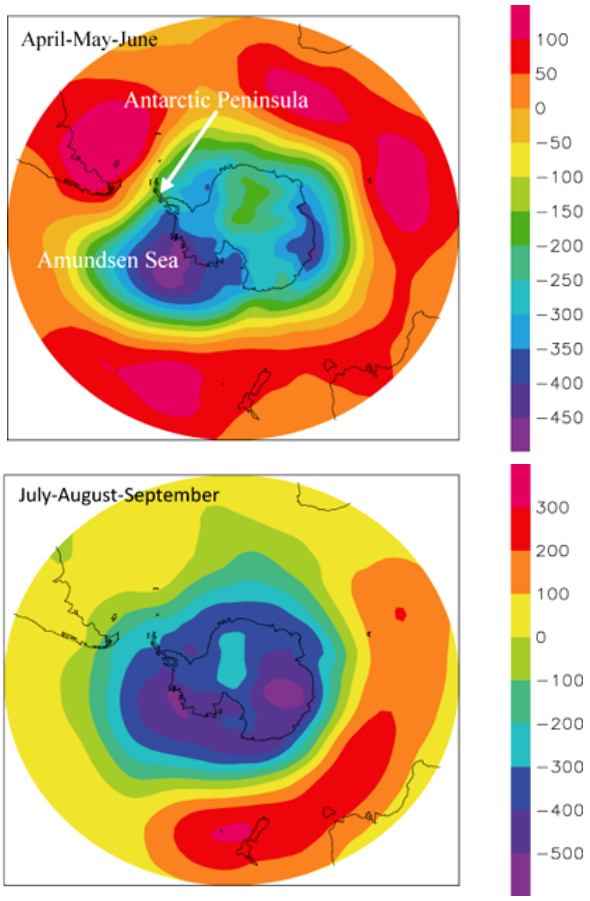

Figure 1.12: Regression between the atmospheric surface pressure and the SAM index for the period 1980-1999 in Pa for (top) the averages in April, May, and June and (bottom) July, August, and September. Data from NCEP-NCAR reanalyses (Kalnay *et al.* 1996). Figures from Goosse *et al.* (2010).

The sea level pressure pattern associated with SAM is a nearly annular pattern with a large low pressure anomaly centered on the South Pole and a ring of high pressure anomalies at mid-high-latitudes (Fig. 1.12).

The SAM contributes a significant proportion of SH midlatitude circulation variability on many time scales (Hartmann and Lo, 1998; Kidson, 1999; Thompson

and Wallace, 2000; Baldwin, 2001). As with the Northern Annular Mode (NAM), the structure and variability of the SAM results mainly from the internal dynamics of the atmosphere and itself is an expression of storm track and jet stream variability (e.g., Hartmann and Lo, 1998; Limpasuvan and Hartmann, 2000).

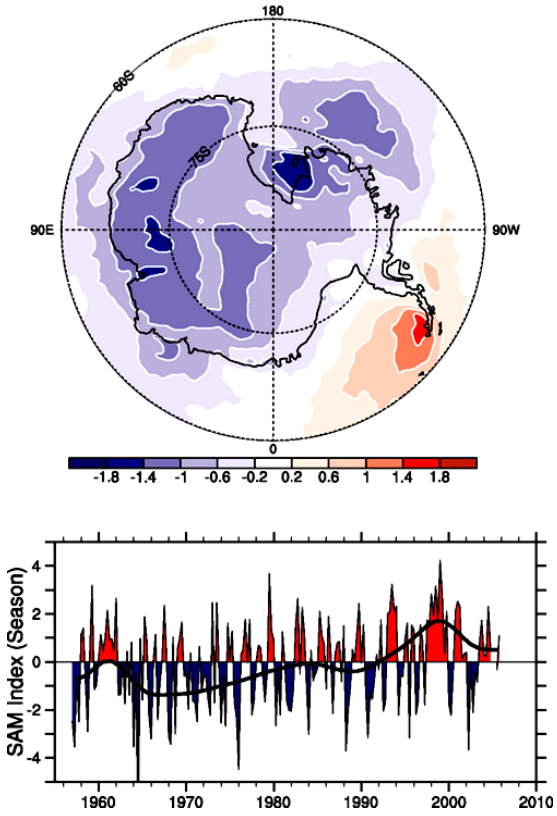

Figure 1.13: (Bottom) Seasonal values of the SAM index calculated from station data (updated from Marshall, 2003). The smooth black curve shows decadal variations. (Top) The regression of changes in surface temperature (°C) over the 23-year period (1982 to 2004) corresponding to a unit change in the SAM index, plotted south of 60°S. Values exceeding about 0.4°C in magnitude are significant at the 1% significance level (adapted from Kwok and Comiso, 2002). Figures from http://www.ipcc.ch.

Poleward eddy momentum fluxes interact with the zonal mean flow to sustain latitudinal displacements of the midlatitude westerlies (Limpasuvan and Hartmann, 2000; Rashid and Simmonds, 2004, 2005). The changing position of the westerly wind belt influences the strength and position of cold fronts and midlatitude storm systems, and is an important driver of rainfall variability in southern Australia.

Marshall (2003) produced a SAM index (Fig.1.12) based on appropriately located station observations, which reveals a general increase in the SAM index beginning in the 1960s consistent with a strengthening of the circum-polar vortex and intensification of the circumpolar westerlies, as observed in northern Antarctic Peninsula radiosonde data (Marshall, 2002). In a positive phase SAM event, the belt of strong westerly winds contracts towards Antarctica. This results in weaker than normal westerly winds and higher pressures with anomalously dry conditions over southern Australia, South America, New Zealand and Tasmania, restricting the penetration of cold fronts inland.

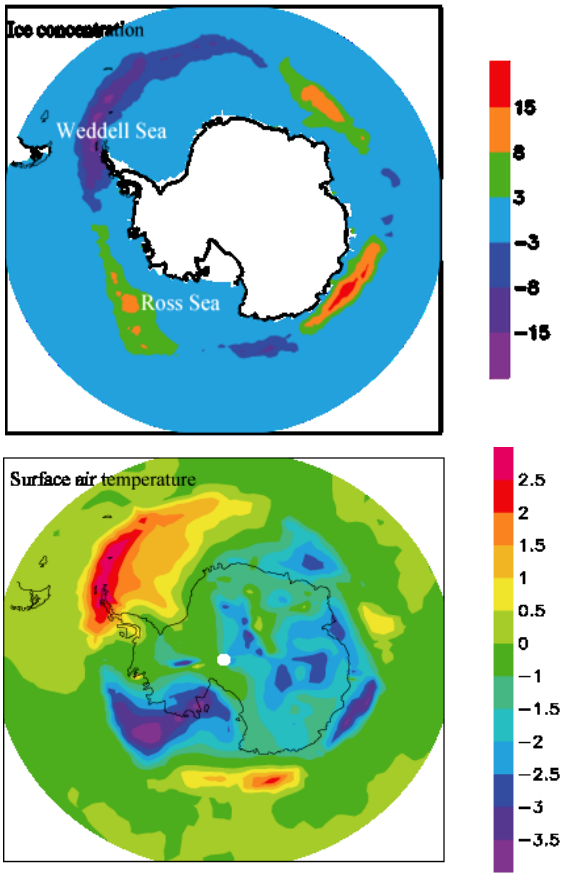

Figure 1.14: Regression between (top) the sea ice concentration in % (data from Rayner *et al.* 2003) and (bottom) the surface air temperature in °C (Kalnay *et al.* 1996) and the SAM index for the averaged over July, August, and September for the period 1980-1999. From Goosse *et al.* (2010).

The stronger westerlies above the Southern Ocean also increase the insulation of Antarctica. As a result, there is less heat exchange between the tropics and the poles, leading to a cooling of the Antarctica and the surrounding seas.

The majority of the effects of SAM could be explained by its annular form and the related changes in zonal winds (Goosse *et al.*, 2010). The departures from this annular pattern have large consequences for sea ice as they are associated with meridional exchanges and thus large heat transport. Hence, the Antarctic Peninsula also warms due to a meridional wind component bringing maritime air onto the Peninsula (Fig. 1.14). In particular, a low pressure anomaly is generally found in the Amundsen Sea during high SAM-index years (Fig. 1.12). This induces southerly wind anomalies in the Ross Sea (Pacific sector of the Southern Ocean) and thus lower temperatures and a larger sea ice extent there (Fig. 1.14). On the other hand, because of the stronger northerly winds, the area around the Antarctic Peninsula is warmer when SAM index is high (Fig.1.13), and sea ice concentration is lower there. Conversely, a negative SAM event reflects an expansion of the belt of strong westerly winds towards the equator. This shift in the westerly winds results in more (or stronger) storms and low pressure systems over southern Australia.

The imprint of SAM variability on the Southern Ocean system is observed as a coherent sea level response around Antarctica (Aoki, 2002; Hughes *et al.*, 2003) and by its regulation of ACC flow through the Drake Passage (Meredith *et al.*, 2004). Changes in oceanic circulation directly alter the Thermohaline Circulation (Oke and England, 2004) and may explain recent patterns of observed temperature change at SH high latitudes described by Gille (2002).

Over the ocean, the stronger westerly winds tend to generate stronger eastward currents, and the divergence of the oceanic surface currents around 60°S is enhanced because of a larger wind-induced Ekman transport[25], resulting in a stronger oceanic upwelling. Indeed, in coastal upwelling regime, wind blows parallel to the coast and surface water has a net movement of 90° to the left respect to it. Because the net surface water flows away from the coast, the water must be replaced with

[25] Ekman theory explains the theoretical state of circulation in the surface layer if currents were driven only by the transfer of momentum from the wind (Colling, 2001; Sverdrup *et al.*, 2005). Surface currents flow at a 45° angle to the wind due to a balance between the Coriolis force and the turbulent drags forces, weakening in magnitude from a maximum at the surface until they dissipate, and also shifting in direction slightly across each subsequent layer (right in the NH and left in the SH), describing the Ekman spiral (Knauss, 2005). Integrating all flow over the Ekman layer, extending from the surface to the point of dissipation of this spiral, the net transportation is at 90° to the right (left) of the surface wind in the northern (southern) hemisphere (Colling, 2001).

water from below (Mann and Lazier, 2006).

Studies has suggested that recent trends in the SH tropospheric circulation can be interpreted as a bias toward the high-index polarity of this pattern, with stronger westerly flow encircling the polar cap (Thompson and Solomon, 2002).

Thus, the observed SAM trend has been related to stratospheric ozone depletion (Sexton, 2001; Thompson and Solomon, 2002; Gillett and Thompson, 2003) and to greenhouse gas increases (Hartmann *et al.*, 2000; Marshall *et al.*, 2004). There is also recent evidence that ENSO variability can influence the SAM in the southern summer (e.g., L'Heureux and Thompson, 2006).

1.6 Air-to-sea carbon fluxes

During the past few decades, the increasing greenhouse gas concentration in the atmosphere is mainly caused by human activities such as fossil fuel burning and Land Use Change (LUC) (Forster *et al.*, 2007). The most important anthropogenic greenhouse gas is carbon dioxide (CO_2), whose atmospheric concentration has been increased from about 280 ppmv (parts per million by volume) in preindustrial times to the present level of about 365 ppmv (Jacob, 1999). However, only about 45% of the total CO_2 emitted from fossil fuels burning and LUC stayed in the atmosphere in the last decades (Le Quéré, 2010). The remaining carbon dioxide was taken up by the carbon reservoirs in the ocean and on the land. The fraction of total CO_2 emissions that remain in the atmosphere is strongly influenced by the impact of climate variability on the CO_2 sinks. Many factors can also play an important role in controlling the airborne fraction such as first the rate of increase in CO_2 emissions, and, second, the level of CO_2 in the atmosphere influencing the uptake by the sinks. The first factor is linked to the fact that sinks are limited by processes that have specific time-scales (e.g. vegetation growth on land and oceanic transport of carbon), whereas the second one is due to the fact that CO_2 fertilisation on land should saturate at high CO_2 and its dissolution in the ocean reduces the chemical capacity of the ocean to take up additional CO_2 (Le Quéré, 2010).

The global oceans absorb a large portion of the atmospheric CO2 as the net oceanic uptake corresponds to approximately one third of the anthropogenic emissions (Sabine *et al.*, 2004). The positive aspect of the oceans carbon uptake is evident. An oceanic uptake of CO2 decreases the atmospheric concentration, and

thereby diminishes the climate effect due to CO2 emissions. The negative aspect is acidification of the oceans due to increased CO2 uptake (Doney *et al.*, 2009; Omstedt *et al.*, 2010). A decreasing pH and a reduction in carbonate ion concentration, which follow an increased CO2 concentration, have a negative impact of the oceans biota, especially the calcification in corals, carolline macroalge and planktonic organisms (Doney *et al.*, 2009; Fabry *et al.*, 2008; Hoegh-Guldberg *et al.*, 2007). High latitude regions are particularly affected by acidification since cold water is more sensitive to changes in partial pressure of CO_2, that mainly controls the CO_2 flux between air and sea surface, and naturally has a low concentration of carbonate ions.

However, the air-to-sea carbon fluxes should take into account that the whole ocean doesn't achieve equilibrium with the atmosphere because of the slow mixing of the ocean, driven by the buoyancy determined by temperature and salinity. Sinking of water from the surface to the deep ocean (*deep water formation*) takes place in polar region where the surface water is cold and salty, hence heavy. Some vertical mixing still occurs near the surface also in other regions, due to wind stress, resulting in an oceanic mixed layer extending to about 100 m depth and exchanging slowly with the deeper ocean. Thus, considering residence time of water in the different oceanic layers, equilibration of the whole ocean in response to a change in atmospheric CO_2 should takes place on a time scale of the order of 200 years (Jacob, 1999). Since the residence time of water in the oceanic mixed layer is only 18 years, the actual fossil fuels CO_2 uptake is strongly determined by the rate of deep water formation. An additional mechanism for CO_2 uptake involves photosynthesis by phytoplankton producing organic carbon, but the biological productivity of the surface ocean is limited in part by upwelling of nutrients from the deep, so that the efficiency of the biological pump is again highly dependent on the vertical oceanic circulation (Jacob, 1999).

Recent model and observational studies indicate the possibility that changes in wind pattern can cause trends in the circulation and biogeochemistry of the Southern Ocean, impacting the air-sea carbon fluxes in the region. Stronger winds over the Southern Ocean are part of the surface signature of the SAM (explained in Section 1.5), that is featured in its positive phase by a poleward shift of the westerlies.

The shift in the austral jet stream has had substantial implications on the hydrological cycle of the SH (Kang *et al.*, 2011). Studies have suggested that an

increasing ventilation of carbon rich deep water driven by the poleward shift of the austral jet stream has both weakened the Southern Ocean carbon sink (Lovenduski *et al.*, 2008), and accelerated ocean acidification (Lenton *et al.*, 2009). In fact, ocean acidification contributes though a positive feedback mechanism to reduce ocean capability to uptake CO_2, increasing atmospheric levels of carbon dioxide. Thus the Southern Ocean, being the primary sink of atmospheric CO_2 in the oceanic carbon cycle, storing up to about 40% of the global oceanic carbon dioxide storage (Sabine *et al.*, 2004), plays an important role on climate change.

Chapter 2

The numerical models and data

This chapter provides a description of the numerical models and the reanalyses data that have been used in the thesis. Specifically, after a first introduction to global Climate Models, I will focus on the definition of High Top (HT) and Low Top (LT) model versions.

2.1 Models general features

The necessity of understanding the Earth system response to external forcings and to investigate climate variability has led to the development of climate numerical models that allow to study both the present climate dynamics and the future projections.

The numerical models that have been used in this work include state of the art parameterizations of all major physical process, i.e. orographic gravity waves drag, shallow and deep convection, large scale precipitation, radiative heat transfer, vertical and horizontal diffusion processes and boundary layer physics.

The dynamical core of the model atmospheric component consists of the primitive equations of the atmosphere. Primitive equations are a set of differential equations that determine the motions of a stratified fluid in a rotating system of spherical geometry, under the approximation that the horizontal scale of motion is smaller than the vertical one, and that each column of air is in hydrostatic equilibrium. Both of these conditions are well satisfied at the relatively coarse horizontal resolutions adopted for climate studies (Holton, 2004).

Moist primitive equations are the mathematical transcription of the following fundamental physical conservation laws:

- The zonal and meridional momentum balance equations
- Vertical momentum balance equation, which, under the cited approximation, becomes the hydrostatic equation
- Heat balance equation
- Conservation of mass
- Conservation of water species: vapour, liquid and ice phase

The equation of state of ideal gases closes the problem by creating a system of nine equations in nine variables: the vorticity (ξ) and the divergence ($\mathcal{D}$) of the horizontal wind field, the temperature T, the logarithm of surface pressure p_s. The concentrations of vapour (q_v), liquid (q_l) and ice (q_i) water, the vertical velocity (ω) and the air density (ρ). The last two variables do not appear as time derived quantities of corresponding prognostic equations. Therefore the thermodynamical state of the atmosphere is defined by the following state vector (X):

$$X = (\xi, \mathcal{D}, T, \log(p_s), q_v, q_l, q_i), \tag{2.1}$$

while ω and ρ are diagnostically computed at every timestep from the state vector itself.

The *physics of the model* includes all those processes participating to atmospheric dynamics which are not explicitly resolved by the primitive equations. They can be separated in two categories:

1. Physical processes that don't pertain fluid dynamics, i.e. radiative heat transfer.
2. Physical processes that pertain fluid dynamics but that can't be resolved by the primitive equations. For example, they can be filtered by the hydrostatic approximation or they can feature spatial or temporal scales which are smaller than those resolved at the model resolution, i.e. clouds, convection, boundary layer turbulence, surface fluxes.

The physics of the model determines the sources and sinks of heat, momentum and moisture, which are the fundamental drivers of the atmospheric circulation. Such processes, which are essential for a realistic climate simulation, are therefore parameterized in function of the resolved state of the atmosphere via best estimate approximate formulas derived by semi-empirical theories and expert judgment.

Thus, the model can be considered composed of two parts: the dynamical core, which by integrating the primitive equations control the time evolution of the atmosphere due to resolved fluid dynamical processes, and a set of parameterized physical processes which provide a forcing on the resolved state of the atmosphere.

The model equations are numerically time forward integrated by discretizing the atmosphere in both the vertical direction and in the horizontal plane. In the used climate models case the atmosphere is divided into layers corresponding to selected values of the vertical coordinates and different numerical techniques allow to solve the set of ordinary differential equations obtained from a series of approximations of the partial differential equation composing the primitive equations.

However, it is necessary to take account of the fact that, despite their progressive development, climate models still present relevant systematic errors that refer to differences between the simulated and the observed climate statistics (Randall *et al.*, 2007). Any systematic errors of models can be identified with different approaches, such as using metrics to evaluate the morphology of climate, defined by the spatial distribution of the statistics of basic climate parameters (Boer, 2000), or simplifying climate models to analyze of how specific processes are effectively simulated in the models (Lin *et al.*, 2006; Lin, 2007; Catto *et al.*, 2010).

2.2 CMIP5 and climate experiments

The Coupled Model Intercomparison Project (CMIP) is a standard experimental protocol to evaluate the outputs of coupled General Circulation Models. It was established in 1995 by the WCRP and provides a wide community infrastructure for sharing and comparing data from Global Climate Models (GCMs) of different climate and meteorological institutes.

Phase 3 of the CMIP project (CMIP3), started in 2004, has been part of the Assessment Report 4 (AR4) by Intergovernmental Panel on Climate Change (IPCC), including simulations for both past and present climate forcing. In September 2008, involving more than 20 different climate modeling groups from all over the world, WCRP launched Phase 5 of the CMIP project, called CMIP5[1] (Taylor *et al.*, 2009), that will be part of the next AR5 (Fifth Assessment Report).

[1] The CMIP5's official website is http://cmip-pcmdi.11n1.gov/cmip5/ .

CMIP5 promotes a standard set of model simulations with different purposes, such as evaluating how realistic the models are in simulating the recent past, providing projections of future climate change on different time scales, and understand some of the factors responsible for differences in model projections.

The CMIP5 protocol includes different typologies of experiments, with standard outputs and predefined forcing, based on two main goals: on the one side, long-term simulations (century time scale), on the other near-term simulations (10-30 years), often defined as decadal predictions. The first kind simulations are initialized from the end of freely evolving simulations of historical period, which will be carried out with Atmosphere-Ocean Global Climate Models (AOGCMs), which in some cases may be coupled to a carbon cycle model. Some of the second type simulations, instead, are initialized with observed ocean state and sea ice.

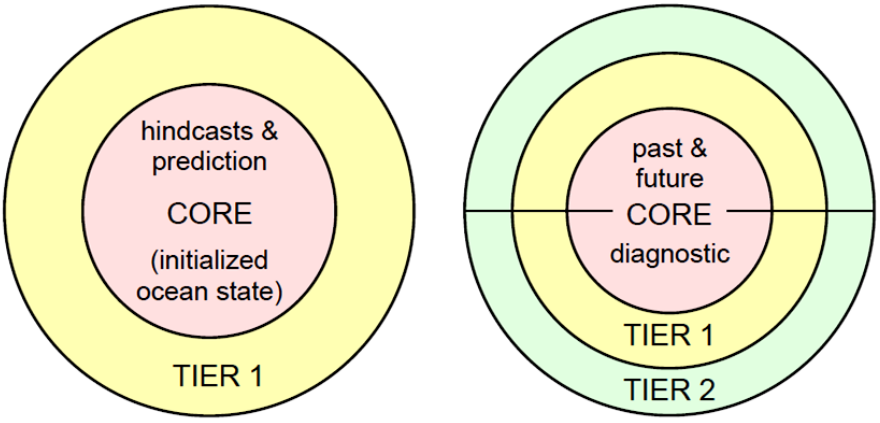

Figure 2.1: Schematic of the two focus areas of CMIP5, with each one divided into prioritized tiers of experiments. The colors used in this figure are also used to indicate the relative priorities of the experiments summarized in the tables that appear later in this document. From Taylor *et al.* (2009).

Since the predefined set of experiments is wide and not all the modeling groups have the possibility to perform them all, a scale of priorities has been defined, defining so-called "time-slice" experiments of both present-day and the future.

Due to the large numbers of simulations included in the CMIP5 framework, historical simulations and long-term simulations lay in the "core" of the experiments demanded to the modeling groups, with then one or two "tiers" (Fig.2.1). Historical simulations can be briefly divided into fully coupled experiments (defined as

historical) and into atmosphere-only experiments (AMIP[2]).

To allow for a systematic model intercomparison and to produce a credible multi-model dataset for analysis, the core experiments have been completed by all groups and these are the simulations that will be used in this work.

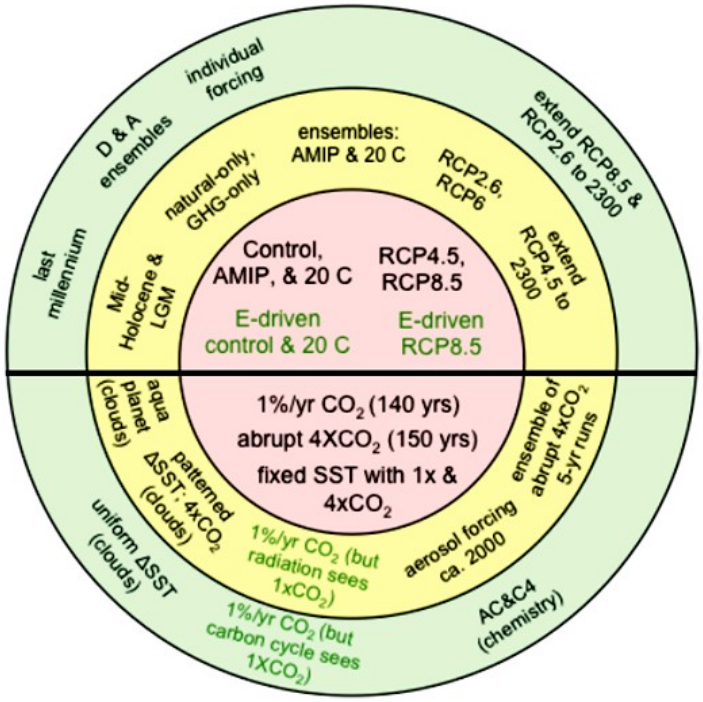

Figure 2.2: Schematic summary of CMIP5 long-term experiments. Green font indicates simulations that will be performed only by models with carbon cycle representation. From Taylor *et al.* (2009).

Turning to the CMIP5 long-term experiments, Fig. 2.2 shows the set of core experiments that include AMIP runs, a coupled control run and at least one 20th century experiment with all forcings, referred also above as an historical run. There are two projection simulations forced with specified concentrations consistent with a high emissions scenario (RCP8.5) and a medium mitigation scenario (RCP4.5). For AOGCMs that have been coupled to a carbon cycle model (subsequently referred to as earth system models or ESMs), there are control, 20th century simulations, and a future simulation with the high scenario (RCP8.5) driven by

[2] The Atmospheric Model Intercomparison Project (AMIP) is a standard for atmospheric model evaluation based on monthly mean observed Sea Surface Temperature and Sea Ice Concentrations.

emissions. The external forcing for the historical and AMIP runs is specified by the CMIP5 protocol. Specifically, well-mixed greenhouse gases are specified individually to the radiation code as CO_2, CH_4, N_2O, CFC-11, CFC-12 and HFC-134-equivalent; anthropogenic three-dimensional sulphate aerosol concentrations are specified considering the direct and first indirect effect; the total solar irradiance (TSI) and the percentage of irradiance in each of the shortwave model radiation bands vary with an 11-year solar cycle (for the TSI an anomaly is added to the 1367 Wm^{-2}); specified monthly-mean ozone fields include variations associated with the solar cycle.

Ozone is specified in most CMIP5 models, based on observational dataset for the past and CCMs (Chemistry Climate Models) simulations for the future.

However, some of the models also include a stratospheric chemistry model, therefore O_3 is prognostic in those models and the coupling between radiative-chemistry-dynamics is explicitly resolved.

2.3 High Top and Low Top Models

CMIP5 dataset gives, for the first time, the possibility to assess climate change in the stratosphere from a multi-model ensemble of coupled atmosphere-ocean-sea ice models. This is due do the fact that in the design of the CMIP5 experiments attention has been paid to the specification of forcings of stratospheric change (such as ozone trends) and also to genuine improvements in the representation of stratospheric processes with respect to previous CMIP model ensembles. One major change in coupled-climate modeling between the third (CMIP3) and fifth (CMIP5) Coupled Model Intercomparison Projects is an increase in the number of models with model tops above the stratopause (nominally located at 1 hPa) and general progress toward a more realistic representation of the stratosphere in coupled climate models. Considering indeed the main differences in simulations of stratospheric climate and variability by models within the CMIP5 it is possible to distinguish an ensemble of these that have a model top above the stratopause and relatively fine stratospheric vertical resolution, the so-called High Top models, from those that have a model top below the stratopause, named Low Top models.

In this study output data coming from the simulation of stratospheric climate and variability by two subensembles (listed in Table 2.1) of CMIP5 climate models,

one containing HT models and one containing LT models, are compared to analyze the different response to ozone-depletion forcing.

As Table 2.1 shows, the CMIP5 models have a wide variety of lid heights, vertical resolutions, and were classified into a HT and LT ensemble based primarily upon their lid height.

Institution	Model	Lid Height	Levels	Subset
BCC CMA	bcc-csm1-1	2.917 hPa	26	LT
CNRM-CERFACS	CNRM-CM5	10 hPa	31	LT
CMCC	CMCC-CESM	0.01 hPa	39	HT
	CMCC-CM	10 hPa	31	LT
	CMCC-CMS	0.01 hPa	95	HT
Consortium of European Weather Services and university groups	EC-Earth	5 hPa	62	LT
LASG-CESS	FGOALS-g2	0.01 hPa	26	LT
NOAA GFDL	GFDL-CM3	0.01 hPa	48	HT
MOHC	HadGEM2-CC	85 km	60	HT
IPSL	IPSL-CM5A-LR	0.04 hPa	39	HT
	IPSL-CM5A-MR	0.04 hPa	39	HT
	IPSL-CM5B-LR	0.04 hPa	39	HT
MIROC	MIROC-ESM-CHEM	0.0036 hPa	80	HT
	MIROC4h	0.04 hPa	56	LT
	MIROC5	3 hPa	56	LT
MPI	MPI-ESM-LR	0.01 hPa	47	HT
	MPI-ESM-MR	0.01 hPa	95	HT
	MPI-ESM-P	0.01 hPa	47	HT
MRI	MRI-CGCM3	0.01 hPa	48	HT
BCC CMA	NorESM1-M	3.54 hPa	26	LT

Table 2.1: Models used this study and their atmospheric features.

The separation is motivated by the assumption that the HT models more realistically include stratospheric processes, for instance planetary wave dissipation

whose breaking level is typically located close to the stratopause.

More specifically, the HT models includes a well-resolved stratosphere in the sense that planetary waves are free to propagate upward above 50–10 hPa and interact with the mean stratospheric flow. Moreover, they include momentum conserving nonorographic and orographic gravity wave drag impacting the stratospheric and mesospheric large-scale flows (Manzini *et al.* 2006; Cagnazzo and Manzini 2009). Since the HT models have indeed an explicit representation of planetary wave-mean flow interaction, the feedback between changes in wave dissipation and wave breaking and changes in zonal mean zonal wind is included.

Given that the top of the LT model ensemble is on average at 10 hPa, this category of models includes only a partial representation of the stratosphere with respect to the HT version, for example they do not include parameterization of non-orographic gravity waves. Moreover the LT models have lower vertical resolution in the upper troposphere and lower stratosphere (UTLS), with relatively large dissipation through a sponge layer, applied between 50 and 10 hPa, to reduce spurious reflection from upward propagating waves and to obtain a realistic mean state. The LT model ensemble has therefore very weak stratospheric variability on daily and interannual time scales. The lack of stratospheric variability in the LT models affects their representation of the stratosphere-troposphere coupling, resulting in short-lived anomalies in the annular modes, which do not produce long-lasting tropospheric impacts, as seen in observations. The lack of stratospheric variability, however, does not appear to have any impact on the ability of the LT models to reproduce for example past stratospheric temperature trends or more in general the stratospheric mean state (Charlton-Perez *et al.*, 2012).

Given that in this kind of models stratospheric variability is removed, there is a virtual lack of sudden stratospheric warming. In LT models planetary waves do not grow enough in the stratosphere and are, indeed, damped in the sponge layer. On the contrary, stratospheric variability measured as the occurrence of major stratospheric warming events has been found to be realistic in the HT models.

Because the middle and high stratospheres are missing in the LT models and planetary waves are subjected to artificial damping in the lower stratosphere of the LT models, the picture that emerge is that wave–mean-flow interaction does not fully occur. Therefore, the interaction between large-scale flow and both planetary and gravity waves is in general misrepresented in the LT models (Cagnazzo *et al.*, 2013).

2.4 Observed data

To investigate the mechanisms by which the various processes occur in the atmosphere and oceans, observations have to be used and compared to model simulations.

2.4.1 ERA-40 reanalyses

Reanalyses is a scientific method for developing a comprehensive record of how weather and climate are changing over time, so it provides the best available homogeneous global and self-consistent dataset of the observed state of the atmosphere for climate studies and for the validation of climate models. These are obtained by assimilating observations of the state of the atmosphere and of the Earth's surface into an Atmospheric General Circulation Model (AGCM), so that its dynamical evolution is bounded to remain close to the actual evolution of the atmosphere. The self consistency is guaranteed by the use of a same data assimilation scheme over the whole analyzed time period. Differences between reanalyses can be due to differences in the set of assimilated observations, in the data assimilation technique or in the numerics and the physics of the AGCM.

ERA-40 is a reanalyses of meteorological observations from September 1957 to August 2002 produced by the European Centre for Medium-Range Weather Forecasts (ECMWF) in collaboration with many institutions. The data is stored in GRIB format and the reanalyses was done in an effort to improve the accuracy of historical weather maps and aid in a more detailed analysis of various weather systems through a period that was severely lacking in computerized data.

The conventional observations for ERA-40 originate from many sources, reflecting the evolution of the global observing system and the archiving by various past users. Most of the data from the numerous pre-1979 sources were collected as a dedicated effort at the National Center for Atmospheric Research (NCAR), and delivered to ECMWF through National Centers for Environmental Prediction (NCEP). The main datasets after 1979 originate from global forecasting centers: ECMWF, NCEP and JMA (Japanese Meteorological Agency).

The observing system changed considerably over this reanalyses period, with assimilable data provided by a succession of satellite-borne instruments from the

1970s onwards, supplemented by increasing numbers of observations from aircraft, ocean-buoys and other surface platforms, but with a declining number of radiosonde ascents since the late 1980s. In the SH and in the tropics the amount of radiosonde data increases gradually. Here, however, over the large ocean areas and over the sparsely populated areas, the conventional observing system alone is not sufficient to produce high quality analysis. Therefore, 1979 brings a more dramatic improvement in the quality and coverage of analysis in the SH than in the NH with the satellite era and with the introduction of a new and significant system of drifting buoys in the SH and tropics.

Satellite and conventional data are extensively used in the analysis of temperature, wind and humidity, but the influence of conventional data is limited to the troposphere and lower stratosphere, while over the large ocean areas and polar regions, as well as in the upper stratosphere above 10hPa, the analysis is mainly driven by the satellite data. If there are no data at all, the analysis is equal to the background. Before 1979 the ozone analysis results from the ozone parameterization and model dynamics, though conditioned by the analysis of temperature and wind. Ozone profiles are also available from a network of radiosonde stations, but they are too sparse and too infrequent to be used in the analysis, although they have an important role in validation, making the more numerous ground-based measurements. After 1979, externally-produced retrievals of total column ozone from TOMS (Total Ozone Mapping Spectrometer) and ozone layer profiles from SBUV (Solar Backscatter Ultra-Violet radiometer) are used.

Atmospheric data assimilation comprises a sequence of analysis steps (or cycles) in which background information for a short period, typically 6 hours, is combined with observations for the period to produce an estimate of the state of the atmosphere at a particular time. The set of observations usually comprises several types of measurement, each with its own accuracy and distribution, whereas the background information comes from a short-range forecast initiated from the most recent previous analysis in the sequence. The observations and background forecast are combined using statistically based estimates of their errors; in variational assimilation this is achieved by minimizing the sum of error-weighted measures of the deviations of analyzed values from the observed and background values. The resulting sequence of initial states provides a record of the evolving atmospheric state that is based on a synthesis of the available observations. The degree of dependence on the model varies with the density and relative accuracy of the

observations (the error statistics), and in general differs from place to place and from variable to variable (e.g. from wind to humidity).

ERA-40 provides fields with higher horizontal and vertical resolutions in the planetary boundary layer and stratosphere than those provided by the earlier reanalyses. This data, in fact, is run through the ECMWF computer model at a 40 km resolution.

Several results demonstrate the marked improvement that was made to the observing system for the SH in the 1970s, particularly towards the end of the decade. In contrast, the synoptic quality of the analysis for the NH is sufficient to provide forecasts that remain skilful well into the medium range for all years. Two particular problems are also identified: excessive precipitation over tropical oceans and a too strong Brewer–Dobson circulation, both of which are pronounced in later years. Expectations that the "second-generation" ERA-40 reanalyses would provide products that are better than those from the first generation ERA-15 and NCEP/NCAR Reanalyses are found to have been met in most cases (Uppala *et al.*, 2005).

Therefore, in conclusion, the ERA-40 reanalyses and related forecast information have considerable potential to contribute to studies of atmospheric, oceanic and land-surface processes, and to studies of the variability and predictability of climate, especially for the period from 1979 onwards for which there is good global observational coverage.

Chapter 3

The stratosphere in Southern Hemisphere long-term changes: starting point of this work

3.1 The ozone hole and the SH circulation

Observations

The atmosphere of the SH high latitudes has been subject to pronounced changes over the past few decades. Total column ozone losses have exceeded 50% during October throughout the 1990s (Jones and Shanklin, 1995), and the Antarctic ozone hole has reached large values in the 2000s (WMO, 2011). The lower stratosphere has cooled by more than 10K since 1985 (WMO, 2011) peaking in October-November and the seasonal breakdown of the polar vortex has been delayed: from early November during the 1970s to late December during the 1990s, in both the troposphere (Hurrell and van Loon, 1994) and the lower stratosphere (Zhou *et al.*, 2000). The cooling has then led to an acceleration of the polar vortex, that interestingly extends down at the surface. Implications of ozone induced cooling therefore include the strengthening of westerly winds in the stratosphere with a later transition to easterlies (Thompson and Solomon 2002). At

the surface, the Antarctic Peninsula has warmed by several degrees over the past several decades, while the internal part of the Antarctic continent has shown a weak cooling (IPCC Fourth Assessment Report). Ice shelves have retreated over the peninsula and sea-ice extent has decreased there, while sea-ice concentration has increased over eastern Antarctica and the Ross Sea (Parkinson, 2002). The stratospheric cooling associated to ozone has been shown to largely project onto the SAM. Indeed, anthropogenic climate change has been particularly strong in the SH summer, within the index of the SAM increasing in the recent past (Thompson and Solomon, 2002). This strong trend in austral summer has been attributed to both increase in GHGs and decrease in stratospheric ozone concentrations (e.g. Thompson and Solomon, 2002; Gillett and Thompson, 2003; Perlwitz *et al.*, 2008; Son *et al.*, 2008). Indeed, it is known that both GHGs increase (e.g., Kushner *et al.*, 2001) and ozone depletion (e.g., Gillett and Thompson, 2003) drive the SH climate in the same direction, toward a positive trend of the SAM index. However, if GHG induced changes occur during all the year, ozone-induced ones occur in the SH summer. Therefore, this is the season when the strongest trends are found. In the troposphere, the SAM is characterized by zonally symmetric, north–south variability in the latitude of the midlatitude jet (Thompson and Wallace, 2000). The high-index polarity of the SAM is marked by poleward displacements of the jet and thus by strengthening of the prevailing atmospheric westerlies.

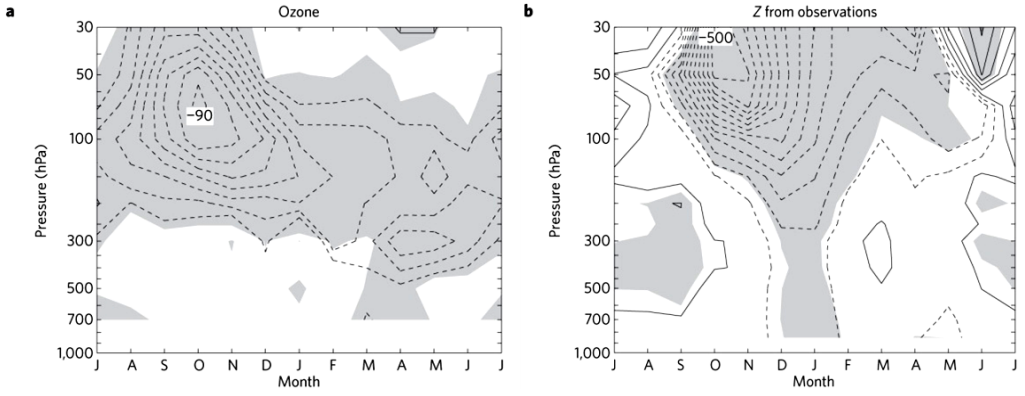

Figure 3.1: Observed composite differences between the pre-ozone-hole and ozone-hole eras in (a) polar ozone from Syowa station (69°S, 40°E; similar results are obtained for other stations within the region of the ozone hole) and (b) polar-mean *Z* from radiosonde data. Contour intervals are (a) 10% depletion for values of 20% and greater and (b) 40 m (–60, –20, 20…). Positive contours are solid, negative contours are dashed. Shading indicates trends significant at the 95% level based on a one-tailed test of the Student's t-statistic. From Thompson *et al.* (2011).

Thompson *et al.* (2011) consider the differences in the SH polar stratosphere between the pre-ozone-hole and ozone-hole eras, making possible to observe monthly mean decreases in lower stratospheric ozone that exceed 80% during the late spring (October–November) and exceed 20% throughout the austral autumn and winter seasons (Fig. 3.1a). The corresponding changes in polar stratospheric geopotential height (*Z*) are indicative of a strengthening of the eastward circumpolar flow persisting through January (Fig. 3.1b).

The eastward acceleration of the lower stratospheric flow due to ozone depletion is particularly relevant for climate change because it extends to the Earth's surface during the summer months (Fig. 3.1b). Deep vertical coupling between the circumpolar tropospheric and stratospheric flow is observed on monthly and daily timescales in both the Northern and Southern Hemispheres (Thompson and Wallace, 2000; Thompson *et al.*, 2005). The changes in the tropospheric flow indicated in Fig. 3.1b suggest that such coupling is also characteristic of the ozone hole.

Reanalyses

Considering ERA 40 Reanalyses on a time period between year 1979 and 1999, Son *et al.* (2010) have demonstrated that ozone impact on the tropospheric circulation is delayed by a few months although its long-term concentration is largest in the late spring, and reaches a maximum in the summer, December-to–February (DJF) (Gillett and Thompson, 2003; Shindell and Schmidt, 2004; Perlwitz *et al.*, 2008; Son *et al.*, 2008). In Figure 3.2 the zonal mean zonal wind long-term mean climatology and linear trend are reported. A rather strong positive trend both in the lower stratosphere at polar latitudes (higher than 60°S) and in the upper troposphere in the circumpolar region are evident, as a result of the temperature meridional gradient increase (see thermal wind equations in Appendix A). This poleward jet displacement also drives the Hadley cell widening towards the same direction (Fu *et al.*, 2006; Hu and Fu, 2007; Seidel *et al.*, 2008; Johanson and Fu, 2009), causing a variation in the arid regions setting.

A simple schematic illustration that can explain how ozone depletion manages to impact down to the surface in SH is reported in Figure 3.3, following the mechanism proposed by Son *et al.* (2010). The proposed mechanism is the following: ozone depletion leads to strong cooling. The cooling over the southern

polar cap in turn accelerates the extratropical zonal-mean zonal wind [u] by enhancing the zonal mean temperature [T] gradient. The stratospheric jet intensification in the polar vortex tends to accelerate tropospheric midlatitude jet in the poleward side implying an intensification of the tropospheric westerly jet. This contributes to a dipolar change of sea level pressure between midlatitude and subpolar regions, equivalent to strengthening of positive trend in the SAM index.

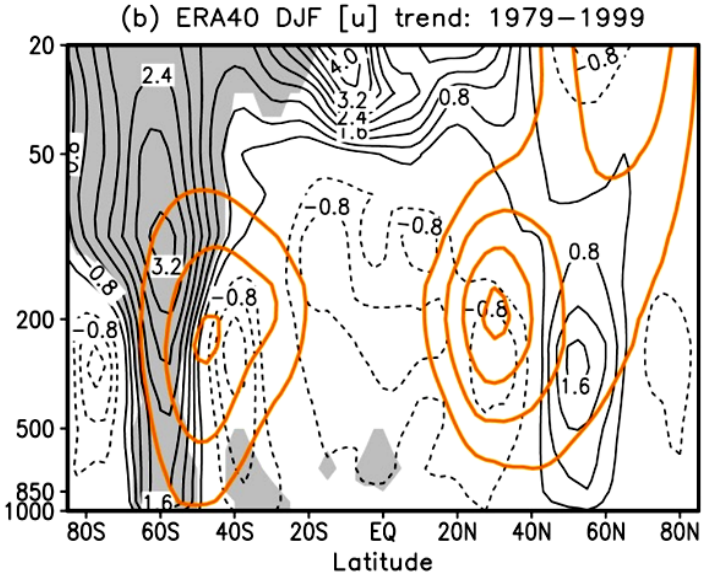

Figure 3.2: The long-term mean (thick orange) and linear trend (thin black contour) of DJF [u] over 1979–1999 ERA40 reanalyses data. Contour intervals of climatological wind and trend are 10 m s^{-1} starting from 10 m s^{-1} and 0.4 ms^{-1}/decade, respectively. Trends which are statistically significant at the 95% confidence level are shaded. Zero contours are omitted. From Son *et al.* (2010).

The opposite is expected when stratospheric ozone increases, as predicted to occur over about the next 50 years (Figure 3.3 *b*ottom). Since circulation changes, driven by ozone recovery, would oppose those by tropospheric GHGs increase, it is anticipated that tropospheric circulation changes in the future will be substantially weaker than, or even the reverse of, those observed in the past (Polvani *et al.*, 2011a,b; Son *et al.*, 2010).

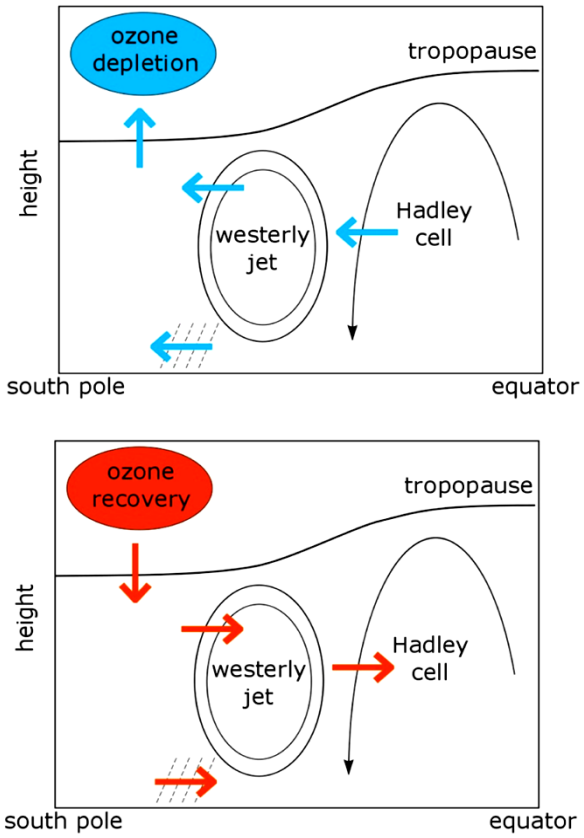

Figure 3.3: A schematic representation of the impact of stratospheric ozone loss and recovery on the tropospheric circulation in the SH summer. Changes in the extratropical tropopause height and location of the westerly jet, storm track (and associated midlatitude precipitation), and the poleward boundary of the Hadley cell are highlighted. From Son *et al.* (2010).

Model simulations

This chain of effects has been verified in long-term simulations. Specifically, Son *et al.* (2010) have derived multi-model linear trend zonal-mean temperature, meridionally integrated on a range between 64°S and 90°S, and multi-model linear trends of the monthly mean zonal-mean zonal wind, integrated from 50°S and 70°S, within simulations performed in the CCMVal-2 model simulations (REF-B1[1] and

[1] REF-B1 is a reference integration for the period 1960-2006, forced with observed GHGs, ozone depleting substances, sea surface temperature (SSTs), sea ice concentrations (SICs), solar variability, and aerosols including volcanic aerosols.

REF-B2[2]). These models manage to successfully reproduce stratospheric ozone depletion in the last 4 decades (e.g., Randel and Wu, 1999), as figure 3.4a shows, then leading to radiative cooling in the lower stratosphere after 1 month-delay (Fig. 3.4b), in agreement with observations (Randel and Wu, 1999; Thompson and Solomon, 2002). Thus, the maximum ozone depletion is found in October in the lower stratosphere, whereas the maximum cooling is in November (Figures 3.4a and 3.4b). This delay is probably caused by the relatively long radiative time scale in the lower stratosphere (e.g. Thompson and Solomon, 2002).

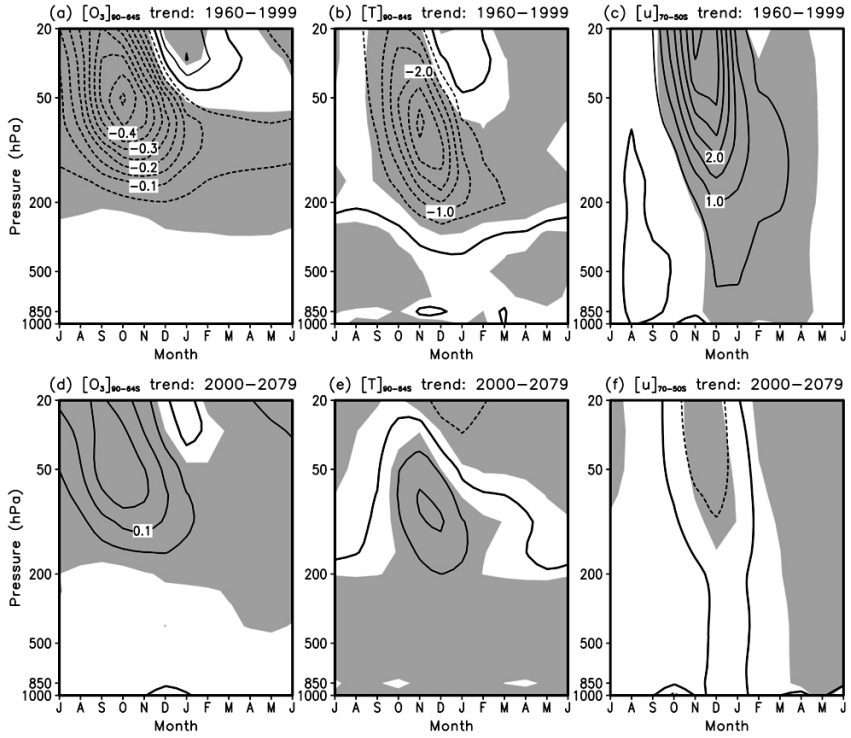

Figure 3.4: Linear trends of (a, d) the monthly mean [O_3], (b, e) [T] integrated south of 64°S, and (c, f) [u] integrated from 70° to 50°S. The multi-model mean trends are computed for the time period of 1960–1999 in the CCMVal-2 REF-B1 runs (a–c) and for the time period of 2000–2079 in the CCMVal-2 REF-B2 runs (Figures d–f). Starting month in the x axis is July, and contour intervals are 0.05 ppmv/decade (a and d), 0.5 K/decade (b and e), and 0.5 m s–1/decade (c and f).Zero lines are denoted with thick black lines, and multi-model mean values exceeding 1 standard deviation are shaded. From Son *et al.* (2010).

[2] REF-B2 is a scenario integration for the period of 1960-2100, based on both observations and scenario forcings. The scenario forcings The scenario forcing are applied after 2000 and are the A1B GHGs scenario, A1 ODSs scenario, modeled SSTs/SICs, and constant solar flux and background surface area density aerosol (Morgenstern *et al.*, 2010).

Models are able to reproduce polar jet acceleration (Figs. 3.4b, 3.4c and 3.5). This acceleration, however, is not confined to the stratosphere, but it penetrates down to the surface after a lag of another 1 to 2 months. The results lead to a significant intensification of the zonal-mean zonal wind in the lower troposphere during DJF (Fig. 3.4c). The consideration that [u] changes in other seasons are almost negligible suggests that tropospheric [u] in the SH extratropics has been driven more by stratospheric ozone than tropospheric GHGs changes in the period of analysis, as it has been seen previously (Polvani *et al.*, 2010).

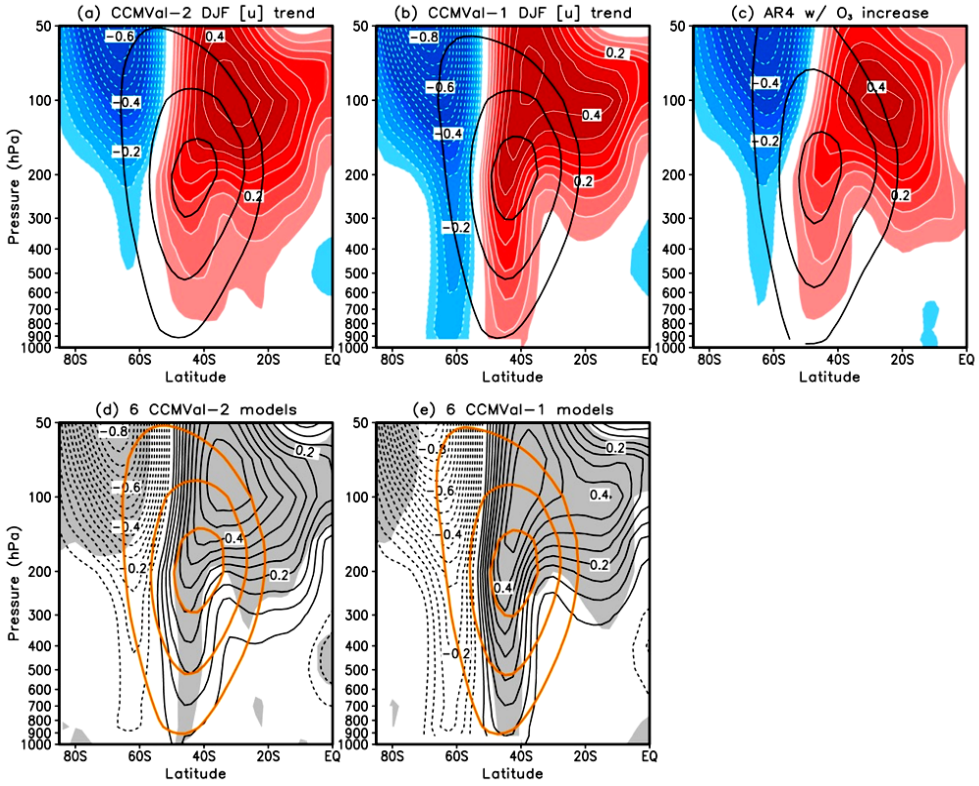

Figure 3.5: The long-term mean (thick black contour) and linear trend (shading with thin contour lines) of DJF [u] over 2001–2050: multi-model mean values are shown for (a) CCMVal-2 REF-B1, (b) CCMVal-1, and (c) AR4 models with prescribing ozone recovery. Contour intervals of climatological wind and trend are 10 m s−1 starting from 10 m s−1 and 0.5 m s−1/decade, respectively. (d, e) Similar to Figures a–c but for the six models which archived both the CCMVal-1 and CCMVal-2 data. Those models are CCSRNIES, CMAM, GEOSCCM, MRI, SOCOL and WACCM. The plot format is the same as Figure 3.2. From Son *et al.* (2010).

Idealized model simulations

Other modeling studies have indeed demonstrated that the role of the ozone is the most important to explain the SH changes. For example, Polvani *et al.* (2011a) have examined the thermal response of an atmospheric general circulation model, the Community Atmospheric Model, version3 (CAM3), to different forcings.

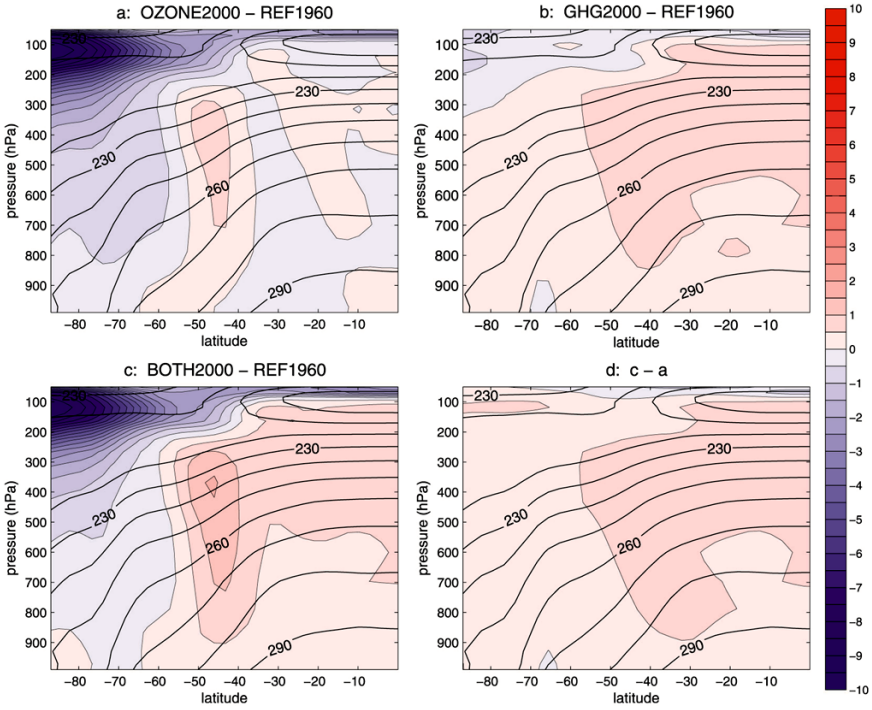

Figure 3.6: Colored contours show the DJF temperature differences between the REF1960 integration and the (a) OZONE2000, (b) GHG2000, and (c) BOTH2000 integrations. (d) The difference between (a) and (c), which should be contrasted with (b). Their similarity leads to the conclusion that the temperature response of our model is roughly linear, except in the polar stratosphere. In all panels the contour interval is 0.5 K. Black contours show the zonal mean, time mean, DJF temperature for the REF1960 integration, with contour intervals of 10 K. From Polvani *et al.* (2011a).

In Figure 3.6 the latitude-pressure, 50-year mean, DJF profiles[3] of temperature differences between the REF1960[4] control integration (representing climate before

[3] These profiles are averaged on the winter season months, i.e. December, January and February.

[4] The reference integration is labeled REF1960: it is forced with SSTs (sea surface temperature and sea ice concentrations) from the Hadley Centre dataset, averaged over the 17-year period 1952–68,

the ozone changes) and OZONE2000[5] (simulation representing climate after the ozone changes from the year 2000, but without the GHG changes), GHG2000[6] (simulation representing climate after the GHG changes from the year 2000, without the ozone changes), and BOTH2000[7] (modeling simulation representing climate after the both ozone and GHG changes from the year 2000) are shown, in order to illustrate that temperature response to stratospheric ozone depletion, while confined to the lower-stratospheric polar cap, is roughly larger than the one associated with GHGs increase in the period between 1960 and 2000. It is also possible to notice how the high-latitude stratospheric cooling associated with greenhouse gas increases is tiny compared with the one caused by ozone depletion.

In particular, by specifying ozone and GHG forcings independently (Fig. 3.6d), and performing long, time-slice integrations, it has been shown that ozone depletion effect is 2-3 times larger than that associated with increased GHGs only, for the SH tropospheric summer circulation.

As noted by Son *et al.* (2009a), stratospheric ozone also influences global hydrology. Expansion of the subtropical dry zone in the recent past is strongly associated with poleward expansion of the Hadley cell[8] (Lu *et al.*, 2007), driven by increasing the tropopause height, strengthening the westerly winds in the polar vortex, and their displacing poleward. Likewise, the poleward displacement of westerly jet largely accompanies a poleward shift of the extratropical storm tracks (e.g., Yin, 2005).

Reanalyses show that the poleward boundary (the extratropical jet) of the Hadley cell is typically located at the latitude of maximum eddy momentum flux convergence (the meridional component of the Eliassen Palm (EP) flux divergence, seen in Appendix A) in the upper troposphere (e.g., Son and Lee, 2005; Fig. 3.7a).

---

with SPARC ozone taken from the year 1960, and with greenhouse gases also taken from the datasets mentioned above for the year 1960.

[5] OZONE2000 is identical to the reference integration in all respects, except for the ozone fields, which are taken from the year 2000 of the SPARC ozone dataset. Note that, in this integration, the halocarbons at 1960 levels are left.

[6] GHG2000 is an integration performed with all forcings at year 2000 levels, except for ozone, which is left at 1960 levels. The SSTs are also averaged over a 17-year period, specifically 1992–2008 (the Hadley Centre SSTs being available only up to 2008 at the time this work was performed).

[7] BOTH2000 is an integration in which all forcings are set at year 2000 levels, performed to evaluate the linearity of the response.

[8] For further information about Hadley cell return back to Chapter 1 and see Section 1.3.7.

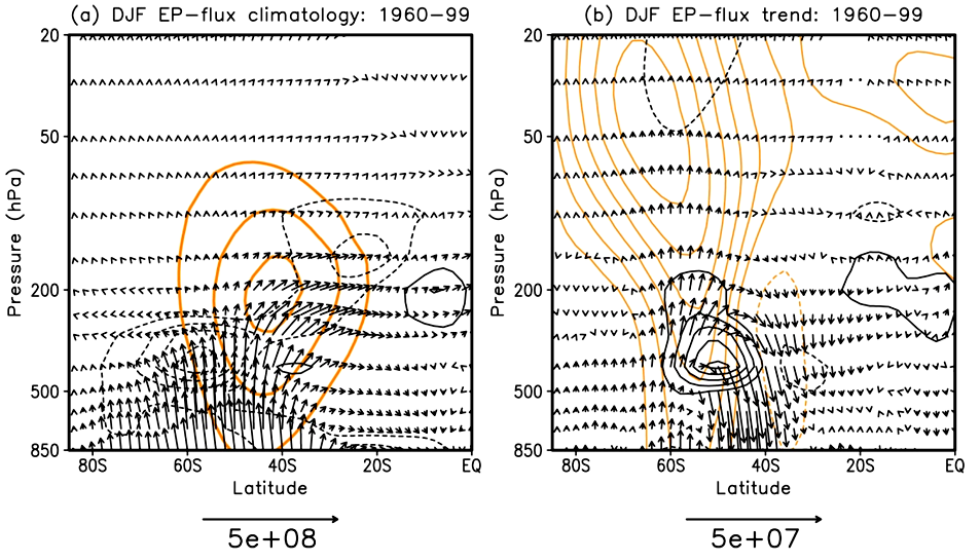

Figure 3.7. The multi-model mean EP flux vectors and divergence in the SH summer: (a) climatology and (b) linear trend between 1960 and 1999. The vertical component of EP flux vector is multiplied by the aspect ratio, and a reference vector is shown in each plot with units of kg s−2 in (a) and kg s−2/decade in (b). The contour intervals of EP flux divergence are 80 kg m−1 s−2 in (a) and 4 kg m−1 s−2/decade in (b). The zero lines are omitted. Superimposed orange lines are DJF [u] climatology in (a) and multi-model trend in (b) in the same time period. Contour intervals are 10 m s−1 and 0.4 m s−1/decade, and the zero lines are omitted. Here multi-model mean values are calculated using the seven CCMVal-2 REF-B1 models which archived zonal mean eddy fields: CMAM, E39CA, GEOSCCM, LMDZrepro, Niwa-SOCOL, SOCOL, and UMUKCA-METO. From Son *et al.* (2010).

Therefore both the jet and the Hadley cell boundary will shift poleward if the eddy fields shift poleward. In the CCMVal-2 REF-B1 model integrations, performed in a modelling study conducted by Son *et al.* (2010), the EP flux has shifted poleward along with the tropospheric circulation in the last four decades (Figure 3.7b). Although this analysis does not provide a causal relationship, it suggests that tropospheric changes, driven by stratospheric ozone loss, are likely mediated by eddies.

3.1.1 Ozone depletion effect at the surface, in the ocean and on air-sea carbon fluxes

Observations show that the Z geopotential height falls in summer in the polar

troposphere (Figs. 3.1b; 3.8), accompanied by a rise at middle latitudes (Fig. 3.8). This strongly resembles the high-index polarity of the leading mode of climate variability in the SH troposphere, the SAM (seen in Chapter1).

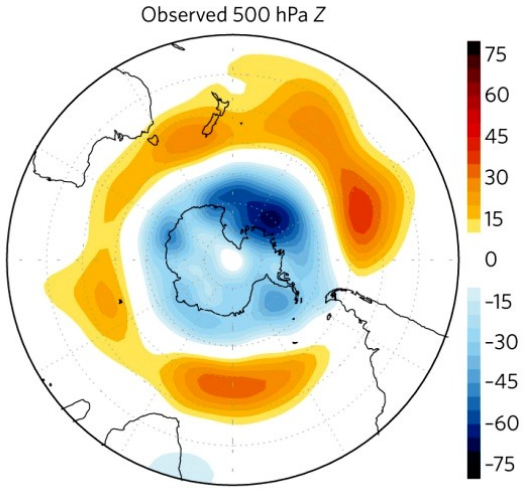

Figure 3.8: Signature of the ozone hole in observed composite differences between the pre-ozone-hole and ozone-hole eras in mean December–February (DJF) 500-hPa *Z* from the NCEP-NCAR Reanalyses in the austral summertime circulation. The contour interval is 5 m and values under 10 m are not contoured. From Thompson *et al.* (2011).

In the troposphere, the SAM high-index polarity is marked by poleward displacements of the jet with a strengthening of the prevailing atmospheric westerly flow near about 60°S and a weakening of the prevailing atmospheric eastward flow near about 40°S. The SAM owes its existence to internal tropospheric dynamics, and its variability is driven by changes in the fluxes of heat and momentum by synoptic-scale (1,000-km-scale) atmospheric waves (Karoly, 1990; Hartmann and Lo, 1998; Limpasuvan and Hartmann, 2000; Lorenz and Hartmann, 2001; Barnes and Hartmann, 2010). Therefore, the link between the ozone hole and the SAM could be due to the effects of ozone depletion on these wave fluxes. In the case of the high-index polarity of the SAM, the changes in the wind field are driven by anomalous poleward wave fluxes of heat in the lower troposphere near 60°S and anomalous poleward wave fluxes of momentum at the tropopause, as shown in Fig. 3.7. In the lower troposphere the synoptic wave fluxes of heat are largely diffusive, that is, they are down-gradient and peak in regions of large temperature gradients

and synoptic wave amplitudes (Held, 1999). Hence, the ozone hole, perturbing the near-surface temperature gradient, influences the diffusive wave fluxes of heat both radiatively and dynamically (Thompson *et al.*, 2011).

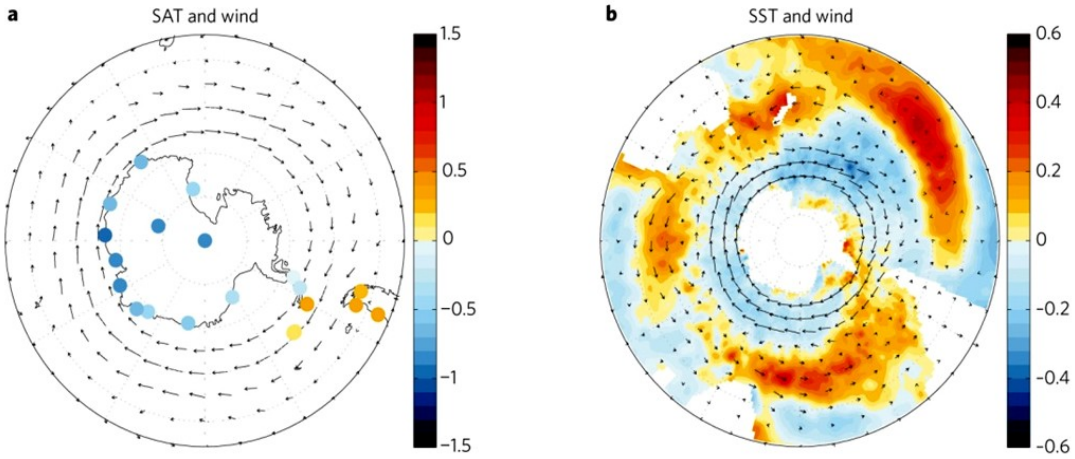

Figure 3.9: Signature of the SAM in austral summertime climate variability. Regressions on the SAM index using DJF monthly mean data showed by results of (a) surface air temperatures (SAT; shading) and (b) sea surface temperatures (SST; shading), both with 925-hPa winds (vectors). Shading interval is (a) 0.1 K and (b) 0.04 K. From Thompson *et al.*, 2011.

In Figures 3.9a and 3.9b the high-index polarity is linked to lower than normal summertime temperatures over much of east Antarctica, consistent with anomalous[9] rising motion and thus a suppression of the katabatic flow over the polar cap, and higher than normal summertime temperatures over Patagonia and the northern reaches of the Antarctic Peninsula, consistent with increased warm temperature advection from the Southern Ocean due to the stronger eastward surface flow (Thompson and Solomon, 2002; Thompson and Wallace, 2000; Marshall *et al.*, 2006; Marshall, 2007; Fig. 3.9a). Besides, detailed analysis of station data indicate that the SAM has a much larger effect on surface temperatures over the eastern side of the Peninsula than the western side because of the orographic effects of the Antarctic Andes (Marshall *et al.*, 2006).

At middle latitudes (about 35–50°S), the high-index polarity of the SAM is characterized by westward anomalies in the surface flow, decelerating the prevailing

[9] Anomalies are defined as departures from the long-term mean (Thompson *et al.*, 2011).

eastward wind and driving a warm near zonal advection in sea surface (Fig. 3.9b).

The high-index polarity of the SAM, modifying wind surface stress, is also linked to pronounced summertime changes in the Southern Ocean (Fig. 3.10). The anomalous eastward atmospheric flow centered near 60°S leads to increased equatorward Ekman transport over much of the Southern Ocean, and thus increased upwelling in the Southern Ocean poleward of 60°S and downwelling at middle latitudes (Cai and Cowan, 2007; Oke and England, 2004; Fyfe and Saenko, 2006; Fyfe *et al.*, 2007). Numerical experiments predict that on timescales shorter than a season, the changes in Ekman flow will tighten the north–south density gradients across the Southern Ocean, and shift the Antarctic Circumpolar Current and the upper limb of the Southern Ocean meridional overturning circulation poleward (Sigmond *et al.*, 2011; Fyfe and Saenko, 2006; Hall and Visbeck, 2002; Sen Gupta and England, 2006). On timescales longer than a season instead, the Ekman-induced changes are predicted to be mostly compensated by the diffusion of density and heat by ocean eddies with length scales of about 10–100 km (Hallberg and Gnanadesikan, 2006; Böning *et al.*, 2008; Screen *et al.*, 2009; Hogg *et al.*, 2008; Salleé *et al.*, 2008; Spence *et al.*, 2010; Farneti *et al.*, 2010; Farneti and Delworth, 2010).

At the ocean surface, the high-index polarity of the SAM is linked in both observations and model experiments to lower than normal summertime sea-surface temperatures (SSTs) around most of Antarctica and higher than normal SSTs in middle latitudes, due not only to changes in the ocean Ekman circulation, but also to the anomalous fluxes of sensible and latent heat at the atmosphere–ocean interface (Sen Gupta and England, 2006; Verdy *et al.*, 2006; Ciasto and Thompson, 2008; Figs. 3.9b and 3.10). For example, the lower than normal SSTs to the southeast of New Zealand are consistent with enhanced ocean heat loss caused by the overlying wind anomalies (Fig. 3.8b). Furthermore, changes in cloudiness and the diffusion of heat by ocean eddies can also likely influence the pattern of SSTs (Figs. 3.9b and 3.10).

The changes in surface climate, partly associated with stratospheric O_3, are also known to affect the upper ocean salinity, as well as upper ocean temperature.

Observational studies have shown that the upper ocean in the southern high latitudes has been freshening over the last 4 decades (Gille, 2002; Böning *et al.*, 2008). This has been attributed in part to the enhanced precipitation over the Southern Ocean resulting from the poleward shift of the tropospheric circulation

(Böning *et al.*, 2008), whereas, as seen previously, the upper ocean temperature might be modulated by surface wind change (Fig. 3.9b) through Ekman transport (e.g., Fyfe *et al.*, 1999). These changes in the upper ocean in turn feedback on the troposphere, possibly amplifying the ozone-induced circulation change in the SH.

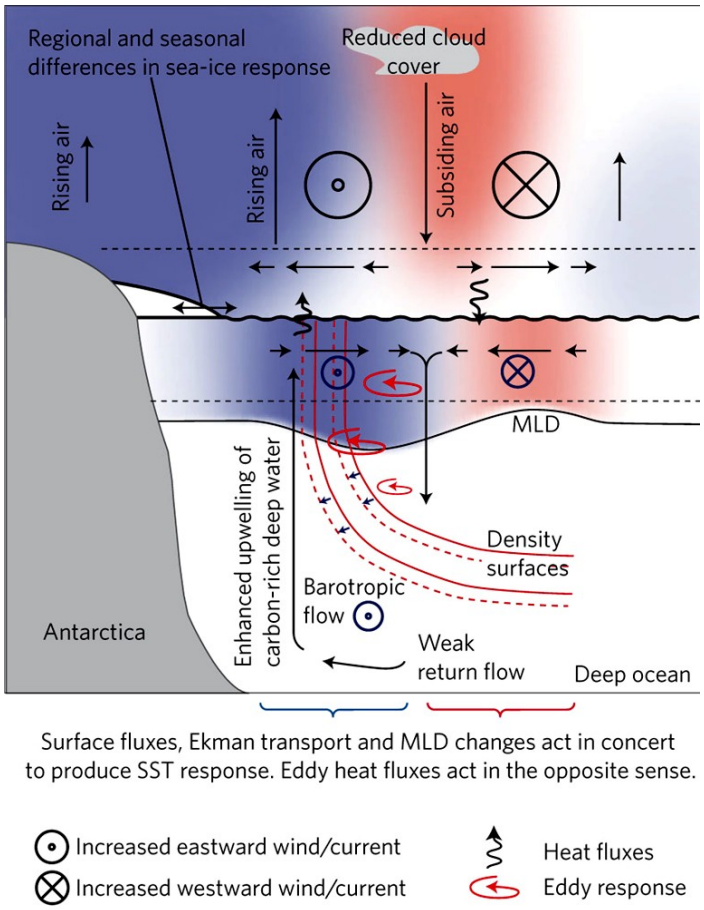

Figure 3.10: Schematic response of the ocean to the high-index polarity of the southern annular mode. Solid arrows indicate meridional and vertical motion in the atmosphere and ocean. Warm colors correspond to increases in temperature or heat content, and cooler colors to decreases. MLD refers to the ocean mixed-layer depth. All other responses are labeled on the figure or in the legend. All results indicate the climate response to the SAM on timescales less than a season with the exception of the oceanic eddy field, which indicates the response on timescales of 2–3 years. From Thompson *et al.* (2011).

Furthermore the increase of wind-stress-driven Ekman pumping gives an important contribute to air-to-sea carbon fluxes: an enhanced poleward upwelling allows deep nutrient-rich-water to rise up to the ocean surface layer reducing the CO_2 partial pressure gradient between the atmosphere and ocean. As it is explained in Chapter 1, this ventilation process implies that the Southern Ocean capacity to work as carbon sink weakens with possible consequences on the ocean acidification and CO_2 atmospheric concentration (Lovenduski *et al.*, 2008; Lenton *et al.*, 2009; Fig. 3.11).

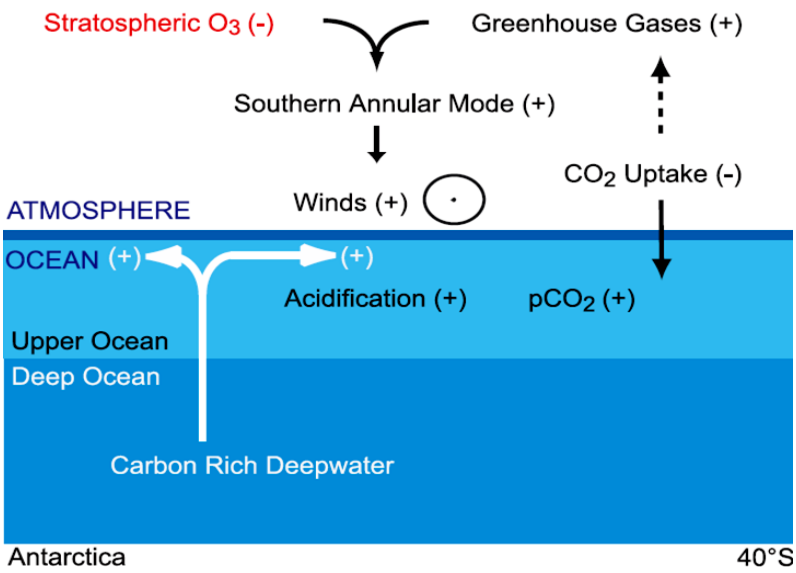

Figure 3.11: Response of the Southern Ocean to stratospheric ozone depletion. Positive (+) represents an increase/strengthening and negative (-) represents a decrease/weakening of a given process. From Lenton *et al.* (2009).

In fact, Southern Ocean plays an important role in mitigating climate change, acting as an important sink of atmospheric CO_2, but its partial pressure variation in atmosphere and oceanic surface, due to the deep water upwelling following the ventilation intensifying, implies carbon concentration changes.

3.2 Role of the representation of the stratosphere in models

If stratospheric cooling deriving from ozone trends is the main responsible for the observed SH changes, is the representation of the stratosphere in models playing a role in reproducing the observed SH long-term changes? And are model projections reliable in this sense?

To answer these questions Cagnazzo *et al.* (2013) have performed two sets of simulations with the HT version and the LT[10] version of the Centro Euro-

[10] The LT model is used for this comparison because it is representative of a CMIP3 (Coupled Model Intercomparison Project—phase 3) standard, including carbon cycle, and it is the predecessor

Mediterraneo sui Cambiamenti Climatici Carbon Earth System Model (CMCC-CESM), that includes processes related to the biological and geochemical parts of the carbon cycle.

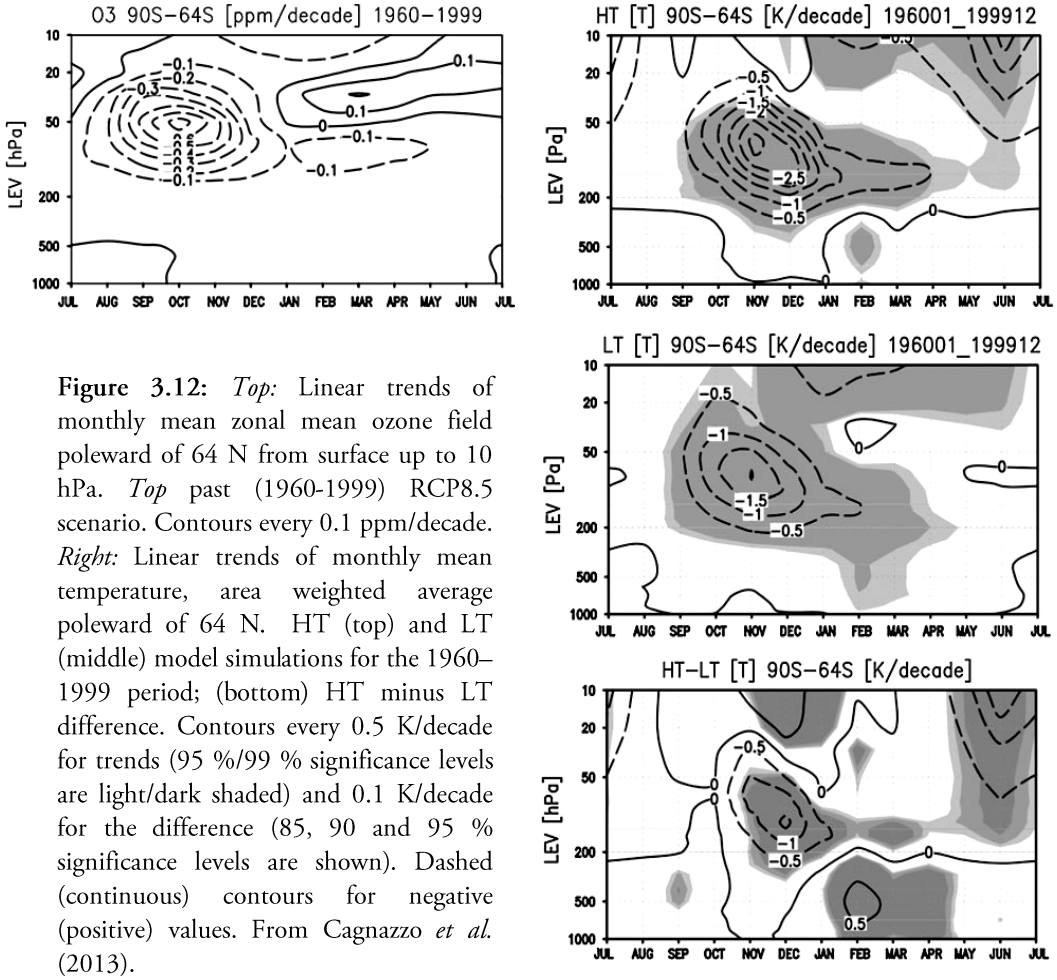

Figure 3.12: *Top:* Linear trends of monthly mean zonal mean ozone field poleward of 64 N from surface up to 10 hPa. *Top* past (1960-1999) RCP8.5 scenario. Contours every 0.1 ppm/decade. *Right:* Linear trends of monthly mean temperature, area weighted average poleward of 64 N. HT (top) and LT (middle) model simulations for the 1960–1999 period; (bottom) HT minus LT difference. Contours every 0.5 K/decade for trends (95 %/99 % significance levels are light/dark shaded) and 0.1 K/decade for the difference (85, 90 and 95 % significance levels are shown). Dashed (continuous) contours for negative (positive) values. From Cagnazzo *et al.* (2013).

Figure 3.12 shows linear trends in the polar cap (64°S–90°S) temperature from surface up to 10 hPa for the 1960-1999 period, for HT and LT models. In agreement with previous modeling studies (e.g. Son *et al.* 2010) and with similar changes deduced from observational datasets (Thompson and Solomon 2002), the two model simulations are characterized by a rapid cooling of the lower

of the current CMCC-CESM (Johns *et al.* 2011; Vichi *et al.* 2011; Patara *et al.* 2012; Fogli *et al.* 2009).

stratosphere, peaking in November. In the stratosphere, the difference between HT (3 K/decade) and LT (1.5 K/ decade) trends shows that the cooling is about two-third larger for the HT than for the LT model with a better agreement with observations for the HT model.

Given that the two models share the same radiation scheme, the diabatic heating change is the same for the two models, then the difference between the two cooling trends can be searched in the dynamical contribution, possibly linked to the different stratospheric representation in models.

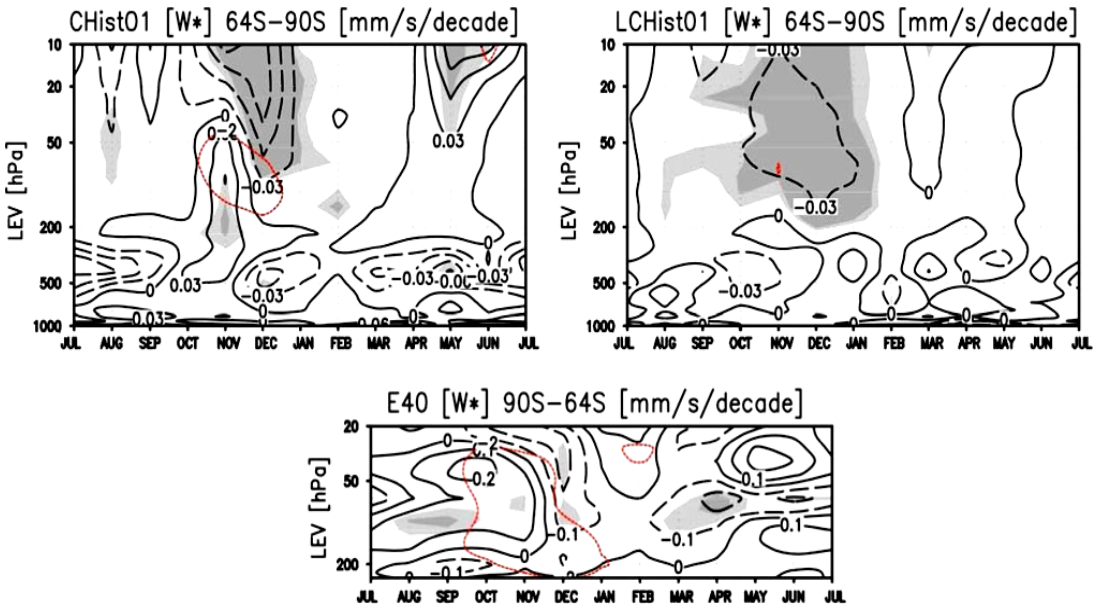

Figure 3.13 Linear Trends of monthly mean vertical residual circulation w* , averaged over the polar cap (64°S-90°S). Two versions of CMCC-CESM model (HT and LT) are reported on the *left* and on the *right* for the period 1960-1999, together with the same trends in ERA40 for the 1979-1999 period (*bottom*). Contours every 0.1 mm/s/decade. (95%) 99% significance are (light) dark shaded. *Red line* represents the -2K/decade temperature trend. From Cagnazzo *et al.* (2013).

The response of zonal mean temperature to stratospheric ozone loss is explained by the following equation[11]:

$$\bar{\theta}_t + \overline{w^*}\theta_{0z} - \bar{Q} = 0 \qquad (3.1)$$

[11] This equation is obtained from motion equations in TEM approximation and is explained in Appendix A.

So if the diabatic term ($\bar{Q}$) in equation is the same, then the difference in cooling trends is mainly searched in the dynamical response of the stratosphere.

This consideration, that is valid in that work because of the experiment design, cannot be verified in our analysis based on multi-models. However, some of our results here will be found to be consistent with that assumption.

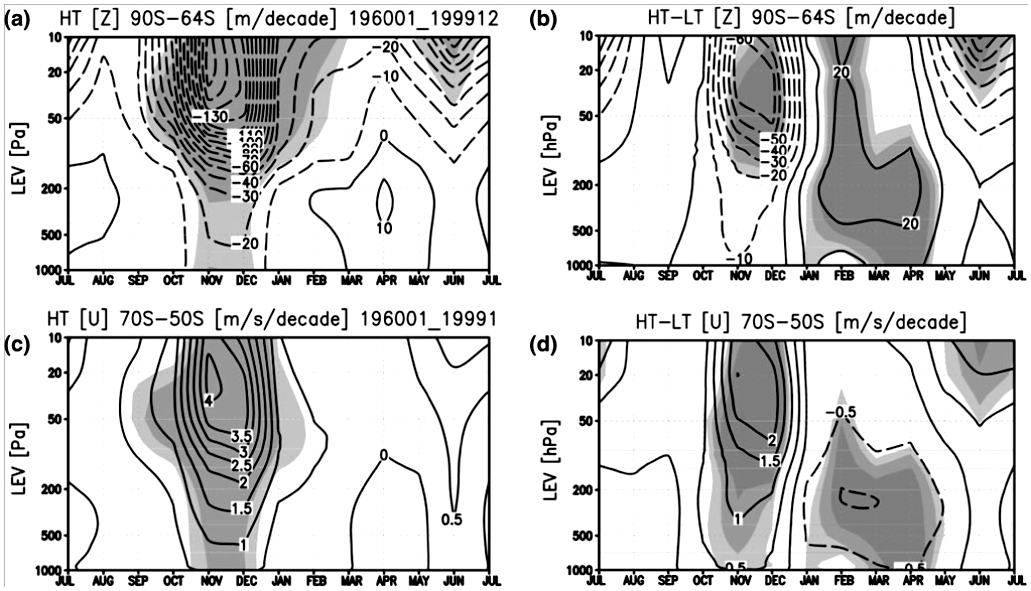

Figure 3.14: s Linear trends of monthly mean polar cap (90°S–64°S) geopotential height (top) and zonal mean of zonal wind (bottom) at 70°S-50°S for the 1960–1999 period. For the HT model (left) and for the HT minus LT difference (right). Contours every 0.5 m/s/decade for trends (95 %/99 % significance levels are light/dark shaded) and 0.1 m/s/decade for the difference (85, 90 and 95 % significance levels are shown). From Cagnazzo *et al.* (2013).

Cagnazzo *et al.* (2013) also show linear trends in the vertical residual circulation w* (reported in Fig. 3.13) together with the same trends in ERA-40 (Uppala *et al.* 2005), highlighting the dynamical contribution to the cooling that comes from a different representation of the stratosphere. Indeed, in this work the LT model is not able to fully simulate observed temperature changes.

The same occurs for changes in the SH circulation (Fig. 3.14) with implications for surface, ocean and air-sea carbon fluxes.

Therefore, if the initial stratospheric cooling is the essential ingredient for a realistic simulation of SH changes to which extent a limited representation of the

dynamical cooling in the lower stratosphere impact the simulation of these changes?

In order to answer this question, we make use of a set of climate models within the CMIP5 project. The starting point is that the majority of these models make use of the same ozone profiles and trends, but have different representations of the stratosphere.

3.3. Ozone recovery: future perspective

Climate models simulations have shown that the observed westerly wind changes likely result from an increase in greenhouse gases and the stratospheric ozone depletion (Gillett and Thompson, 2003; Shindell and Schmidt, 2004; Arblaster and Meehl, 2006), but the relative contribution of these two effects remains an open question. This is true especially for the 21st century when stratospheric ozone is expected to recover as a result of the implementation of the Montreal Protocol.

A first sign of ozone recovery is already present in the most recent observations (Eyring *et al.*, 2007; Yang *et al.*, 2005). The marked decrease in stratospheric ozone concentration has stopped around the 2000, and ozone levels has started to increase since that year. Although weak, this increasing trend is found in almost all ground-based and satellite observations (Yang *et al.*, 2005).

An important question is how the different climate models succeed in representing ozone recovery and the consequent effects deriving therefrom.

In a study conducted by Son *et al.* in 2008, a comparison between the Intergovernmental Panel on Climate Change/Fourth Assessment Report (IPCC/AR4) models and Chemistry-Climate Model Validation (CCMVal) models is performed. Unlike the AR4 models, the CCMVal models have a fully interactive stratospheric chemistry, a high vertical resolution in the stratosphere, and a model top located above the stratopause, on average at 50 km. Most AR4 models, instead, have the model top well below the stratopause (Meehl *et al.*, 2007; Cordero and Forster, 2006) and time changes in stratospheric ozone concentrations are ignored by quite half the models. In the remaining group, the ozone recovery is specified either as simple linear time function or from the output of two-dimensional models, which are driven by halogen loading consistent with the Montreal Protocol (Meehl *et al.*, 2007).

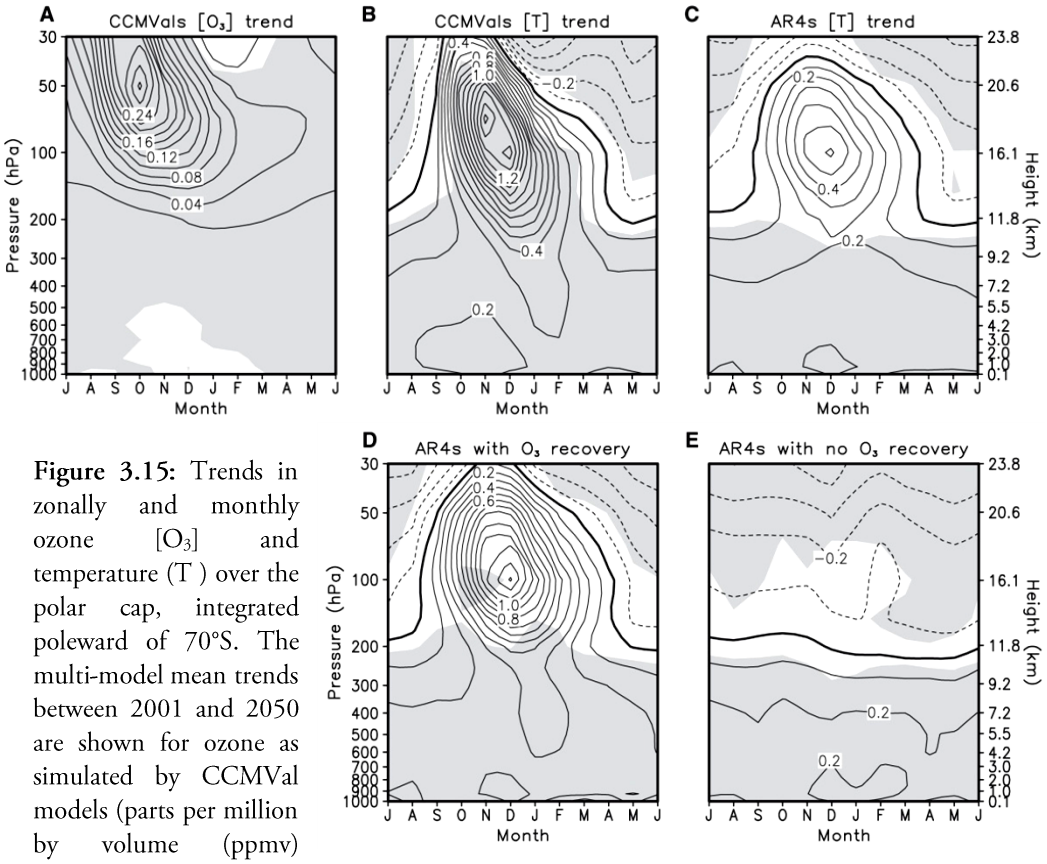

Figure 3.15: Trends in zonally and monthly ozone [O_3] and temperature (T) over the polar cap, integrated poleward of 70°S. The multi-model mean trends between 2001 and 2050 are shown for ozone as simulated by CCMVal models (parts per million by volume (ppmv) decade^{-1}) (A), temperature as simulated by CCMVal models (K decade^{-1}) (B), temperature as simulated by AR4 models (K decade^{-1}) (C), temperature as simulated by AR4 models with prescribed ozone recovery (D), and temperature as simulated by AR4 models with no ozone recovery (E). Values that are greater than one SD are shaded. From Son *et al.* (2008).

Because of the expected disappearance of the ozone hole in the first half of the 21st century, the CCMVal models predict that the tropospheric westerlies in SH summer will be decelerated, on the poleward side, in contrast with the prediction of most IPCC/AR4 atmosphere-ocean-coupled models, whose multi-model mean indicates that the SH westerlies acceleration will continue in 21st century, although at a weaker rate (Miller *et al.*, 2006; Figs. 3.4d, 3.4f, 3.5d and 3.5e).

Since the stratospheric ozone is predicted to increase approximately linearly[12]

[12] Changes in stratospheric ozone concentration in CCMVal model integrations are not perfectly linear, but almost all CCMVal models predict a slow increase until 2010 and a relatively faster increase thereafter until about 2060.

from 2001 to 2050 in almost all CCMVal model integrations (Eyring *et al.*, 2007), it is useful observe linear trends of zonal fields in this time period. Therefore, considering how ozone recovery affects the temperature in the upper troposphere and lower stratosphere, it is possible to see that lower stratospheric temperatures over the SH polar cap increase substantially (Fig. 3.15B), following the strong ozone recovery, whose maximum is found in October at 50 hPa and at lower altitudes in the following months (Fig. 3.15A), as predicted by multi-model mean of CCMVal models. This warming reaches down into the upper troposphere, as has been noted in stratospheric-resolving general circulation model experiments with prescribed ozone depletion (Gillett and Thompson, 2003) and chemistry-climate model integrations for the recent past (Perlwitz *et al.*, 2008). It needs to note that, because of its strong seasonality (Fig. 3.15A), ozone recovery plays a minimal role during other seasons (Perlwitz *et al.*, 2008).

The multi-model mean trend of the polar cap temperature, predicted by all AR4 models, in Figure 3.15C shows instead a much weaker warming and is not statistically significant in the upper troposphere and lower stratosphere. This is due to the way in which ozone is prescribed in the AR4 models. In fact, half of those models have no ozone recovery, and this results in the absence of warming in the lower stratosphere for those models (Fig. 3.15E).

Even when ozone recovery is prescribed (Fig. 3.15D), the AR4 models produce less intense polar cap warming than the CCMVal models because of the large inter-model difference in temperature trends.

The ozone-induced temperature change in the lower-stratospheric polar cap strongly influences the pressure and wind fields in the troposphere below (Thompson and Solomon, 2002; Shindell and Schmidt, 2004; Arblaster and Meehl, 2006). Analyzing the multi-model mean trend in December-to-February mean SH westerlies simulated by CCMVal models (Fig. 3.16A), these winds result to be decelerated on the poleward side, implying a negative trend in Southern SAM index in the future. This result is opposite to the one predicted by the multi-model mean of AR4 models, which shows acceleration on the poleward side of the jet (Fig. 3.16B). The importance of warming, due to ozone increasing, can be cleared if one compares AR4 models with and without a prescribed ozone recovery.

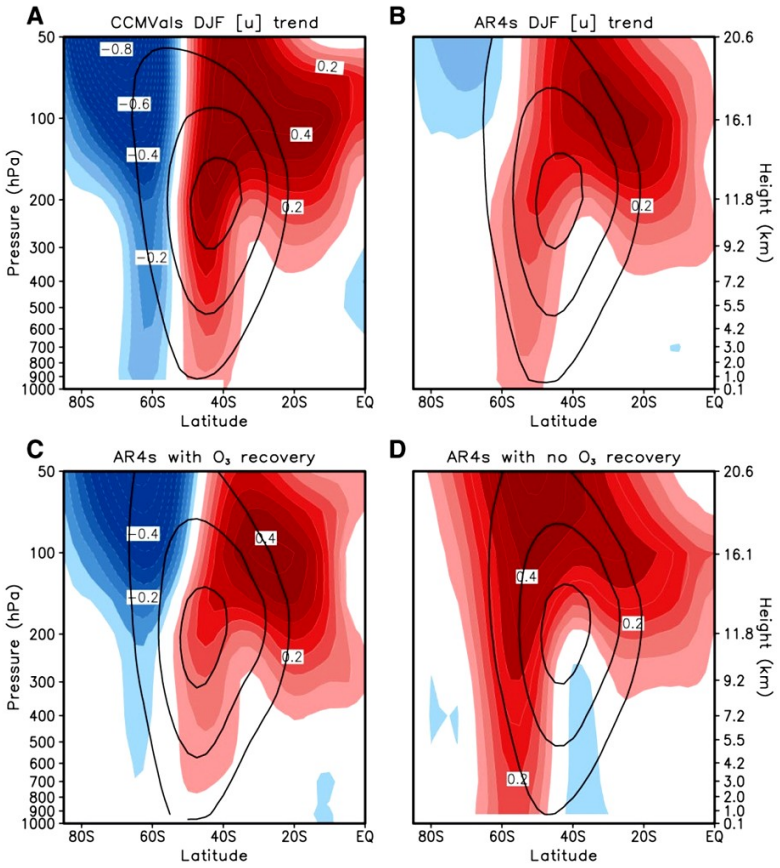

Figure 3.16: Trends in December-to-February (DJF) zonal-mean zonal wind. The multi-model mean trends between 2001 and 2050 are shown for the CCMVal models (A), the AR4 models (B), the AR4 models with prescribed ozone recovery (C), and the AR4 models with no ozone recovery (D). Shading and contour intervals are 0.05 ms–1 decade–3. Deceleration and acceleration are indicated with blue and red colors, respectively, and trends weaker than 0.05 ms–1 decade–1 are omitted. Superimposed black solid lines are DJF zonal-mean zonal wind averaged from 2001 to 2010, with a contour interval of 10 ms^{-1}, starting at 10 $ms^{-3.}$ EQ, equator. From Son *et al.* (2008).

In the first case, the multi-model mean trend for the subset of AR4 integrations with ozone recovery exhibits features qualitatively similar to those in CCMVal models, although the dipolar pattern is weaker and does not reach to the surface (Fig. 3.16C). When the ozone recovery is neglected (Fig. 3.16D), instead, the AR4 models predict the opposite trend in the extratropics. This result indicates that the effect of ozone-induced warming overwhelms that of GHG–induced cooling in the lower-stratospheric polar cap and plays an important role in the acceleration of the tropospheric westerlies during the SH summer.

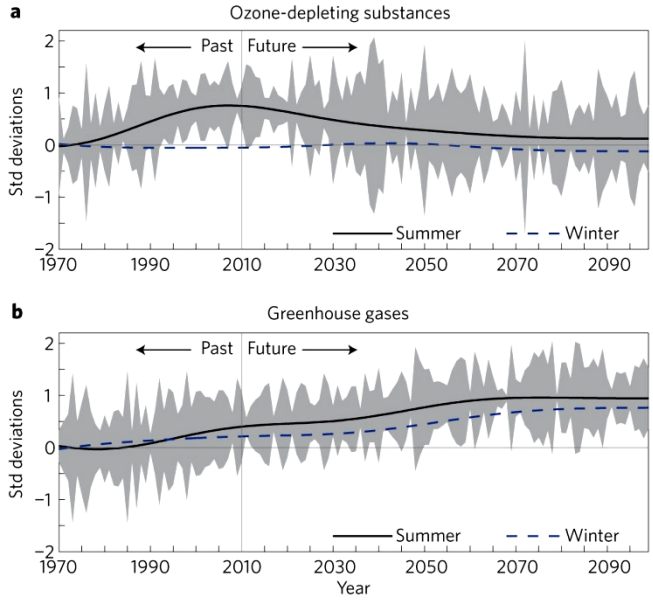

Figure 3.17: Time series of the southern annular mode from transient experiments forced with time-varying ozone-depleting substances and greenhouse gases. Results are from experiments published in ref. 28. a, Forcing with ozone-depleting substances; b, forcing with greenhouse gases. The SAM index is defined as the leading principal component time series of 850-hPa Z anomalies 20–90° S: positive values of the index correspond to anomalously low Z over the polar cap, and vice versa. Lines denote the 50-year low-pass ensemble mean response for summer (DJF; solid black) and winter (JJA; dashed blue). Grey shading denotes ± one standard deviation of the three ensemble members about the ensemble mean (see Methods for details). The long-term means of the time series are arbitrary and are set to zero for the period 1970–1975. Past forcings are based on observational estimates; future forcings are based on predictions reviewed in McLandress *et al.* (2011). From Thompson *et al.* (2011).

Furthermore, climate change experiments have revealed also an intense SAM response to both future increases in GHGs (Son *et al.*, 2009b; Sigmond *et al.*, 2011; McLandress *et al.*, 2011; Shindell and Schmidt, 2004; Arblaster and Meehl, 2006; Fyfe *et al.*, 1999; Kushner *et al.*, 2001; Cai *et al.*, 2003; Brandefelt and Kallen, 2004; Yin, 2005; Lu *et al.*, 2008; Arblaster *et al.*, 2011), and future recovery of the ozone hole (Son *et al.*, 2008, 2009b; Sigmond *et al.*, 2011; McLandress *et al.*, 2011; Shindell and Schmidt, 2004; Arblaster and Meehl, 2006; Perlwitz *et al.*, 2008; Arblaster *et al.*, 2011). Ozone recovery is predicted to lead to a negative trend in the SAM that is limited to the summer months (Fig. 3.17a), whereas GHGs are predicted to lead to a positive trend that extends across both summer and winter seasons (Fig. 3.17b).

Thus, during the summer over the next 50 years, the ozone recovery is expected

to have an effect on the SAM that is equal and opposite to that due to increasing greenhouse gases. During other seasons, instead, the SAM trend is expected to be driven only by GHGs increase towards a high index polarity (Son *et al.*, 2008, 2009a, 2010; Sigmond *et al.*, 2011; McLandress *et al.*, 2011; Shindell and Schmidt, 2004; Arblaster and Meehl, 2006; Perlwitz *et al.*, 2008; Arblaster *et al.*, 2011; Polvani *et al.*, 2011b).

Thus, ozone recovery results to be able to affect SH climate in several way (Son *et al.*, 2009b), so it is really important to include this condition in predictions of the SH climate in the 21st century.

Therefore, if the representation of the stratosphere can imply a different representation of SH changes to which extent, future projections made by models with a limited representation of stratospheric dynamics are reliable?

Chapter 4

Response in zonal mean zonal wind and temperature fields

In the following two chapters, the original analysis performed within this thesis work is shown. I have used NetCDF[1] (*Network Common Data Form*) starting data files, downloaded by the CMIP5 website (indicated previously in Section 2.2). The data files have been processed in order to obtain zonal and meridional means, long-term means, linear trends, significance tests and to select specific variables, pressure levels, months and years, used in the analysis. To this aim, I have I have written scripts in UNIX language and used the CDO (*Climate Data Operators*) software and IDL (*Interactive Data Language*) language. The figures reported in Chapter 4 and Chapter 5 have been realized by using IDL and GrADS[2] (Grid Analysis and Display System).

In this particular section we discuss past changes in the stratosphere and the troposphere of the SH in reanalyses data and CMIP5 models. Specifically, this chapter is dedicated to highlight and comment if different stratospheric dynamics in models can imply significant differences in response to forcing. Here, all the figures will represent zonal mean climatologies of temperature and zonal wind fields together with their linear trends over 1979-1999. The time period has been chosen because it corresponds to the strongest ozone reduction in the SH and because reanalyses in the SH are more robust after the assimilation of satellite products. It is

[1] NetCDF is a set of software libraries and self-describing, machine-independent data formats that support the creation, access, and sharing of array-oriented scientific data. For further information see the website: http://www.unidata.ucar.edu/software/netcdf/ .

[2] See the website: http://www.iges.org/grads/.

known indeed that before and after 1979, reanalyses in the stratosphere do show "jumps", and therefore cannot be used for estimating linear trends (Randel, W., personal communication). Linear regressions on monthly mean fields have been calculated using least square fit analysis; 90, 95 and 98 % significances following a 2-tailed t-Student test are reported.

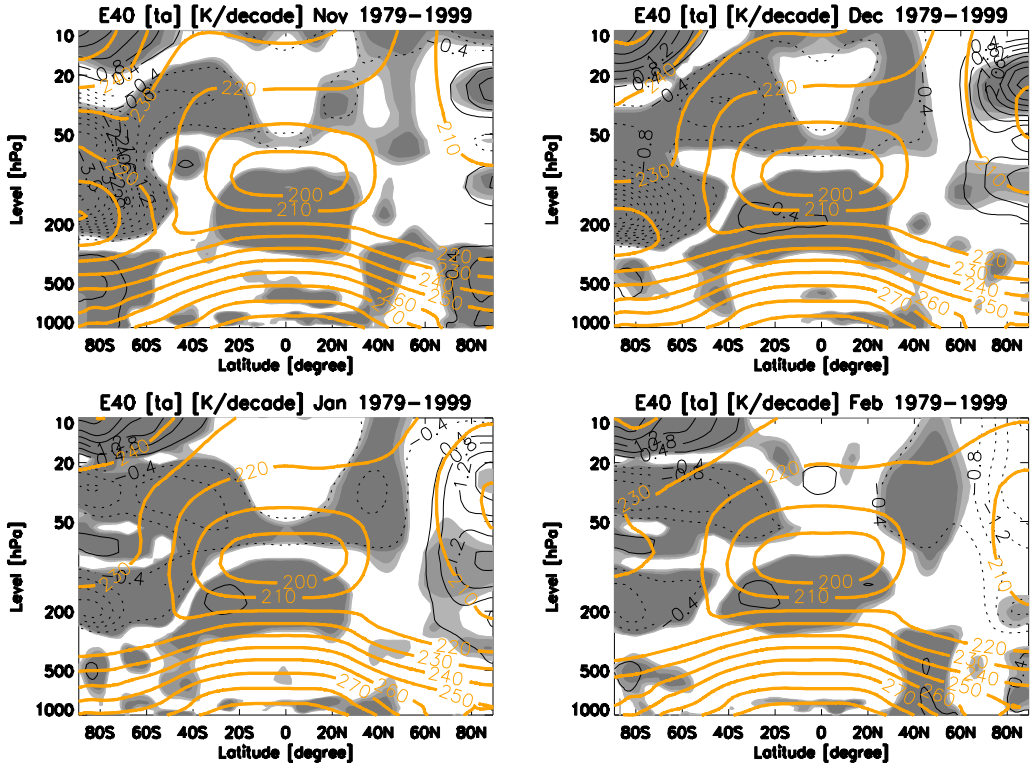

Figure 4.1: The long-term mean (thick orange) and linear trend (thin black contour) of : (*top left*) November, (*top right*) December, (*bottom left*) January, (*bottom right*) February zonal mean temperature [ta] over 1979–1999 ERA40 reanalysis data. Contour intervals of climatological temperature and trend are 10 K starting from 200 K and 0.4 K/decade, respectively. Trends which are statistically significant at the 90, 95 and 98% confidence levels are shaded. Zero contours are omitted.

4.1 Zonal mean temperature in ERA-40 reanalyses

The ozone trend in the stratosphere is the maximum in spring (October) and continues until December-January (summer, see Figure 3.12*top*). However, the effect on the temperature in the stratosphere is delayed of about one month (in

November, see Figure 3.12*right*); this delay is consistent with observations and likely caused by the relatively long radiative time scale in the lower stratosphere, which is about a month (Thompson and Solomon, 2002). We can therefore expect the strongest effect on circulation in the summer season (DJF for the SH).

Figure 4.1 shows the global zonal mean temperature field climatologies and trends derived from ERA-40 reanalysis data in the November-to-February period. It is possible to see that in November (Fig. 4.1 *top left*) a rather strong cooling (-3.6 K/decade) occurs at level pressure between 50 and 200 hPa over the SH polar cap. At correspondent pressure levels at equatorial latitudes, instead, there is a warming in the upper troposphere, which is found throughout the year because of GHGs increase. At and above 200 hPa pressure level, for example, an equatorial warming trend found at the same time as the polar cooling trend implies an intensification of the temperature meridional gradient. The stratospheric cooling tends to persist in December (Fig. 4.1 *top right*) and then, quickly reduces in January and February (Figs. 4.1 *bottom*). Furthermore, the long-term mean (the *climatology*) contours show the mean thermal structure of the atmosphere. As a consequence of the strong stratospheric cooling over polar cap region, the tropopause tends to rise at high latitudes with respect to normal conditions.

4.2 Zonal mean temperature in HT Models

Same zonal mean temperature trends for a subset[3] of HT models participating in CMIP5 simulations are shown in Figures 4.2a,b. As the majority of the models use the same ozone forcing data derived from observations (Cionni *et al.*, 2011), we could expect a similar response in the lower stratospheric temperature, over the same period as for reanalyses. However, not all the models have used the same ozone profiles. Some of them for example have either used ozone fields derived from CCM simulations, or they have simulated their own ozone because they have an interactive chemistry module in the stratosphere.

The analysis has been performed for all the models described in Table 2.1 in Section 2.3 (all the models are shown in Appendix B), however here we report results for the following models: CMCC-CMS, GFDL-CM3, MIROC-ESM-

[3] Results of the whole set of CMIP5 climate models used in this study represented in graphics reported in Appendix B.

CHEM, and MPI-ESM-MR. This subset has been chosen to describe the possible range of responses found across the models. The other models report a behaviour similar to one of the four models shown in Figures 4.2a,b.

MIROC-ESM-CHEM and GFDL-CM3 report a cooling in November and December, that is much stronger than ERA-40 (maximum -12 K/decade for MIROC-ESM-CHEM, -15 K/decade for GFDL-CM3) between 50 and 200 hPa (Figs. 4.2a,b). These two HT models are also among the models including an interactive chemistry module in their simulations, possibly explaining the strong temperature trends. The other two chosen models are the CMCC-CMS and MPI-ESM-MR model (Fig. 4.2a). CMCC-CMS reports a SH polar lowest cooling in November of about -6.4 K/decade, larger than ERA-40 but smaller than GFDL-CM3 and MIROC-ESM-CHEM. MPI-ESM-MR model instead is not able to reproduce any cooling in November. In the following months the four models show a different behaviour in the polar stratosphere: CMCC-CMS has a cooling in line with ERA-40 (about 2K/decade in December, 0.8 K/decade in January), smaller in February only; GFDL-CM3 a much stronger cooling from December to February; MIROC-ESM-CHEM a stronger cooling in December only and then a cooling in good agreement with ERA-40; MPI-ESM-MR is never able to reproduce a reliable cooling until January and February.

Therefore, three of the models show a cooling trend stronger than ERA-40 reanalysis in November at altitudes between 50 and 200 hPa, with a better agreement with reanalysis found in the CMCC-CMS. An equatorial warming due to annual increase of GHGs can also be found in the troposphere. In the CMCC-CMS indeed there is a very significant warming trend (0.4 K/decade) at tropical latitudes between 500 hPa and just above the equatorial tropopause that persists in the whole November-to-February season (in February moves also just below 500 hPa), together with another warming component of the same intensity at polar latitudes, where disappearing in February. Specifically, in November the warming trend is in part confined in the troposphere more near to the surface (although statistically insignificant) over a region poleward of about 70°S and in part extends from about 300 hPa downward to the surface with a good significance level, located in the circumpolar area at latitudes between 50°S and 70°S. In December instead, the circumpolar component trend moves poleward and is found over the polar cap between 70°S and 90°S in the mid-lower troposphere. In the other two models (MIROC-ESM-CHEM and GFDL-CM3) a similar polar cap warming trend

cannot be found, therefore in less agreement with reanalyses. GFDL-CM3 shows a stronger warming (0.8 K/decade) between 40°S and 70°S only in the mid-lower troposphere in the December-January months with 90-95% confidence level, whereas the equatorial trend can be observed in February only in the entire troposphere. MIROC-ESM-CHEM instead presents a warming of about 0.8 K/decade at the equatorial tropopause only. Comparing to ERA-40 results, we can see that CMCC-CMS shows on average a better overall agreement in both the stratosphere , the troposphere and in the seasonality of the cooling.

Another particularity of the three model trends, as also found in reanalyses, is given by the appearances of a strong warming above the lower stratosphere cooling, in correspondence of the polar cap between 64°S and 90°S. The warming response in the upper stratosphere is a typical dynamical response found in HT models possibly deriving from the gravity waves-mean flow interaction, initiated in the upper stratosphere and mesosphere, that in those models are represented (Manzini *et al.,* 2003). Specifically, this dynamical warming can be associated to increase in the gravity wave induced downwelling because of increased gravity wave momentum flux deposition in the lower mesosphere. In ERA-40 this dynamical contribution persists in the whole November-to-February season with the warming confined above 20 hPa, between nearly 40°S and 90°S, reaching maximum value in December (2,4 K/decade). In GFDL-CM3 the trend is found above 20 hPa in November, and it moves downward in the following months, reaching down 50 hPa in February. In this HT model, the dynamical warming is quite intense (6 K/decade) in November. CMCC-CMS reports a weaker warming (2 K/decade) and limited to November. MIROC-ESM-CHEM instead seems to dynamically respond with 1-month delay in December with a maximum warming trend comparable to that of CMCC-CMS (2 K/decade).

The fourth chosen model is MPI-ESM-MR (Fig. 4.2b). This HT model presents an irregular behaviour in its long-term trend over the 1979-1999 resulting in a weak warming in November in the lower stratosphere rather than a cooling, and a following weak cooling in December-to-February. Given that this model use the same ozone profile as CMCC-CMS, we expect that the difference come from both the parameterization of radiation in the SW domain within the model itself and the feedback in dynamical cooling (the two models have the same representation of the stratosphere).

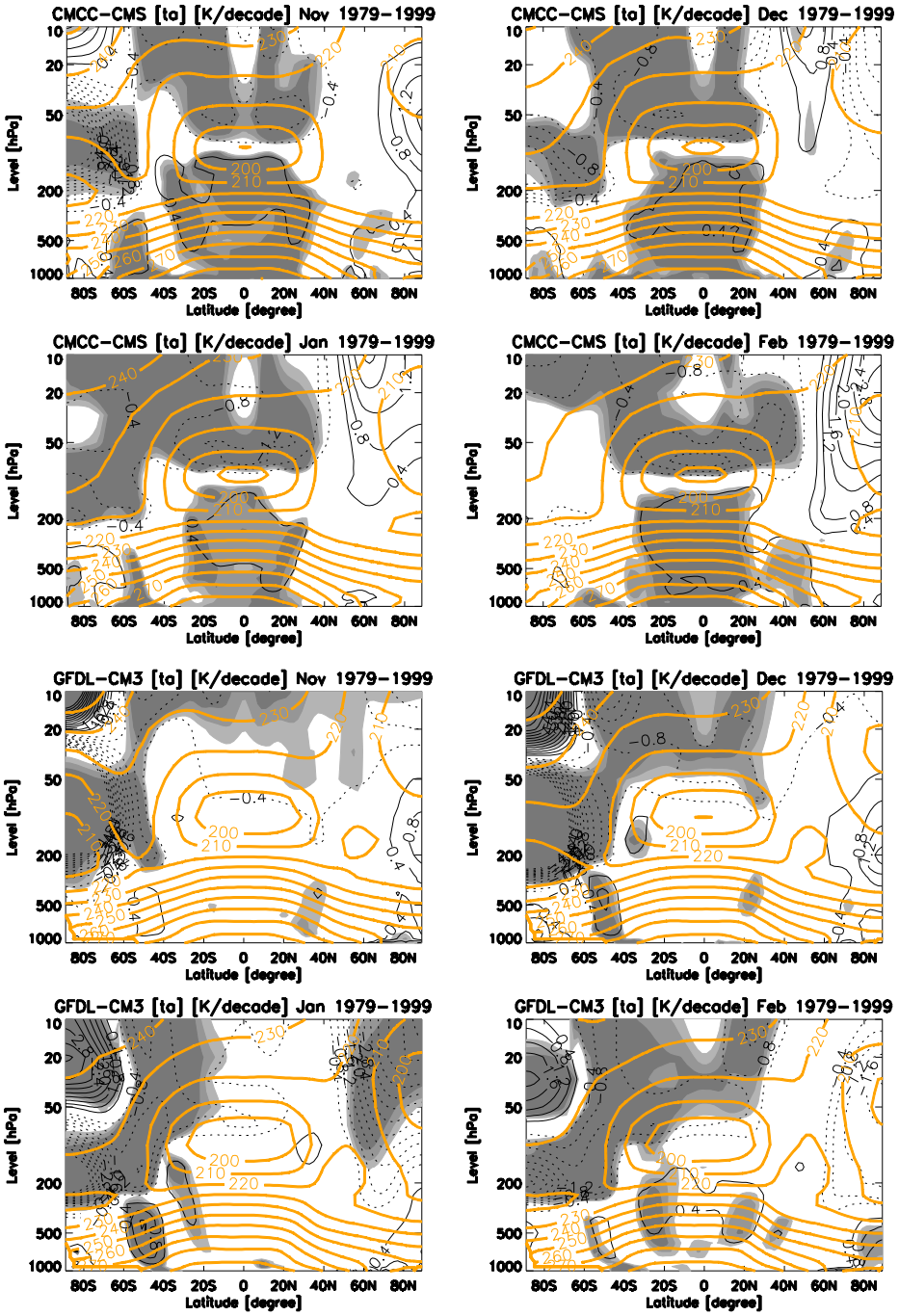

Figure 4.2a: The long-term mean (thick orange) and linear trend (thin black contour) of November, December, January, and February zonal mean temperature [ta] over 1979–1999: (*left*)CMCC-CMS, and (*right*) GFDL-CM3 HT model data. Contour intervals of climatological temperature and trend are 10 K starting from 190 K and 0.4 K/decade, respectively. Trends which are statistically significant at the 90, 95 and 98% confidence levels are shaded. Zero contours are omitted.

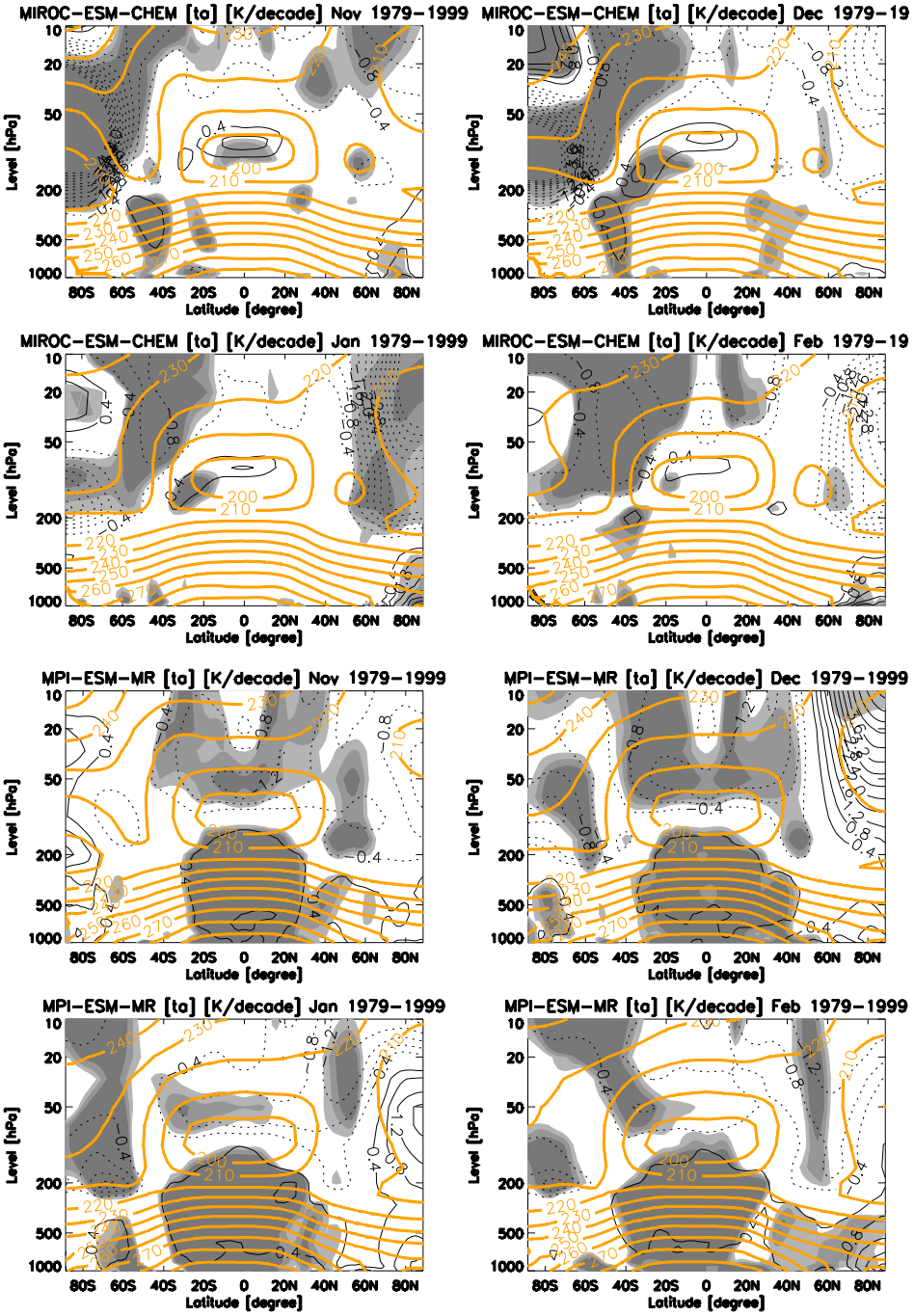

Figure 4.2b: The long-term mean (thick orange) and linear trend (thin black contour) of November, December, January, and February zonal mean temperature [ta] over 1979–1999: (*left*) MIROC-ESM-CHEM, and (*right*) MPI-ESM-MR HT model data. Contour intervals of climatological temperature and trend are 10 K starting from 190 K and 0.4 K/decade, respectively. Trends which are statistically significant at the 90, 95 and 98% confidence levels are shaded. Zero contours are omitted.

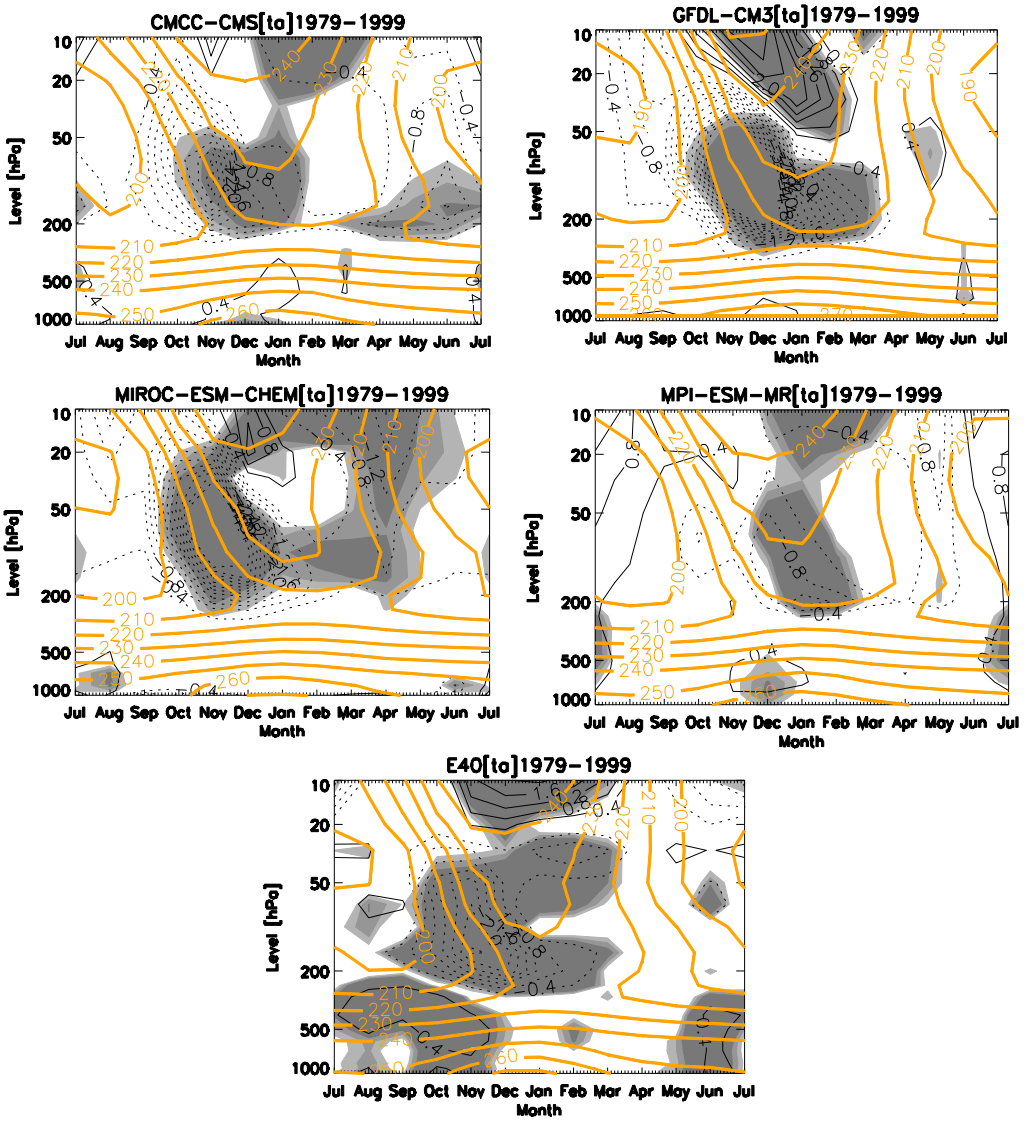

Figure 4.3: The long-term monthly mean (thick orange) and linear trend (thin black contour) of zonal mean temperature [ta] over 1979–1999, averaged poleward of 64°S: (*top left*) CMCC-CMS, (*top right*) GFDL-CM3, (*middle left*) MIROC-ESM-CHEM, (*middle right*) MPI-ESM-MR HT models, and (*bottom*) ERA-40 reanalysis data. Contour intervals of climatological temperature and trend are 10 K starting from 190 K and 0.4 K/decade, respectively. Trends which are statistically significant at the 90, 95 and 98% confidence levels are shaded. Zero contours are omitted.

In order to analyze the seasonality of the zonal mean temperature trends over the polar cap region, we plot trends averaged over latitudes between 64°S and 90°S, as a function of the altitude coordinate and month. The same CMIP5 HT models shown in the previous figure are reported in Figures 4.3a and 4.3b. GFDL-CM3

(Fig. 4.3 *top right*) and MIROC-ESM-CHEM (4.3 *middle left*) report a really strong stratospheric cooling on the spring SH polar cap, as discussed before.

We note a significant maximum cooling in November-December period with a larger intensity in GFDL-CM3 (-15 K/decade, against the -3 K/decade for ERA-40 maximum trend) between the 50 and 200 hPa pressure levels (MIROC-ESM-CHEM maximum results to be located higher between about 100 and 30 hPa), with a warming above, again larger in GFDL-CM3 model (2.8 K/decade) than MIROC-ESM-CHEM trend (1.2 K/decade) at 10-20 hPa altitudes, in the same months. CMCC-CMS also has similar negative-trend peaking in November with a weaker maximum (about -3.6 K/decade) at 50-200 hPa, overtopped by smaller warming (1.2 K/decade). Indeed these three HT models represent the seasonality in the ozone-depletion response similar to stratospheric response given by ERA-40 reanalyses, shown in Fig. 4.3 *bottom right.* The zonal mean temperature negative-trend in these HT models response tends to persists in time and maintaining its intensity also until January or February in the middle and lower stratosphere, determining different tropopause height (not shown) and different temperature climatologies.

MPI-ESM-MR is a very singular case among the HT models. It tends to cool very weakly with a very small temperature trend (-0.8 K/decade) during SH summer (December to February).

In the troposphere (below 200 hPa), ERA-40 reanalyses make evident the presence of weak warming trend (0.4 K/decade) in both June and the July-to-November period and with 95-98% significance level. These trends are partially shown also in MIROC-ESM-CHEM, GFDL-CM3 and CMCC-CMS. The first shows positive polar-cap temperature trends in the July-August period below 500 hPa reaching the surface (although with lower significance), whereas the other two models display a positive trend in the November-to-January months (CMCC-CMS with 90% significance whereas GFDL-CM3 gives insignificant positive trend). MPI-ESM-MR shows a significant positive trend in the November-to-January and July months at 500-850 hPa levels, in agreement with ERA-40.

4.3 Zonal mean temperature in LT Models

The same analysis conducted on LT models is shown in the following figures. Here again, the following four LT models are discussed in detail: bcc-csm1-1,

CMCC-CM, FGOALS-g2, and MIROC4h.

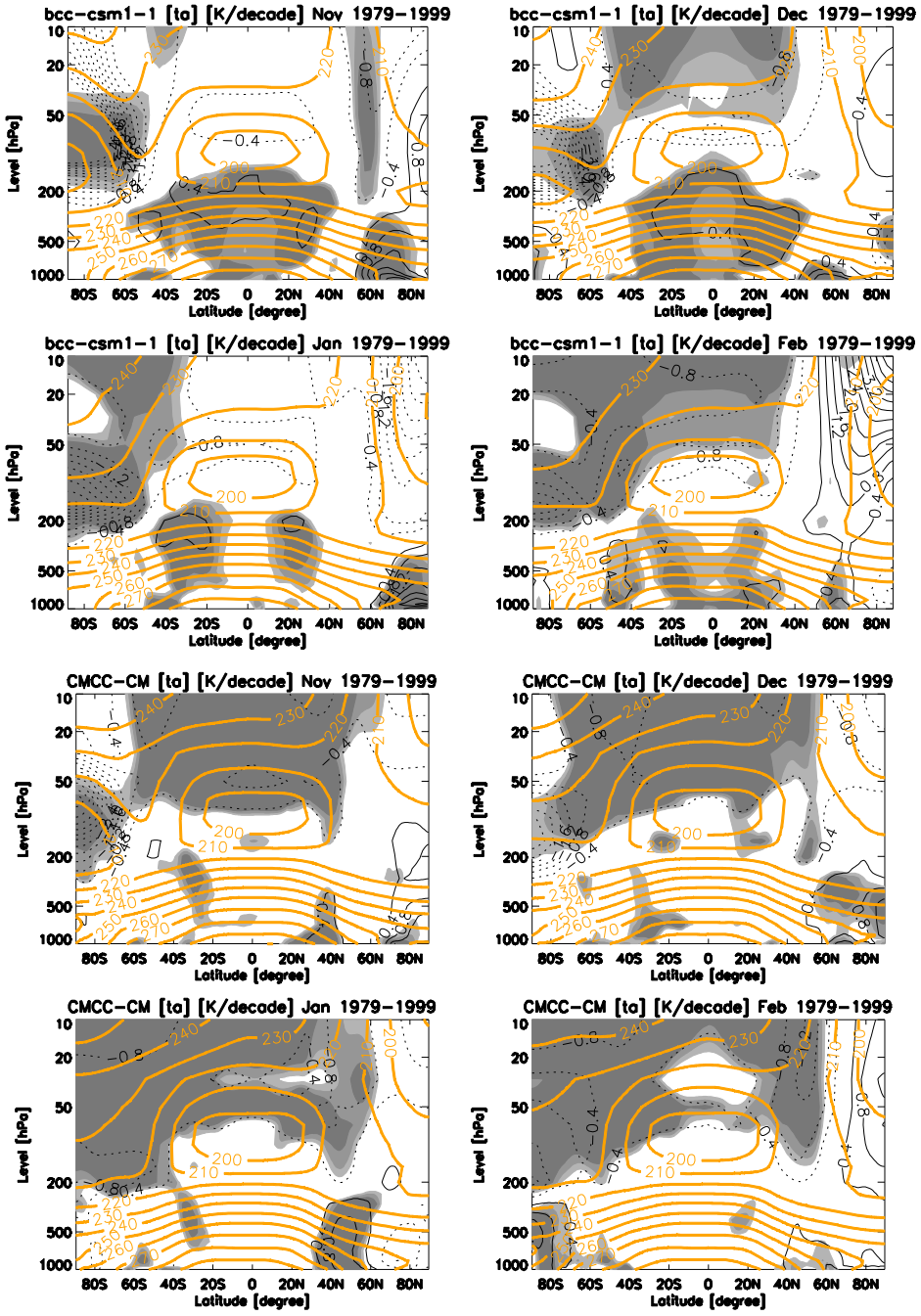

Figure 4.4a: The long-term mean (thick orange) and linear trend (thin black contour) of November, December, January, and February zonal mean temperature [ta] over 1979–1999: (*left*) bcc-csm1-1, and (*right*) CMCC-CM LT model data. Contour intervals of climatological temperature and trend are 10 K starting from 190 K and 0.4 K/decade, respectively. Trends which are statistically significant at the 90, 95 and 98% confidence levels are shaded. Zero contours are omitted.

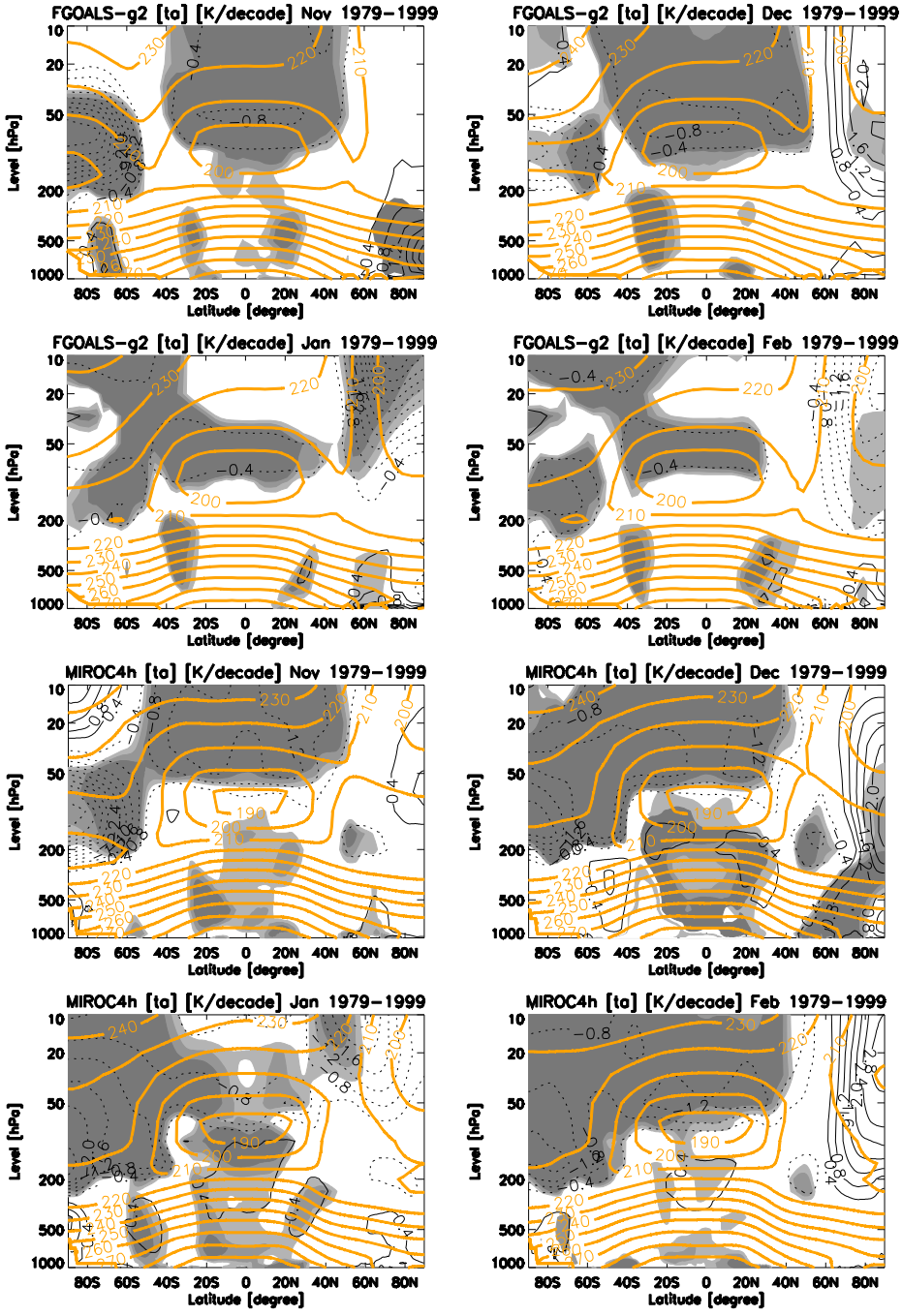

Figure 4.4b: The long-term mean (thick orange) and linear trend (thin black contour) of November, December, January, and February zonal mean temperature [ta] over 1979–1999: (*left*) F-GOALS-g2, and (*right*) MIROC4h LT model data. Contour intervals of climatological temperature and trend are 10 K starting from 190 K and 0.4 K/decade, respectively. Trends which are statistically significant at the 90, 95 and 98% confidence levels are shaded. Zero contours are omitted.

LT model typical response is given by a relatively weaker cooling trend during November in the SH polar stratosphere between 50 and 200 hPa with respect to HT models but in agreement with reanalyses, with a quite rapid attenuation in magnitude just in December, as we can see in CMCC-CM, FGOALS-g2, and MIROC4h models (Figs. 4.4a and 4.4b). In the first model indeed, the negative trend results to be very strong (-4.8 K/decade), although its rapid attenuation. Moreover, in this class of models the warming representative of dynamical response in the upper stratosphere is missing, except for a few of them.

For example, an upper stratospheric warming trend is found in MIROC4h model (although it is not statistically significant), which is the LT model more similar to a HT model, with a rather intense significant lower stratospheric cooling (4 K/decade) over polar cap and a climatological lower stratosphere temperatures more similar to the other HT models than those deriving from the LT models. In bcc-csm1-1 model, where it is present a stronger stratospheric cooling in spring (-4.8 K/decade), it also found an equatorial warming in December, due to GHGs contribute in the upper troposphere (Fig. 4.4a). MIROC4h indeed presents similar equatorial trends in December-January.

Concerning tropospheric trends, we can find a significant circumpolar warming in FGOALS-g2 at 60°S-80°S latitudes in November, and in MIROC4h in February (it has indeed a midlatitude tropospheric warming in January), below 300 hPa. More intense is the CMCC-CM polar warming (1.2 K/decade) in February with 95-98% significance level, consistent with reanalyses but 2-months shifted with respect to these.

As in previous section, in Figure 4.5 trends in the 64°S -90°S latitudinally averaged zonal mean temperatures are shown.

FGOALS-g2 model (Fig. 4.5 *middle left*) response shows to have an isolated cooling trend in the lower stratosphere with a maximum in October-November with a 95% confidence level, consistently with ERA-40 reanalyses results (Fig. 4.5 *bottom right*). Indeed this model presents also a second cooling in the same atmospheric region in February but with weaker intensity. Bcc-csm1-1 (Fig. 4.5 *top left*) and MIROC4h (Fig. 4.5 *middle right*) report a cooling that involves also the middle-upper stratosphere in early September (although insignificant), and then moves down to the lower stratosphere where it registers a maximum value around November. However, MIROC4h also presents upper-stratospheric warming in November. CMCC-CM reports a weaker lower stratospheric cooling trend in

November and a middle-upper stratospheric warming in early spring (Fig. 4.5 *top right*).

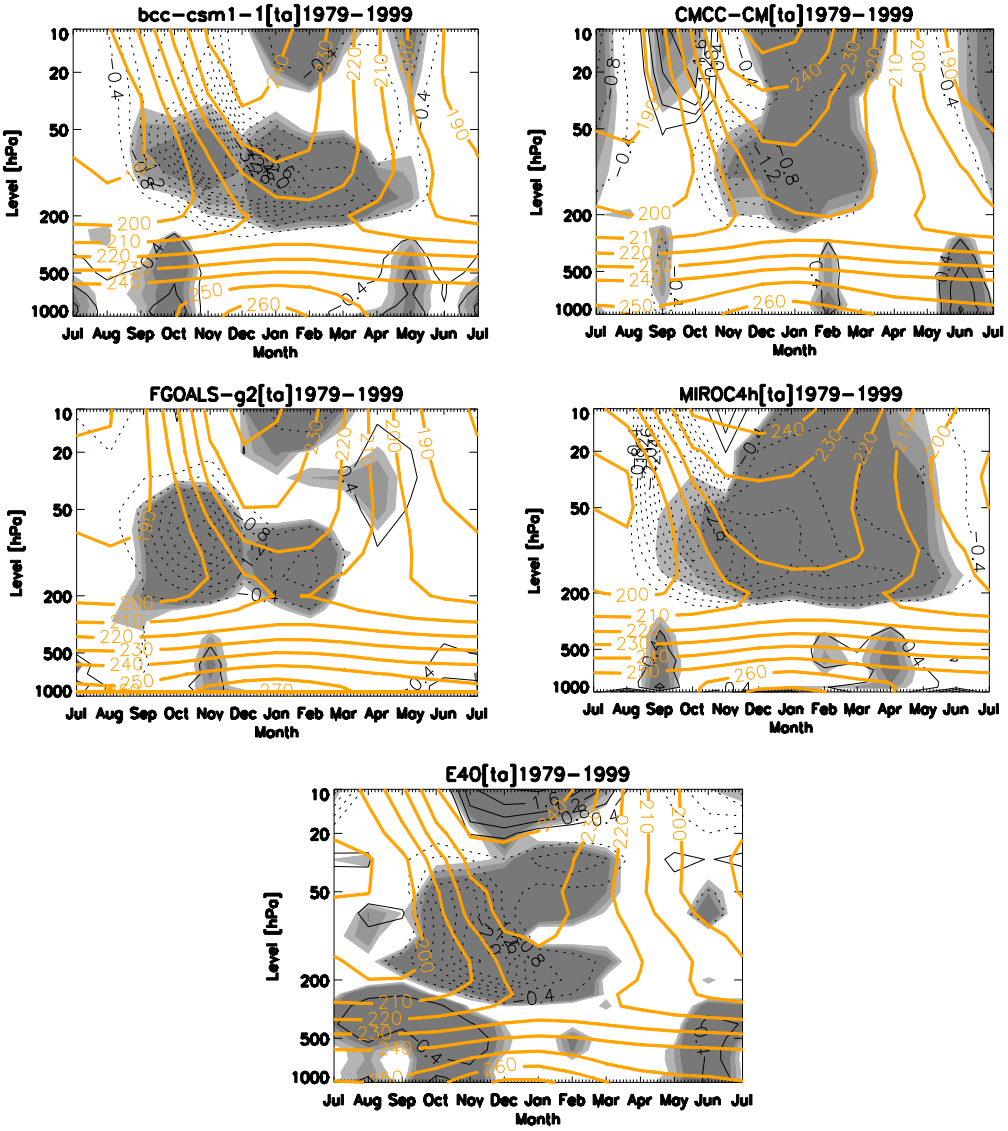

Figure 4.5: The long-term monthly mean (thick orange) and linear trend (thin black contour) of zonal mean temperature [ta] over 1979–1999, averaged poleward of 64°S: (*top left*) bcc- csm1-1, (*top right*) CMCC-CM, (*middle left*) FGOALS-g2, (*middle right*) MIROC4h LT models, and (*bottom*) ERA-40 reanalysis data. Contour intervals of climatological temperature and trend are 10 K starting from 190 K and 0.4 K/decade, respectively. Trends which are statistically significant at the 90, 95 and 98% confidence levels are shaded. Zero contours are omitted.

Furthermore, bcc-csm1-1, CMCC-CM, and MIROC4h are the LT models

that best represent significant tropospheric polar warming ascribed to GHGs increase, found in the May-to-November period in ERA-40. Specifically, CMCC-CM shows a warming in June-July significant at 98%, whereas bcc-csm1-1 presents it in February-October months. MIROC4h has positive tropospheric trend in September, but it also shows a second warming pattern in February-to-May period.

To summarize, the difference in the temperature response between the chosen HT and LT models is mainly related to the absence of a dynamical upper stratospheric warming over the spring-summer cooling in LT models. This cooling then appears to be much larger in HT models with an interactive chemistry scheme than in reanalyses, smaller in LT models. However, the cooling itself has a very spread representation (i.e. it is not possible to clearly derive a typical HT versus LT response).

4.4 Multi-Model averages of zonal mean temperature

In order to highlight major differences between the HT and LT models response to ozone depletion here we show a multi-model analysis distinguishing between the two climate model versions which have different stratospheric representations. In this section all CMIP5 models reported in Table 2.1 (except EC-Earth, that misses the 10 hPa level) have been used.

Before performing multi-model averages, an interpolation of all the model variables on a new common horizontal and vertical grid has been performed. We have chosen a T42 grid in latitude and longitude and selected the same vertical levels (from 1000 hPa up to 10 hPa) for each model. After interpolation multi-model averages and trends have been calculated.

As it has been seen for single-model analysis, HT models are characterized by their strong cooling trend peaking in November in the polar SH lower stratosphere due to both radiative and dynamical reasons, overtopped by the adiabatic-heating positive trend possibly due to a model dynamical response involving gravity waves. The ozone-depletion derived cooling maintains its magnitude until December, progressively weakening from January. These results are also featured by a 98% confidence level (Fig. 4.6 *top left*). Both the climatologic responses in zonal mean temperature are quite consistent with observations, represented in Figure 4.6 *bottom*

right through ERA-40 reanalysis data.

LT multi-model-mean trend for the zonal mean temperature response, instead, has a similar profile but shows a smaller intensity and a faster attenuation. The climatology contours instead seems to be similar to those of HT multi-model case.

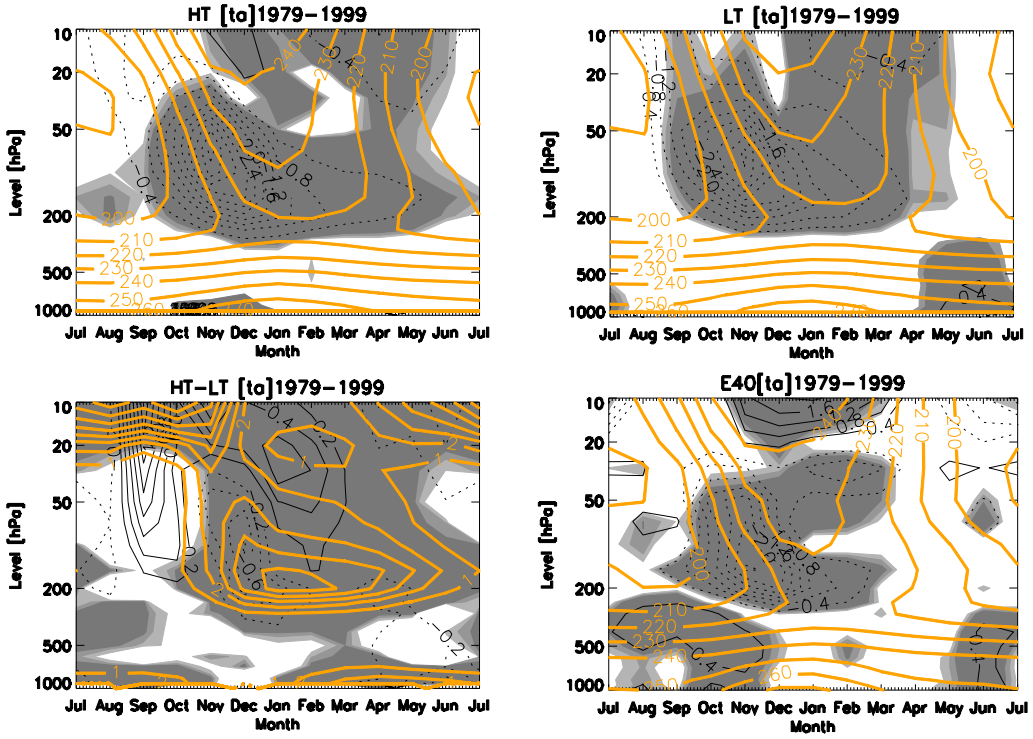

Figure 4.6: The long-term monthly mean (thick orange) and linear trend (thin black contour) of zonal mean temperature [ta] over 1979–1999, averaged poleward of 64°S: (*top left*) HT multi-model mean, (*top right*) LT multi-model mean, (*bottom left*) HT minus LT difference, (*bottom right*) ERA-40 reanalysis data. Contour intervals of climatological temperature and trend are 10 K starting from 190 K and 0.4 K/decade, respectively in *top* and *bottom right* figures. In *bottom left* figure, contour intervals of climatological temperature and trend are 1 K starting from 1 K and 0.2 K/decade, respectively. Trends which are statistically significant at the 90, 95 and 98% confidence levels are shaded. Zero contours are omitted.

Analyzing HT minus LT multi-models response difference (Fig. 4.6 *bottom left*), it is very interesting to identify higher climatologic temperatures in both SH summer lower stratosphere and SH winter middle-upper stratosphere. Specifically, the higher climatologic polar zonal mean temperature maintains until the austral winter beginning. Observing HT and LT single climatologies and comparing these

with ERA-40, we can immediately deduce that the first class of models is more in agreement with reanalysis results. Concerning trend differences, HT models display a summer cooling about 30% larger than LT models.

4.5 Zonal mean zonal wind in ERA-40 reanalyses

As expected, the cooling and enhanced temperature gradient between high and low latitudes in the lower stratosphere induce a zonal mean zonal wind acceleration that propagates from the stratosphere down to the surface, influencing the tropospheric midlatitude jet, as shown in Figure 4.7 for ERA40.

Linear trends have been estimated for the same period as temperature trends (1979-1999). It is possible to note that the strongest significant zonal mean zonal wind polar jet acceleration in the stratosphere is found in November at around 60°S, 50-20 hPa (peaking at about 3.2 m/s/decade; Fig. 4.7 *top left*) in correspondence with the maximum of the jet in that season (orange contours) and in correspondence with the strongest temperature trend discussed above. The stratospheric jet trend is still present in December (Fig. 4.7 *top right*), when the climatology has reversed to easterlies (no orange contours). These trends are consistent with a later transition to easterlies in this season. Moreover, in December the wind trend is found down at the tropopause level and at the surface, with a contour of about 0.4 m/s/decade. These trends in the troposphere correspond with a westerly acceleration of the mid-latitude jet on its poleward side.

At the equator, an alternating pattern of positive and negative winds is found following the vertical structure of the QBO (Quasi-Biennial Oscillation). The wind acceleration in December (Fig. 4.7 *top right*) has a maximum at 50 hPa (lower than the November maximum) coming down at 60°S-50°S. This propagation to the troposphere continues also in January (Fig. 4.7 *bottom left*), when the climatological midlatitude tropospheric jet in SH is strongly accelerated with a maximum on average at 50°S below tropopause set at 200 hPa. In this month, the maximum of the jet is located at the tropopause level, suggesting that feedbacks involving synoptic scale eddies could be invoked to explain such a persistence (the cooling peaks at 200 hPa, though reduced in amplitude). In January, in particular, we can see a positive linear trend exactly on the poleward side of climatological jet, meaning an acceleration in this side, against the equatorial side that is weakly decelerated. In

this way we could expect that climatological jet position is moved poleward (jet shift consideration will be drawn in the next chapter). The shift of the jet is then associated with a change in the cyclonic and anticyclonic wave breaking regions at the two sides of the jet (Ndarana *et al.*, 2010) Then, this trend becomes weaker until it disappears in February (Fig. 4.7 *bottom right*).

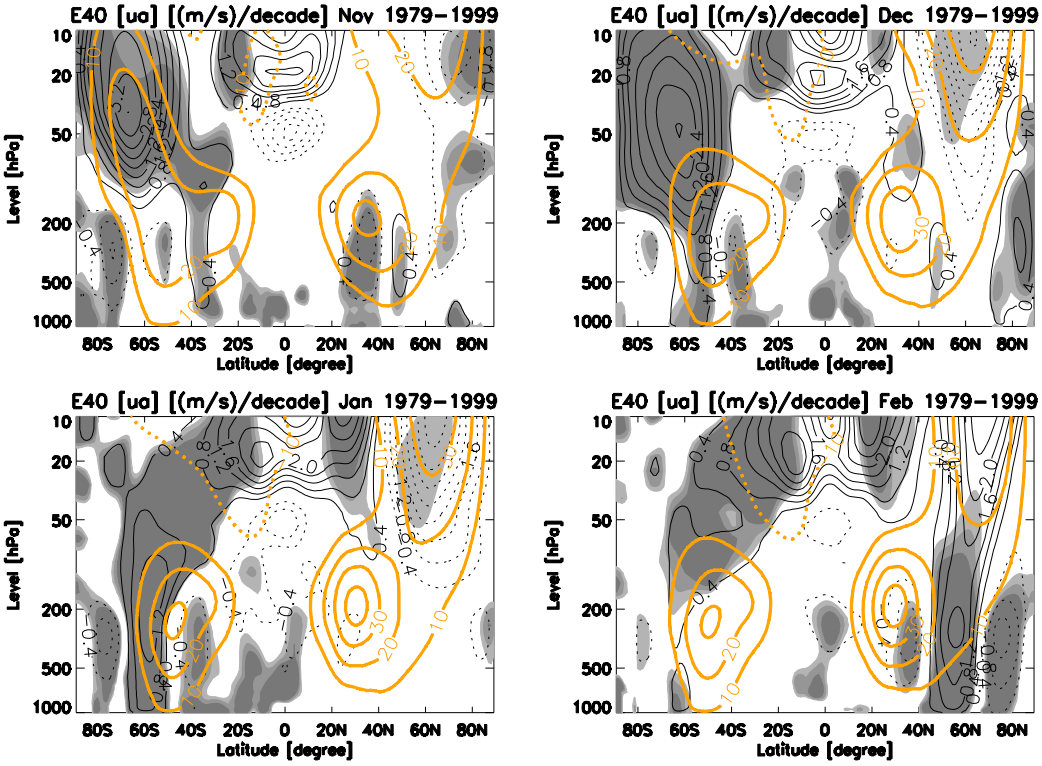

Figure 4.7: The long-term mean (thick orange) and linear trend (thin black contour) of : (*top left*) November, (*top right*) December, (*bottom left*) January, (*bottom right*) February zonal mean zonal wind [ua] over 1979–1999 ERA40 reanalysis data. Contour intervals of climatological wind and trend are 10 m s^{-1} starting from 10 m s^{-1} and 0.4 (m s^{-1})/decade, respectively. Trends which are statistically significant at the 90, 95 and 98% confidence levels are shaded. Zero contours are omitted.

4.6 Zonal mean zonal wind in HT Models

The same analysis has been conducted on the same subset of HT models, discussed in the previous sections (CMCC-CMS, GFDL-CM3, MIROC-ESM-CHEM, and MPI-ESM-MR).

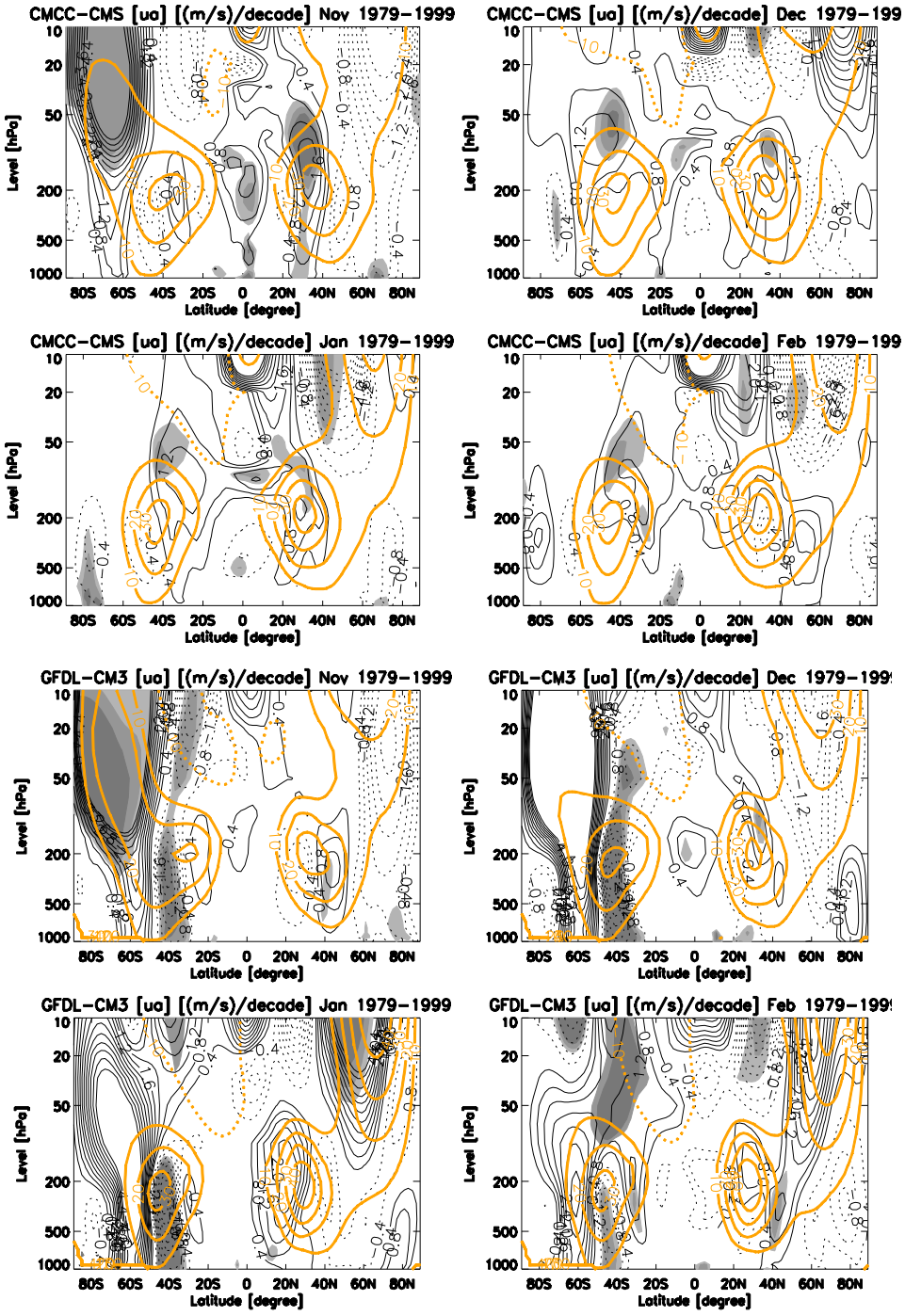

Figure 4.8a: The long-term mean (thick orange) and linear trend (thin black contour) of November, December, January, and February zonal mean zonal wind [ua] over 1979–1999: (*left*) CMCC-CMS, and (*right*) GFDL-CM3 HT model data. Contour intervals of climatological wind and trend are 10 m s^{-1} starting from 10 m s^{-1} and 0.4 (m s^{-1})/decade, respectively. Trends which are statistically significant at the 90, 95 and 98% confidence levels are shaded. Zero contours are omitted.

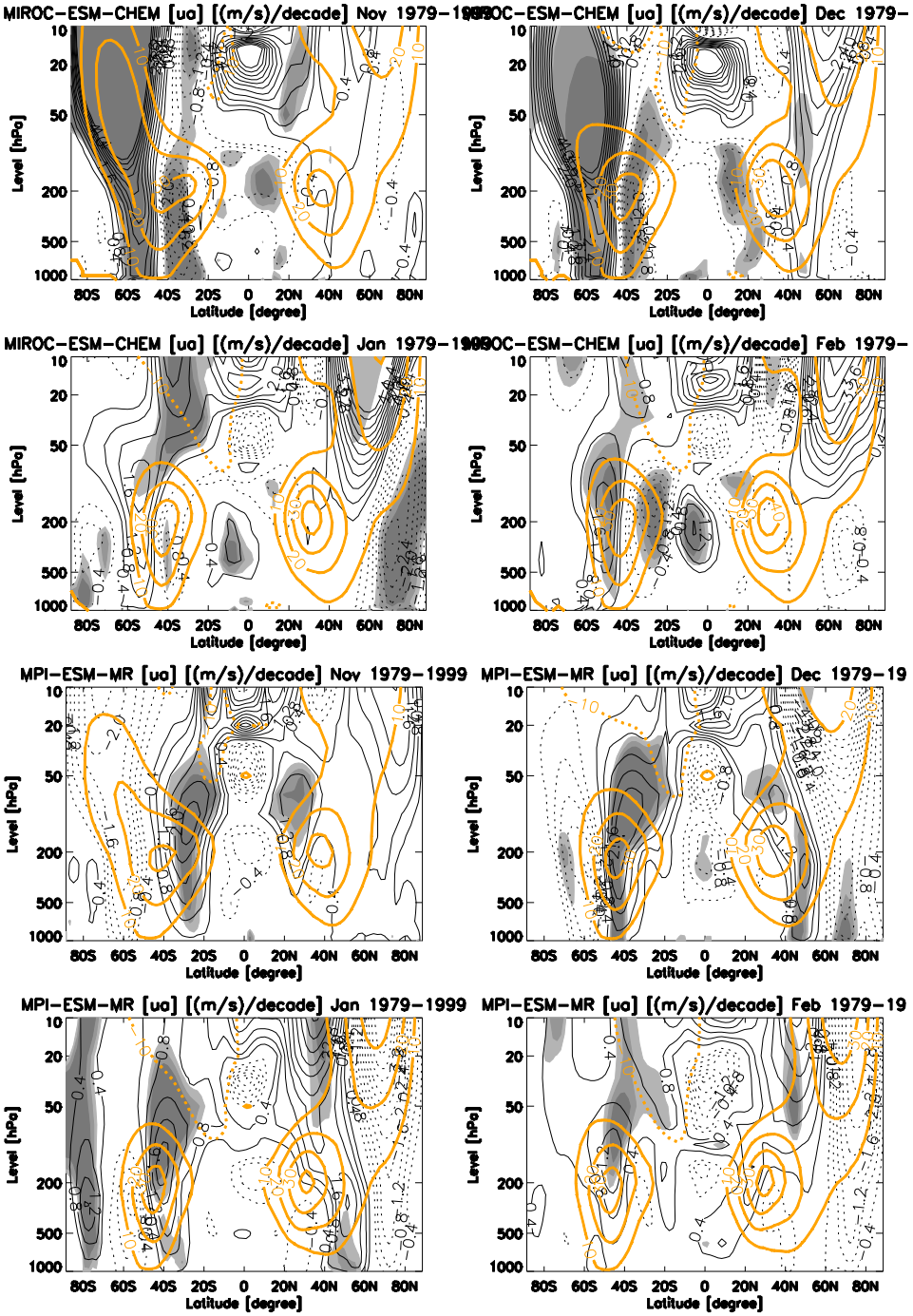

Figure 4.8b: The long-term mean (thick orange) and linear trend (thin black contour) of November, December, January, and February zonal mean zonal wind [ua] over 1979–1999: (*left*) MIROC-ESM-CHEM, and (*right*) MPI-ESM-MR HT model data. Contour intervals of climatological wind and trend are 10 m s^{-1} starting from 10 m s^{-1} and 0.4 (m s^{-1})/decade, respectively. Trends which are statistically significant at the 90, 95 and 98% confidence levels are shaded. Zero contours are omitted.

Here, the monthly climatologies and linear trend of zonal mean zonal winds for November-to-February for the four models are reported (Figs. 4.8a,b).

Some HT climate models, such as MIROC-ESM-CHEM (Fig. 4.8b) and GFDL-CM3 (Fig. 4.8a) respond to the stratospheric cooling deriving from ozone depletion with a very strong stratospheric circumpolar jet intensification (the first 4.8 m/s/decade, the second 4.4 m/s/decade) in November and in December, propagating from the middle-upper stratosphere downward to the surface and maintaining its magnitude in December. This is consistent with the very strong cooling discussed in the previous sections. The significant positive trend however persists also in January and February, shifting towards midlatitudes (about 40-60°S) and propagating downward to the surface implying a tropospheric jet acceleration on the poleward side. Both these two models responds also with a significant negative jet trend from the equatorward side of the climatological midlatitude tropospheric jet stream. In GFDL-CM3 the westerly polar jet trend maintains very strong in the November-to-February period (maximum from 4.4 m/s/decade in November to 2.8 m/s/decade in February). Thus, even if the easterly tropospheric trend becomes more intense (maximum of the order of -3.2 m/s/decade), especially in December and January, it results to be smaller than the positive trend on the poleward side. In MIROC-ESM-CHEM the westerly polar jet trend weakens in January-February and the negative trend intensity is smaller than the positive one, except in February (the negative trend is -2.4 m/s/decade and the positive 1.6 m/s/decade).

CMCC-CMS (Fig. 4.8 a) presents a rather intense polar stratospheric westerly jet trend (4.4 m/s/decade; larger than ERA-40 but smaller than the other two models) extending in the whole stratosphere in November (it reaches down to the surface but without any confidence level), but with a smaller intensity in the following months. Furthermore, a small easterly trend on the poleward side of the tropospheric climatological jet can be found in January and February.

In Section 4.2 we have discussed the very weak signal in temperature reported by MPI-ESM-MR. We therefore expect a weak signal in winds too. In Figure 4.8b, indeed, we can see very anomalous wind response in MPI-ESM-MR: negative circumpolar jet trend (-2.4 m/s/decade) in the stratosphere where we expect to find a positive one (that instead is found at 20-40°S with intensity 2.2 m/s/decade, lower than that of ERA-40). Therefore, this model responds to ozone depletion by

weakening the climatological tropospheric midlatitude jet on the poleward side and strengthening it on the equatorward side, implying a tropospheric jet shift towards lower latitudes. Hence, MPI-ESM-MR represents an outlier model respect to the other CMIP5 models. We briefly mention here that the HT models that are not shown, tend to be similar to one of these discussed models. For example, models as CMCC-CESM, MPI-ESM-P and MPI-ESM-LR results more similar to the CMCC-CMS model; IPSL-CM5B-LR, IPSL-CM5A-MR and MRI-CGCM3 seems to have a behaviour similar to that of MIROC-EMS-CHEM, whereas IPSL-CM5A-LR results to be more similar to GFDL-CM3. HadGEM2-CC, instead, is the model that is quite similar to MPI-ESM-MR. The Figures, equivalent to those reported here, for these other HT models can be found in Appendix B.

4.7 Zonal mean zonal wind in LT Models

The same response for the LT models is now shown in Figures 4.9a,b. The models considered are the ones discussed in previous sections (bcc-csm1-1, CMCC-CM, FGOALS-g2, and MIROC4h).

Results show that models as CMCC-CM (Figs. 4.9a) have an immediate response to stratospheric cooling with a westerly trend (3.2 m/s/decade, like in ERA-40 reanalyses) in middle stratosphere during November; this trend does not reach down the surface in December-to-February, differently than in what found in the HT model case. In this model only in November the circumpolar jet positive trend is significant, whereas in January there is a westerly tropospheric jet trend in the equatorward side of the climatological midlatitude jet around 20°S.

The bcc-cms1-1 (Fig. 4.9a) shows a stronger stratospheric polar jet trend in November (4.4 m/s/decade) rather comparable with that of HT models. In December it tends to propagate to the surface but without significant patterns. Moreover, it persists also in January and February with stronger response in January with respect to ERA-40 and a different seasonality: February patterns resemble January ERA-40 patterns. The persistence in the polar jet trend can be consistent with the absence of a clear “onset”, “growth” and “decay” stage of the jet response to cooling, as proposed by Orr *et al.* (2012).

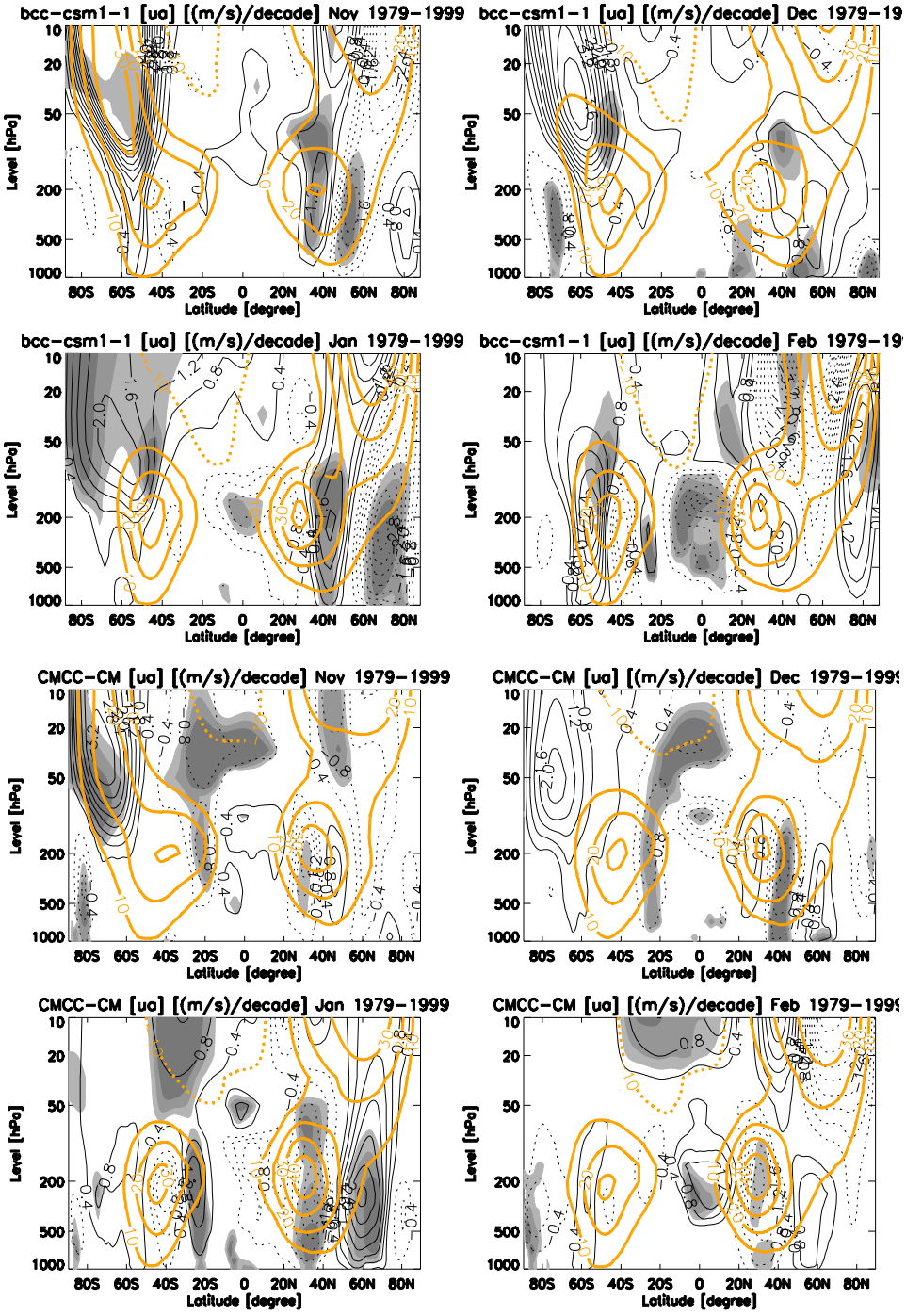

Figure 4.9a: The long-term mean (thick orange) and linear trend (thin black contour) of November, December, January, and February zonal mean temperature [ta] over 1979–1999: (*left*) bcc-csm1-1, and (*right*) CMCC-CM HT model data. Contour intervals of climatological wind and trend are 10 m s^{-1} starting from 10 m s^{-1} and 0.4 (m s^{-1})/decade, respectively. Trends which are statistically significant at the 90, 95 and 98% confidence levels are shaded. Zero contours are omitted.

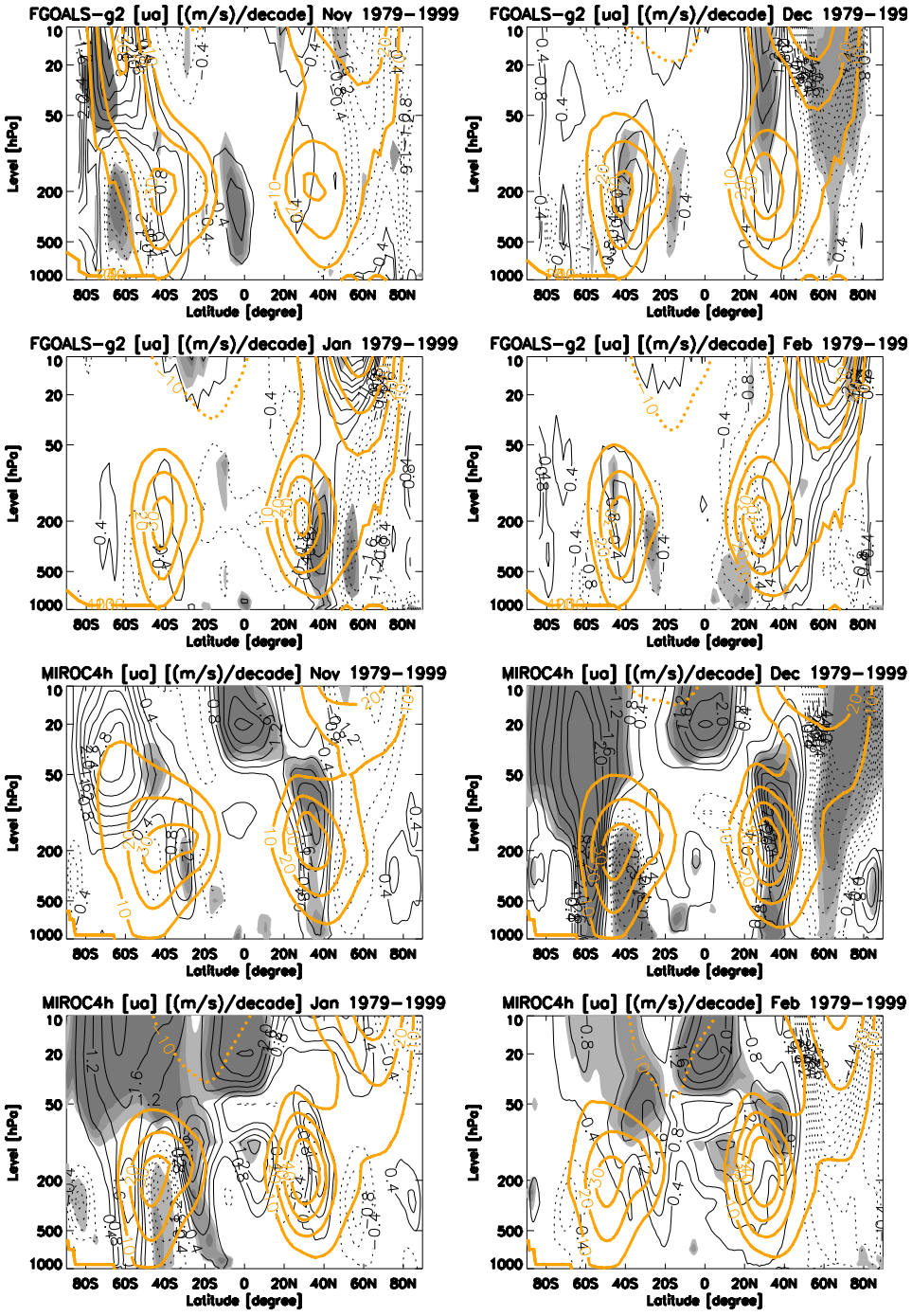

Figure 4.9b: The long-term mean (thick orange) and linear trend (thin black contour) of November, December, January, and February zonal mean temperature [ta] over 1979–1999: (*left*) FGOALS-g2, (*right*) MIROC4h model data. Contour intervals of climatological wind and trend are 10 m s^{-1} starting from 10 m s^{-1} and 0.4 (m s^{-1})/decade, respectively. Trends which are statistically significant at the 90, 95 and 98% confidence levels are shaded. Zero contours are omitted.

A different behavior is reported by MIROC4h (Fig. 4.8b), which presents a circumpolar jet westerly trend that extends from the stratosphere down to the surface, accelerating the tropospheric midlatitude jet in the poleward side and decelerating it in the equatorward side in December (3.2 m/s/decade), in agreement with reanalyses.

The FGOALS-g2 model seems to respond in terms of zonal mean zonal wind only in November with a quite significant westerly trend (3.2 m/s/decade) above 50 hPa only. No other trends are found in the following months, totally inconsistent with observations.

Concerning the other LT models, NorESM1-M seems to be similar to CMCC-CM model, whereas MIROC5 is similar to MIROC4h. EC-Earth and CNRM-CM5, instead results to be more similar to bcc-csm1-1. FGOALS-g2 represents an anomalous case for the LT models set.

4.8 Multi-Model averages of zonal mean zonal wind

In this section we compare multi-model averages in zonal mean zonal wind with the same methodology used for the temperature.

In November and December HT multi-model mean (Figs. 4.10 *top*) show strong jet westerly trend (5.6 m/s/decade in November, 4 m/s/decade in December) in the middle-upper stratosphere over the SH circumpolar region, that remains confined to the lower stratosphere, with a 98% significance in November, whereas in December this signal propagates from the stratosphere down to the surface but it results to be statistically insignificant, due probably to the great variability present in few HT models (e.g. MPI-ESM-MR model).

The LT multi-model mean has a similar behaviour but: the polar jet trend is smaller in November and especially in December (2 m/s/decade); the surface trends are smaller (0.4 m/s/decade) and confined on a smaller region at 60°S. However, for the LT average, December trends in the stratosphere are significant. We ascribe the difference in the significances to a smaller variability across LT models.

In January surface trends persist in both HT and LT models, however in LT models this trends is a half of the one found in ERA-40 and HT models. Moreover LT models display a persistent trend in the stratosphere not found in both

reanalyses and HT models.

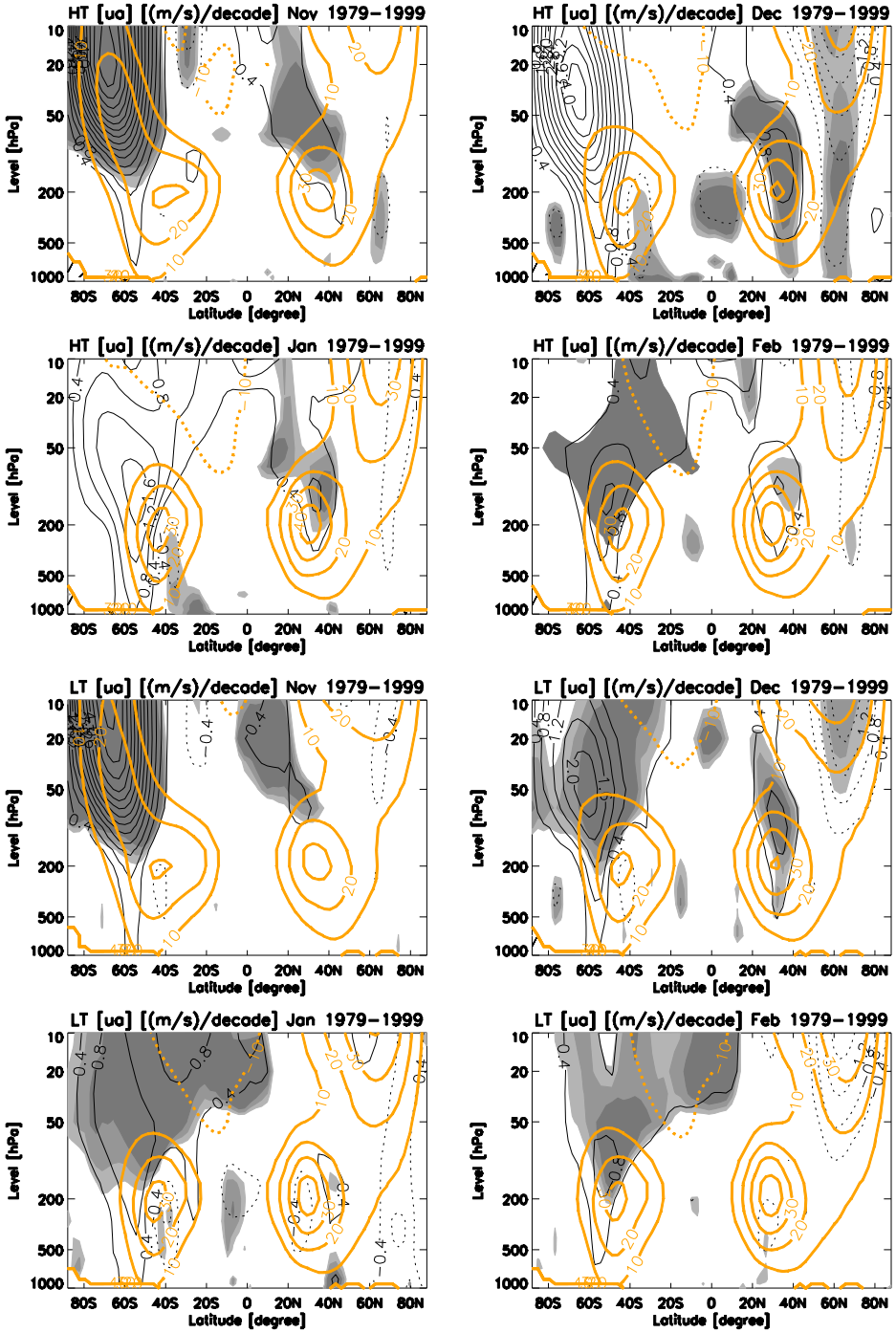

Figure 4.10: The long-term mean (thick orange) and linear trend (thin black contour) of November, December, January, and February zonal mean temperature [ta] over 1979–1999: (*top*) HT, (*bottom*)LT multi-model data. Contour intervals of climatological wind and trend are 10 m s^{-1}

starting from 10 m s^{-1} and 0.4 (m s^{-1})/decade, respectively. Trends which are statistically significant at the 90, 95 and 98% confidence levels are shaded. Zero contours are omitted.

This can be due to the absence in LT models of a westward acceleration in the middle stratosphere, consistent with the "decay" stage described in Orr *et al.* (2012) and consistent with Cagnazzo *et al.* (2013) driven by stratospheric dynamics.

In ERA-40 and HT models January trends are the strongest at the tropopause level, consistent with increases in the synoptic wave fluxes of heat and momentum (Cagnazzo *et al.*, 2013). These trends persist in February in both HT and LT models, though larger in HT multi-model. Both HT and LT multi-model also show an easterly jet trend on the equatorward side of the tropospheric jet of the same magnitude of ERA-40, resulting in a poleward jet shift.

4.9 Discussion

In this chapter, we have analyzed the thermal and dynamical response of the HT and LT models to ozone changes. Concerning the temperature trends found in the lower stratosphere, these are well simulated in both the model versions on average, with a similar seasonality and magnitude. However, when looking at multi-model averages, the HT models report an about 30% stronger trend in the December lower stratosphere. We ascribe this difference to enhanced cooling deriving from the dynamical component in HT models, that also appears as a summer warming overtopping the cooling. Moreover, the stratospheric cooling is more persistent in LT models in February and March. Concerning zonal mean zonal wind trends, HT models respond with a stronger stratospheric jet trend and display a more persistent surface response. Moreover, LT models report a too persistent stratospheric zonal wind trends in January.

Our interpretations of these differences are indeed related to the definition of the stratosphere in the two model categories. Specifically, the LT models are missing the wave-mean flow interaction initiated in the upper stratosphere by critical level filtering of gravity waves and propagated down by planetary waves (Manzini *et al.*, 2003). The interplay between large-scale flow and both planetary and gravity waves is the stratospheric dynamical response to the ozone induced cooling in the lower stratosphere that can be misinterpreted in LT models. This can be seen in the winds

response too: associated to a stronger cooling is a stronger jet response in the stratosphere in November and December. This jet trend is too strong in HT models and too weak in LT multi-model average. Moreover, it is too persistent in the stratosphere in LT models, consistent with the interpretation of a missing "decay" stage (Orr *et al.*, 2012) due to a westward acceleration driven by stratospheric dynamics. However, within the HT models, there are some models with an interactive stratospheric chemistry module. These models tend to bias the HT multi-model average toward a too strong cooling. In order to better isolate the role of a dynamical stratosphere, the same analysis should be performed excluding those models.

Finally, in these two sets of model simulations, trends at the tropopause are interpreted as due to increases in synoptic wave fluxes of heat and momentum in January and February, stronger in HT than LT models. A subsequent analysis on surface trends should then follow.

Chapter 5

Correlation between tropospheric jet trend and stratospheric cooling in models

In this chapter we study the inter-model variability of the poleward shift of the austral jet stream in the CMIP5 integrations linked to the representation of stratospheric cooling in the 1979-1999 period. We therefore stratify the models in terms of their representation of lower stratospheric radiative and dynamical cooling and in terms of their tropospheric jet response. Thus, we study the correlation between tropospheric jet intensity and jet shift trend and the lower stratospheric cooling trend across the models. To reach this purpose we construct indices representing these trends for each CMIP5 model considered in this work (reported in Table 2.1) and for ERA-40 reanalyses. The same analysis has been performed for the 1960-1999 period (not reported here) however in that case there are no available observations that can be used for estimating linear trends in the SH.

5.1 Indices

5.1.1 Stratospheric cooling

The lower stratospheric cooling trend across the CMIP5 models has been determined in Chapter 4. The linear trend of the long-term zonal mean temperature has been estimated for different seasons. Almost all the models show a maximum

stratospheric cooling in November persisting in December (the maximum in general is found in November, but few models can respond with about 1-month delay) and January. Moreover, since the cooling trend maximum is located between 64°S and 90°S in latitude and between 50 hPa and 200 hPa altitude, we estimate the average cooling in this region for the November-December (ND) mean. The vertical mean is calculated over the following pressure levels: 50 hPa, 100 hPa, 150 hPa and 200 hPa. In this way we manage to obtain the cooling trend index representative of the lower stratosphere region inside polar vortex, shown in Figure 5.1.

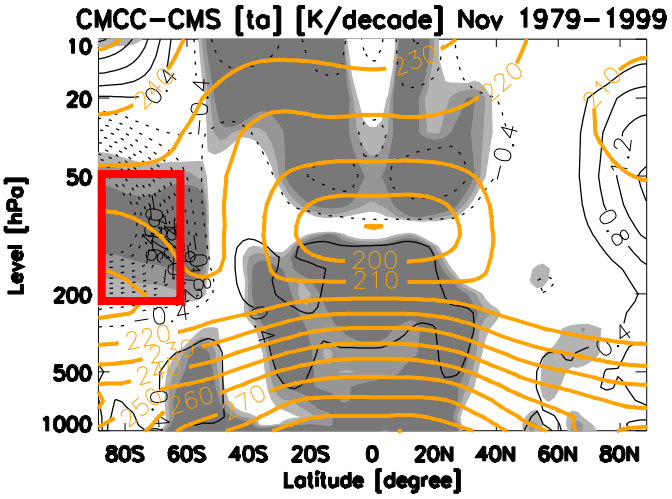

Figure 5.1: An example-figure (taken from Fig. 4.2a in Section 4.2) to show the region selected (red rectangle) to calculate the stratospheric cooling trend index.

Another methodology is to estimate the vertical integral of the cooling, by pressure-weighting the trends over the pressure level thickness of each level. We have obtained the pressure thickness value (dp_i) of each layer as the semi-difference between the reference level and the pressure of the second level above, and we have referred the temperature of the each layer top to the entire layer temperature (T_i).

So, we can calculate the vertically mean temperature $\bar{T}$, as follows:

$$\bar{T} = \frac{\Sigma_i T_i \cdot dp_i}{\Sigma_i dp_i} \tag{5.1}$$

5.1.2 Jet trend and jet shift

We have estimated both the trend in the strength of the jet and the trend in the latitudinal position of the jet (the jet shift). The first index is obtained by meridionally averaging the zonal mean zonal wind trends between 50°S and 70°S, the latitudes where jet positive trend is found to be the strongest across the models from the tropopause to the surface. The choice of averaging over a quite large latitudinal band, is related to the fact that the jet response is related to the mean climatological position of the jet itself: low latitude jets are able to shift more poleward than high latitude ones (Kidston and Gerber, 2010). This index has been estimated in the NDJ, DJ or NDJF season (where N, D, J, and F indicate respectively November, December, January, and February) in order to obtain the maximum mean jet trend magnitude. The reason of working with three seasons is linked to the different models response. Most models respond in December but few models tend to respond before in November or later, in January. This is also related to the vertical resolution of models: models with a low vertical resolution tend to respond very fast to the stratospheric cooling, therefore mostly in November-December, whereas the high resolution ones tend to respond in December-January.

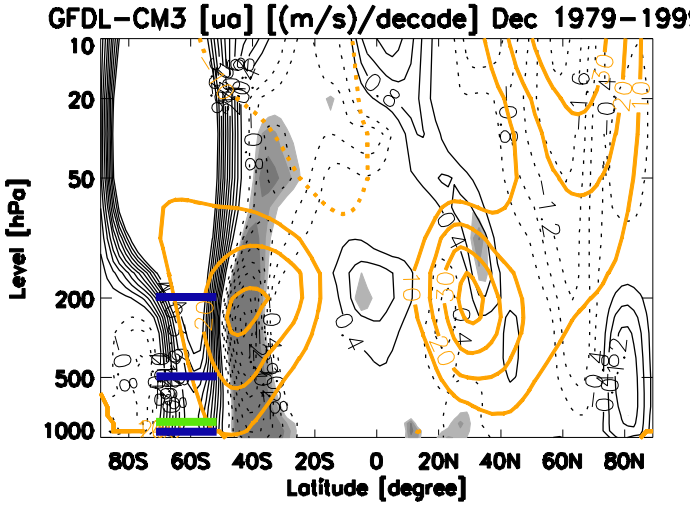

Figure 5.2: An example-figure (taken from Fig. 4.8a in Section 4.6) to show the levels selected (blue and green lines) to calculate the tropospheric jet trend index and the level selected (green line only) to calculate jet shift trend index.

Here we show results for the whole NDJF season. Moreover, we select four different levels (200, 500, 850, and 925 hPa) for analyzing the jet strength trend in the troposphere, as shown in Figure 5.2, in order to analyze the maximum correlation at different altitudes (although we expect to obtain similar results at the different model levels because of the barotropicity of the jet stream).

For the jet shift index we have defined the latitude of the eddy-driven jet stream, taken as the latitude of the maximum zonal mean zonal wind at 850 hPa. The surface winds reflect the convergence of westerly momentum aloft due to the meridional propagation of eddies away from the baroclinic source region, which is damped by friction near the surface (Held, 1975), and so serve as a good indicator of the position of the barotropic jet streams. We have therefore constructed the time series of this maximum in different seasons: NDJ, DJ, and NDJF seasons and then calculated their linear trends. Latitudes sign is considered negative when the jet moves poleward.

5.2 Scatter plot and correlation

In this section, we report the indices correlations in HT and LT models. Two typologies of scatter plot are realized, one using the tropospheric jet trend index for the four different pressure levels mentioned before (three similar cases have been indeed examined, distinguished by the NDJ, DJ, and NDJF seasonal average), and another one with the jet shift trend at 850 hPa for the three seasons. We also introduce ERA-40 indices in scatter plots and in the correlation coefficient determination.

Figure 5.3 shows the scatter plot of the jet trend index in the NDJF season versus the stratospheric cooling index (derived from the vertical average and not the vertical integral; results for the vertical integral show slightly smaller correlations and are displayed in Appendix B). This is the season when the best correlation is found: the largest correlation is estimated for a jet index at 200 hPa (-0.70). This is expected, because the larger is the polar cap cooling, the stronger is the jet intensification at the tropopause level. From this figure, we deduce that HT models (represented by blue symbols) have a stronger cooling and stronger jet response but do show a larger spread, whereas LT models (represented by green symbols) tend to report a smaller but more similar across them long-term response. We interpret the

difference in the spread by the fact that LT models are again missing a correct representation of the stratospheric variability, and therefore their long-term response is less variable across the models.

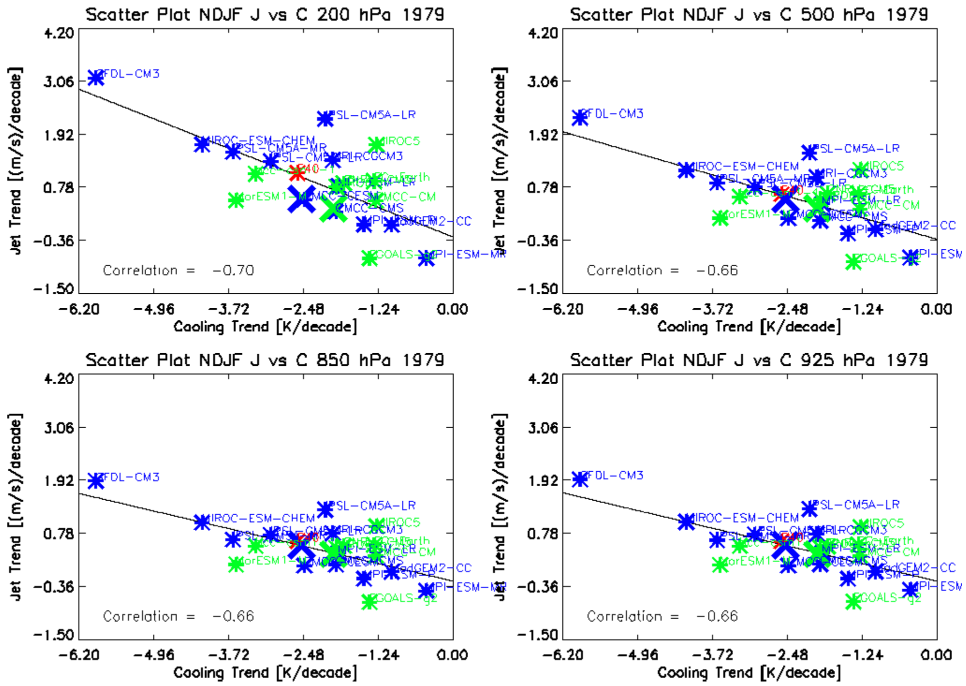

Figure 5.3: Scatter plot of the HT (blue symbols), LT (green symbols), and ERA-40 reanalyses (red symbol) mean trends over the 1979-1999 period at: (*top left*) 200 hPa, (*top right*) 500 hPa, (*bottom left*) 850 hPa, and (*bottom right*) 925 hPa pressure level of the tropospheric jet. The correlation between the ND mean lower stratospheric cooling trend and the NDJF mean tropospheric jet trend is showed. The cooling trend is averaged at 50-200 hPa pressure level and over a region between 64°S and 90°S. The jet trend is averaged on latitude only, between 50°S and 70°S.

Interestingly we find a linear correlation between HT and LT models indices, with ERA-40 (red symbol) exactly lying along the linear fit, overplotted to the scatter points. Moreover ERA-40 results are about in the center of the models distribution. This implies that the physical mechanisms linking the stratospheric cooling to the jet strength trend that are acting in the models and in the reanalyses are the same.

We can see how models like GFDL-CM3 and MIROC-ESM-CHEM tend to be located in upper right corner of the scatter plots, in perfect agreement with previous chapter consideration. These HT models report a very stronger cooling in

the stratosphere (possibly due to their representation of the ozone) and, in response to it, a more intense jet acceleration in the troposphere. MPI-ESM-MR, instead is found in the opposite corner of the plot, in according with its anomalous behaviour seen in Chapter 4.

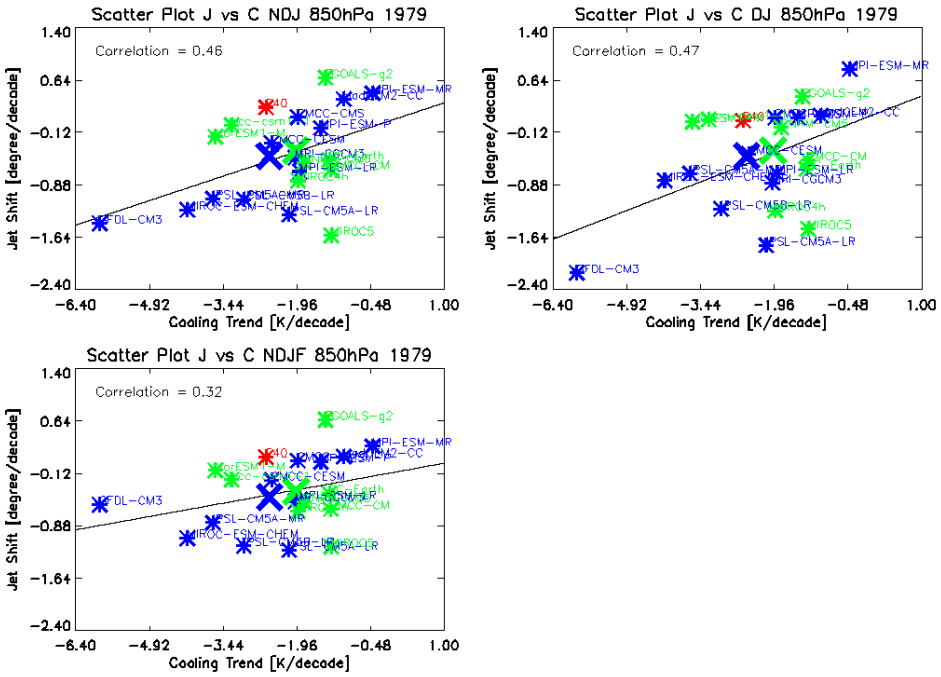

Figure 5.4: Scatter plot of the HT (blue symbols), LT (green symbols), and ERA-40 reanalyses (red symbol) mean trends over the 1979-1999 period at 850 hPa in: (*top left*) NDJ, (*top right*) DJ, and (*bottom*) NDJF mean season, relative to the tropospheric jet shift only. The correlation between the ND mean lower stratospheric cooling trend and the mean tropospheric jet shift trend is shown. The cooling trend is averaged at 50-200 hPa pressure level and over a region between 64°S and 90°S. The jet shift trend is averaged on the different seasons only.

However, in general we find that models that report a stronger cooling in the lower stratosphere over polar cap tend to have a larger intensification of the midlatitude jet trend in the troposphere and down at the surface.

In Figure 5.4 we report the scatter plot of the jet shift trend index versus the stratospheric cooling. Again, we find that HT models tend to be widespread, whereas LT models are located in the upper right corner of the plot. Better correlations (0.47) are found in the DJ mean period (although smaller than the previous case). In this case, models with a stronger cooling tend to result in a more

poleward eddy-driven jet. However, the shift of the jet is also function of its climatological mean position, therefore it can happen that strong cooling does not result in a strong jet, if the model has a too poleward-biased jet. This could explain indeed the maximum correlations (0.47) between the two quantities, lower than the correlations discussed above. The dependence of the jet shift on its mean climatological position can be explained in terms of basic geometric constraints. The jet stream simply has more room to shift poleward in models that begin with an equatorward bias, and so appears more sensitive to external forcing. In other words, the radiative forcing of the atmosphere, as the one coming from the ozone or GHGs change, ultimately sets a high-latitude limit on the location of the eddy-driven jet, and it is likely that models, which are closer to this limit, are unable to shift the jet very far. Additional figures are reported in Appendix B.

5.3 Discussion

Summarizing, we find that the jet trend from the tropopause down to the surface is significantly linearly correlated to the lower stratospheric cooling itself across the models, with reanalyses very well fitting this linear relationship.

HT models appear to have a stronger cooling and stronger jet response but show a larger spread, whereas LT models tend to report a smaller but more similar long-term response. We interpret the difference in the spread by the fact that LT models are again missing a component (in this case a correct representation of the stratospheric variability), and therefore their long-term response is less variable across the models. Although large differences in the models used in this work could render uneasy to derive a clear and consistent role of the dynamical stratosphere, our analysis points out that in the long-term response to ozone changes the representation of the stratosphere can be important.

In conclusion, we can confirm that the representation and the magnitude of the initial cooling in the lower stratosphere (depending on the model representation of the stratosphere itself) is the essential ingredient, because it results to be rather strongly correlated to the tropospheric midlatitude jet shift in both HT and LT models.

Chapter 6

Summary and conclusions

Purpose of the work

This thesis is devoted to study how ozone depletion in the lower stratosphere have influenced the tropospheric long-term changes in the SH. In this work we have addressed the long-term changes in the stratosphere and in the troposphere, by making use of state-of-the art climate model simulations. One of the main purposes of this analysis has been to identify the role of the stratospheric dynamics in surface tropospheric changes. To this aim we have made use of a large number of model simulations reproducing past climate, performed with coupled atmosphere-ocean-sea-ice models. The simulations were performed with different model configurations; we have specifically focused on the configurations named HT and LT, where the representation of the stratosphere, within the atmospheric component, is different. However, the models also differ in many other aspects. Therefore, our purpose has been to clearly identify the role of the stratospheric dynamics within a set of models presenting large differences in several modeling aspects. If on one side this choice could mask a clear stratospheric signal, on the other hand a successful analysis would give physical robustness to our hypothesis. The model simulations used in this work are part of the CMIP5 project and reproduce the historical period (1850-2005) together with the ERA40 reanalyses.

Specifically, we have defined the data, the simulations and the HT and LT model configurations in *Chapter 2*.

Involved phenomenology

Ozone induced cooling in the stratosphere is associated with the strengthening of westerly winds in the stratosphere with a later transition to easterlies (Thompson and Solomon, 2002), a poleward shift of the mid-latitudes westerly jet in the troposphere during SH summer (e.g. Perlwitz *et al.*, 2008; Son *et al.*, 2010) and a projection of these long-term changes onto a high-index polarity of the Southern Annular Mode (SAM; e.g. Thompson and Solomon 2002; Fogt *et al.* 2009). The projection onto the SAM positive polarity can explain why climate change over Antarctica is characterized by a cooling over the continent and a warming over the peninsula. The shift in the extratropical SH jet has then consequences on the hydrological cycle deep into the subtropical regions (Kang *et al.*, 2011). Tropospheric warming induced by increase in greenhouse gas (GHG) concentrations also results in a poleward shift of the tropospheric jet (e.g. Kushner *et al.* 2001), so that ozone depletion and GHGs increase have both acted in the past to drive changes in the SH circulation. Moreover, recent analysis performed with General Circulation Models (e.g. Perlwitz *et al.*, 2008; McLandress *et al.*, 2011; Polvani *et al.*, 2011a) and multi-model studies (e.g. Son *et al.* 2008; Gerber *et al.*, 2012) have confirmed that ozone induced cooling in the lower stratosphere has dominated past changes in the SH climate. A number of studies have analyzed the downward propagation of variations of the SH stratospheric flow affecting the tropospheric circulation (e.g. Graversen and Christiansen, 2003; Polvani and Kushner, 2002; Gillett and Thompson, 2003; McLandress *et al.,* 2010). Changes in the SAM polarity are characterized by reduced atmospheric pressure at polar latitudes and raised pressure at mid-latitudes, corresponding to a strengthening and poleward shifting of the tropospheric jet. At the surface, the mid-latitude westerlies drive the Antarctic Circumpolar Current (ACC), therefore influencing the ocean meridional overturning (e.g. Toggweiler and Lea, 2010). An increase in ACC transport and a southward shift of its mean position has been estimated indeed (Boening *et al.*, 2008). Moreover, recent studies have connected changes in atmospheric circulation to sea-ice extent (Goosse *et al.*, 2009) and found consistency between sea ice concentration trend patterns in Antarctica and 500 hPa

geopotential height patterns (Turner *et al.*, 2009). However, there is no clear evidence of the impact of ozone changes on the sea-ice and the oceanic circulation (Sigmond and Fyfe, 2010). A detailed description of the possible mechanisms linking stratospheric ozone depletion and summertime changes in atmospheric and oceanic circulation, as well as air-to-sea carbon fluxes, have been presented in *Chapter 3*, mainly reviewing recent literature.

Why the stratospheric dynamics?

In the past, the two-way interaction between the stratosphere and the Earth climate system below was not considered as important, thus the stratosphere representation was not included in climate model simulations and the models were missing part of the variability induced by the troposphere-stratosphere interaction. However, there is now increasing evidence that a better representation of the stratosphere in climate models could lead to improved predictability of the climate system at different timescales (e.g. Gerber *et al.*, 2012; Charlton *et al.* 2012; Manzini *et al.*, 2012). In this work we deal with long timescales (longer than decadal) and at these timescales the anthropogenic forcing (GHGs and ozone depleting substances increase) is dominant with respect to natural variability. Even if the chain of mechanisms linking stratospheric cooling associated with ozone depletion to the surface long-term changes are still under investigation, recently, it has been proposed that a limited representation of stratospheric processes in climate models aiming to simulate past and predict future SH climate change could led to a bias in the representation of long-term tropospheric changes in those climate model simulations. The object of discussion is to which extent a well resolved stratosphere can improve future climatic prediction of the SH changes in models and what we do miss in models that not correctly represent the stratospheric dynamics.

Recent analyses performed on historical and scenario model simulations (Son *et al.*, 2010; Gerber *et al.*, 2012) confirm that multi-model means of HT (CCMVal2) and mostly LT (AR4) models are both able to reproduce changes in the tropospheric circulation of the SH austral summer induced by ozone changes. However, multi-model assessments were not able to estimate the role of improved stratospheric representation and variability in HT models in simulating surface changes.

Our results

As expected and consistent with the above-mentioned works, in our analysis both kinds of model simulations (HT and LT) are able to reproduce past changes in the SH circulation induced by ozone changes (e.g., Thompson and Solomon 2002), however differences emerge and are here analyzed.

This work has been developed into two main sections. The first part (*Chapter 4*) has been dedicated to understand how different HT and LT models respond to the ozone depletion forcing in the stratosphere and in the troposphere, subdividing the models in two categories, mainly based on their stratospheric representation. In order to quantify to which extent the different models are able to represent the lower stratospheric cooling and the stratospheric and tropospheric jet changes in response to it, climatologies and linear trends of the temperature and of the zonal mean zonal wind fields have been analyzed, focusing particularly attention onto the lower stratosphere temperature field at latitudes between 60°S and 90°S and zonal mean zonal winds between 50°S and 70°S in the November to March season. As we have expected from the initial hypotheses, we have found that HT models (that have a good representation of the stratospheric dynamics) have represented on average a stronger lower stratospheric cooling than LT models (that have a limited stratospheric dynamics representation). Specifically, the temperature trends in the lower stratosphere have been well simulated in both the model versions with similar seasonality and magnitude. However, when looking at multi-model averages, the HT models have reported an about 30% stronger trend in the December lower stratosphere. We have ascribed this difference to enhanced cooling deriving from the dynamical component in HT models. The role of the stratospheric dynamics also has appeared as a summer warming above the cooling. Moreover, the stratospheric cooling has been more persistent in LT models in February and March. Concerning zonal mean zonal wind trends, HT models have responded with a stronger stratospheric jet trend and displayed a more persistent surface response. Moreover, LT models have reported a too persistent stratospheric zonal wind trends in January.

The second part of this work (*Chapter 5*) has been devoted to stratify the models in terms of their representation of lower stratospheric radiative and dynamical cooling and in terms of their tropospheric jet response. One of our main findings is that the representation and magnitude of the initial radiative and

dynamical cooling in the lower stratosphere in models is the key factor controlling the subsequent tropospheric response and how the cooling itself depends on the representation of the stratospheric dynamics. In this section, we have constructed two indices to build correlations across the models. Specifically, the lower stratospheric polar cooling index, the tropospheric midlatitude jet trend and the jet shift trend. By looking at the existing correlation among the indices, we have found that the jet trend from the tropopause down to the surface has resulted to be significantly linearly correlated to the lower stratospheric cooling itself across the models, with reanalyses very well fitting this linear relationship. Interestingly, HT models appear to have a stronger cooling and stronger jet response but do show a larger spread, whereas LT models tend to report a smaller but more similar long-term response.

Our interpretations

Our interpretations of these differences are indeed related to the definition of the stratosphere in the two model categories. Specifically, the LT models are missing the wave-mean flow interaction initiated in the upper stratosphere by critical level filtering of gravity waves and propagated down by planetary waves (Manzini *et al.*, 2003). The interplay between large-scale flow and both planetary and gravity waves is the component of the stratospheric dynamical response to the ozone induced cooling in the lower stratosphere that is very difficult to represent in models and therefore that can be lively source of errors, especially in LT models. This can be seen in the winds response too: associated with a stronger cooling is a stronger jet response in the stratosphere in November and December. In HT models, this jet trend is too strong in HT models and too weak in LT multi-model average. Moreover, it is too persistent in the stratosphere in LT models, consistent with the interpretation of a missing "decay" stage (Orr *et al.*, 2012) due to a westward acceleration driven by stratospheric dynamics. However, within the HT models, there are some models with an interactive stratospheric chemistry module. These models tend to bias the HT multi-model average toward a too strong cooling. In order to better isolate the role of a dynamical stratosphere, the same analysis should be performed after excluding those models.

In these two sets of model simulations, trends at the tropopause are interpreted as due to increases in synoptic wave fluxes of heat and momentum in January and February, stronger in HT than LT models.

Considering the correlation study conducted in the second part of the work, we interpret the difference in the spread by the fact that LT models are again missing a component, that is in this case a correct representation of the stratospheric variability, and therefore their long-term response is less variable across the models. Although large differences in the models used in this work could render difficult to derive a clear and consistent role of the dynamical stratosphere, our analysis points out that in the long-term response to anthropogenic changes the representation of the stratosphere can be important. Moreover, since in the future, it is expected that stratospheric ozone will recover and GHGs and ozone changes will no longer combine to project onto the SAM high-index polarity, the stratospheric representation can be important also for producing realistic climate change future projection over Antarctica.

Therefore with this work, we have confirmed the importance of including a proper representation of the stratosphere, at least with a certain degree of detail, in order to obtain more reliable long-term climate simulations and projections in the SH circulation patterns.

Future perspectives

Perspectives of this analysis include: an extension to all the CMIP5 database; repeating the same analysis by including the HT and LT models that do use the same identical ozone forcing (no interactive chemistry, ozone fields based on observations only); making use of future projections; extending this study to changes in the SAM across the models as well as top changes in the oceanic circulation and, for the subset of models including an explicit representation of the carbon cycle, to implications for the air-to sea carbon fluxes in the Southern Ocean and at the global level.

Appendix A

Geostrophic approximation and geostrophic wind

In the atmosphere air parcels naturally move from areas of high pressure to areas of low pressure, due to the pressure gradient force. As soon as the air starts to move, however, the Coriolis Force deflects it, rightward in the Northern Hemisphere, and leftward in the Southern Hemisphere. As the air moves from the high pressure area, its speed increases and so does its Coriolis deflection. The deflection increases until the Coriolis and pressure gradient forces are in *geostrophic balance*: at this point, the air flow is no longer moving from high to low pressure, but instead moves along an isobar[1].

To explain what the geostrophic balance is it's necessary to start considering the motion equations. It's possible to see that eliminating of terms on scaling considerations not only has the advantage of simplifying the mathematics, but the small terms elimination in some cases has the important property of filtering an unwanted type of motion. For synoptic scale motions, the equations can be simplified defining characteristic scales of the field variables based on observed values for midlatitude synoptic systems.

The complete equations of motion, that describe all types and scales of atmospheric motions, derive from Newton's second law of dynamics. If only the pressure gradient, gravity and friction act on an air parcel, the motion equations can be write as follows :

$$\frac{D\mathbf{U}}{Dt} = -2\boldsymbol{\Omega} \times \mathbf{U} - \frac{1}{\rho}\boldsymbol{\nabla} p + \mathbf{g} + \mathbf{F}_r \qquad \text{(A.1)}$$

[1] Note that this explanation assumes that the atmosphere starts in a geostrophically unbalanced state and describes how such a state would evolve into a balanced flow. In practice, the flow is nearly always balanced.

where the bold symbolizes a vector, **U** is the velocity field of the air, **Ω** is the angular velocity vector of the Earth planet, ρ is the density of the air, p is the air pressure, $\mathbf{F_r}$ is the friction and **g** is the acceleration vector due to gravity. These are known as the Navier-Stokes equations. Locally this can be expanded in Cartesian coordinates, with a positive u representing an eastward direction and a positive v representing a northward direction. Neglecting friction[2] and vertical motion[3], we have:

$$\frac{Du}{Dt} = -\frac{1}{\rho}\frac{\partial p}{\partial x} + f \cdot v \tag{A.2a}$$

$$\frac{Dv}{Dt} = -\frac{1}{\rho}\frac{\partial p}{\partial y} - f \cdot u \tag{A.2b}$$

$$\frac{Dw}{Dt} = -\mathrm{g} - \frac{1}{\rho}\frac{\partial p}{\partial z} \tag{A.2c}$$

where $f \equiv 2\Omega \sin\phi$ is called the *Coriolis parameter* (approximately equal to 10^{-4} s^{-1}, varying with latitude), with ϕ which represents the latitude.

For midlatitude synoptic scale disturbances the Coriolis force and the pressure gradient force are in approximate balance. Then, retaining only these two terms in (A.2a) and (A.2b) gives as a first approximation the *geostrophic* relationship:

$$-fv \approx -\frac{1}{\rho}\frac{\partial p}{\partial x} \tag{A.3a}$$

$$fu \approx -\frac{1}{\rho}\frac{\partial p}{\partial y} \tag{A.3b}$$

This condition is called *geostrophic balance* and this is a *diagnostic*[4] espression that gives the approximate relationship between the pressure field and horizontal velocity in large-scale extratropical systems.

---

[2] The molecular friction term is so small that it may be neglected for all motions except the smallest scale turbulent motions near the ground, where vertical wind shears can become very large and the molecular friction term must be retained (Holton, 2004).

[3] The inertial component of synoptic scale vertical acceleration is very smaller than the other vertical components.

[4] The reason for which the geostrophic relationship is called "diagnostic" expression is that the approximate equations (A.5) and (A.6) contain no reference to time and therefore cannot be used to predict the evolution of the velocity field.

By analogy to the geostrophic approximation it's possible to define a horizontal velocity field, called the *geostrophic wina*, that can be expressed in vectorial form, as follows:

$$\boldsymbol{V}_{\mathrm{g}} = \mathbf{k} \times \frac{1}{\rho f} \nabla \mathrm{p} \tag{A.4}$$

where $\mathbf{k}$ is the wave vector.

By substituting using the third equation (A.2c) above considering vertical acceleration being zero (hydrostatic equilibrium), it's possible to obtain the geostrophic wind in isobaric coordinated:

$$f \cdot v = \mathrm{g} \frac{\frac{\partial p}{\partial x}}{\frac{\partial p}{\partial z}} = \mathrm{g} \frac{\partial z}{\partial x} \tag{A.5a}$$

$$f \cdot u = -\mathrm{g} \frac{\frac{\partial p}{\partial y}}{\frac{\partial p}{\partial z}} = -\mathrm{g} \frac{\partial z}{\partial y} \tag{A.5b}$$

with z the height of the constant pressure surface satisfying the equation:

$$dp = \frac{\partial p}{\partial x} dx + \frac{\partial p}{\partial y} dy + \frac{\partial p}{\partial z} dz = 0 \tag{A.6}$$

Defining the gravity in terms of the gradient of a potential function Φ:

$$\nabla \Phi = -\mathbf{g} \tag{A.7}$$

Since $\mathbf{g} = -\mathrm{g}\boldsymbol{k}$ where $\mathrm{g} \equiv |\mathbf{g}|$, it's clear that $\Phi = \Phi(\mathrm{z})$ and $\frac{d\Phi}{dz} = \mathrm{g}$. Thus, horizontal surfaces on the earth are surfaces of constant geopotential.

In this way the geostrophic wind components $(u_{\mathrm{g}}, v_{\mathrm{g}})$ can be expressed in terms of the gradient of the geopotential height Φ on a surface of constant pressure:

$$u_{\mathrm{g}} = -\frac{1}{f} \frac{\partial \Phi}{\partial y} \tag{A.8a}$$

$$v_{\mathrm{g}} = \frac{1}{f} \frac{\partial \Phi}{\partial x} \tag{A.8b}$$

The validity of this approximation depends on the local Rossby number, a dimensionless number used in describing fluid flow to characterize the importance of Coriolis accelerations arising from planetary rotation. It is calculated as the ratio of inertial to Coriolis force terms, $v \cdot \nabla v \sim \frac{U^2}{L}$ and $\Omega \times v \sim U\Omega$ in the Navier-Stokes equations.

The Rossby number is defined as:

$$R_o = \frac{U}{Lf} \tag{A.9}$$

It is invalid at the equator, because f is equal to zero there, and therefore generally not used in the tropics.

Therefore the geostrophic wind is a theoretical wind that would result from an exact balance between the Coriolis effect and the pressure gradient force, directed parallel to isobars (lines of constant pressure at a given height).

This balance seldom holds exactly in nature. The true wind almost always differs from the geostrophic wind due to other forces such as friction from the ground. Thus, the actual wind would equal the geostrophic wind only if there were no friction and the isobars were perfectly straight. Despite this, much of the atmosphere outside the tropics is close to geostrophic flow much of the time and it is a valuable first approximation. Geostrophic flow in air or water is a zero-frequency inertial wave (Holton, 2004).

Thermal wind

The geostrophic wind must have vertical shear in the presence of a horizontal temperature gradient, as it's possible to see with simple physical considerations based on hydrostatic equilibrium (Holton, 2004). This vertical shear is called *thermal wind* but its name is a misnomer, because the thermal wind is not actually a wind, but rather a wind shear.

The geostrophic wind is proportional to the slope of geopotential on a surface of constant pressure. In a *barotropic* atmosphere, one where density is a function only of pressure (so that isobaric surfaces are also surfaces of constant density), the

slope of isobaric surfaces is independent of temperature, so geostrophic wind does not increase with height. This does not hold true in a *baroclinic* atmosphere, one where density is a function of both pressure and temperature. Horizontal temperature gradients cause the thickness of gas layers between isobaric surfaces to increase with higher temperatures. When multiple atmospheric layers are stacked upon each other, the slope of isobaric surfaces increases with height. This also causes the magnitude of the geostrophic wind to increase with height.

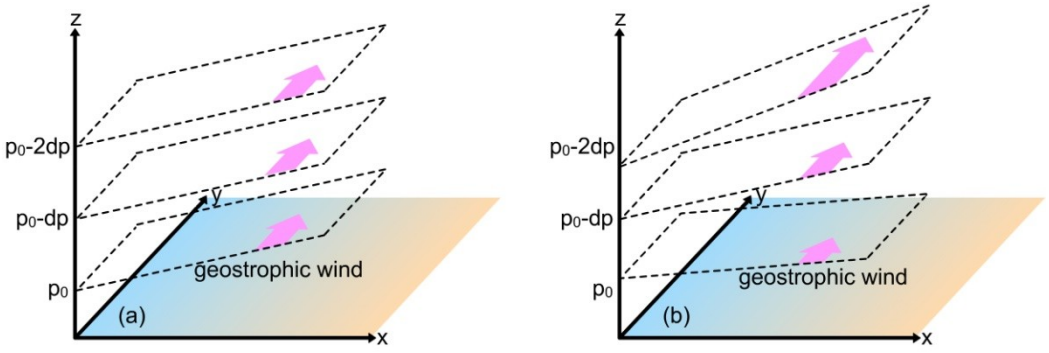

Figure A.1: The vertical variation of geostrophic wind in a barotropic atmosphere (a) and in a baroclinic atmosphere (b). The blue portion of the surface denotes a cold region while the orange portion denotes a warm region. The temperature difference is restricted to the boundary in (a) and extends through the region in (b). The dotted lines enclose isobaric surfaces which remain at constant slope with increasing height in (a) and increase in slope with height in (b). This causes thermal wind to occur only in a baroclinic atmosphere.

The geopotential thickness of an atmospheric layer is described by the hypsometric equation result. This is obtained considering the *hydrostatic equation*, that describes the balance of the gravity force by the vertical component of the pressure gradient force in the absence of atmospheric motions:

$$\frac{dp}{dz} = -\rho g \tag{A.10}$$

Integrating this condition from a height z to the top of the atmosphere it can found that:

$$p(z) = \int_z^\infty \rho \, g dz \tag{A.11}$$

so that the pressure at any point is simply equal to the weight of the unit cross section column of air overlying the point. Thus, mean sea level pressure $p(0)$=1013.25 hPa is simply the average weight per square meter of the total atmosphere column[5] (Holton, 2004).

Noting that $d\Phi = \mathrm{g}dz$ and from the equation of state for an ideal gas that $\alpha = \frac{1}{\rho} = \frac{RT}{p}$, where α is specific volume, R is the gas constant for dry air[6] and T is the air temperature, the hydrostatic equation can be expressed in the form:

$$\mathrm{g}dz = d\Phi = -\frac{dp}{\rho} = -\left(\frac{RT}{p}\right)dp = -RTd\ln p \tag{A.12}$$

Thus, the variation of geopotential with respect to pressure depends only in temperature. Integrating this expression in the vertical, a form of the *hypsometric equation* is yielded:

$$\Phi(\mathrm{z}_1) - \Phi(\mathrm{z}_0) = \mathrm{g}_0(Z_1 - Z_0) = R\int_{p_0}^{p_1} T\, d\ln p \tag{A.13}$$

Here $Z \equiv \frac{\Phi(\mathrm{z})}{\mathrm{g}_0}$, is the *geopotential height*, where $\mathrm{g}_0 \equiv 9.80665$ m s^{-2} is the global average of gravity at mean sea level.

Defining a layer mean temperature:

$$\langle T\rangle = \frac{\int_{p_0}^{p_1} Td\ln p}{\int_{p_0}^{p_1} d\ln p} \tag{A.14}$$

and a layer mean scale height $H \equiv \frac{R\langle T\rangle}{\mathrm{g}_0}$ the result of the hypsometric equation results to be:

$$\Phi_1 - \Phi_0 \equiv \mathrm{g}Z_t = R\langle T\rangle \ln\frac{p_0}{p_1} \tag{A.15}$$

where the quantity Z_t is the thickness of the layer between p_0 and p_1 measured in units of geopotential meters. This formula shows that the thickness is proportional to the mean temperature in the layer. Hence, lines of equal Z_t (isolines of thickness)

[5] For computational convenience, the mean surface pressure is often assumed to equal 1000 hPa.
[6] The gas constant R for dry air is equal to 287 J kg^{-1} K^{-1}.

are equivalent to the isotherm of mean temperature in the layer.
When there is a horizontal temperature gradient, the thickness of the layer would be greatest where the temperature is greatest.

Then, differentiating the geostrophic wind, written in the vectorial form in the isobaric coordinate system as:

$$\mathbf{V}_g = \frac{1}{f}\mathbf{k} \times \boldsymbol{\nabla}_\mathbf{p} \Phi \tag{A.16}$$

where f is the Coriolis parameter, $\mathbf{k}$ is the wave vector, and the subscript "p" on the gradient operator denotes gradient on a constant pressure surface. Integrating from pressure level p_0 to p_1, the thermal wind equation can be obtained:

$$\mathbf{V}_T = \frac{1}{f}\mathbf{k} \times \boldsymbol{\nabla}_\mathbf{p}(\Phi_1 - \Phi_0) \tag{A.17}$$

.

Alternatively, the thermal wind can be expressed for a given layer in terms of the horizontal gradient of the vertically mean temperature, substituting the expression (A.15), resulting from the hypsometric equation (A.13):

$$\mathbf{V}_T = \frac{R}{f}\mathbf{ln}\left(\frac{p_0}{p_1}\right)\mathbf{k} \times \boldsymbol{\nabla}_\mathbf{p}\langle \mathrm{T} \rangle \tag{A.18}$$

It's clear that the thermal wind blows parallel to the isotherms (lines of constant thickness) with the warm air to the right facing downstream in the Northern Hemisphere (Holton, 2004), while, in the Southern Hemisphere, the change in sign of f flips the direction.
If a component of the geostrophic wind is parallel to the temperature gradient, the thermal wind will cause the geostrophic wind to rotate with height: if the geostrophic wind blows from cold air to warm air (*cold advection*) the geostrophic wind will turn counterclockwise with height, a phenomenon known as *wind backing*; otherwise, if the geostrophic wind blows from warm air to cold air (*warm advection*) the wind will turn clockwise with height, also known as *wind veering*.
Wind backing and veering allow to estimate the horizontal temperature gradient with data from an atmospheric sounding (Holton, 2004).

Quasi-geostrophic theory

The effect of friction, between the air and the land, breaks the geostrophic balance. Friction slows the flow, lessening the effect of the Coriolis force. As a result, the pressure gradient force has a greater effect and the air still moves from high pressure to low pressure, though with great deflection. This explains why high pressure system winds radiate out from the center of the system, while low pressure systems have winds that spiral inwards.

The geostrophic wind neglects frictional effects, which is usually a good approximation for the synoptic scale instantaneous flow in the midlatitude mid-troposphere (Holton, 2004). Although ageostrophic terms are relatively small, they are essential for the time evolution of the flow and in particular are necessary for the growth and decay of storms.

The *quasi-geostrophic theory* helps to understand how the mass fields (via horizontal temperature advection) and the momentum fields (via horizontal vorticity advection) interact to create vertical circulations that result in realistic synoptic-scale weather patterns.

For extratropical synoptic-scale motions, however, the horizontal velocities are approximately geostrophic. Such motions, which are usually referred to a *quasi-geostrophic*, are simpler to analyze than are tropical disturbances or planetary scale disturbances. The quasi-geostrophic system is constituted by the equations of hydrostatic and geostrophic balance that constrain the baroclinic motions so that to a good approximation the structure the evolution of the three-dimensional velocity field are determined by the distribution of geopotential height on isobaric surfaces.

Therefore, for this analysis, it's convenient to use the isobaric coordinate system, simplifying the dynamical equations.

Horizontal velocity can be separated into a mean component and an instability term, the geostrophic and ageostrophic components :

$$\mathbf{V} = \mathbf{V}_g + \mathbf{V}_a \tag{A.19}$$

where the first term is the geostrophic wind and the second is the ageostrophic wind, given by the difference between the horizontal wind and the geostrophic wind.

Assuming that the meridional length scale, L, is small compared to the radius of

the earth, $\mathbf{V}_g$ is calculated using a constant reference latitude value of the Coriolis parameter. For the systems of interest the geostrophic term is much greater than the ageostrophic term. More precisely, the ratio of the magnitudes of the ageostrophic and geostrophic winds is the same order of magnitude as the Rossby number (A.14). So, horizontal advection is accomplished by only the geostrophic winds and the vertical advection term disappears from the total derivative:

$$\frac{D}{Dt} = \left(\frac{\partial}{\partial t}\right)_p + (\mathbf{V}\cdot\boldsymbol{\nabla})_p + \omega\frac{\partial}{\partial p} \tag{A.20}$$

where $\omega = \frac{Dp}{Dt}$ is the pressure change following the motion. As a consequence, the rate of change of momentum following the total motion is then approximately equal to the rate of change of the geostrophic momentum following the geostrophic wind, so $\frac{D\mathbf{V}}{Dt} \approx \frac{D_g\mathbf{V}_g}{Dt}$, where $\frac{D_g}{Dt} = \frac{\partial}{\partial t} + \mathbf{V}_g\cdot\boldsymbol{\nabla}$.

Although a constant f_0 can be used in defining $\mathbf{V}_g$, it is still necessary to retain the dynamical effect of the variation of the Coriolis parameter with latitude in the Coriolis force term in the momentum equation. This variation can be approximated by expanding the latitudinal dependence of f in a Taylor series about a reference latitude ϕ_0 and retaining only the first two terms to yield:

$$f = f_0 + \beta y \tag{A.21}$$

where $\beta \equiv \left(\frac{df}{dy}\right)_{\phi_0} = \frac{2\Omega\cos\phi_0}{a}$ (with a representing the Earth radius) is the constant meridional gradient in the Coriolis parameter and y=0 at ϕ_0. This approximation is usually referred to as the *midlatitude β-plane* approximation[7]. For synoptic-scale motions, the ratio of the first two terms in the expansion of f has an order of magnitude as the Rossby number order and this justifies letting the Coriolis parameter have a constant value in the geostrophic approximation and approximating its variation in the Coriolis force term by (A.21).

The difference between the Coriolis force and the pressure gradient force depends on the departure of the actual wind from the geostrophic wind. Hence, it's not permissible to simply replace the horizontal velocity by its geostrophic value ion

[7] This approximation is a geometrical simplification consisting in replacing the spherical coordinates (x,y), and in restricting the flow domain to some neighborhood of the latitude ϕ_0.

the Coriolis term. Using the geostrophic relation (A.16) to eliminate the pressure gradient force and neglecting the ageostrophic wind compared to the geostrophic wind in the term proportional to βy. Therefore, the approximate horizontal momentum equation has the form:

$$\frac{D_g \boldsymbol{V}_g}{Dt} = -f_0 \boldsymbol{k} \times \boldsymbol{V}_a - \beta y \boldsymbol{k} \times \boldsymbol{V}_g \tag{A.22}$$

where every term has an order of magnitude of the Rossby number compared to the pressure gradient force, whereas terms that have an order of magnitude of the square of Rossby number or smaller are neglected.

Furthermore, the geostrophic wind has a null divergence, so the only contribute to the field divergence is given by the ageostrophic wind and the continuity equation can be rewritten as:

$$\frac{\partial u_a}{\partial x} + \frac{\partial v_a}{\partial y} + \frac{\partial \omega}{\partial p} = 0 \tag{A.23}$$

which shows that ω is determined only by the ageostrophic part of the wind field (Holton, 2004).

First, stretching is directly related to convergence by the continuity equation:

$$\frac{\partial u_a}{\partial x} + \frac{\partial v_a}{\partial y} = -\frac{\partial \omega}{\partial p} \tag{A.24}$$

so that when the vertical column is stretched, horizontal convergence tends to occur. Alternatively, horizontal divergence is associated with compression of the vertical column. The process can also be illustrated by visualizing a parcel whose volume remains constant but whose vertical and horizontal dimensions are allowed to change. If the parcel is stretched, then it will contract horizontally (converge), whereas when it is compressed, it will expand horizontally (diverge).

The absolute vorticity is made up of two parts: relative vorticity or that which is moving along with the rotating coordinate system on earth and the earth's vorticity (f) due to the earth's rotation.

The vertical component of the relative vorticity can be defined, approximating geostrophically, as:

$$\xi_{\mathrm{g}} = \frac{\partial v_{\mathrm{g}}}{\partial x} - \frac{\partial u_{\mathrm{g}}}{\partial y} \tag{A.25}$$

This equation shows the combined effects of how the north-south wind varies in the east-west direction and how the east-west wind varies in the north-south direction. In other words, relative vorticity represents a point measure of the rotation of the airflow moving along with the rotating coordinate system on the Earth.

To obtain the quasi-geostrophic vorticity equation, the x and y components of the quasi-geostrophyc momentum equation (A.22) can be expressed as:

$$\frac{D_{\mathrm{g}} u_{\mathrm{g}}}{Dt} - f_0 v_a - \beta y v_{\mathrm{g}} = 0 \tag{A.26a}$$

$$\frac{D_{\mathrm{g}} v_{\mathrm{g}}}{Dt} + f_0 u_a - \beta y u_{\mathrm{g}} = 0 \tag{A.26b}$$

Deriving (A.8a) respect to x and (A.8b) respect to y, and using the fact that the geostrophic wins is nondivergent, yields the vorticity equation:

$$\frac{D_{\mathrm{g}} \xi_{\mathrm{g}}}{Dt} = -f_0 \left(\frac{\partial u_a}{\partial x} + \frac{\partial v_a}{\partial y} \right) - \beta v_{\mathrm{g}} \tag{A.27}$$

The divergence of the ageostrophic wind can be eliminated in favor of ω, using (A.24), and noting that f depends only on y, the vorticity equation becomes:

$$\frac{\partial \xi_{\mathrm{g}}}{\partial t} = -\mathbf{V}_{\mathrm{g}} \cdot \boldsymbol{\nabla}(\xi_{\mathrm{g}} + f) + f_0 \frac{\partial \omega}{\partial p} \tag{A.28}$$

which states that the local rate of change of geostrophic vorticity is given by the sum of the advection of the absolute vorticity by the geostrophic wind plus the concentration or dilution of vorticity by stretching or shrinking of fluid columns.

If advection is ignored, thus, geostrophic relative vorticity is tending to decrease with time because of either compression or divergence and to increase because of either stretching or convergence. Returning to the parcel illustration, as the parcel expands vertically, air converges towards the axis of rotation causing it to rotate faster. When the parcel compresses vertically, air diverges from the axis of rotation causing the parcel to spin more slowly.

The advection term, however, is the dominant term in the upper levels. In essence, despite a decreasing trend in geostrophic relative vorticity due to the vertical motion pattern, the fast wind speeds and high values of vorticity aloft produce a more dominant advection pattern which increases the geostrophic vorticity downstream of the trough with time.

A change in the vertical shear of the horizontal wind associated with differential (height dependent) vorticity advection will drive an ageostrophic vertical circulation, which adiabatically adjusts the horizontal temperature gradient to maintain thermal wind balance. The convergence and divergence fields associated with this vertical circulation will not only modify the effects of vorticity advection at upper levels, but will force changes in the vorticity distribution in the lower troposphere where advection may be very weak. In an analogous manner, thermal advection, which is often strong near the surface, induces a vertical circulation which alter the vorticity fields both near the surface and aloft that thermal wind balance is maintained.

The Eulerian-mean equations

Many of the middle-atmosphere phenomena can be regarded as resulting of the interaction of a mean flow with disturbances, the so-called *eddies*, that are superimposed upon it. Thus, the zonal wind field can be separated into a zonal-mean part and a disturbance quantity, which can be written for the mean flow on a β-plane as:

$$u \equiv u'(x, y, z, t) + \bar{u} \tag{A.29a}$$

where the zonal mean wind is given by the relation:

$$\bar{u}(y, z, t) \equiv {a_0}^{-1} \int_0^{a_0} u(x, y, z, t) dx \tag{A.29b}$$

where $a_0 \equiv 2\pi a \cos \phi_0$ is the length of the latitude circle at $\phi = \phi_0$.

This average is an example of an *Eulerian*[8] mean, since it's taken over the longitudinal coordinate (in β-plane approximation this coordinate is y), at fixed values of the other coordinates.

In the quasi-geostrophic approximation on the β-plane, the primitive equations from which starting to obtain the Eulerian-mean equations are:

$$\frac{Du}{Dt} - fv + \frac{\partial \Phi}{\partial x} = X \tag{A.30a}$$

$$\frac{Dv}{Dt} + fu + \frac{\partial \Phi}{\partial y} = Y \tag{A.30b}$$

$$\frac{\partial \Phi}{\partial z} = H^{-1} R\theta e^{-kz/H} \tag{A.30c}$$

$$\frac{\partial \mathrm{u}}{\partial x} + \frac{\partial \mathrm{v}}{\partial y} + \frac{1}{\rho_0}\frac{\partial(\rho_0 \mathrm{w})}{\partial z} = 0 \tag{A.30d}$$

$$\frac{D\theta}{Dt} = Q \tag{A.30e}$$

where (X,Y) are the horizontal component of friction or of other non-conservative mechanical forcing, Φ is the geopotential height, $Q \equiv \left(\frac{J}{c_p}\right) e^{kz/H}$ is the diabatic heating, with J is the diabatic heating rate per unit mass (which in the middle atmosphere equals the net radiative heating rate per unit mass plus a small thermal conduction term) and H is a vertical scale parameter. Here the pressure gradient force is expressed as the geopotential height gradient and last two equations, representing the continuity of mass equation and the thermodynamic relation between diabatic heating and the material rate of change of potential temperature θ, are added respect to the previous paragraphs.

Separating each variable into a zonal-mean component and a disturbance one, as in (A.29b), substituting into (A.30), taking the zonal average and performing a little manipulation, we obtain the following set of quasi-geostrophic equations, dropping subscripts *g* on geostrophic quantities, but retaining subscripts *a* on ageostrophic variables:

[8] The Eulerian mean is taken considering fixed locations in the space through which the fluid flows as time passes; whereas, another kind of average is the Lagrangian mean, which is taken over a specified set of fluid parcels following their moving in the space.

$$\frac{\partial \bar{u}}{\partial t} - f_0 \bar{v}_a - \bar{X} = -\frac{\partial(\overline{v'u'})}{\partial y} \tag{A.31a}$$

$$\frac{\partial \theta}{\partial t} + \bar{w}_a \frac{\partial \theta_0}{\partial z} - \bar{Q} = -\frac{\partial(\overline{v'\theta'})}{\partial y} \tag{A.31b}$$

$$\frac{\partial \bar{v}_a}{\partial y} + \frac{1}{\rho_0}\frac{\partial(\rho_0 \bar{w}_a)}{\partial z} = 0 \tag{A.31c}$$

$$f_0 \frac{\partial \bar{u}}{\partial z} + \frac{Re^{-kz/H}}{H}\frac{\partial \bar{\theta}}{\partial y} = 0 \tag{A.31d}$$

These equations form a closed set for the mean-flow variables ($\bar{u}$,$\bar{\theta}$, $\bar{v}_a$,$\bar{w}_a$), given the rectified eddy-forcing terms on the right, $\bar{X}$, $\bar{Q}$, and apposite boundary and initial conditions. In the upper troposphere and in the middle atmosphere, as well as in the boundary layer, the zonally averaged turbulent drag $\bar{X}$ result to be important because represents stresses due to unresolved eddies (such as gravity waves). The y component is absent because in the case of quasi-geostrophic flow on a β-plane the zonal-mean geostrophic wind is purely zonal by periodicity:

$$\bar{v}_g \equiv a_0^{-1} \int_0^{a_0} \frac{\partial \psi}{\partial x} dx = 0 \tag{A.32}$$

where $\psi(x, y)$ is the stream function[9], whose spatial derivations give the components of a two-dimensional wind field with a null divergence ($\partial u_g/\partial x + \partial v_g/\partial y = 0$).

However, the Eulerian-mean equations govern the zonal-mean flow, whereas the eddy component can be described by similar equations but these are more useful in studies of small-amplitude departures from the zonal-mean state because, in this case, they can be linearized in amplitude and eventually solved numerically (Andrews *et al.*, 1987).

Returning to the mean flow equations, to understand how this flow respond to eddy fluxes, it's convenient to transform the mean-flow equations to an alternative form, as we'll see in the next section.

[9] For horizontal non-divergent motion, the flow field can be represented by a stream function $\psi(x, y)$ defined so that the velocity components are given as $u = -\partial\psi/\partial y$, $v = \partial\psi/\partial x$ (Holton, 2004).

The transformed Eulerian-mean equations

For a better understanding of the properties that regulate the interaction between the zonal-mean flow and eddy forcing, it would be more useful to use another type of approach that takes account of the fact that in (A.31b) there tends to be a strong annulment between the eddy heat flux convergence and adiabatic cooling, while the diabatic heating term is a small residual. Since in the mean an air parcel tends to rise to a higher equilibrium altitude only if its potential temperature is increased by diabatic heating, it triggers the *residual meridional circulation* associated with diabatic processes that is directly related to the mean meridional mass flow (Holton, 2004). Therefore, it can firstly define this residual mean meridional circulation $(0,\bar{v}^*, \bar{w}^*)$ for β-plane geometry and in a quasi-geostrophic case, by:

$$\bar{v}^* \equiv \bar{v}_a - \frac{1}{\rho_0}\frac{\partial(\rho_0\overline{v'\theta'}/\theta_{0z})}{\partial z} \tag{A.33a}$$

$$\bar{w}^* \equiv \bar{w}_a + \frac{\partial(\overline{v'\theta'}/\theta_{0z})}{\partial y} \tag{A.33b}$$

where the vertical derivation of potential temperature is simplified by the notation $\theta_{0z} = \partial\theta_0/\partial z$.

On substituting for $(\bar{v}^*, \bar{w}^*)$ in (A.31), the following quasi-geostrophic *transformed Eulerian-mean* (TEM) set is obtained:

$$\frac{\partial\bar{u}}{\partial t} - f_0\bar{v}^* - \bar{X} = -\frac{1}{\rho_0}\boldsymbol{\nabla}\cdot\mathbf{F} \tag{A.34a}$$

$$\frac{\partial\theta}{\partial t} + \bar{w}^*\frac{\partial\theta_0}{\partial z} - \bar{Q} = 0 \tag{A.34b}$$

$$\frac{\partial\bar{v}^*}{\partial y} + \frac{1}{\rho_0}\frac{\partial(\rho_0\bar{w}^*)}{\partial z} = 0 \tag{A.34c}$$

$$f_0\frac{\partial\bar{u}}{\partial z} + \frac{Re^{-kz/H}}{H}\frac{\partial\bar{\theta}}{\partial y} = 0 \tag{A.34d}$$

where the vector $\mathbf{F} \equiv (0, -\rho_0\overline{v'u'}, \rho_0\overline{v'\theta'}/\theta_{0z})$, in the transformed mean

zonal momentum equation (A.34a), is the only explicit eddy-forcing term in the TEM equations, considering that, in fact, in the thermodynamic equation (A.34b) the eddy forcing result to be negligible.

Therefore, according to what has been said, the eddy momentum flux $\overline{v'u'}$ and eddy heat flux $\overline{v'\theta'}$ act in combination, through the divergence of the *Eliassen-Palm flux* (EP flux) **F:**

$$\boldsymbol{\nabla \cdot F} \equiv -\frac{\partial(\rho_0 \overline{v'u'})}{\partial y} + \frac{\partial(\rho_0 f_0 \overline{v'\theta'}/\theta_{0z})}{\partial z} \qquad \text{(A.35)}$$

Statistic significance and t-Student test

In this section it is considered how the statistical significance of individual trends should be assessed when the data are strongly autocorrelated and how the significance of trends difference should be estimated to identify small trend differences embedded in noisy time series.

The first issue is important primarily within the framework of a model consisting of a linear trend plus noise, where the noise is assumed to have a lag-1 autocorrelation structure. The sensitivity of trend significance depends from the assumptions made in accounting for temporal autocorrelation (Santer *et al.*, 2000). Deducing cause and effect is hampered by: the short length (20 years or less) of the available deep-layer temperature time series; the forcing uncertainties and model errors, which lead to uncertainties in the climate-change signals associated with anthropogenic and natural external forcing; the inadequate knowledge of the statistical properties of such signals (i.e., a lack of ensembles of experiments with different forcing mechanisms); the large high-frequency noise contributions from natural modes of variability; the poor understanding of possible linkages between anthropogenic forcing and changes in the frequency, intensity, and duration of these modes (Corti *et al.*, 1999; Hasselmann *et al.*, 1999).

Considering a time series, for example, of global-mean seasonal-mean temperature anomalies, $x(t)$, for some specified atmospheric layer and data set, with the number of time samples in each series that is equal to n_t. The least squares linear regression estimate of the trend in $x(t)$, b, minimizes the squared differences between $x(t)$ and the regression line $\hat{x}(t)$:

$$\hat{x}(t) = a + bt \; ; \qquad t = 1, \dots, n_t. \tag{A.36}$$

The regression residuals, e(t), are defined as:

$$e(t) = x(t) - \hat{x}(t); \qquad t = 1, \dots, n_t. \tag{A.37}$$

For statistically independent values of e(t), the standard error of b is defined as:

$$s_b = \frac{s_e}{\left[\sum_{t=1}^{n_t}(t-\bar{t})^2\right]^{1/2}} \tag{A.38}$$

where ${s_e}^2$, the variance of the residuals about the regression line, is given by:

$$s_e^2 = \frac{1}{n_t - 2}\sum_{t=1}^{n_t} e(t)^2 \tag{A.39}$$

(see, e.g., Wilks, 1995). It is necessary to note that in some studies, it is implicitly (and often incorrectly) assumed that values of $e(t)$ are statistically independent (e.g., Balling *et al.*, 1998).

If a trend in $x(t)$ is significantly different from zero is tested by computing the ratio between the estimated trend and its standard error:

$$t_b = b/s_b \tag{A.40}$$

Under the assumption that t_b is distributed as Student's *t*, the calculated t ratio is then compared with a critical t value, t_{crit}, for a stipulated significance level α and $n_t - 2$ degrees of freedom. If values of $e(t)$ are not statistically independent, as is often the case with temperature data, this approach, referred to as "NAIVE", must be modified. There are various ways of accounting for temporal autocorrelation in $e(t)$ (see, e.g., Wigley and Jones, 1981; Bloomfield and Nychka, 1992; Wilks, 1995; Ebisuzaki, 1997; Bretherton *et al.*, 1999). The simplest way (Bartlett, 1935; Mitchell *et al.*, 1966) uses an effective sample size n_e based on r_1, the lag-1 autocorrelation coefficient of $e(t)$:

$$n_e \approx n_t \frac{1-r_1}{1+r_1} \tag{A.41}$$

By substituting the estimated effective sample size n_e for n_t in (A.39), one obtains "adjusted" estimates of the standard deviation of regression residuals (s'_e) and hence of the standard error (s'_b) and *t* ratio (t'_b).

One interesting issue is whether r_1 should be estimated directly from $x(t)$ or from the regression residuals $e(t)$. In the presence of a large overall trend in $x(t)$, the former approach yields higher estimates of r_1, since the trend inflates the lag-1 autocorrelation.

If there are instead two samples data, it is possible to use two approaches to assess the significance of the trends difference. Considering two time series, $x(t)$ and $y(t)$, with least squares linear trends b_x and b_y and estimated standard errors s_{bx} and s_{by}. In the first approach, it is possible to examine whether there is overlap between the regions defined by $b_x \pm s_{bx}$ and $b_y \pm s_{by}$ (or between the "adjusted" confidence intervals, $b_x \pm s'_{bx}$ and $b_y \pm s'_{by}$). The second method uses the difference time series $d(t) = x(t) - y(t)$ and then determines whether b_d, the trend in $d(t)$, is significantly different from zero. Operating on the difference time series it is much important because it allows to reduce noise levels by subtracting variability common to $x(t)$ and $y(t)$. This facilitates identification of real trend differences that may exist between the two time series. In the first approach it is tested if the individual trends in $x(t)$ and $y(t)$ belong to the same population. In the second method, it is tested if difference in data treatment (e.g. measurements methods, spatial coverage, the version of the dataset) have a significant effect on the trends.

Given the raw standard errors s_{bx} and s_{by}, the *P*% confidence intervals for b_x and b_y can be determined assuming that the sampling distributions of b_x and b_y are Gaussian. This is a reasonable assumption if the temporal sample size is large (larger than 30), as in calculation of the unadjusted standard errors s_{bx} and s_{by}. To determine the 95% confidence intervals for s'_{bx} and s'_{by}, it is more appropriate to assume that b_x and b_y are distributed as Student's *t*.

Since the *t* distribution gives greater "weight" (i.e., assigns greater probability) to the tails than the normal distribution (e.g., Wilks, 1995), the small-sample confidence intervals estimated with the *t* distribution are wider than the corresponding confidence intervals estimated with the normal distribution.

However, b_x and b_y are normally distributed for calculating unadjusted 95% confidence intervals. Adjusted 95% confidence intervals can be calculated by inverting Student's t distribution to obtain t_{inv} for n_e degrees of freedom and p = 0.975 (two-tailed test). The adjusted 95% confidence interval is simply $b_x \pm t_{inv}$ (s_{bx}).

Appendix B

List of additional figures

Temperature

HT models

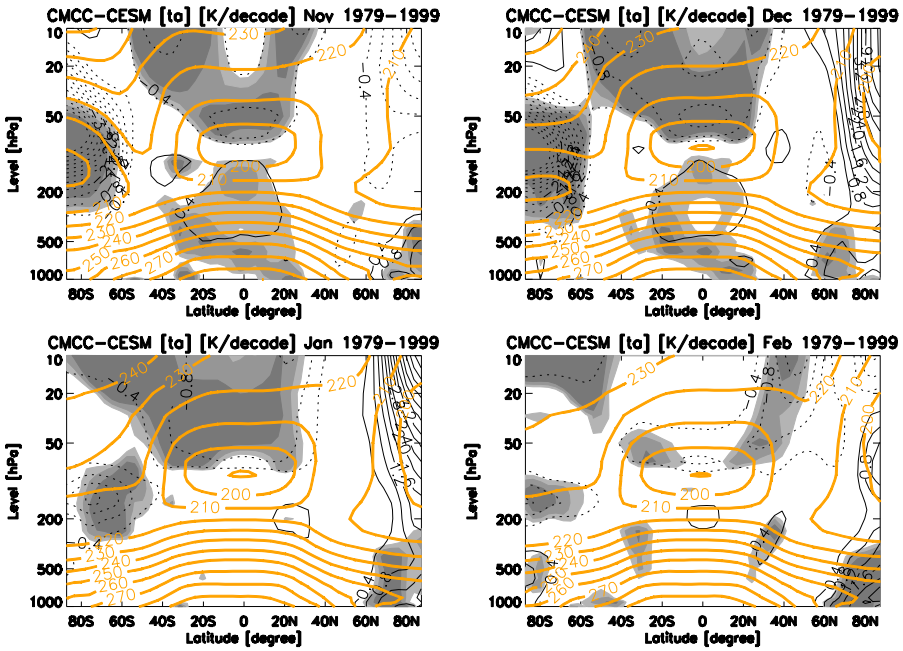

Figure B.1: as Figure 4.2.

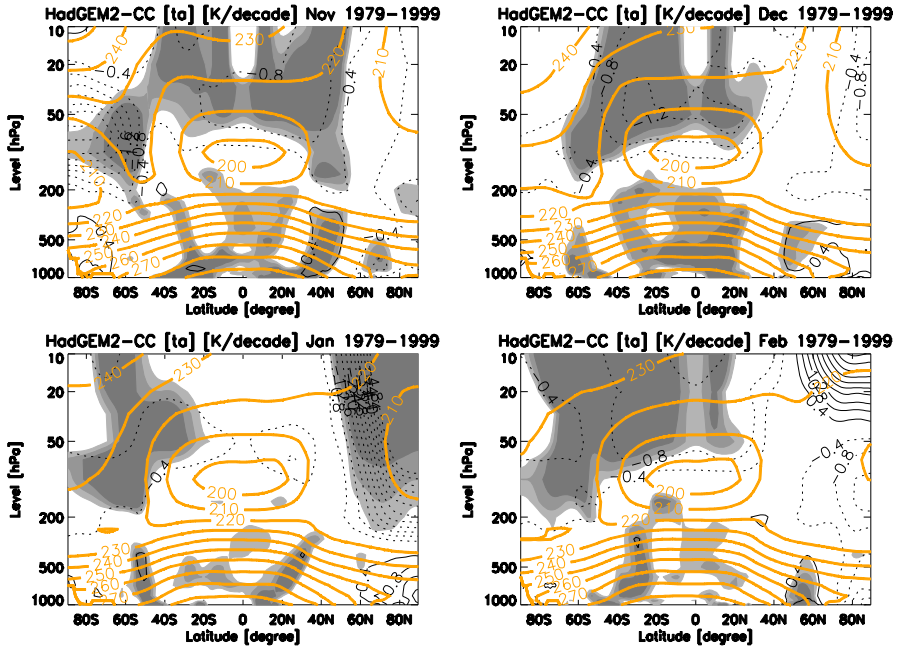

Figure B.2: as Figure 4.2.

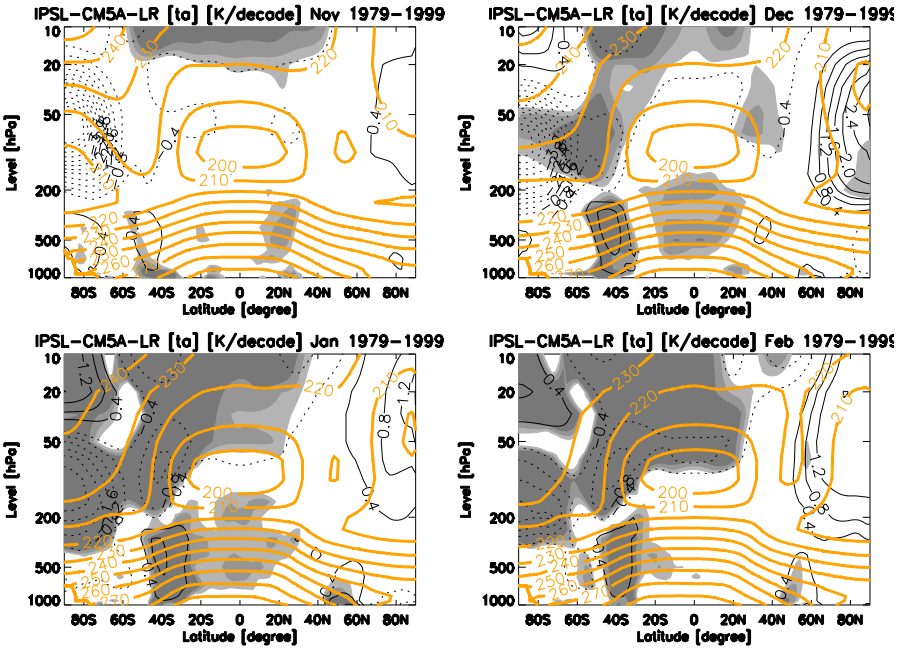

Figure B.3: as Figure 4.2.

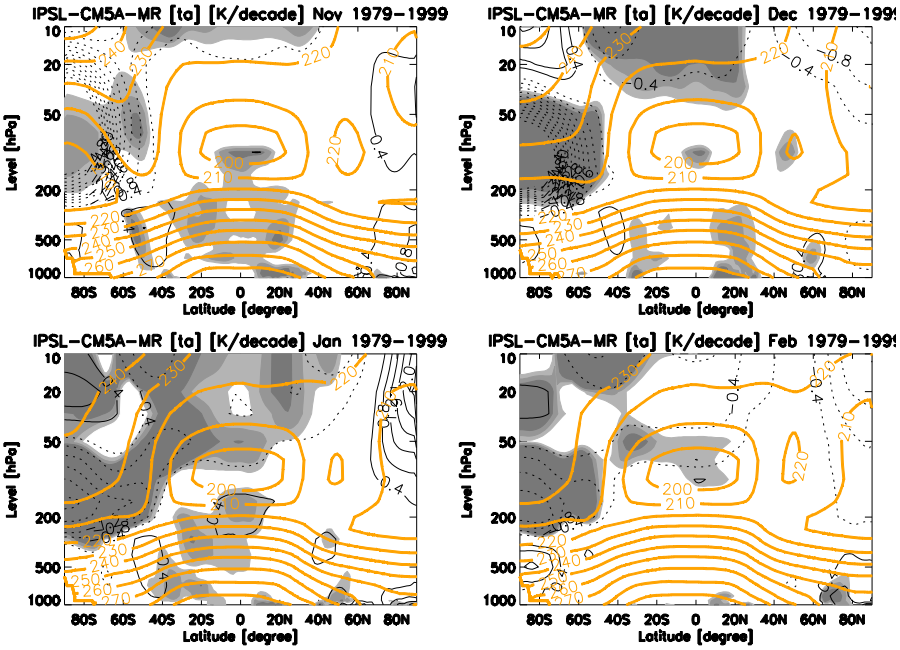

Figure B.4: as Figure 4.2.

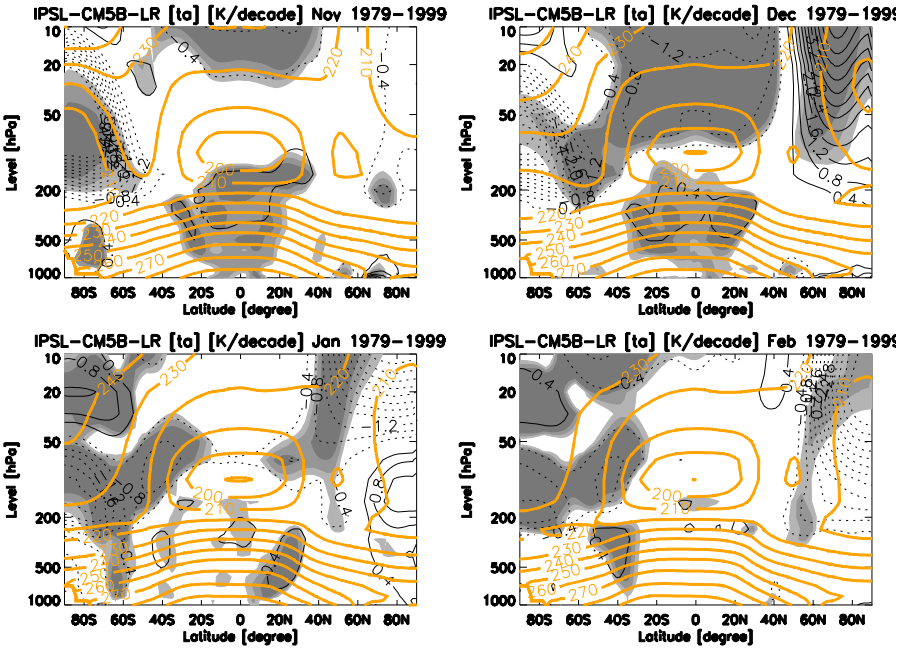

Figure B.5: as Figure 4.2.

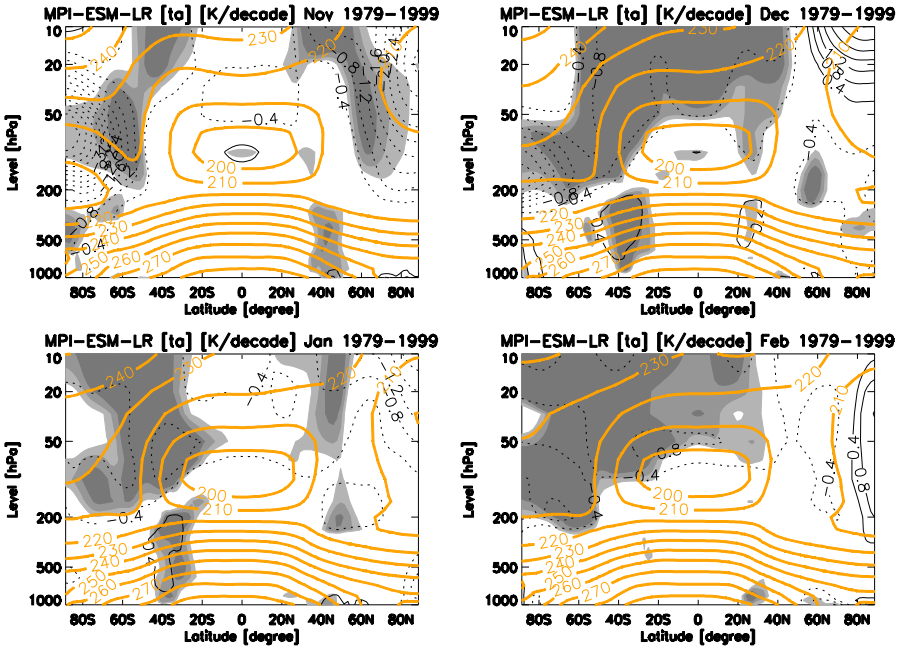

Figure B.6: as Figure 4.2.

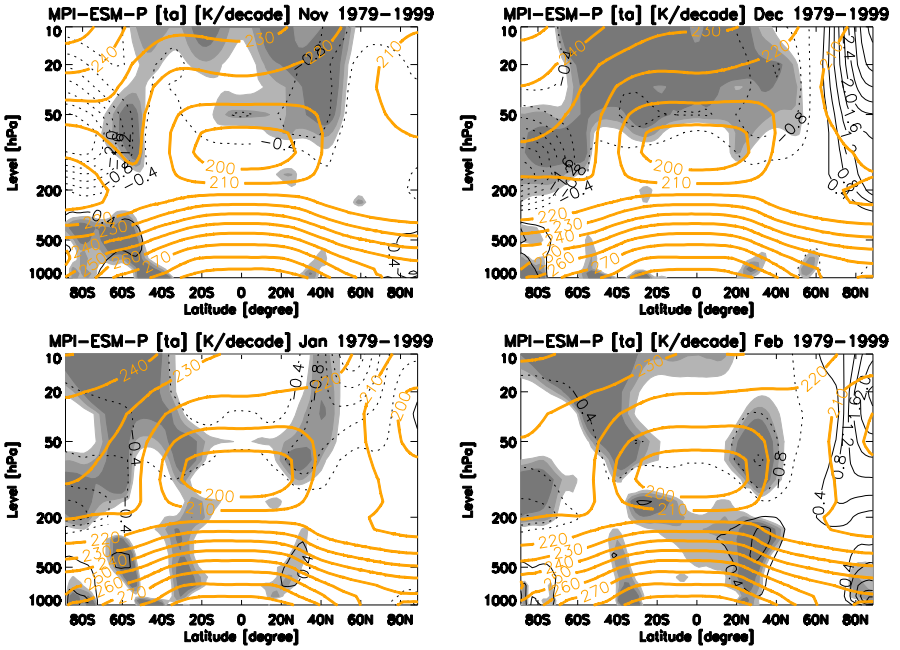

Figure B.7: as Figure 4.2.

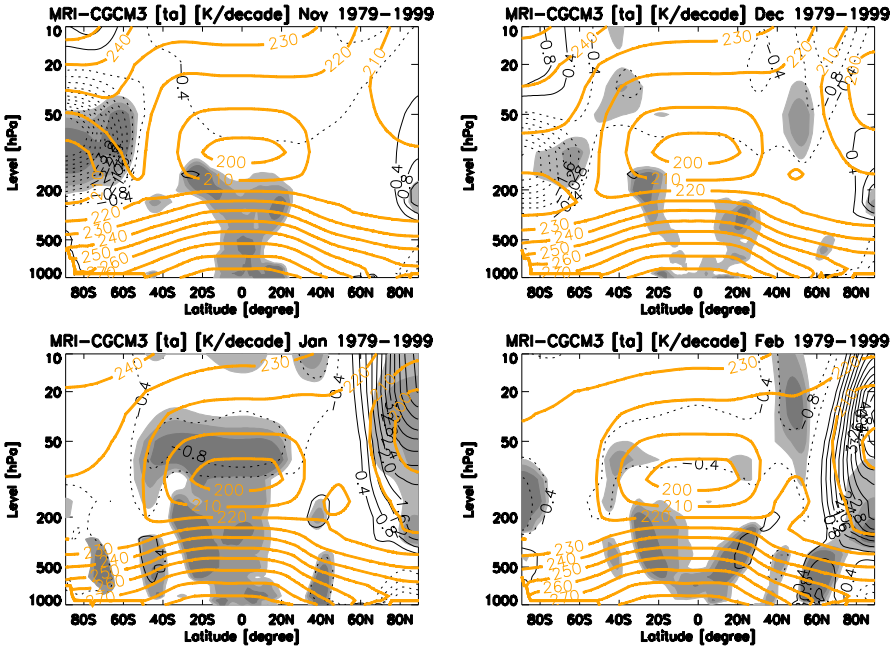

Figure B.8: as Figure 4.2.

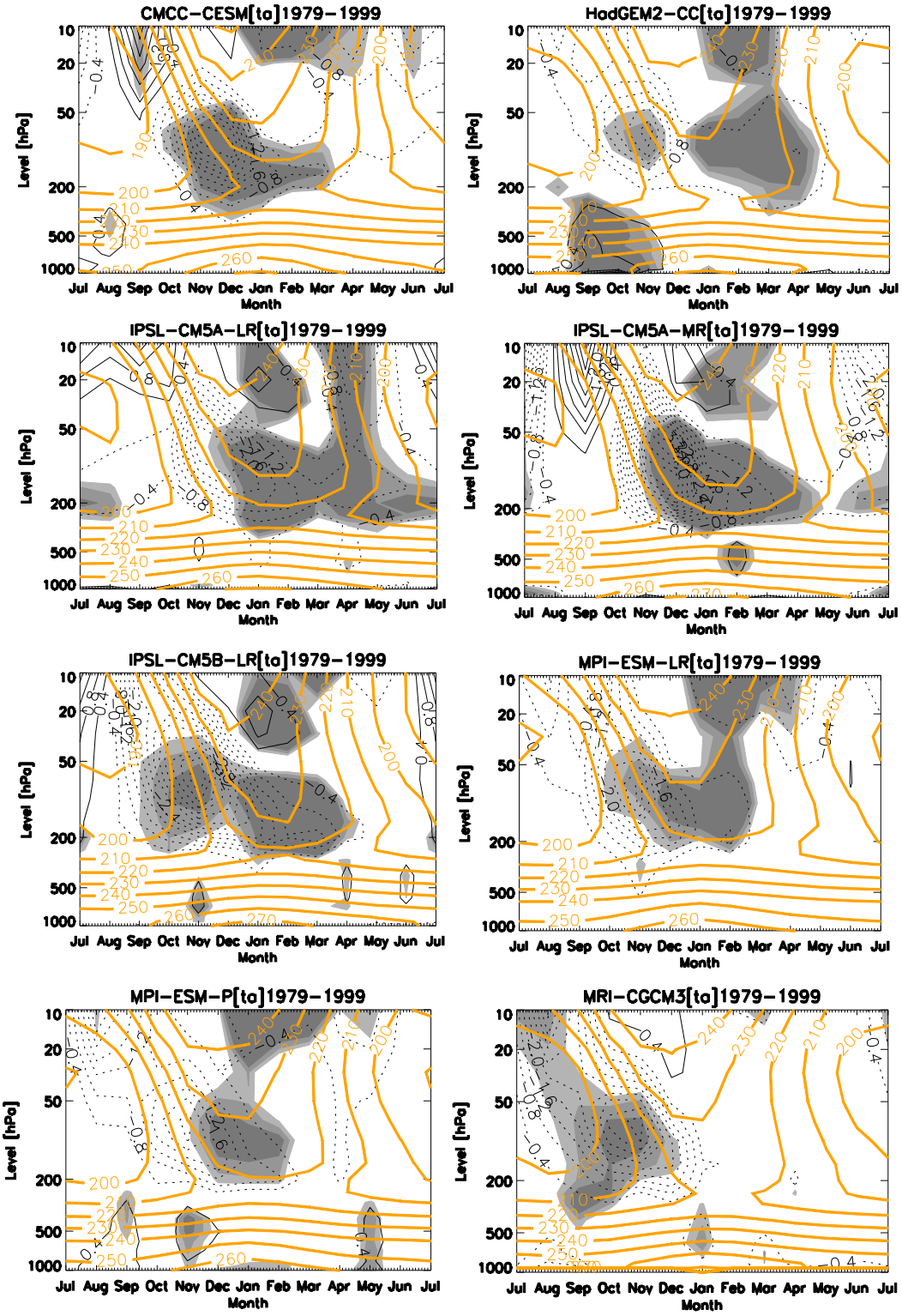

Figure B.9: as Figure 4.3.

LT models

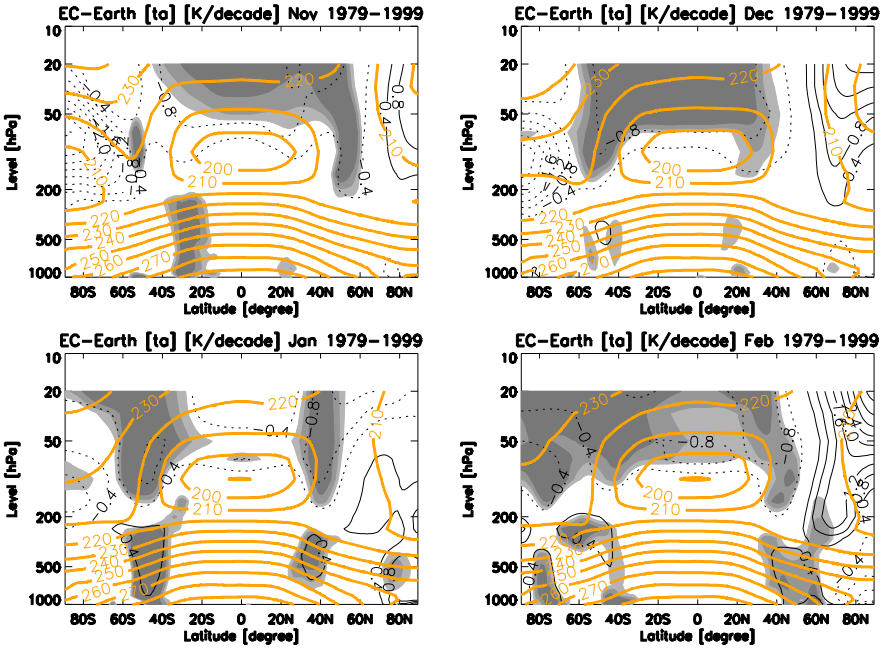

Figure B.10: as Figure 4.4.

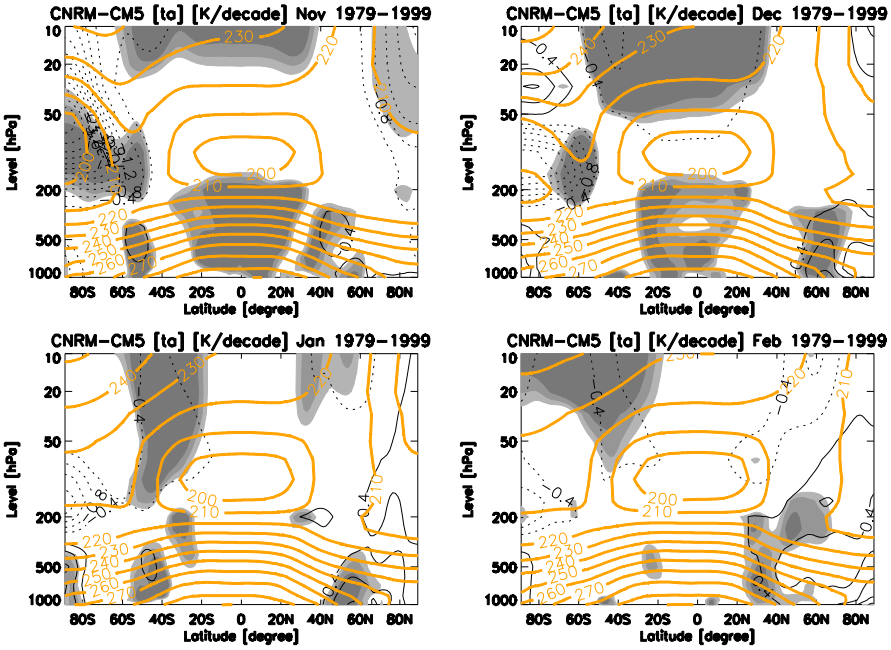

Figure B.11: as Figure 4.4.

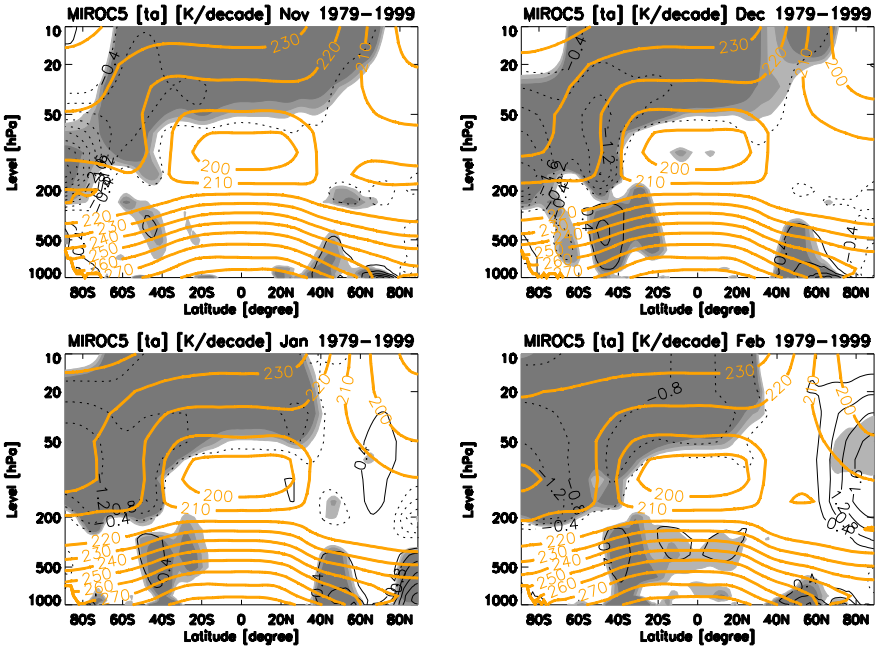

Figure B.12: as Figure 4.4.

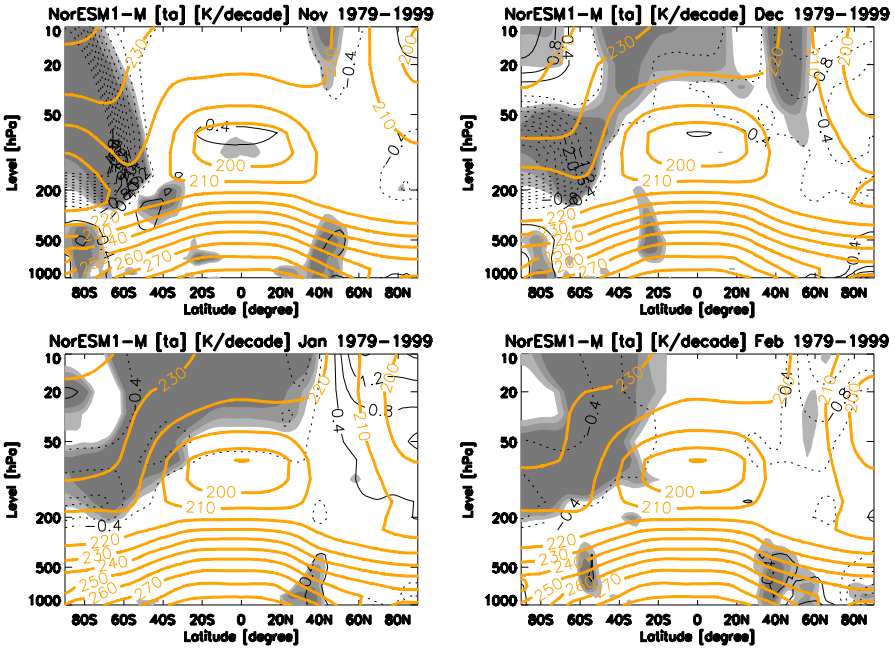

Figure B.13: as Figure 4.4.

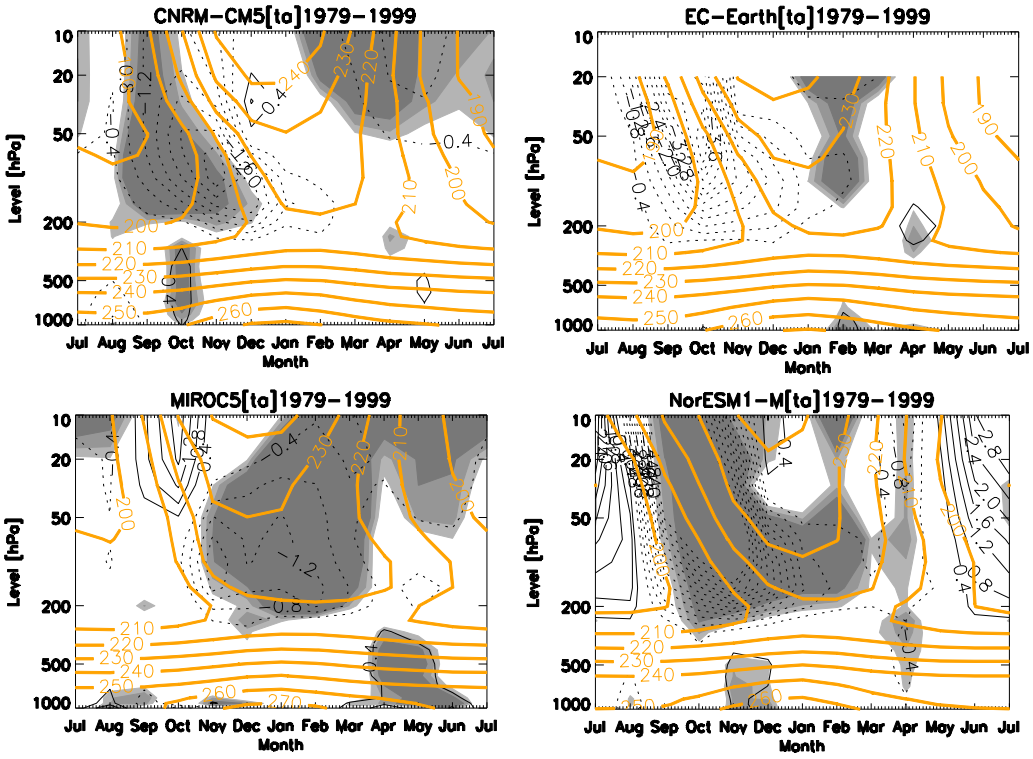

Figure B.14: as Figure 4.5.

Multi-model

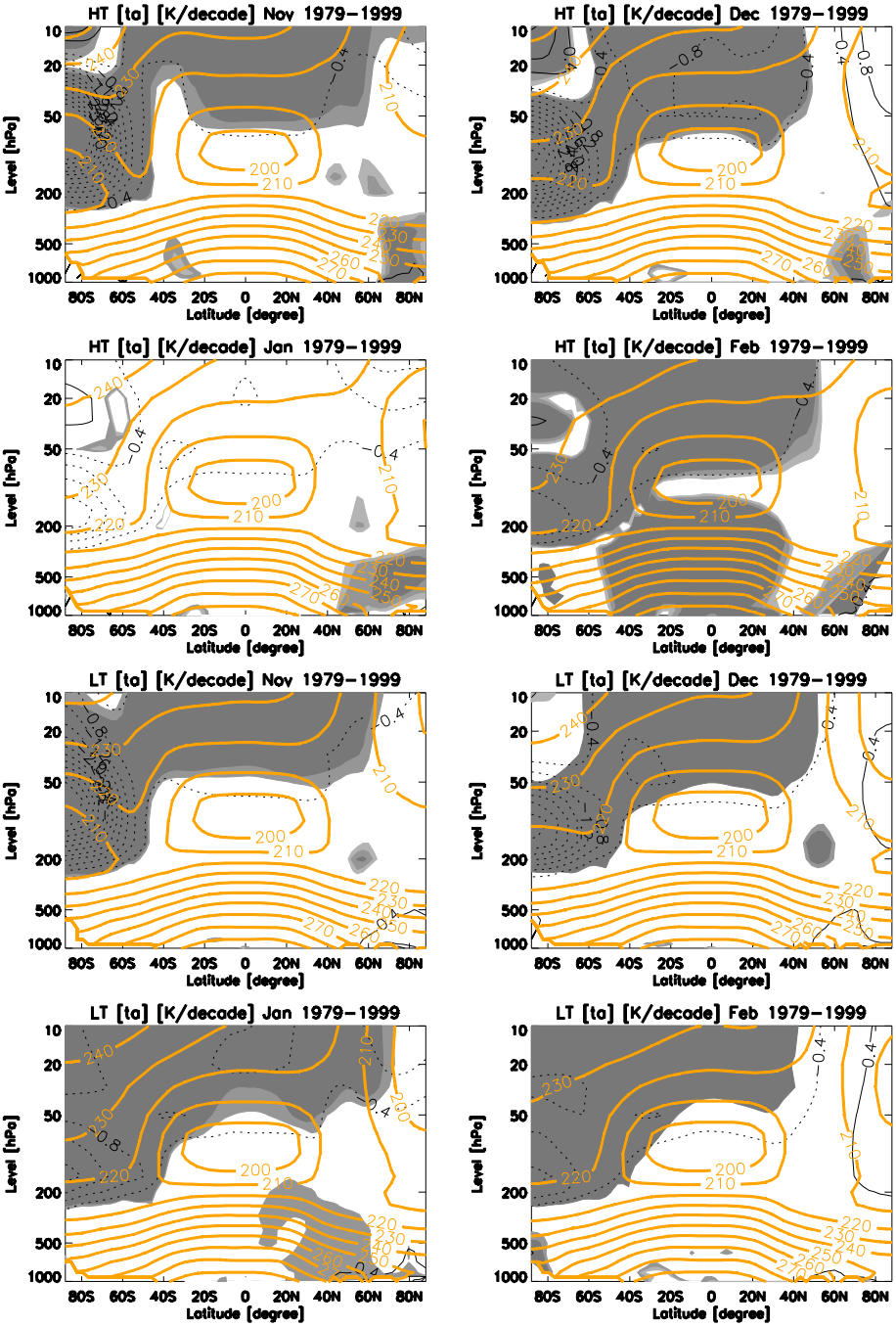

Figure B.15: as Figure 4.10 but for the zonal mean temperature field.

Zonal wind

HT models

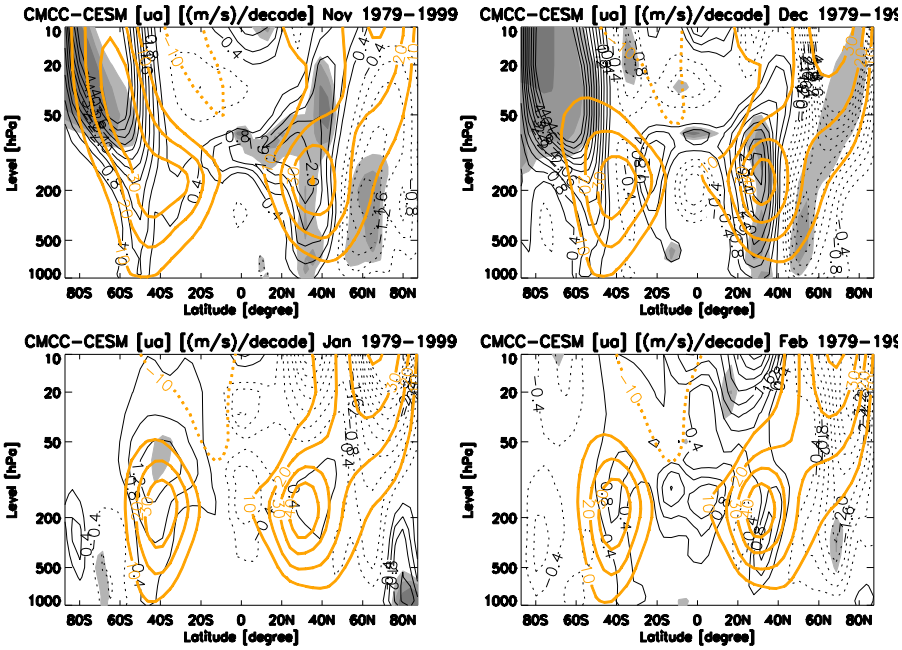

Figure B.16: as Figure 4.8.

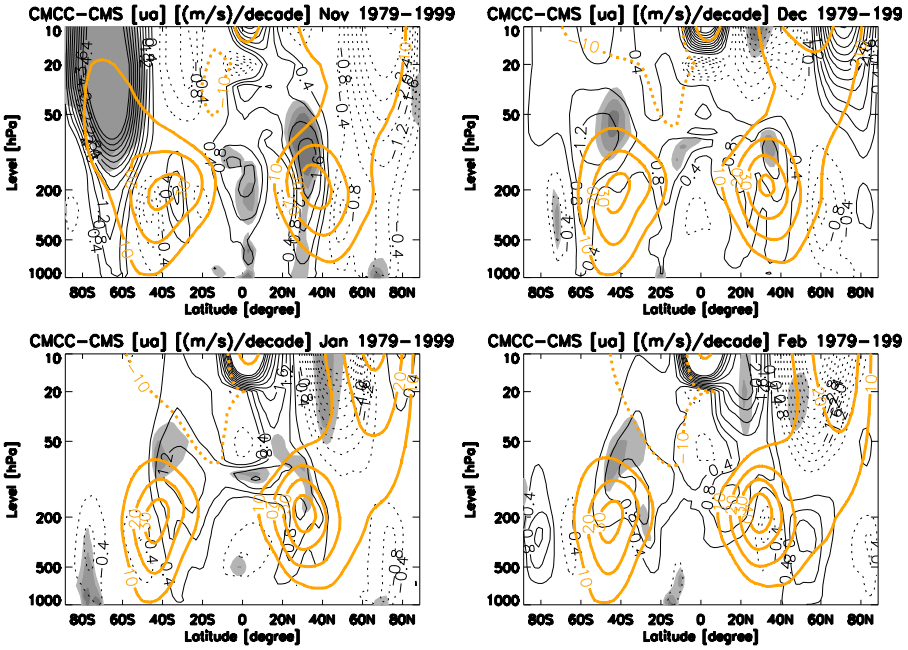

Figure B.17: as Figure 4.8.

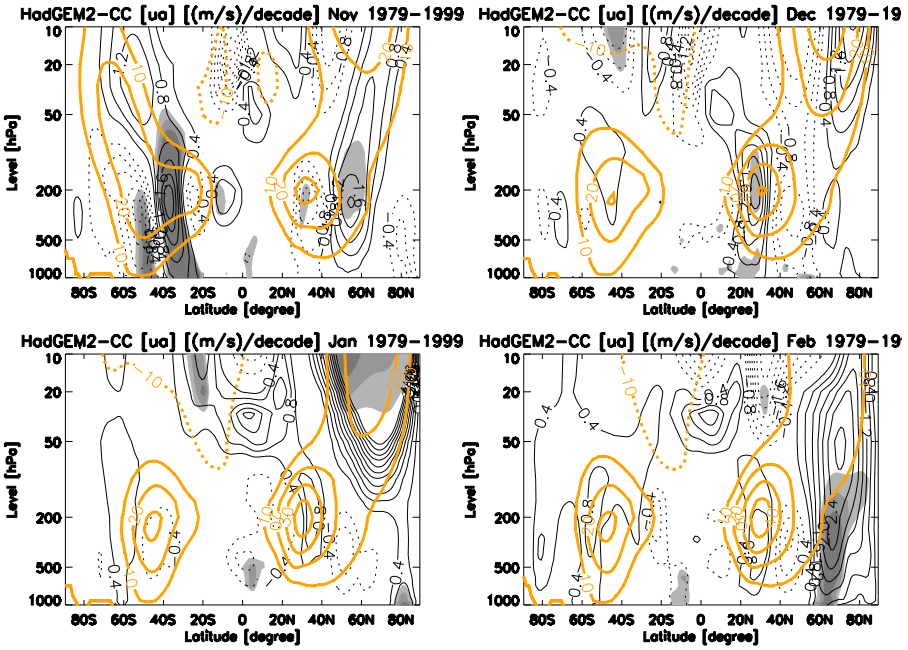

Figure B.18: as Figure 4.8.

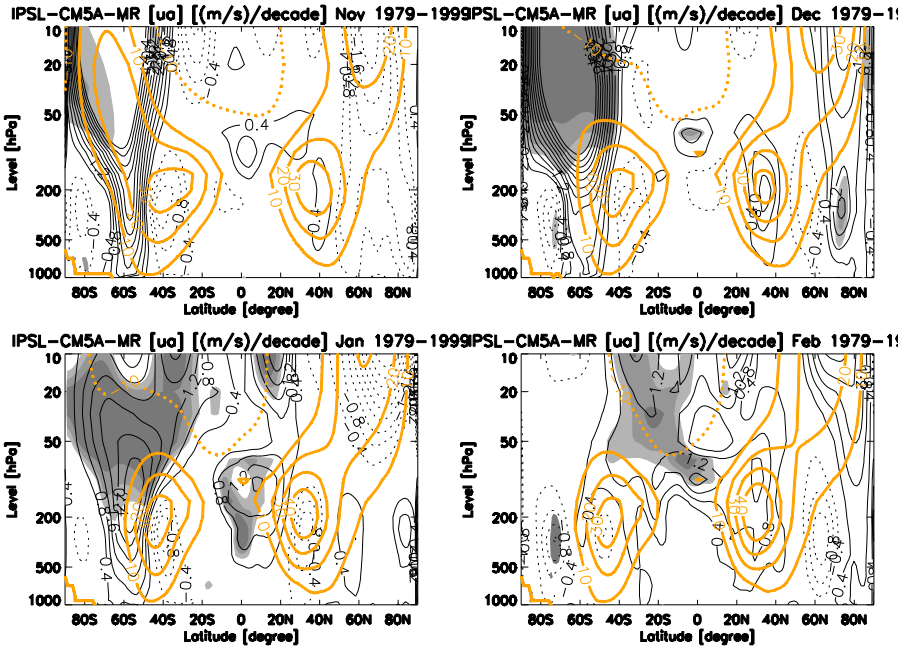

Figure B.19: as Figure 4.8.

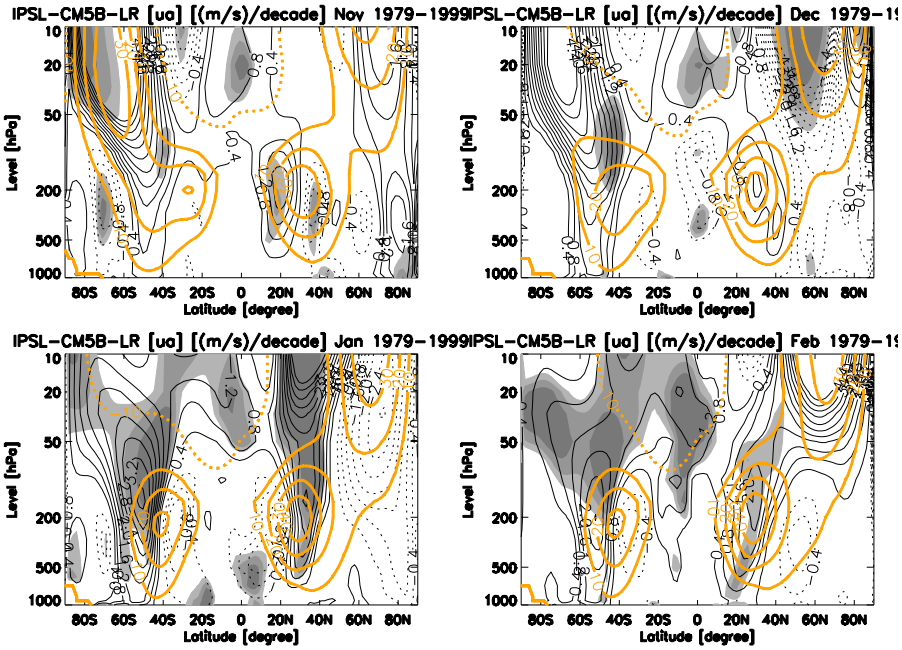

Figure B.20: as Figure 4.8.

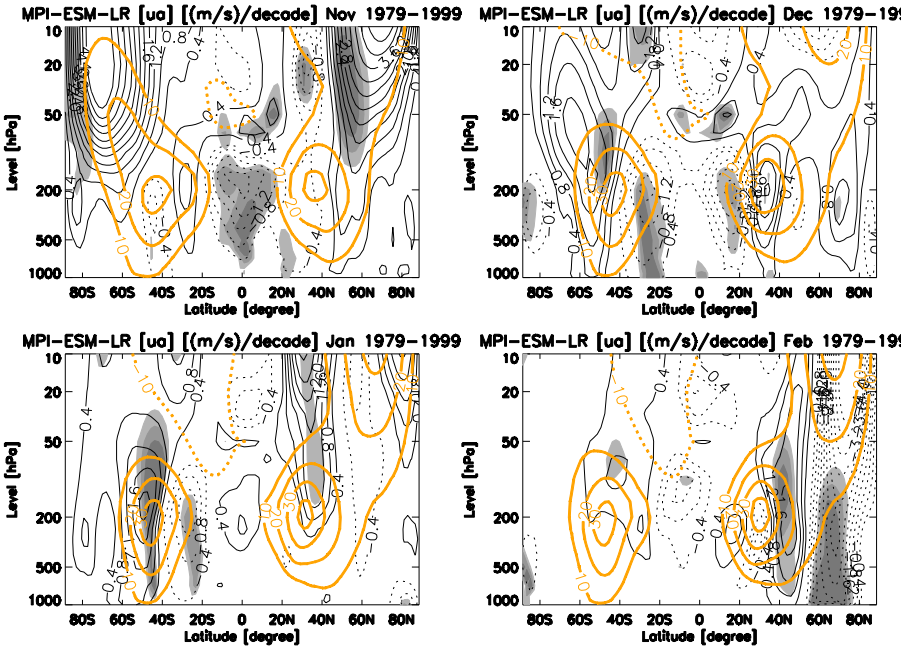

Figure B.21: as Figure 4.8.

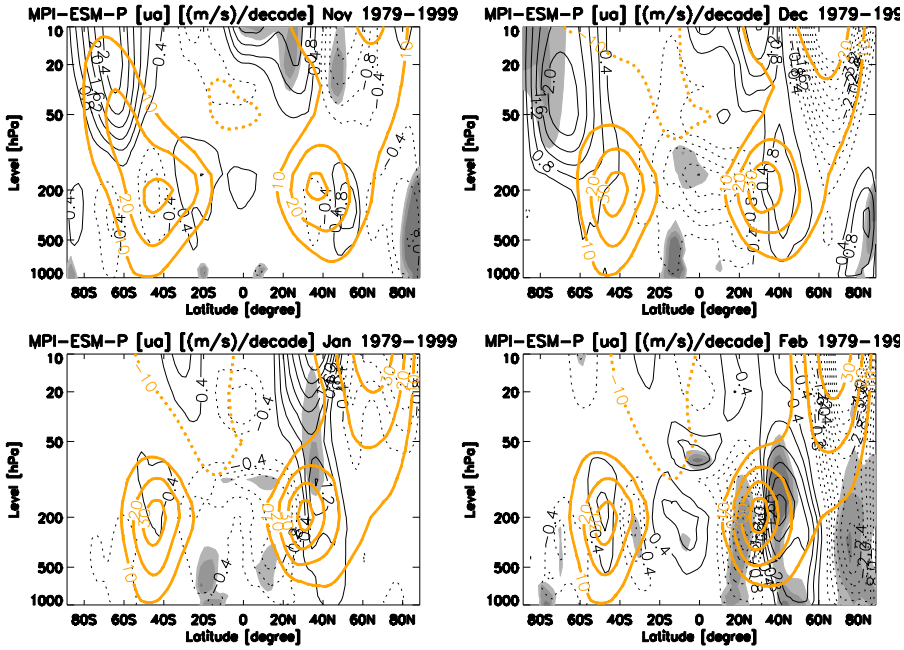

Figure B.22: as Figure 4.8.

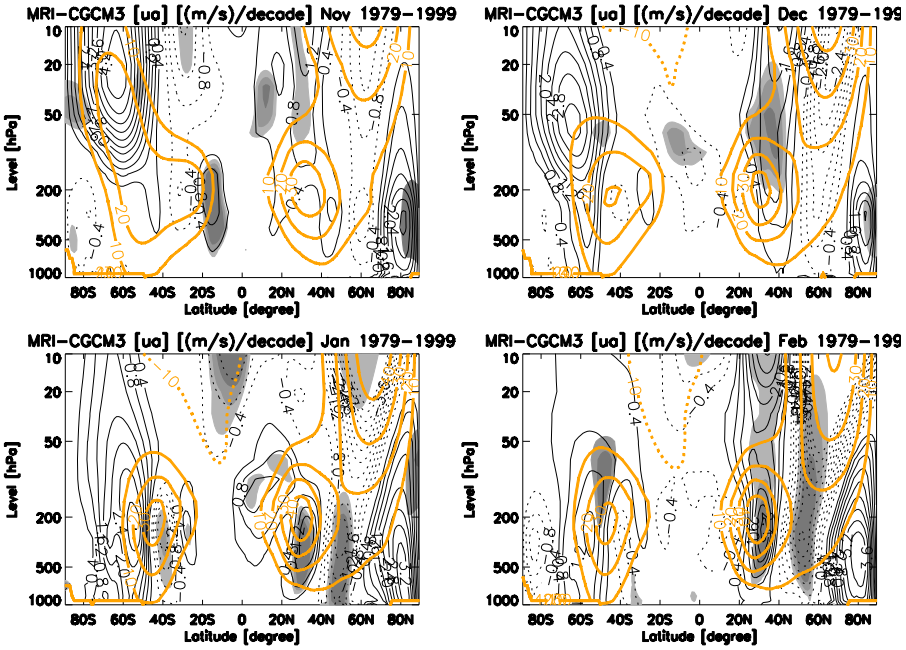

Figure B.23: as Figure 4.8.

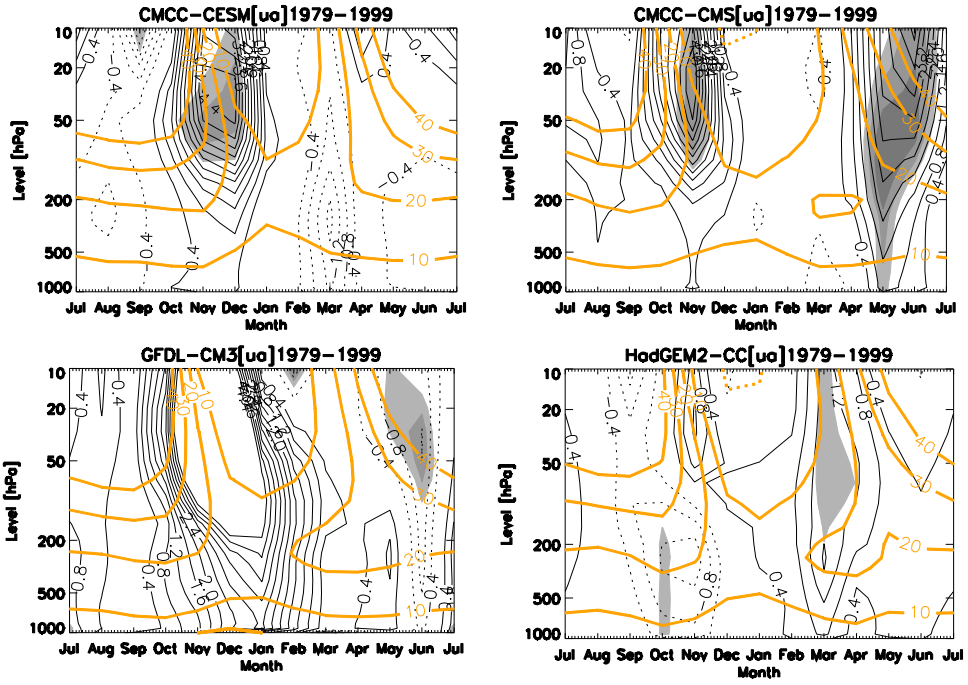

Figure B.24a: as Figure 4.3 but for the zonal mean zonal wind field (not shown in thesis chapters).

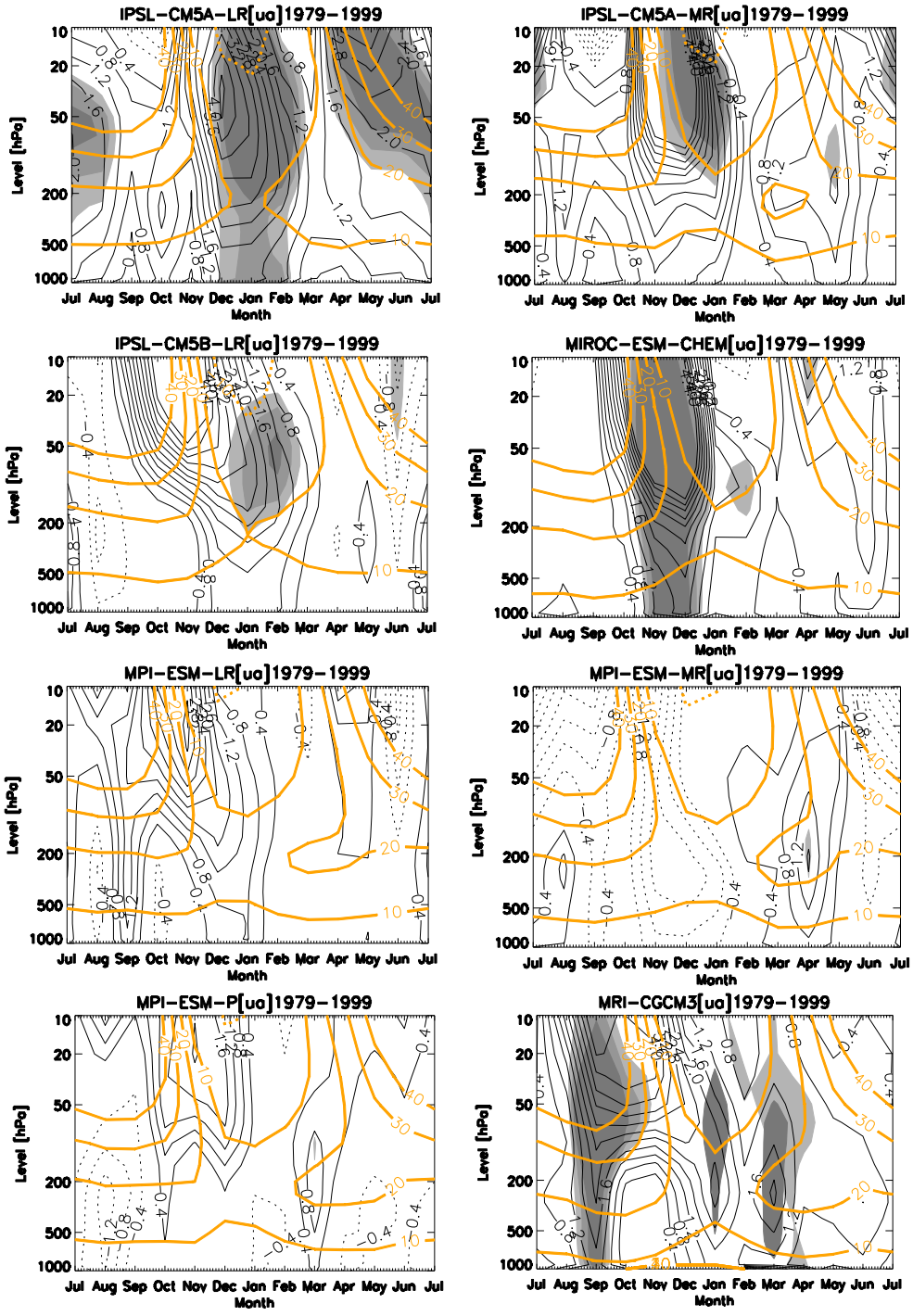

Figure B.24b: as Figure 4.3 but for the zonal mean zonal wind field (not shown in thesis chapters).

LT models

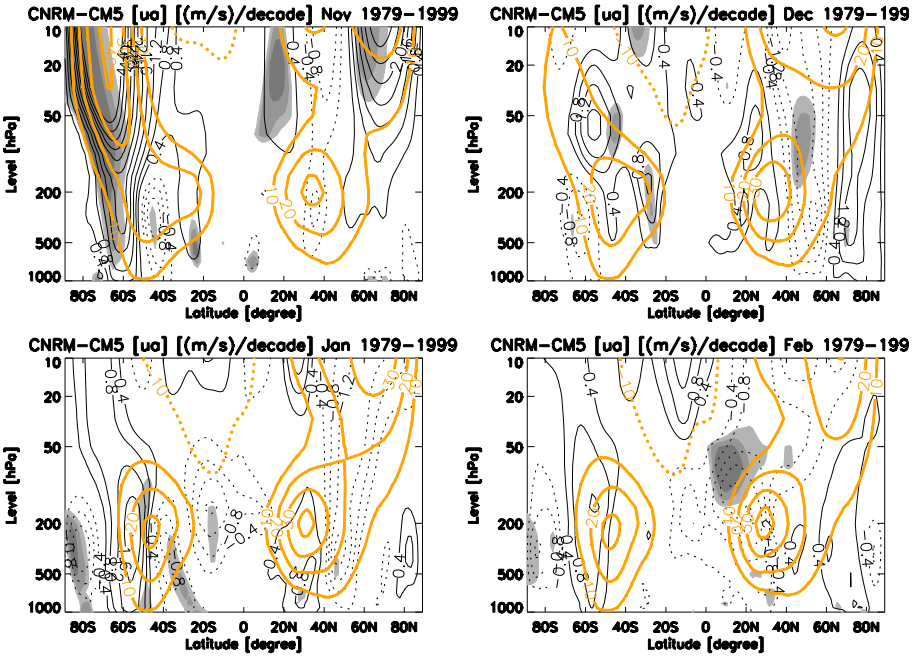

Figure B.25: as Figure 4.9.

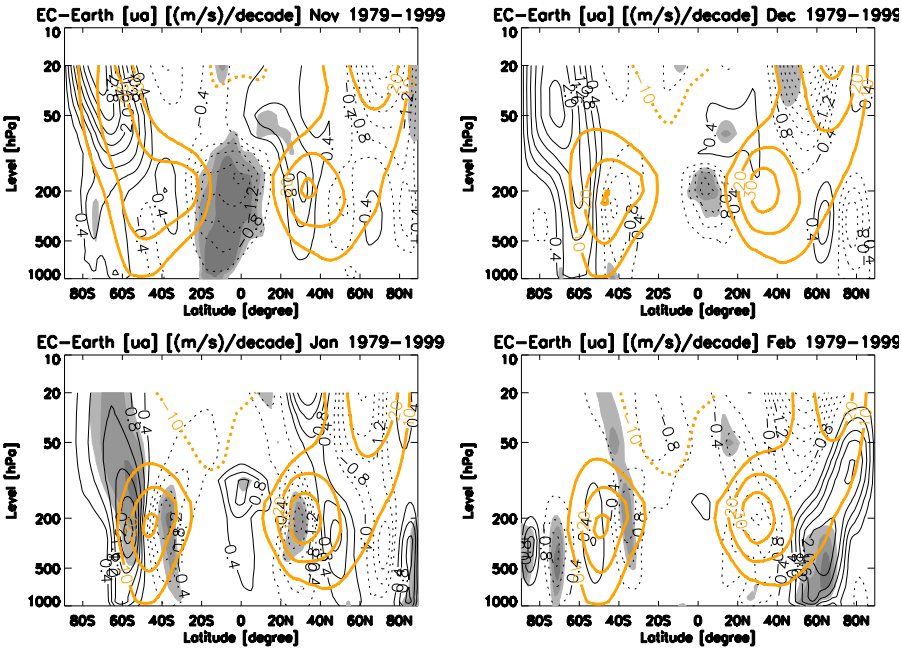

Figure B.26: as Figure 4.9.

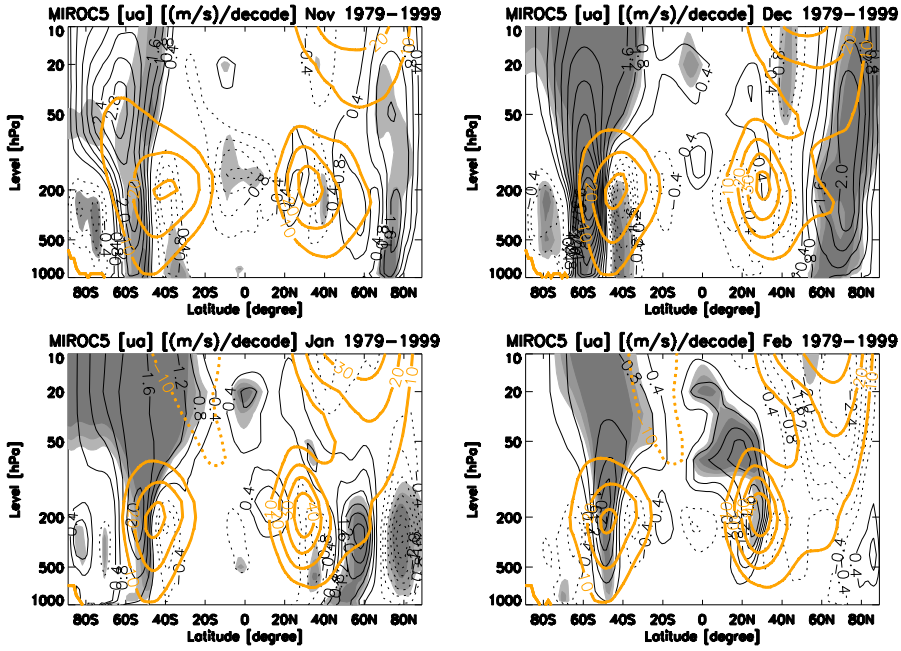

Figure B.27: as Figure 4.9.

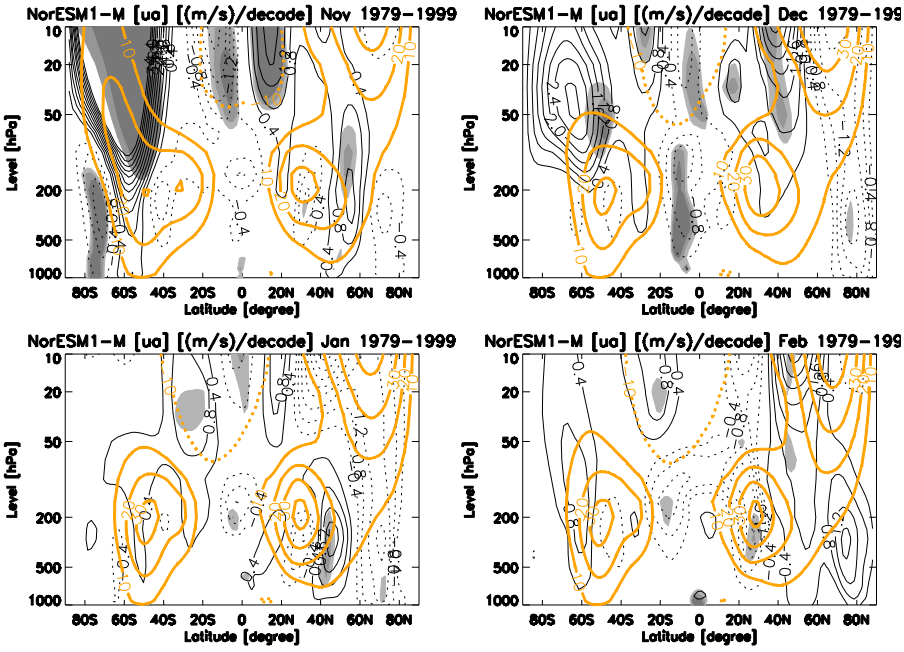

Figure B.28: as Figure 4.9.

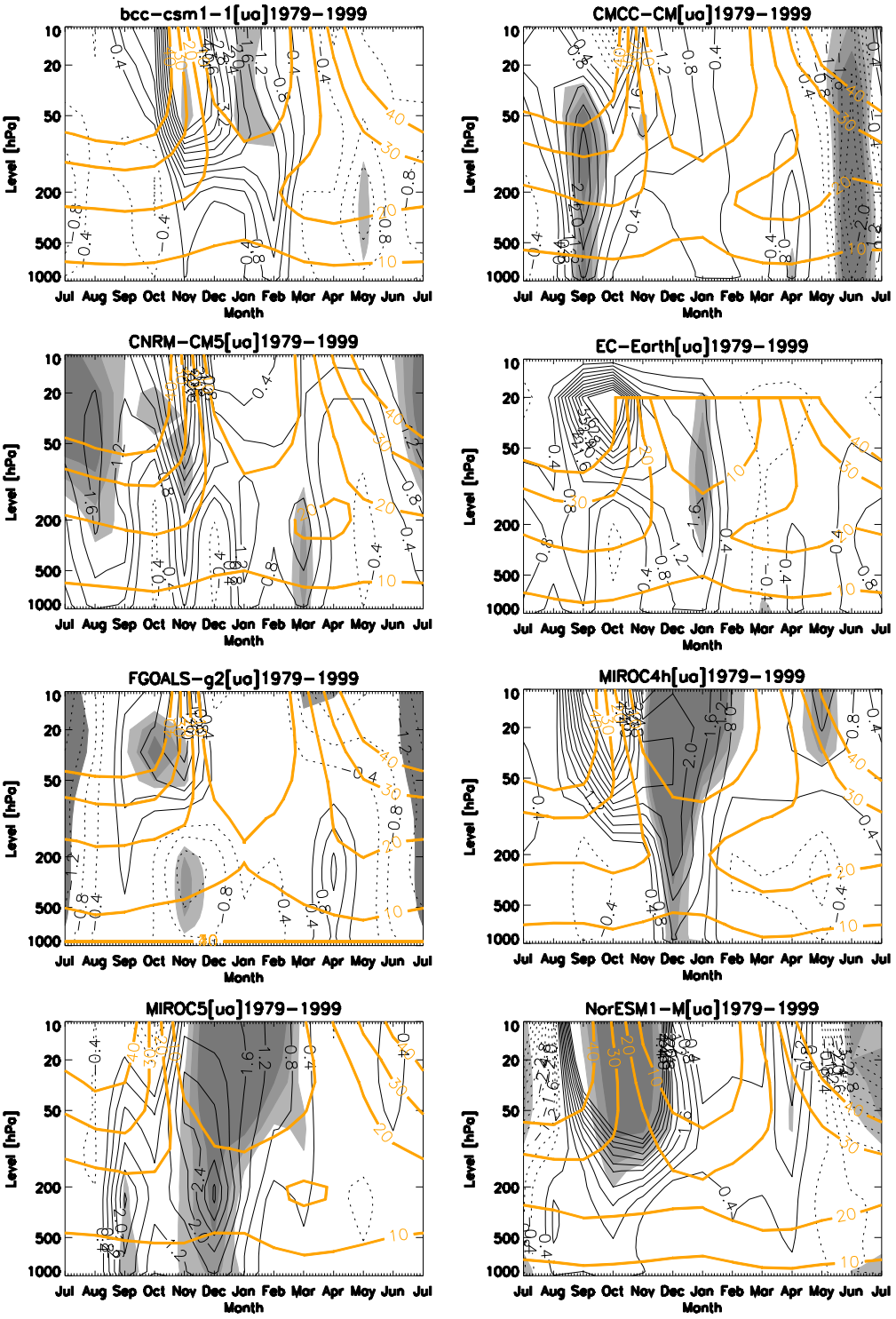

Figure B.29a: as Figure 4.6 but for the zonal mean zonal wind field (not shown in thesis chapters).

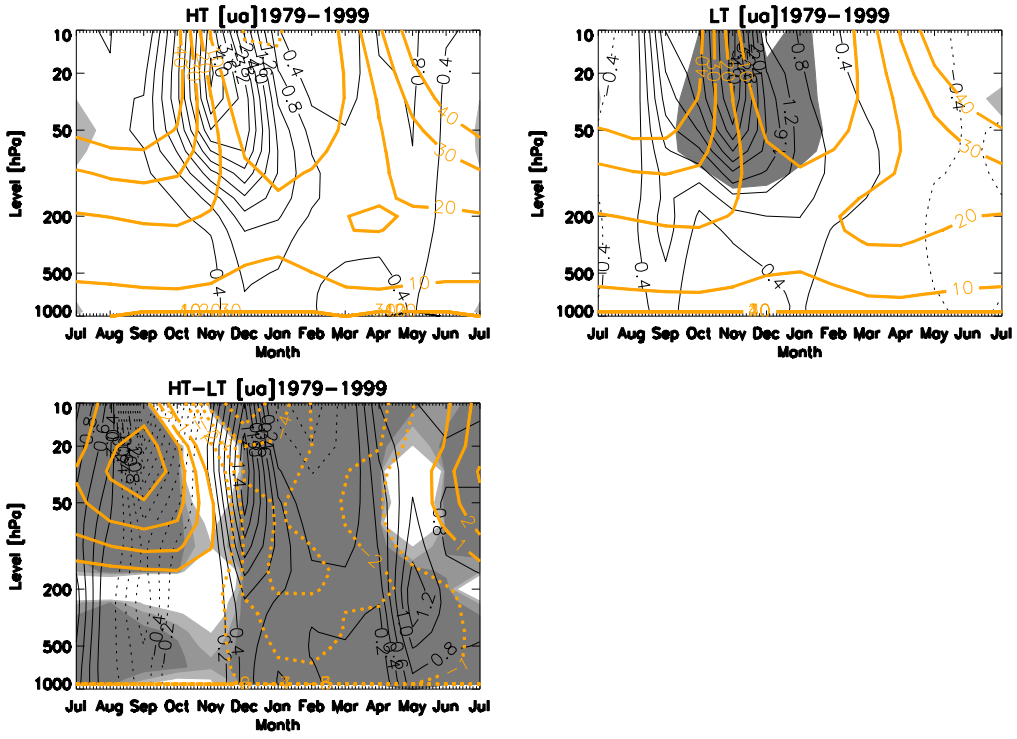

Figure B.29b: as Figure 4.6 but for the zonal mean zonal wind field (not shown in thesis chapters).

Scatter plot

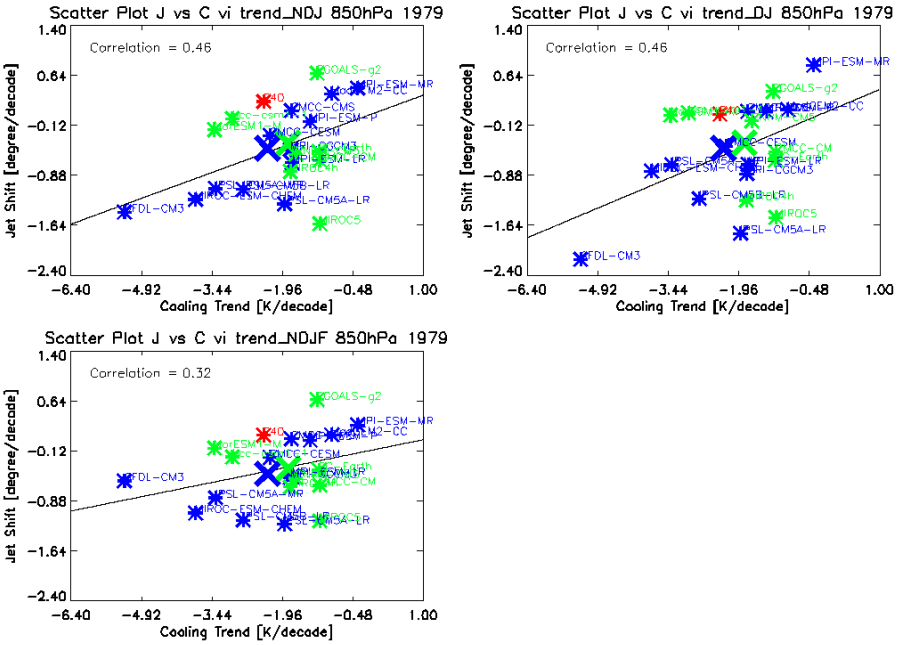

Figure B.30: as Figure 5.4 but with the jet shift trend constructed by vertical integration.

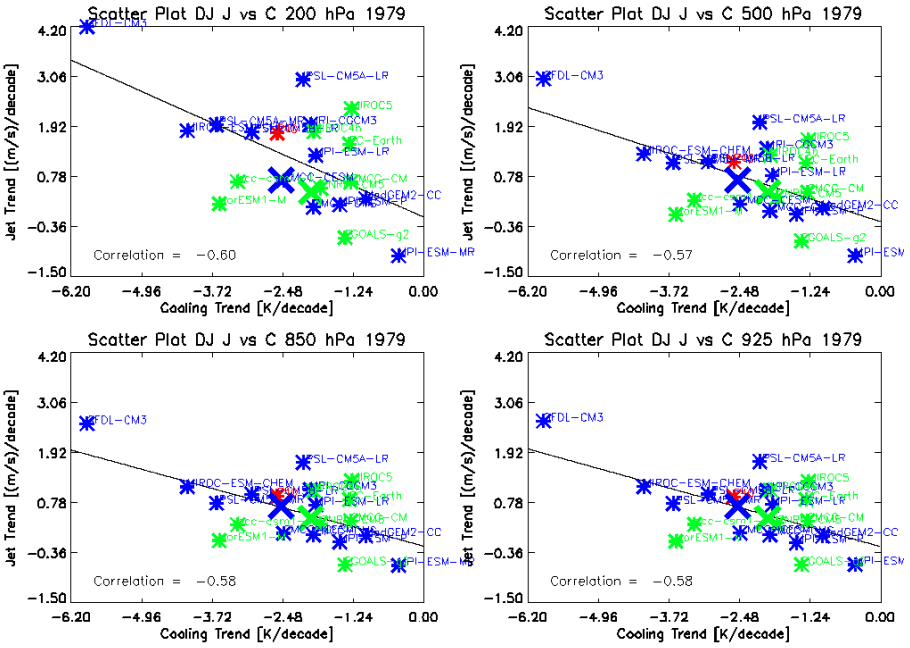

Figure B.31: as Figure 5.3 but with the jet shift trend constructed averaging on DJ season.

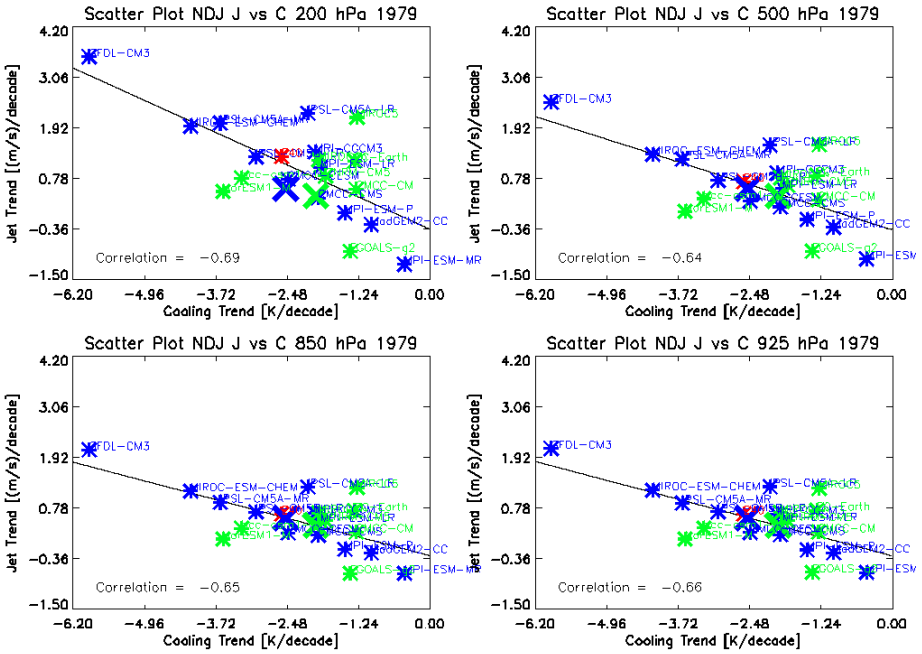

Figure B.32: as Figure 5.3 but with the jet shift trend constructed averaging on NDJ season.

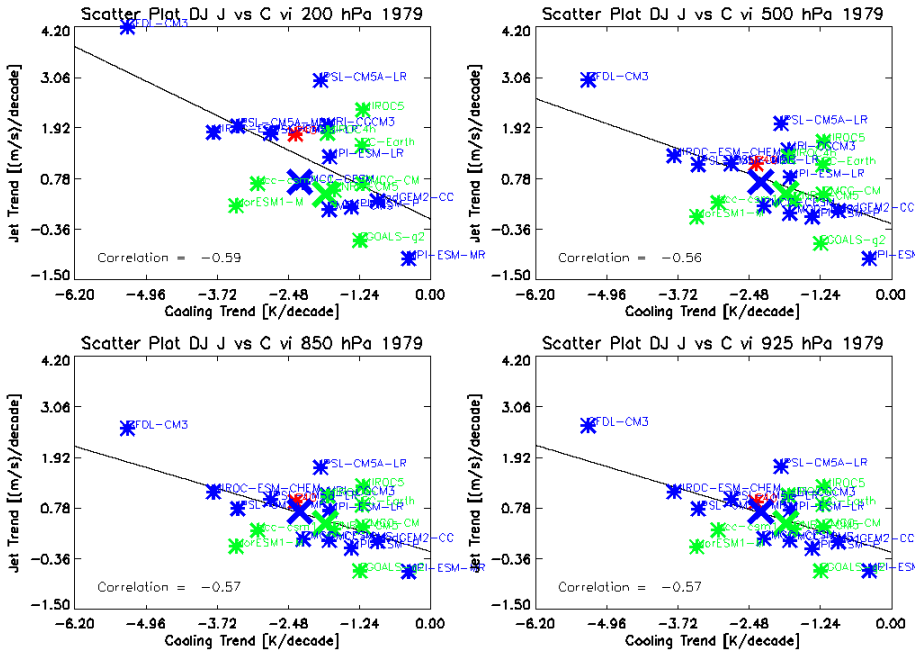

Figure B.33: as Figure 5.3 but with the jet shift trend constructed averaging on DJ season.

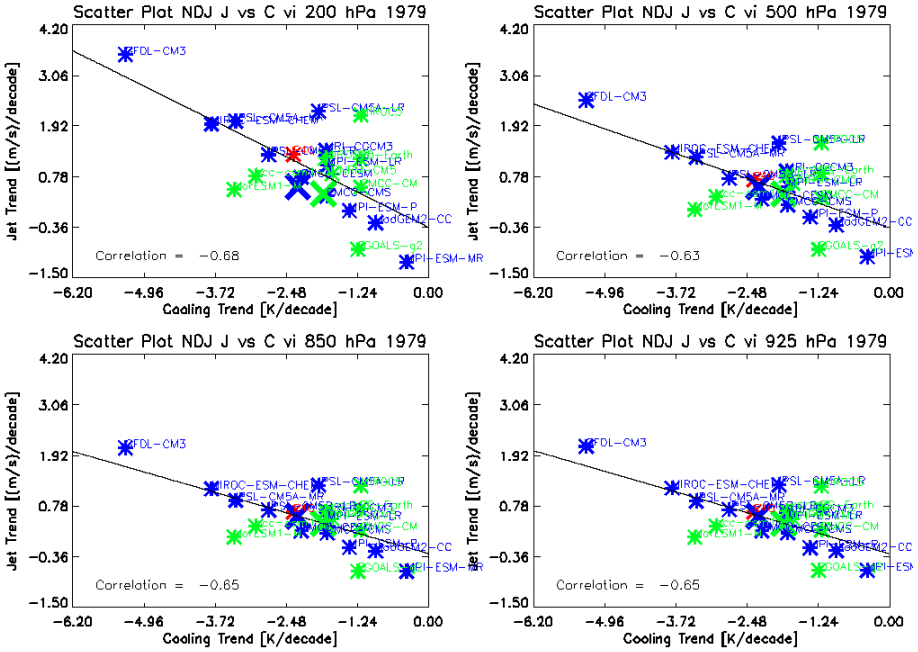

Figure B.34: as Figure 5.3 but with the jet shift trend constructed averaging on NDJ season and with the jet shift trend constructed by vertical integration.

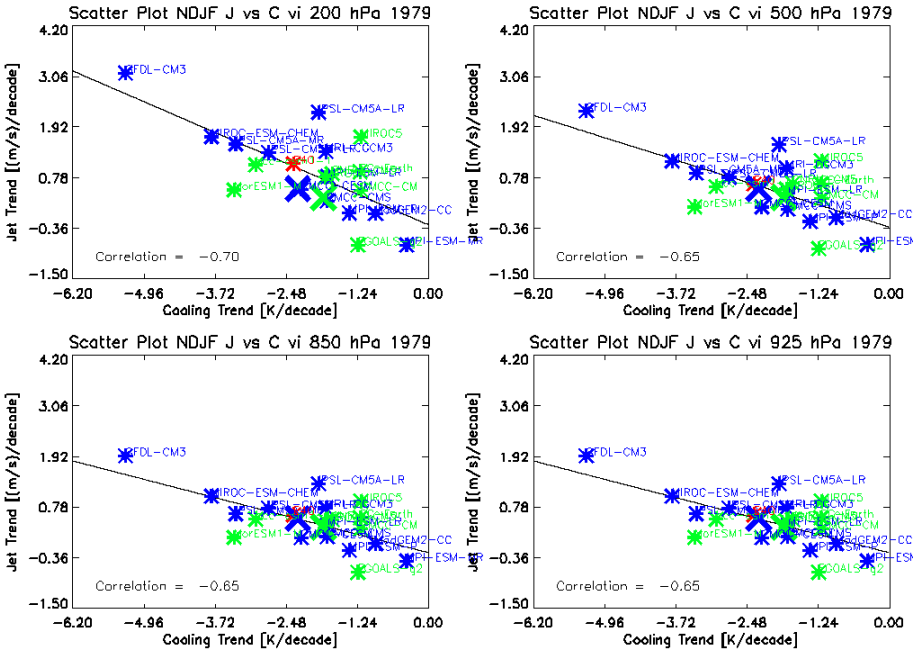

Figure B.35: as Figure 5.3 but with the jet shift trend constructed averaging on NDJF season and with the jet shift trend constructed by vertical integration.

Appendix C

Acronyms

AMIP	Atmospheric Model Intercomparison Project
AOGCM	Atmosphere-Ocean Global Climate Models
AR	Assessment Report
AO	Antarctic Oscillation
CAM3	Community Atmospheric Model, version 3
CCM	Chemistry Climate Model
CCMVal	Chemistry Climate Model Validation
CFC	Chlorofluorocarbon

CMIP	Climate Model Intercomparison Project
CMIP3	CMIP Phase 3
CMIP5	CMIP phase 5
ENSO	El Niño-Southern Oscillation
GCM	Global Climate Model
EP	Eliassen Palm
ESM	Earth System Model
ERA-40	ECMWF 40 Year Re-analysis
ECMWF	European Centre for Medium-Range Weather Forecasts
GHG	Greenhouse Gas
HT	High Top
IPCC	Intergovernmental Panel on Climate Change
JMA	Japanese Meteorological Agency

LT	Low Top
LUC	Land Use Change
NAM	Northern Annular Mode
NCAR	National Center for Atmospheric Research
NCEP	National Centers for Environmental Prediction
NH	Northern Hemisphere
PSC	Polar Stratospheric Cloud
RWB	Rossby Wave Breaking
SAM	Southern Annular Mode
SBUV	Solar Backscatter Ultra-Violet radiometer
SH	Southern Hemisphere
SPARC	Stratospheric Processes and Their Role in Climate

SSW	Stratospheric Sudden Warming
TEM	Transformed Eulerian Mean
TOMS	Total Ozone Mapping Spectrometer
TSI	Total Solar Irradiance
WMO	World Meteorological Organization
WRCP	World Climate Research Programme

References

Andrews, D. G., Holton, J. R., Leovy, C. B., 1987: *Middle Atmospheric Dynamics*, Academic Press, 489 pp.

Ambaum, M. H. P., and B. J. Hoskins, 2002. The NAO troposphere-stratosphere connection. *J. Climate,* **15**,1969–78.

Aoki, S., 2002: Coherent sea level response to the Antarctic Oscillation, *Geophysical Research Letters*, **29** (20), 11-1.

Arblaster, J. M., and G. A. Meehl, 2006: Contribution of external forcings to southern annular mode trends, *J. Clim.*, **19**, 2896–2905.

Arblaster, J. M., Meehl, G. A., Karoly, D. J., 2011: Future climate change in the Southern Hemisphere: Competing effects of ozone and greenhouse gases. *Geophys. Res. Lett.* **38,** L02701.

Balling, R. C., P. J. Michaels, and P. C. Knappenberger, 1998: Analysis of winter and summer warming rates in gridded temperature time series, *Clim. Res.*, **9**, 175–181.

Baldwin M. P., and T. J. Dunkerton, 1999: Propagation of the Arctic Oscillation from the stratosphere to the troposphere. *J. Geophys. Res.,***104**, 30937-46.

Baldwin M. P., and T. J. Dunkerton, 2001: Stratospheric harbingers of anomalous weather regimes. *Science,* **294**, 581-84.

Baldwin M. P., D. B. Stephenson, D. W. J. Thompson, T. J. Dunkerton, A. J. Charlton, and A. O'Neill, 2003: Stratospheric memory and skill of extended-range weather forecasts. *Science,* **301**, 636-40.

Barnes, E. A., & Hartmann, D. L., 2010: Influence of eddy-driven jet latitude on North Atlantic jet persistence and blocking frequency in CMIP3 integrations.*Geophysical Research Letters*, **37** (23).

Bartlett, M. S., 1935: Some aspects of the time-correlation problem in regard to tests of significance, *J. R. Stat. Soc.*, **98**, 536–543.

Black R. X., 2002. Stratospheric forcing of surface climate in the Arctic Oscillation. J. *Climate,* **15**, 268–277.

Bloomfield, P., and D. Nychka, 1992: Climate spectra and detecting climate change, *Clim. Change*, **21**, 275–287.

Böning, C. W., Dispert, A., Visbeck, M., Rintoul, S. R., Schwarzkopf, F. U., 2008: The response of the Antarctic circumpolar current to recent climate change, *Nat. Geosci.*, **1**, 864–869.

Boer, G. J., & Lambert, S. J., 2001: Second-order space-time climate difference statistics, *Climate dynamics*, **17** (2-3), 213-218.

Boville B. A., 1984: The influence of the polar night jet on the tropospheric circulation in a GCM. *J. Atmos. Sci.,* **41**, 1132–1142.

Brandefelt, J., and E. Källén, 2004: The response of the Southern Hemisphere atmospheric circulation to an enhanced greenhouse gas forcing. *Journal of climate*, **17** (22), 4425-4442.

Brayshaw, David James, Brian Hoskins, and Michael Blackburn, 2009: The basic ingredients of the North Atlantic storm track. Part I: Land-sea contrast and orography. *J. Atmos. Sci.,* **66** (9), 2539-2558.

Bretherton, C. S., M. Widmann, V. P. Dymnikov, J. M. Wallace, and Ileana Bladé, 1999: The effective number of spatial degrees of freedom in a spatial field, *J. Clim.*, **12**, 1990–2009.

Butchart, N. and A, A. Scaife, 2001: Removal of chlorofluorocarbons by increased mass exchange between the stratosphere and troposphere in a changing climate, *Nature*, **410**, 799-802.

Butchart, N. et al., 2006: Simulations of anthropogenic change in the strength of the Brewer–Dobson circulation, *Clim. Dyn.*, **27** (7-8), 727-741.

Cash, B. A., P. J. Kushner, and G. K. Vallis, 2005: Zonal asymmetries, teleconnections and annular patterns in a GCM. *J. Atmos. Sci.,* **62**, 207–219.

Cagnazzo, C., Manzini, E., 2009: Impact of the stratosphere on the winter tropospheric teleconnections between ENSO and the North Atlantic and European region, *J. Clim.*, **22**, 1223–1238.

Cagnazzo, C., Manzini, E., Fogli, P. G., Vichi, M., Davini, P., 2013: Role of stratospheric dynamics in the ozone-carbon connection in the Southern Hemisphere, *Clim. Dyn.*, 1-16.

Cai, W., Whetton, P., Karoly, D., 2003: The response of the Antarctic Oscillation to increasing and stabilized atmospheric CO2. *J. Clim.* **16,** 1525–1538.

Catto, Jennifer L., Len C. Shaffrey, Kevin I. Hodges, 2010: Can Climate Models Capture the Structure of Extratropical Cyclones?. *J. Climate*, **23**, 1621–1635.

Charlton, A. J., A. O'Neil, W. A. Lahoz, and A. C. Massacand., 2004: Sensitivity of tropospheric forecasts to stratospheric initial conditions, *Q. J. R. Meteorol. Soc.*, **130**, 1771-1792.

Charlton-Perez, A., et al. (2012), Mean Climate and Variability of the Stratosphere in the CMIP5 models, *J. Geophys. Res.*, *submitted*

Chen, P., Robinson, W. A., 1992: Propagation of planetary waves between the troposphere and stratosphere, *J. Atmos. Sci.*, **49** (24), 2533-2545.

Christiansen, B., 1999: Stratospheric vacillations in a general circulation model. *J. Atmos. Sci.,* **56,** 1858–1872.

Ciasto, L. M. and D. W. J. Thompson, 2008: Observations of large-scale ocean–atmosphere interaction in the Southern Hemisphere. *J. Clim.* **21,** 1244–1259.

Cionni, I., Eyring, V., Lamarque, J. F., Randel, W. J., Stevenson, D. S., Wu, F., Bodeker, G. E., Shepherd, T. G., Shindell, D. T., and Waugh, D. W., 2011:

Ozone database in support of CMIP5 simulations: results and corresponding radiative forcing, *Atmos. Chem. Phys.*, **11**, 11267-11292.

Colling, A., 2001: *Ocean Circulation,* Open University Course Team. Second Edition.

Cordero, E., Newman, P. A., Weaver, C., and E. Fleming, 2012: *Stratospheric ozone. An Electronic Textbook*, Chapter 6.

Cordero, E. C., & Forster, P. D. F., 2006: Stratospheric variability and trends in models used for the IPCC AR4. *Atmospheric Chemistry and Physics*, **6** (12), 5369-5380.

Corti, S., F. Molteni, and T. N. Palmer, 1999: Signature of recent climate change in frequencies of natural atmospheric circulation regimes, *Nature*, **398**, 799–802.

Doney, S. C., Fabry, V. J., Feely, R. A., Kleypas, J. A., 2009: Ocean acidification: the other CO2 problem. *Marine Science*, **1**.

Ebisuzaki, W., 1997: A method to estimate the statistical significance of a correlation when the data are serially correlated, *J. Clim.*, **10**, 2147–2153.

Eyring, V., et al., 2007: Multimodel projections of stratospheric ozone in the 21st century, *Journal of Geophysical Research: Atmospheres (1984–2012)* **112**, D16.

Fabry, V. J., et al., 2008: Impacts of ocean acidification on marine fauna and ecosystem processes, *ICES Journal of Marine Science: Journal du Conseil* **65** (3), 414-432.

Farneti, R., Delworth, T. L., Rosati, A. J., Griffies, S. M., Zeng, F., 2010: The role of mesoscale eddies in the rectification of the Southern Ocean response to climate change. *J. Phys. Oceanogr.* **40,** 1539–1557.

Farneti, R. and T. L. Delworth, 2010: The role of mesoscale eddies in the remote oceanic response to altered Southern Hemisphere winds. *J. Phys. Oceanogr.* **40,** 2348–2354.

Feldstein S., and S. Lee, 1998: Is the atmospheric zonal index driven by an eddy feedback? *J. Atmos. Sci.,* **55**, 3077-86.

Fleming, James R. (1990). *Meteorology in America, 1800-1870*. Baltimore, MD: Johns Hopkins University Press.

Fogt, R. L., Perlwitz, J., Monaghan, A. J., Bromwich, D. H., Jones, J. M., and G. J. Marshall, 2009: Historical SAM variability. Part II: twentieth-century variability and trends from reconstructions, observations, and the IPCC AR4 models, *J. Clim.*, **22**; 5346–5365.

Forster, Piers, et al., 2007: Changes in atmospheric constituents and in radiative forcing." *Climate change,* **20**.

Fu, Q., Johanson, C. M., Wallace, J. M., Reichler, T., 2006: Enhanced mid-latitude tropospheric warming in satellite measurements. *Science*, **312** (5777), 1179-1179.

Fyfe, J. C., Boer, G. J., Flato, G. M., 1999: The Arctic and Antarctic oscillations and their projected changes under global warming. *Geophys. Res. Lett.* **26,** 1601–1604.

Fyfe, J. C. and O. A. Saenko, 2006: Simulated changes in the extratropical Southern Hemisphere winds and currents. *Geophys. Res. Lett.*, **33**, L06701.

Fyfe, J. C., Saenko, O. A., Zickfeld, K., Eby, M., Weaver, A. J., 2007: The role of poleward-intensifying winds on Southern Ocean warming. *J. Clim.* **20,** 5391–5400.

Gerber, E. P. et al., 2010: Stratosphere-troposphere coupling and annular mode variability in chemistry-climate models, *J. Geophys. Res.*, **115**, D00M06.

Gerber, E. P., et al., 2012: Assessing and understanding the impact of stratospheric dynamics and variability on the earth system, *Bull. Amer. Meteor. Soc.*, **93**, 845–859.

Gille, S. T., 2002: Warming of the Southern Ocean since the 1950s, *Science*, **295** (5558), 1275-1277.

Gillett N. P., M. P. Baldwin, D.W. J. Thompson, E. F. Shuckburgh, W. A. Norton, and J. L. Neu, 2003. Report on the SPARC workshop on the role of the stratosphere in tropospheric climate.

Gillett, N. P., Thompson, D. W. J., 2003: Simulation of recent Southern Hemisphere climate change. *Science*, **302**, 273–275.

Goosse, H., Arzel, O., Bitz, C. M., de Montety, A., Vancoppenolle, M., 2009: Increased variability of the Arctic summer ice extent in a warmer climate, *Geophys. Res. Lett.*, **36**, L23702.

Goosse H., P.Y. Barriat, W. Lefebvre, M.F. Loutre, and V. Zunz, 2010: Introduction to climate dynamics and climate modeling. Online textbook available at http://www.climate.be/textbook.

Gray, L. J., 2003: The influence of the equatorial upper stratosphere on stratospheric sudden warmings. *Geophys. Res. Lett.,* **30**, 1166.

Graversen, R. G., Christiansen, B., 2003: Downward propagation from the stratosphere to the troposphere: A comparison of the two hemispheres, *J. Geophys. Res.*, **108**, D24.

Hall, A. and M. Visbeck, 2002: Synchronous variability in the Southern Hemisphere atmosphere, sea ice, and ocean resulting from the Annular Mode. *J. Clim.* **15,** 3043–3057.

Hallberg, R. and A. Gnanadesikan, 2006: The role of eddies in determining the structure and response of the wind-driven Southern Hemisphere overturning: Results from the Modeling Eddies in the Southern Ocean (MESO) project. *J. Phys. Ocean.* **36,** 2232–2252.

Hartley,D. E., J. T.Villarin, R. X. Black, and C. A. Davis, 1998: A new perspective on the dynamical link between the stratosphere and troposphere. *Nature,* **391**, 471–74.

Hartmann, D. L., and F. Lo, 1998: Wave-driven zonal flow vacillation in the Southern Hemisphere. *J. Atmos. Sci.,* **55**,1303-15.

Hartmann, D. L., J. M.Wallace, V. Limpasuvan, D.W. J. Thompson, and J. R. Holton, 2000: Can ozone depletion and global warming interact to produce rapid climate change? *Proc. Nat. Acad. Sci. (Wash. DC),* **97**,1412–17.

Hartmann, D. L., 2004: The stratosphere in the climate system. *SPARC Newsletter,* **22**, 15-18.

Hasselmann, K., 1999: Linear and nonlinear signatures, *Nature*, **398**, 755–756.

Haynes, P. H., and T. G. Shepherd, 1989: The importance of surface-pressure changes in the response of the atmosphere to zonally-symmetric thermal and mechanical forcing. *Quart. J. Roy. Meteor. Soc.,* **115,** 1181–1208.

Haynes, P. H., C. J.Marks, M. E.McIntyre, T. G. Shepherd, and K. P. Shine, 1991: On the "downward control" of extratropical diabatic circulations by eddy-induced mean zonal forces. *J. Atmos. Sci.,* **48**, 651–78.

Haynes, P. H., 2005: Stratosphere-Troposphere Dynamical Coupling, *SPARC Newsletter,* **25**, 27-31.

Haynes, P.H., 2005: Stratospheric dynamics. *Ann. Rev. Fluid Mech.,* **37**, 263-293.

Held, I. M., 1975: Momentum Transport by Quasi-Geostrophic Eddies, *J. Atmos. Sci.*, **32**, 1494–1497.

Held, I. M., Arthur Y. Hou, 1980: Nonlinear Axially Symmetric Circulations in a Nearly Inviscid Atmosphere, *J. Atmos. Sci.*, **37**, 515–533.

Held, I. M., 2000: The general circulation of the atmosphere, Proc. Prog. Geophys. Fluid Dyn.

Hoegh-Guldberg, Ove, et al., 2007: Coral reefs under rapid climate change and ocean acidification, *Science,* **318** (5857), 1737-1742.

Hogg, A., Meredith, M., Blundell, J., Wilson, C., 2008: Eddy heat flux in the Southern Ocean: Response to variable wind forcing. *J. Clim.* **21,** 608–620.

Holton, J. R., Mass, C., 1976: Stratospheric vacillation cycles, *Journal of the Atmospheric Sciences*, **33** (11), 2218-2225.

Holton, J. R., P. H. Haynes, and M. E. McIntyre, A. R. Douglass, R. B. Rood, and L. Pfister, 1995: Stratosphere–troposphere exchange. *Revs. Geophys.,* **33**, 403–39.

Holton, J. R., 2004: *An introduction to Dynamic Meteorology*, Elsevier Academic Press, 535 pp.

Hoskins, B. J., and Karoly, D. J.,1981: The steady linear response of a spherical atmosphere to thermal and orographic forcing, *J. Atmos. Sci.*, **38** (6), 1179-1196.

Hoskins, B. J., James, I. N., White, G. H., 1983: The shape, propagation and mean-flow interaction of large-scale weather systems. *J. Atmos. Sci.*, **40** (7), 1595-1612.

Hu, Y., & Fu, Q., 2007: Observed poleward expansion of the Hadley circulation since 1979. *Atmospheric Chemistry and Physics*, **7** (19), 5229-5236.

Hughes, C. W., Woodworth, P. L., Meredith, M. P., Stepanov, V., Whitworth, T., & Pyne, A. R., 2003: Coherence of Antarctic sea levels, southern hemisphere annular mode, and flow through Drake Passage, *Geophysical Research Letters*, **30** (9).

Hurrell, J.W., and H. van Loon. 1994: A modulation of the atmospheric annual cycle in the southern hemisphere, *Tellus*, **46A**, 325-338.

Jacob, D. J., 1999: *Introduction to Atmospheric Chemistry*, Princeton University Press, 260 pp.

Johanson, C. M., and Q. Fu, 2009: Hadley cell widening: Model simulations versus observations. *Journal of Climate*, **22** (10), 2713-2725.

Jones, A. E., J. D. Shanklin, 1995: Continued decline of total ozone over Halley, Antarctica, since 1985, *Nature*, **376**, 409-411.

Kang, S. M., Polvani, L. M., Fyfe, J. C., and M. Sigmond, 2011: Impact of polar ozone depletion on subtropical precipitation, *Science*, **332**, 951–954.

Kalnay, E. and twenty-one others, 1996: The NCEP/NCAR 40-year reanalysis project, *Bull. Amer. Meteor. Soc.*, **77**, 437-471.

Kalnay, E. et al., 2003: Global analyses of sea surface temperature, sea ice, and nigh marine aire temperature since the late nineteenth century. *J. Geophys. Res.,* **108**, D14, 4407.

Kang, S. M., Polvani, L. M., Fyfe, J. C., Sigmond, M., 2011: Impact of polar ozone depletion on subtropical precipitation, *Science,* **332,** 951–954.

Karoly, D. J., 1990: The role of transient eddies in low-frequency zonal variations of the Southern Hemisphere circulation. *Tellus* **42A,** 41–50.

Kaspi, Yohai, and T. Schneider, 2011: Winter cold of eastern continental boundaries induced by warm ocean waters, *Nature,* **471** (7340), 621-624.

Kidson, John W., 1999: Principal modes of Southern Hemisphere low-frequency variability obtained from NCEP-NCAR reanalyses, *Journal of Climate* **12** (9), 2808-2830.

Kidston, J., and E. P. Gerber., 2010: Intermodel variability of the poleward shift of the austral jet stream in the CMIP3 integrations linked to biases in 20th century climatology, *Geophys.Res. Lett.,* **37**:9, L09708.

Knauss, J.A., 2005: *Introduction to Physical Oceanography*, Waveland Press. Second Edition.

Kodera, K., K. Yamazaki, K. Chiba, and K. Shibata, 1990: Downward propagation of upper stratospheric mean zonal wind perturbation to the troposphere. *Geophys. Res. Lett.,* **17**,1263-66.

Kushner, P. J., Held, I. M., Delworth, T. L., 2001: Southern Hemisphere atmospheric circulation response to global warming, *J. Clim.*, **14**, 2238–2249.

Kushner, P. J., and L. M. Polvani, 2004: Stratosphere-troposphere coupling in a relatively simple AGCM: the role of eddies. *J. Clim.,* **17**, 629-639.

Kwok, R., and J. C. Comiso, 2012: Spatial patterns of variability in Antarctic surface temperature: Connections to the Southern Hemisphere Annular Mode and the Southern Oscillation, *Geophysical Research Letters* **29** (14), (2002): 50-1.

L'Heureux, Michelle L., David W. J. Thompson, 2006: Observed Relationships between the El Niño–Southern Oscillation and the Extratropical Zonal-Mean Circulation. *J. Climate*, **19**, 276–287.

Labitzke, K., 1972: Temperature Changes in the Mesosphere and Stratosphere Connected with Circulation Changes in Winter. *J. Atmos. Sci.*, **29**, 756-766.

Lachlan-Cope, T., & Connolley, W., 2006: Teleconnections between the tropical Pacific and the Amundsen-Bellinghausens Sea: Role of the El Niño/Southern Oscillation, *J. Geophys. Res.: Atmospheres (1984–2012)*, **111**, D23.

Le Quéré, C. et al., 2007: Saturation of the Southern Ocean CO2 sink due to ecent climate change, *Science*, **316**:1735–1738.

Le Quéré, C., Takahashi, T., Buitenhuis, E. T., Rödenbeck, C., Sutherland, S. C., 2010: Impact of climate change and variability on the global oceanic sink of CO2, *Global Biogeochemical Cycles*, **24** (4).

Ledley, T. S., E. T. Sundquist, S. E. Schwartz, D. K. Hall, J. D. Fellows, and T. L. Killeen, 1999: Climate change and greenhouse gases, *Eos Trans. AGU*, **80**, 39, 453–458.

Lenton, A., Codron, F., Bopp, L., Metzl, N., Cadule, P., Tagliabue, A., Le Sommer, J., 2009: Stratospheric ozone depletion reduces ocean carbon uptake and enhances ocean acidification, *Geophys. Res. Lett.*, **36**, L12606.

Li, C. and J.J. Wettstein, 2012: Thermally-driven and Eddy-driven Jet Variability in Reanalysis, *J.Climate*, **25**, 1587-1596.

Limpasuvan, V., and D. L. Hartmann, 1999: Eddies and the annular modes of climate variability, *Geophysical Research Letters*, **26** (20), 3133-3136.

Limpasuvan, V., and D. L. Hartmann, 2000: Wave-maintained annular modes of climate variability. *J. Climate,* **13**, 4414-29.

Lin, Jia-Lin, et al., 2006: Tropical intraseasonal variability in 14 IPCC AR4 climate models. Part I: Convective signals, *Journal of climate,* **19** (12), 2665-2690.

Lin, J. L., 2007: Interdecadal variability of ENSO in 21 IPCC AR4 coupled GCMs. *Geophysical research letters*, **34** (12), L12702.

Lorenz, D. J., & Hartmann, D. L., 2001: Eddy-zonal flow feedback in the Southern Hemisphere. *Journal of the atmospheric sciences*, **58** (21), 3312-3327.

Lovenduski, N. S., Ito, T., 2009: The future evolution of the Southern Ocean CO2 sink, J. Mar. Res., **67**, 597–617.

Lovenduski, N. S., Gruber, N., Doney, S. C., 2008: Toward a mechanistic understanding of the decadal trends in the Southern Ocean carbon sink, *Global Biogeochem. Cycles*, **22**, GB3016.

Lu, J., Vecchi, G. A., & Reichler, T., 2007: Expansion of the Hadley cell under global warming. *Geophysical Research Letters*, **34** (6).

Lu, J., Chen, G. and D. Frierson, 2008: Response of the zonal mean atmospheric circulation to El Niño versus global warming. *J. Clim.* **21**, 5835–5851.

Lutgens, F. K., and E. J. Tarbuck, 2001: *The Atmosphere: an Introduction to Meteorology*,

Mann, K.H. and Lazier J.R., 2006: *Dynamics of Marine Ecosystems*, Blackwell Publishing. Third Edition.

Manzini, E., and L. Bengtsson, 1996: Stratospheric climate and variability from a general circulation model and observations, *Climate. Dyn.*, **12**, 615-639.

Manzini, E., Steil, B., Bruhl, C., Giorgetta, M. A., Kruger, K., 2003: A new interactive chemistry-climate model: 2. Sensitivity of the middle atmosphere to ozone depletion and increase in greenhouse gases and implications for recent stratospheric cooling, *J. Geophys. Res.*, **108**, D14, 4429.

Manzini, E., Giorgetta, M. A., Esch, M., Kornblueh, L., Roeckner, E., 2006: The influence of sea surface temperatures on the northern winter stratosphere: ensemble simulations with the MAECHAM5 model. *J. Clim.*, **19**, 3863–3881.

Manzini, E., Cagnazzo, C., Fogli, P. G., Bellucci, A., Muller, W. A., 2012: Stratosphere-troposphere coupling at inter-decadal time scales: implications for the North Atlantic Ocean, *Geophys. Res. Lett.*, **39**, L05801.

Marshall, G. J., 2002: Trends in Antarctic geopotential height and temperature: A comparison between radiosonde and NCEP-NCAR reanalysis data. *Journal of Climate*, **15** (6), 659-674.

Marshall, G. J., 2003: Trends in the Southern Annular Mode from observations and reanalyses, *J. Climate*, **16** (24), 4134-4143.

Marshall, G. J., Stott, P. A., Turner, J., Connolley, W. M., King, J. C., & Lachlan-Cope, T. A., 2004: Causes of exceptional atmospheric circulation changes in the Southern Hemisphere, *Geophysical Research Letters*, **31** (14).

Marshall, G. J., Orr, A., van Lipzig, N. P. M., King, J. C., 2006: The impact of a changing Southern Hemisphere Annular Mode on Antarctic peninsula summer temperatures. *J. Clim.* **19,** 5388–5404.

Marshall, G. J., 2007: Half-century seasonal relationships between the Southern Annular Mode and Antarctic temperatures. *Int. J. Climatol.* **27,** 373–383.

McIntyre, M. E., and T. N. Palmer, 1983: Breaking planetary waves in the stratosphere, *Nature,* **305** (5935), 593-600.

McLandress, C., Jonsson, A. I., Plummer, D. A., Reader, M. C., Scinocca, J. F., Shepherd, T. G., 2010: Separating the dynamical effects of climate change and ozone depletion. Part I: southern Hemisphere stratosphere, *J. Clim.*, **23**, 5002–5020.

McLandress, Charles, Theodore G. Shepherd, John F. Scinocca, David A. Plummer, Michael Sigmond, Andreas I. Jonsson, M. Catherine Reader, 2011: Separating the Dynamical Effects of Climate Change and Ozone Depletion. Part II: Southern Hemisphere Troposphere, *J. Climate*, **24**, 1850–1868.

Meehl, Gerard A., et al., 2007: Global climate projections, *Climate change,* 747-845.

Meredith, M. P., Woodworth, P. L., Hughes, C. W., & Stepanov, V., 2004: Changes in the ocean transport through Drake Passage during the 1980s and 1990s, forced by changes in the Southern Annular Mode, *Geophysical Research Letters*, **31** (21).

Miller, R. L., Schmidt, G. A., Shindell, D. T., 2006: Forced annular variations in the 20th century intergovernmental panel on climate change fourth assessment report models. *Journal of Geophysical Research*, **111** (D18), D18101.

Mitchell, J. M., Jr., B. Dzerdzeevskii, H. Flohn, W. L. Hofmeyr, H. H. Lamb, K. N. Rao, and C. C. Wallén, 1966: *Climatic Change*, *Techn. Note 79*, World Meteorol. Org., Geneva, 79 pp.

Ndarana, T and D.W. Waugh, 2010: The link between cut-off lows and Rossby wave breaking in the Southern Hemisphere, *Quart. J. Royal. Met. Soc.*, **136**, 869-885.

Norton, W. A., 2003: Sensitivity of northern hemisphere surface climate to simulation of the stratospheric polar vortex. *Geophys. Res. Lett.* **30**, 1627.

Oke, P. R., & England, M. H., 2004: Oceanic response to changes in the latitude of the Southern Hemisphere subpolar westerly winds, *Journal of Climate*, **17** (5), 1040-1054.

Omstedt, A., Edman, M., Anderson, L. G., Laudon, H., 2010: Factors influencing the acid–base (pH) balance in the Baltic Sea: a sensitivity analysis, *Tellus B*, **62** (4), 280-295.

Orr, A., Bracegirdle, T. J., Hosking, S. J., 2012: Possible dynamical mechanisms for Southern Hemisphere climate change due to the ozone hole, *J. Atmos. Sci.*, **69**, 2917–2932.

Parkinson, C. L., 2002. Trends in the length of the Southern Ocean sea-ice season, 1979-99. *Annals of Glaciology*, **34** (1), 435-440.

Peixoto, J. and A. Oort, 1992: *Physics of Climate*. Aip Press, 520 pp.

Perlwitz, J., and N. Harnik, 2003: Observational evidence of a stratospheric influence on the troposphere by planetary wave reflection. *J. Climate,* **16**, 3011-3026.

Perlwitz, J., and N. Harnik, 2004: Downward coupling between the stratosphere and the troposphere: the relative roles of wave and zonal mean processes. *J. Climate,* **17**, 4902-4909.

Perlwitz, J., Pawson, S., Fogt, R. L., Nielsen, J. E., Neff, W. D., 2008: Impact of stratospheric ozone recovery on Antarctic climate, *Geophys. Res. Lett.*, **35**, L08714.

Plumb, R. A., 1977: The interaction of two internal waves with the mean flow: implications for the theory of the quasi-biennial oscillation. *J. Atmos. Sci.,* **34**, 1847–1858.

Plumb, R. A., and K. Semeniuk, 2003: Downward migration of extratropical zonal wind anomalies. *J. Geophys. Res.,* **108**, 4223,

Polvani, L. M., and P. Kushner, 2002: Tropospheric response to stratospheric perturbations in a relatively simple general circulation model, *Geophys. Res. Lett.,* **29,** 1114.

Polvani, L. M., Waugh, D. W., Correa, G. J. P., and S.-W. Son, 2010: Stratospheric ozone depletion: The main driver of 20th century atmospheric circulation changes in the Southern Hemisphere, *J. Clim., in press*.

Polvani, L. M., Waugh, D. W., Correa, G. J. P., Son S.-W., 2011a: Stratospheric ozone depletion: the main driver of twentieth-century atmospheric circulation changes in the Southern Hemisphere, *J. Clim.*, **24**, 795–812.

Polvani, L. M., Previdi, M., Deser, C., 2011b: Large cancellation, due to ozone recovery, of future Southern Hemisphere atmospheric circulation trends, *Geophys. Res. Lett.*, **38**, L04707.

Pond, S. and Pickard, G. L., 1983: *Introductory Dynamical Oceanography*, Pergamon Press. Second edition.

Randall, D. A. et al., 2007: Climate models and their evaluation. *Climate change*, **323**.

Randall, D. A., 2013 : *An Introduction to the general circulation of the atmosphere*. Available online on: http://kiwi.atmos.colostate.edu/group/dave/at605.html.

Randel, W. J., & Wu, F., 1999: A stratospheric ozone trends data set for global modeling studies. *Geophysical Research Letters*, **26** (20), 3089-3092.

Rashid, H. A., Simmonds, I., 2004: Eddy-zonal flow interactions associated with the Southern Hemisphere annular mode: Results from NCEP-DOE reanalysis and a quasi-linear model, *Journal of the atmospheric sciences*, **61** (8), 873-888.

Rashid, H. A., Simmonds, I., 2005: Southern Hemisphere annular mode variability and the role of optimal nonmodal growth, *Journal of the atmospheric sciences*, **62** (6), 1947-1961.

Rayner, N. A., et al., 2003: Global analyses of sea surface temperature, sea ice, and night marine air temperature since the late nineteenth century, *Journal of Geophysical Research: Atmospheres (1984–2012),* **108**, D14.

Robinson, W. A., 1991: The dynamics of the zonal index in a simple model of the atmosphere, *Tellus,* **43A**, 295–305.

Sabine, Christopher L., et al., 2004: The oceanic sink for anthropogenic CO2, *Science,* **305** (5682), 367-371.

Salleé, J. B., Speer, K., Morrow, R., 2008: Response of the Antarctic Circumpolar Current to atmospheric variability. *J. Clim.* **21,** 3020–3039.

Santer, B. D., Wingley, T. N. L., Boyle, J. S., Gaffen, D. J., Hnilo, J. J., Nychka, D., Parker, D. E., and K. E. Taylor, 2000: Statistical significance of trends and trend differences in layer-average atmospheric temperature time series, *J. Geophys. Res*, **105**, 7337-7356.

Scherhag, R., 1952: Die explosionsartigen Stratospären-eruärmungen des Spätuinters 1951/52, *Berichte d. Dt. Uetterd. US-Zone,* **38**, 51 – 63.

Schneider, T., 2006: The general circulation of the atmosphere, *Annual Reviews of Earth and Planetary Sciences*, **34**, 655-688.

Scinocca, J. F., Haynes, P. H., 1998: Dynamical forcing of stratospheric planetary waves by tropospheric baroclinic eddies, *J. atmos. sciences*, **55** (14), 2361-2392.

Scott, R. K., and L. M. Polvani, 2004. Stratospheric control of upward wave flux near the tropopause, *Geophys. Res. Lett.,* **31**, L02115.

Screen, J. A., Gillett, N. P., Stevens, D. P., Marshall, G. J., Roscoe, H. K., 2009: The role of eddies in the Southern Ocean temperature response to the Southern Annular Mode. *J. Clim.* **22,** 806–818

.

Shindell, D. and G. A. Schmidt, 2004: Southern Hemisphere climate response to ozone changes and greenhouse gas increases. *Geophys. Res. Lett.* **31**, L18209.

Shine, K. P., 1987: The middle atmosphere in the absence of dynamical heat fluxes, *Q. J. Roy. Met. Soc.,* **113**, 603-633.

Sigmond, M., Fyfe, J. C., 2010: Has the ozone hole contributed to increased Antarctic sea ice extent?, *Geophys. Res. Lett.*, **37**, L18502.

Sigmond, M., Reader, M. C., Fyfe, J. C., Gillett, N. P., 2011: Drivers of past and future Southern Ocean change: stratospheric ozone verses greenhouse gas impacts. *Geophys. Res. Lett.* **38,** L12601.

Seidel, D. J., Q. Fu, W.J. Randel and T. Reichler, 2008: Widening of the tropical belt in a changing climate. *Nature Geoscience*, **1**, 21-24

Sen Gupta, A. and M. H. England, 2006: Coupled ocean-atmosphere-ice response to variations in the Southern Annular Mode. *J. Clim.* **19,** 4457–4486.

Sexton, D. M. H., 2001: The effect of stratospheric ozone depletion on the phase of the Antarctic Oscillation, *Geophysical research letters,* **28** (19), 3697-3700.

Song, Y., and W. A. Robinson, 2004: Dynamical mechanisms of stratospheric influences on the troposphere, *J. Atmos. Sci.,* **61**, 1711-25.

Son, S. W., & Lee, S., 2005: The response of westerly jets to thermal driving in a primitive equation model. *Journal of the atmospheric sciences*, **62** (10), 3741-3757.

Son, S.-W., Polvani, L. M., Waugh, D. W., Akiyoshi, H., Garcia, R., Kinnison, D., Pawson, S., Rozanov, E., Shepherd, T. G., Shibata, K., 2008: The impact of stratospheric ozone recovery on the Southern Hemisphere westerly jet, *Science*, **320**, 1486–1489.

Son, S-W., Tandon, N. F., Polvani, L. M. & Waugh, D. W., 2009a: Ozone hole and Southern Hemisphere climate change. *Geophys. Res. Lett.* **36,** L15705.

Son, S.-W., L. M. Polvani, D. W. Waugh, T. Birner, H. Akiyoshi, R. R. Garcia, A. Gettelman, D. A. Plummer, and E. Rozanov, 2009b: The impact of stratospheric ozone recovery on tropopause height trends, *J. Clim.*, **22**, 429–445.

Son, S.-W., et al., 2010: Impact of stratospheric ozone on the Southern Hemisphere circulation changes: a multimodel assessment, *J. Geophys. Res.*, **115**, D00M07.

Spence, P., Fyfe, J. C., Montenegro, A., Weaver, A. J., 2010: Southern Ocean response to strengthening winds in an eddy-permitting global climate model. *J. Clim.* **23**, 5332–5343.

Strong, C., and G. Magnusdottir, 2008: Tropospheric Rossby wave breaking and the NAO/NAM, *J. Atmos. Sci.,* **65** (9), 2861-2876.

Sverdrup, K.A., Duxbury, A.C., Duxbury, A.B., 2005: *An Introduction to The World's Oceans*, McGraw-Hill. Eighth Edition.

Taylor, K. E., Stouffer, R. J., & Meehl, G. A., 2009: A summary of the CMIP5 experiment design. *WCRP, submitted.*

Thompson, D. W. J., and J. M. Wallace, 2000: Annular modes in the extratropical circulation. Part I: Month-to-month variability, *J. Climate,* **13**, 1000-1016.

Thompson, D.W.J., J.M. Wallace, and G.C. Hegerl, 2000: Annular modes in the extratropical circulation. Part II: Trends, *J. Clim.,* **13**, 1018–1036.

Thompson, D. W. J., Baldwin, M. P. and S. Solomon, 2005: Stratosphere–troposphere coupling in the Southern Hemisphere, *J. Atmos. Sci.,* **62**, 708–715.

Thompson, D.W. J., and S. Solomon, 2002: Interpretation of recent Southern Hemisphere climate change, *Science*, **296**, 895–899.

Thompson, D. W., Solomon, S., Kushner, P. J., England, M. H., Grise, K. M., & Karoly, D. J., 2011: Signatures of the Antarctic ozone hole in Southern Hemisphere surface climate change, *Nature Geoscience*, **4** (11), 741-749.

Toggweiler, J. R., and D. W. Lea, 2010: Temperature differences between the hemispheres and ice age climate variability, Paleoceanography, **25**, PA2212.

Trenberth, K.E., and L. Smith, 2005: The mass of the atmosphere: A constraint on global analyses, *J. Clim.*, 18, 864–875.

Turner, J., et al., 2009: Non-annular atmospheric circulation change induced by stratospheric ozone depletion and its role in the recent increase of Antarctic sea ice extent, *Geophys. Res. Lett.*, **36**, L08502.

Uppala, Sakari M., et al., 2005: The ERA-40 re-analysis, *Quarterly Journal of the Royal Meteorological Society,* **131** (612), 2961-3012.

Vallis, Geoffrey K. 2006: *Atmospheric and oceanic fluid dynamics: fundamentals and large-scale circulation*. Cambridge University Press.

Verdy, A., Marshall, J., Czaja, A., 2006: Sea surface temperature variability along the path of the Antarctic Circumpolar Current. *J. Phys. Oceanogr.* **36,** 1317–1331.

Wigley, T. M. L., and P. D. Jones, 1981: Detecting CO2-induced climate change, *Nature*, **292**, 205–208.

Wignall, P. B., 2001: Large igneous provinces and mass extinctions, *Earth Science Rev.*, **53**, 1-33.

Wilks, D. S., 1995: *Statistical Methods in the Atmospheric Sciences*, Academic, San Diego, Calif., 467 pp.

WMO (World Meteorological Organization), 2011: Scientific Assessment of Ozone Depletion: 2010, *Global Ozone Research and Monitoring Project–Report No. 52*, Geneva, Switzerland, 516 pp.

Yang, E. S., Cunnold, D. M., Newchurch, M. J., & Salawitch, R. J., 2005: Change in ozone trends at southern high latitudes. *Geophysical research letters*, **32** (12).

Yin, J. H., 2005: A consistent poleward shift of the storm tracks in simulations of 21st century climate. *Geophysical Research Letters*, **32** (18).

Yoden, S., M. Taguchi, and Y. Naito, 2002: Numerical studies on time variations of the troposphere- stratosphere coupled system, *J. Met. Soc. Japan,* **80**, 811–830.

Zhou, S., M. E. Gelman, A. J. Miller, and J. P. McCormack, 2000: An inter-hemisphere comparison of the persistent stratospheric polar vortex, *Geophys. Res. Lett.*, **27**, 1123–1126.

Acknowledgments

I dearly want to thank all the persons who helped me during this long "trip" of my university life. I would like to start thanking Chiara Cagnazzo, a great teacher, a helpful mentor, who made me part of her research project and addressed me to a new walking in the scientific international community. With her constant enthusiasm, patience, cheerfulness, she dedicated me time to discuss together the issues I've had to face during this work, always willing to accept my "help requests". I am extremely grateful also to Federico Fierli who gave me the chance to work with him and his work team, and addressed me to the better project for my interests. He had been always available to help me and clear every my doubts. My gratitude goes also to ISAC-CNR Roma and to the wonderful people (from both the scientific and the human point of view) that I met during my staying at CNR, in particular Marcel Snels and Francesco Cairo who contributed to make my work less stressful, and helped me a lot with different parts of it. I am also grateful to Prof. Andrea Buzzi who helped me with his wise advices and gave me the possibility to work to ISAC-CNR Bologna and to let me work at Roma in under Chiara supervision. I thank the University of Bologna and, again, ISAC-CNR for their support. An important part of my gratefulness goes for my friends and family. My mom, my dad, my sister who had always support me and make me feel confident, who gave me a warm hug during my ups and downs and try to make less stressful preparing my exams and thesis. I thank my friends who there had always been for me, who make me laugh, feel strong and loved, and make this "trip" so beautiful, special, full of beautiful moments, silly ones, but most of all full of joy. In particular I thank Flovia for her unlimited patience in my regard. I would like to thank Bologna too, which let me be part of its chaotic life, full of different students, full of different cultures, made me know Verdi's Square, the artery of students life. I love Bologna even thought I still get lost. At last but not for the importance I would love to thank a very special person for me, who with his presence fills this so hard period full of joy and love.